AN INVESTIGATION OF THE REGENERATION OF CARBONISED CATALYST PELLETS IN A PACKED BED REACTOR

BY

BEREND JAGER M.Sc.Eng. (Rand)

A thesis submitted in partial fulfillment of the requirements for the degree of Doctor of Philosophy in the Department of Chemical Engineering, University of Natal, South Africa.

Durban
August, 1973

To Rosil

PREFACE

The work described in this thesis was carried out in the Department of Chemical Engineering of the University of Natal. The work is original, except where specifically stated in the text, and no part of this thesis has been submitted for a degree at any other university. This research was supported by grants from the South African Council for Scientific and Industrial Research for which I express my grateful thanks.

I would like to express my grateful appreciation for the assistance and guidance I obtained from Dr. R. P. King, who supervised the work.

I would also like to express my grateful appreciation towards Professor E.T. Woodburn, the head of the department, for his interest in this work and the opportunities he provided which made completion of it possible. I also would like to thank him, as well as all my colleagues in the department, for the invaluable stimulation they provided during the time of this investigation.

The catalyst needed for this work was donated by the South African Coal, Oil and Gas Corporation for which I express my grateful thanks. In particular I appreciate the interest show in this work by Mr. R. Bettman of the South African Coal, Oil and Gas Corporation. He suggested the problem.

I would like to thank Mr. D. Penn and his staff, in particular Messrs. E. Magnus and J. Botha for their able and willing help in the construction and maintenance of the experimental equipment.

The help of Mr. G. L. Webb, Director of the Computer Centre of the University of Natal, and his staff, in particular, Mrs. M. Wright, is sincerely appreciated.

Mrs. B. Hudson and Mrs. J. M. Garcia I would like to thank for typing this thesis.

Lastly my grateful appreciation and thanks goes to my wife Rosil for her forbearance which contributed so much towards the completion of this work.

SUMMARY

A numerical model is proposed which simulates the regeneration of carbonised pellets by combustion with oxygen. The rate of combustion may either be reaction rate or reaction rate and diffusion rate controlled.

Experimental data was obtained from a 0,914 m long fixed bed reactor, 0,050 m in diameter in the temperature range of 750°K to about 1000°K for carbonised 6,4 mm x 6,4 mm cylindrical pellets. The initial carbon content of the pellets was 4,8 or 6,9% by weight. Diffusivities were experimentally determined for several individual pellets and found to be of the Knudsen type.

Pre-exponential factors and an activation energy were obtained for the model, to fit the experimental temperature profiles. The effect of different parameters on predicted temperature profiles was investigated.

The effect of gas flow reversal on the regeneration times for short beds or high flowrates was investigated. Depending on the degree of regeneration required, reductions of up to 30% in regeneration times are predicted.

O P S O M M I N G

'n Numeriese model word voorgestel wat die regenerasie (deur verbranding met suurstof) simuleer van katalisatorkorrels, waarop koolstof neergeslaan is. Die verbrandingsnelheid word deur die reaksiesnelheid of deur die reaksiesnelheid saam met die diffusiesnelheid, beheer.

Experimentele gegewens is versamel in 'n temperatuurgebied van 750°K tot 1000°K, van 'n vaste bed reaktor, 0,914 m lang en 0,050 m in deursnee, gevul met silindriese korrels, 6,4 mm lang en 6,4 mm in deursnee. Die aanvangskonsentrasie van koolstof in die korrels was 4,8% of 6,9% per gewig. Diffusie koeffisiente is experimenteel bepaal vir verskeie korrels. Diffusie het geblyk om van die Knudsen tipe te wees.

Voor-exponentiële faktore en 'n aktieveringsenergie is verkry vir die model, om die experimentele temperatuur profiele te simuleer. Die invloed van verskeie parameters op die temperatuur profiele is ondersoek.

Die invloed van omkering van die vloeirigting van die gas op die regenerasie tyd, vir kort beddens of vir hoe vloeisnelhede, is ondersoek. Afhangende van die graad van verlangde regenerasie, is verminderings in regenerasie tyd van tot 30% voorspel.

TABLE OF CONTENTS

Chapter: Page

LIST OF FIGURES

C H A P T E R 1

INTRODUCTION

1.1 Definition of the Problem

Heterogeneous reactions taking place in fixed or slowly moving beds are frequently met in the chemical and metallurgical industries. One of the more complex of these reactions is the regeneration of catalyst which becomes carbonised and deactivated during cracking or reforming of hydrocarbons in the petroleum industries. Carbon is deposited on the catalyst in the form of a coke or char. This has to be removed by burning off the coke in a hot stream of gas containing a small amount of oxygen.

The combustion of coke is highly exothermic and in a fixed bed this results in a transient, more or less sharp, temperature peak travelling along the bed. If the bed is long enough, the actual burning of the coke is limited to a more or less well defined burning zone which also moves along the bed at a velocity which may be less or exceed that of the temperature profile.

Depending on the nature of the catalyst material, there is a temperature limitation above which the catalyst will be permanently damaged and deactivated. The problem then is to burn off the coke as quickly as possible without exceeding the maximum allowable temperature.

The design of satisfactory control systems for the regenerator depends critically on the availability of a satisfactory model for the regeneration process. The use of ordinary feed back control loops is not

feasible because the hot spots in the bed are mobile and therefore are not always detected by a feed back detector. The position and intensity of the heat wave passing through the bed must be precisely predictable from observations dispersed sparsely throughout the bed; for this a viable model is essential.

Initially the object of this project was to use the existing models available in order to develop a control system and policy for the regeneration of a fixed bed of carbonised pellets. This appeared to have important industrial applications for the clay treatment process used at the South African Coal, Oil and Gas Corporation (SASOL) where the main reactions are dehydration of alcohols and the shifting of olefin bonds. The regeneration of catalyst associated with this treatment, took about twice as long as the "on line" period, and manual control of the process proved to be not very satisfactory. During regeneration, temperature run-aways would occasionally occur and the catalyst had to be replaced at approximately half-yearly intervals owing to the loss of activity due to overheating. Accurate automatic control could prevent overheating, prevent permanent deactivation of the catalyst and give it a longer life, reducing operating costs.

It was found however, that the models available for the regeneration of carbonised catalyst, could not predict the experimental results obtained from a small pilot plant fixed bed. A new model had therefore to be developed that would be able to predict the behaviour of a fixed bed regenerator. The main object of the project then became the development of such a model and its experimental verification.

1.2 The Fixed Bed

Methods for estimating temperature profiles in fixed beds during regeneration of carbonised catalyst were proposed by van Deemter (1953,1954), Johnson, Froment and Watson (1962), Schulman (1963), Gonzalez and Spencer (1963), Olson, Luss and Amundson (1968) and Ozawa (1969). In all the models derived, axial diffusion of heat and mass were neglected. All the models derived assumed adiabatic beds except for Schulman's model which incorporated heat losses through the wall of the reactor. He assumed, however, that the only resistance to heat transfer in the bed was at the wall of the reactor. Together with the assumption of plug flow in the bed, these assumptions preclude the need for a two-dimensional bed model since radial gradients in both concentration and temperature will be zero in the bed.

The characteristics of the different models and other major assumptions made are tabulated in Table 1.1 and compared with those evenally used for the model derived in the present work.

In the present work the overall behaviour of the reactor was found to be very much temperature dependent. This immediately precluded the use of models proposed by van Deemter and Johnson, et. al. Schulman, Gonzalez and Spencer, and Ozawa included the effect of temperature by using an Arrhenius type expression to describe the reaction rate. Like van Deemter and Johnson, they assume a homogeneous reaction rate which does not take into account any diffusional resistances to the overall rate at a particulat point in the bed. It appeared that one of these models might be used to simulate the experimental data obtained in this work. When the model proposed by Gonzalez

TABLE 1.1 MODELS FOR SIMULATING REGENERATION OF CARBONISED FIXED BEDS

Variable or mechanism:	Van Deemter (1953,1954)	Johnson et.al. (1962)	Schulman (1963)	Gonzalez & Spencer (1963)	Olson et.al. (1968)	Ozawa (1969)	Present work
Interphase: mass transfer:	∞	∞	∞	∞	finite	∞	finite
heat transfer:	∞	∞	∞	finite	finite	∞	finite
Adiabatic bed:	yes	yes	no	yes	yes	yes	no
Homogeneous reaction:	yes	yes	yes	yes	no	yes	no
Rate expression:*	constant	$Py_g \frac{\bar{C}}{\bar{C}_o} \exp(k_o)$	$Py_g \bar{C} \exp(k_o - \frac{E}{R'T})$	$PY \frac{\bar{C}}{\bar{C}_o} \exp(k_o - \frac{E}{R'T})$	Diffusion control	$Py_g \frac{\bar{C}}{\bar{C}_o} \exp(k_o - \frac{E}{R'T})$	$\frac{Py_g C}{R'T\bar{C}_o} \exp(k_o - \frac{E}{R'T})$
CO_2/CO produced:	constant	constant	constant	constant	constant	constant	temp. dependent
Diffusivity in pellet:					$De(T)^{\frac{1}{2}}$		$De(T)^{\frac{1}{2}}$
G	constant	constant	constant	constant	constant	constant	constant
M_g	"	"	"	"	"	"	"
c_g	"	"	"	"	temp. dependent	"	temp. dependent
c_s	"	"	"	"	temp. dependent	"	temp. dependent
P	"	"	"	"	constant	"	constant
ρ_b	"	"	"	"	"	"	"
ρ_g	"	"	"	"	temp. dependent	"	temp. dependent
$-\Delta H$	"	"	"	"	weak temp. dep.	"	strong temp. dep.
Method of solution:	Analytical: method of characteristics; construction.	Analytical: assuming no transient period.	Numerical: "partial integration".	Numerical: predictor-corrector.	Numerical: Runge-Kutta-Gill.	Numerical: method of characteristics.	Numerical: predictor-corrector.

* $\bar{C}$ denotes average carbon concentration in the pellet.

and Spencer was used, taking into account heat losses from the reactor through the wall, better fits were obtained than with Johnson's model; however, the shape of the curves were still quite dissimilar.

From visual observations then made on pellets regenerated at different temperatues, it was clear that conditions did arise in the reactor where considerable carbon was still present at the center of the pellet when the carbon close to the surface had been completely removed. Diffusional resistances to the transfer of oxygen to the reaction sites were obvious and the assumption of a completely homogeneous bed was clearly not applicable.

Based on this type of consideration, Olson, Luss and Amundson (1968) proposed a model for the regeneration of carbonised catalyst beds, which assumed that the intrinsic reaction rate was so fast that diffusional resistances were completely controlling. In such a case oxygen in a pellet cannot diffuse past any carbon and there exists a sharp interface between the carbonised and completely regenerated catalyst material. Then the overall reaction rate which is the rate at which oxygen diffuses towards the interface, can be directly used in the material balance to compute the rate at which this interface moves towards the center of the pellet.

When diffusion controls, the temperature dependence of the diffusion coefficient becomes important and since at elevated temperatures for most porous catalysts, diffusion is of the Knudson type, a half-order dependence on temperature may be expected. Because of the relative insensitivity of the diffusion process to temperature as compared to that of the intrinsic reaction rate process, for Olson's model it then becomes important to include the comparable temperature dependence

of specific heats, gas density and heat of reaction.

From the visual observations made on pellets regenerated in different temperature regions, reality for the present work presented itself as one wherein both reaction rate and diffusion rate controlled. The relative importance of the two mechanisms varied depending on the temperature prevailing at a particular time and position in the bed. It was therefore important to consider what happened inside a pellet more closely.

1.3 The Pellet

In a great majority of instances, the analysis of solid-gas reactors has been based on the unreacted shrinking core model as shown by Yagi and Kunii (1953). This was the approach used by Olson, Luss and Amundson (1968). Ausman and Watson (1962) derived a homogeneous model using a pseudo steady state approximation for the gas distribution in a spherical catalyst pellet and assuming a first order reaction with respect to oxygen for isothermal combustion of carbon. They differentiated between a "constant rate" period, when the homogeneous reaction takes place throughout the pellet, and a "falling rate" period when all the carbon has been removed from the external surface of the pellet and when the reaction takes place in the receding carbonised central core of the catalyst pellet. The constant rate was possible owing to the assumption of zero order reaction rate with respect to carbon. The effective diffusivity of oxygen in the pellet was assumed constant and independent of the carbon concentration.

Ishida and Wen (1968) elaborated on this and considered different diffusivities in the regenerated and unregenerated parts of the catalyst pellet. They showed that the model converts to the unreacted core shrinking model, for Thiele's modulus greater than 100 when the reaction rate is high, and for oxygen diffusivities much greater in the regenerated or "ash" layer than in the carbonised core. They derived an effectiveness factor which is constant during the "constant rate" period but changes with degree of regeneration during the "falling rate" period.

A weakness of the homogeneous model as proposed by either Ausman and Watson or Ishida and Wen as far as the regeneration of carbonised catalyst is concerned, is that it is zero order with respect to carbon. Most experimental evidence indicates a first order dependence (section A 1.4.3). Another serious shortcoming, especially when mainly the reaction rate is controlling, is that their models only deal with the isothermal case.

Shettigar and Hughes (1972), based on work by Bowen and Cheng (1969), derived a model to describe the regeneration of carbonised catalyst in which the reaction rate depends on both oxygen and carbon concentration and on temperature. However, the combustion is assumed to take place in a narrow zone which is small compared to the radius of the unreacted core. The model, therefore, more accurately describes a process which, although not quite that of a shrinking core, has diffusion very much in control of the overall rate of combustion.

For the present work, over the temperature range of interest, the control changes from the rate of reaction at low temperatures to the rate of diffusion at high temperatures. Shettigar's model does

not therefore apply, nor does the pure unreacted core shrinking model. For the present work the basic differential expressions used by Ausman and Watson and Ishida and Wen have been retained, but a more general reaction rate expression to incorporate dependence on both oxygen and carbon as well as temperature, is used. This precludes the use of an analytical solution and a numerical approach has been adopted. The numerical solution makes the retention of temperature dependence for all important parameters in the model quite feasible. This is of importance when the rate of diffusion in the pellet becomes controlling and temperature dependence of specific heats, gas concentration and especially the relative rate at which carbon dioxide and carbon monoxide are formed and the associated heat of reaction, become comparable to that of the diffusivity of oxygen in the pellet.

The model adopted for the pellet is incorporated with a model for the bed similar to that proposed by Gonzalez and Spencer (1963), to predict temperature profiles which are compared with experimentally obtained results.

1.4 Flow Reversal

Early on in the investigation it was noticed from observations made that provided enough reaction time was allowed for the burning zone to move through the entire bed, the extent of regeneration would be smallest at the entrance of the bed notwithstanding the higher oxygen concentrations near the inlet. Since the entrance of the bed is always the coolest part of the bed, this indicated strong temperature dependence for the rate of carbon removal. In accordance with

this view, raising the temperature at the entrance of the bed would increase the rate of carbon removal in this part of the bed. This could be achieved by reversing the flowrate to the bed at some stage. Gas heated in the hot sections of the bed would then heat up what would have been the relatively cool entrance. A secondary object of this investigation then became to show that reversal of flowrate could decrease the time required for overall regeneration and that there was an optimum time at which flow reversal should be implicated.

CHAPTER 2

EXPERIMENTAL PROCEDURE

2.1 Introduction

Considerable experimentation was done on the design of a suitable reactor system to investigate the regeneration of carbonised catalyst pellets. Initially a system was designed with a view to investigating the dynamic control of the regeneration reactor. The reactor system incorporated internal heat exchange to use the heat produced by the reaction to preheat the feed flowing on the outside of the reactor. The reactor consisted of a 0,914 m long stainless steel tube 0,051 m in diameter. Interesting results were obtained in that the feedback of heat from a primary moving burning zone and temperature wave, through the heated feed gas, produced a second burning zone and heat wave. This occurred at the entrance of the bed owing to a combination of higher temperatures and high inlet oxygen concentrations with the still considerable amounts of carbon left at the entrance, when initially the reaction temperatures were relatively low. Typical temperature profiles obtained are shown in figure 2.1.

The system although giving interesting results, was too complex to be dealt with from a modelling point of view with the limited data available at that stage of the investigation and with the then current expertise in the field. A simpler and more direct approach was adopted and a reactor was designed in which the inlet conditions could be kept constant and in which the interchange of heat between the reactor and its

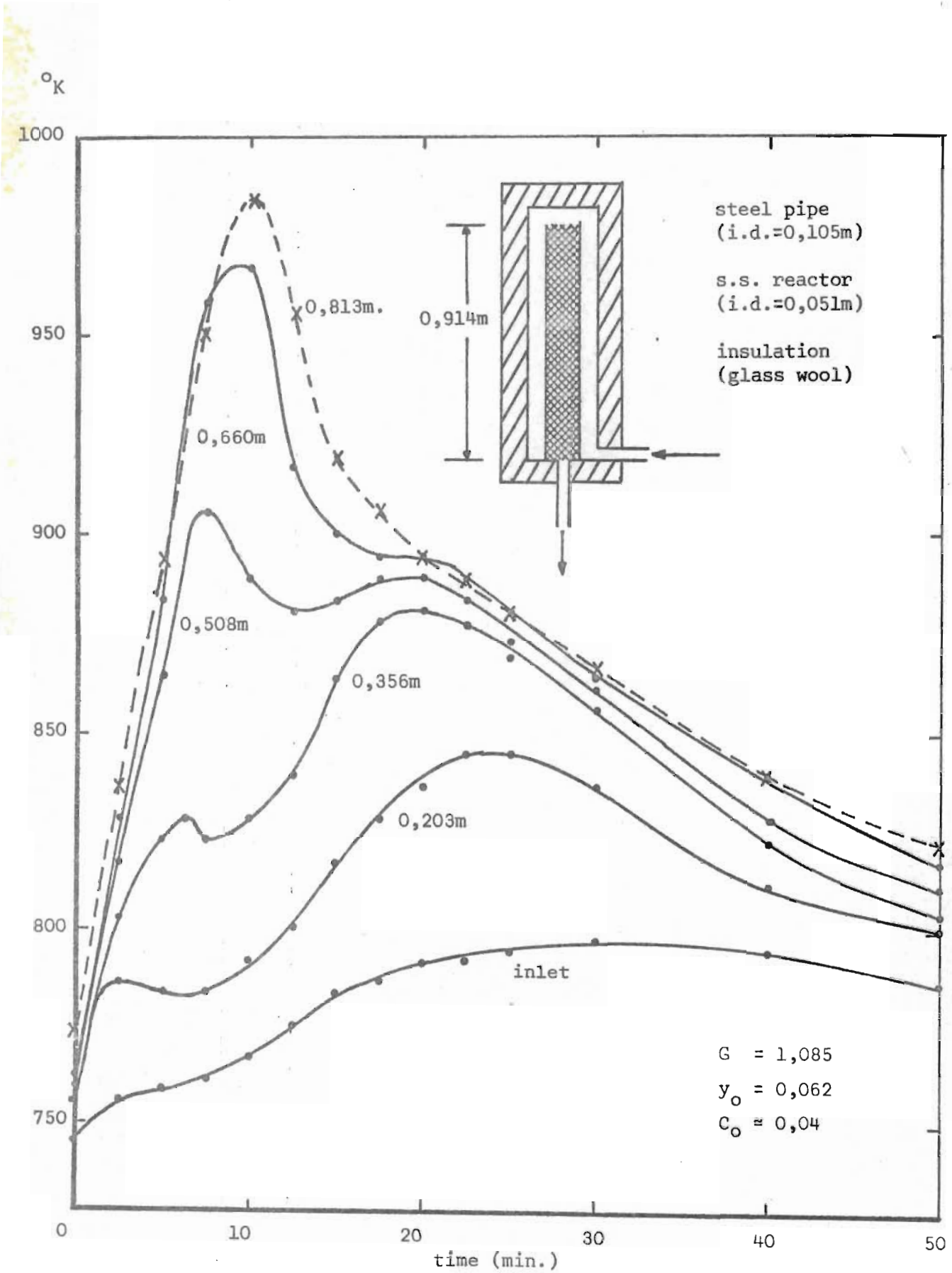

FIGURE 2.1 TEMPERATURE PROFILES FROM INITIAL REACTOR DESIGN.

surroundings, as well as between different parts of the reactor were reduced to a minimum. The design of this system is described in later sections.

Thermo-couples were used throughout to measure temperatures. Initially millivolt readings of all the thermo-couples were recorded manually through a combination of a rotary switch and a single millivoltmeter. This unsatisfactory system was soon replaced by a semi-automatic system for which a complex electronic timing and gating device was built. This sampled all the thermo-couples in rotation and produced a single voltage signal containing successive bits produced by the different thermo-couples. The signal was frequency modulated and together with a timing signal to define the signal bit lengths, stored on double track magnetic tape. From the tape the frequency modulated signal and timing signal were played back to counting equipment, which, controlled by the timing signal, counted the impulses in every single bit. The counts were recorded in print and punched on cards. The cards were then read into a computer, decoded and the temperatures printed. Although a vast improvement, this system was still unsatisfactory in many ways. It was temperamental and noise in the timing signal would necessitate editing of the decoded results. Because of this and the slowness of counting, temperature profiles would normally not be available till three days after the experiment was performed.

When a logging computer became available, however, all these problems disappeared. Recording became reliable and results were produced in real time with a resolution at least twice that obtained with magnetic

tape recording. For all but the preliminary runs, the temperature profiles reported were obtained using this system. It is further described in later sections.

2.2 Reactor

The reactor shown in figure 2.2, consisted of a vertical mullite tube, 0,914 m long with an internal diameter of 0,050 m and an external diameter of 0,059 m. It was held inside a 0,10 m steel pipe by means of asbestos flanges 0,0127 m thick, two at the top and one at the bottom. In order to prevent gas from flowing between the outside of the reactor tube and the inside of the pipe, the space between the two top flanges was filled with alumina wool which was highly compressed by forcing the very top flange down hard. All three flanges were held in place by steel sleeves which were held inside the pipe by means of grub screws. The flanges and sleeves were furthermore sealed by a mixture of an alumina cement and waterglass. In an attempt to approach the adiabatic conditions of industrial practice, the annular space between the tube and pipe was filled with alumina wool. Asbestos cloth was wrapped around the pipe, around which resistance wire was wound. This was again covered with asbestos cloth and the whole lagged with glass wool. Removeable steel blank flanges were bolted to the top and bottom of the pipe to facilitate charging and discharging of the reactor. The bed was held in place by removable perforated plates in the top and bottom of the mullite tube. Gas inlet and outlet sockets were welded into the side of the pipe at the top and bottom between the asbestos and blank flanges. The top and bottom flanges were lagged with removable alumina wool.

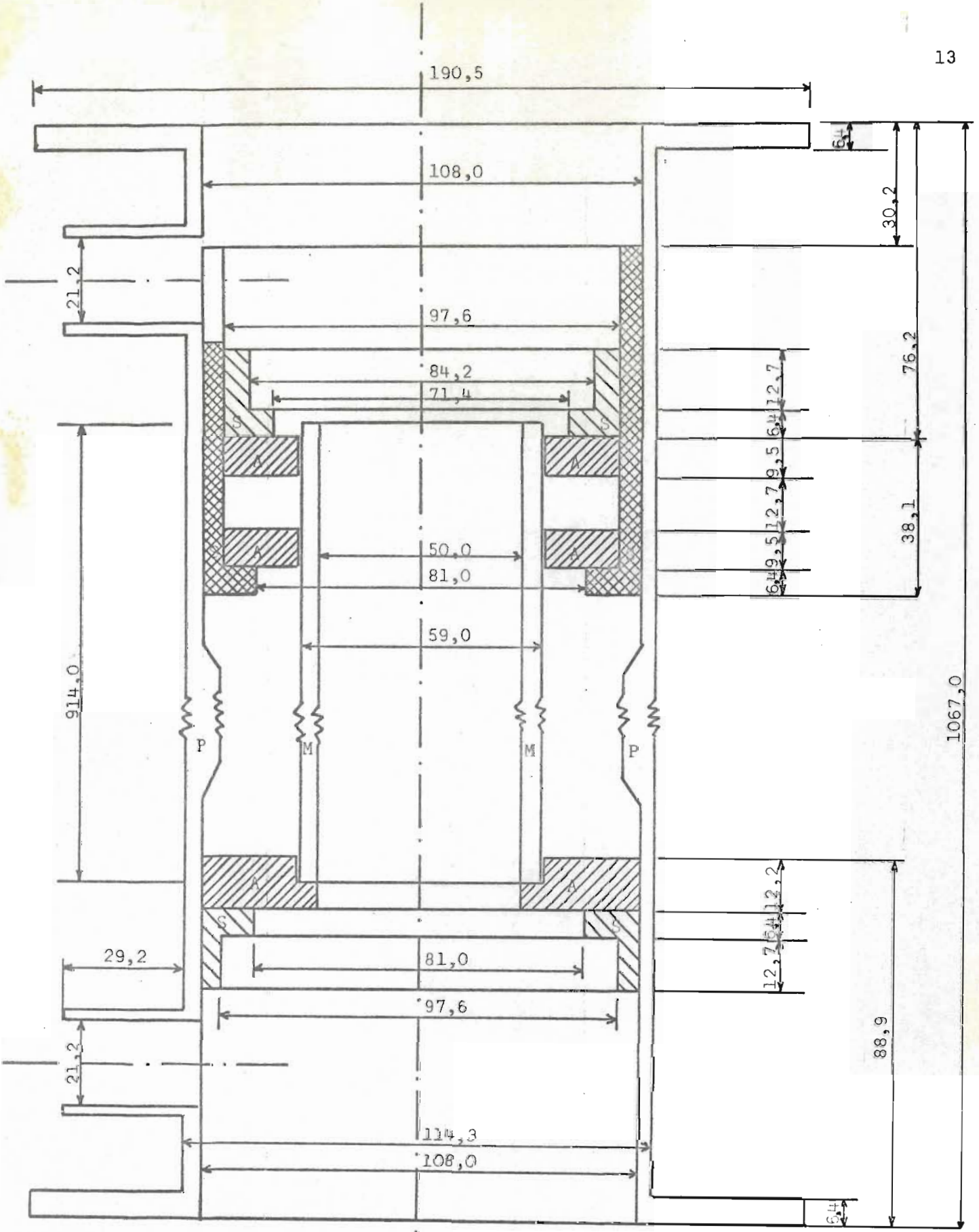

A - Asbestos Flanges
S - Steel Sleeves
M - Mullite Reactor Tube
P - Pipe Wall

Scale 1 cm = 25,4 mm
(measurements in mm.)

FIGURE 2.2 REACTOR WITHOUT FLANGES

Just below the top blank flange there was a spacer ring with small holes and asbestos fibre packed stuffing boxes, through which passed 6 inconel clad, alumina packed, chromel-alumel thermo-couples which had an outside diameter of 2 mm. These thermo-couples were distributed along the circumference of the reactor tube to pass from the top of the reactor along the inside of the tube wall to where they were bent towards the centre of the tube to measure temperatures at the centre line of the reactor. This is pictured in figure 2.3. Inlet and outlet temperatures were measured by means of thermo-couples above and below the bed.

The thermo-couple below the bed passed through a stuffing box in the removable bottom flange and had its hot junction about 5 cm below the bottom perforated plate support at about 2 cm from the centre line. It was placed in this position to prevent the hot junction from coming into contact with a bracket, attached to the support plate, which was needed for its removal when discharging the reactor. The thermo-couple above the bed passed through the top flange but had its hot junction about 8 cm from the top of the bed in order to prevent contact with the thermo-couples passing through the ring between the top flange and reactor jacket. All the thermo-couples had their hot junctions exposed and unprotected to give as quick a response as possible. Their positions in the reactor bed are shown in figure 2.4.

The heat losses towards the ends of the reactor were greater than those at the centre owing to the flanges not being heated. To compensate for this, the resistance wire was wound around the pipe in three sections, and the voltage to the middle and bottom sections could be individually

FIGURE 2.3 THERMO-COUPLE ASSEMBLY IN THE REACTOR SEEN FROM THE TOP

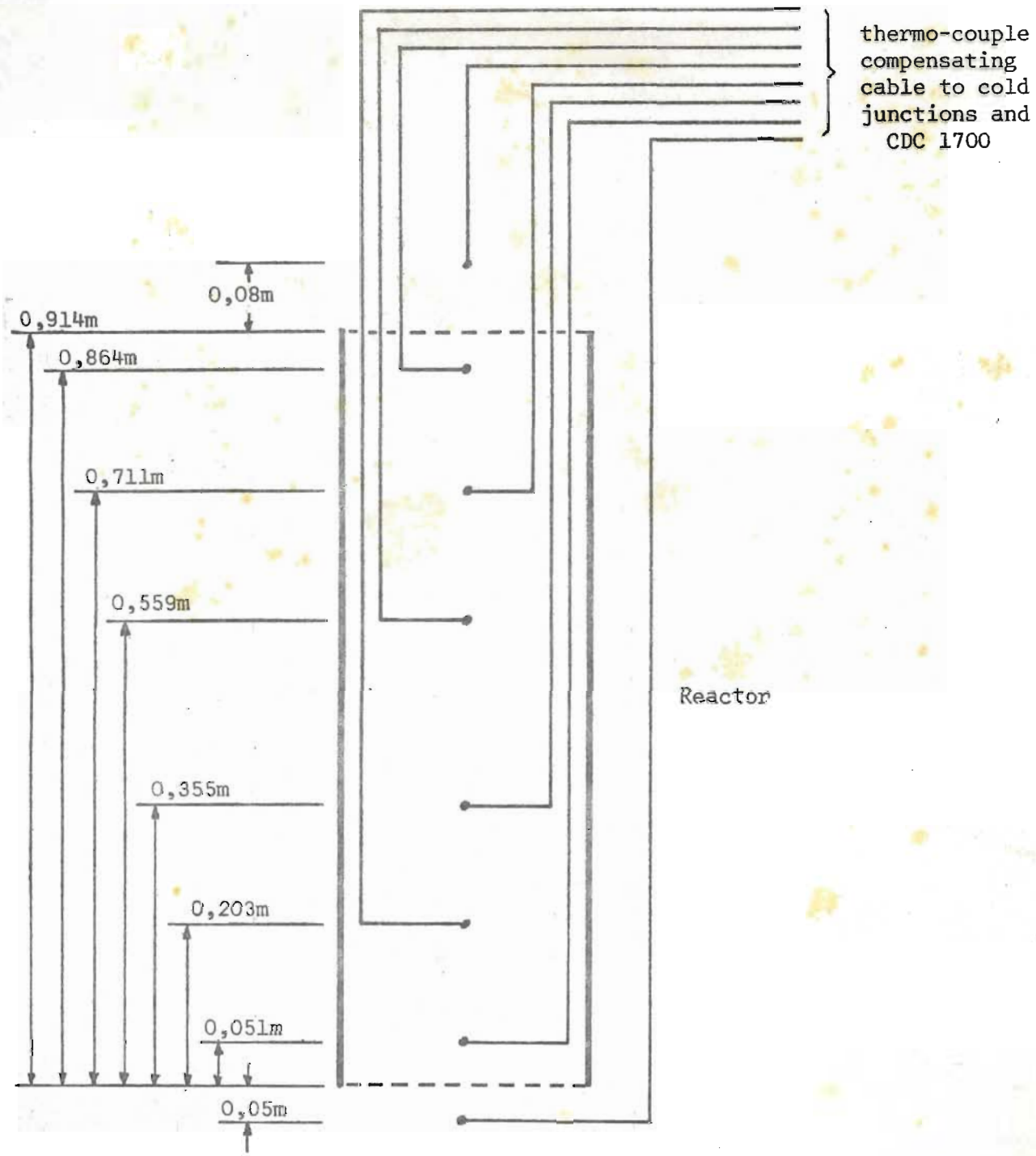

FIGURE 2.4 POSITION OF THERMO-COUPLES IN BED

adjusted by 1 KVA auto transformers. The two adjustable transformers and topsection were supplied from a third adjustable 2 KVA auto transformer. Within limits, with this arrangement, it was possible to adjust the relative heat inputs for the different sections in such a way that once the transformers were properly adjusted, only adjustment of the common transformer would be needed to give the same required temperature for all three sections. The actual settings required for a particular temperature were found by trial and error under no flow conditions.

2.3 Plant Lay-out

The plant lay-out was as shown in figure 2.5.

The oxygen supply was from a single gas bottle and nitrogen was supplied from two gas bottles which could be individually isolated from a common manifold, so that empty bottles could be replaced during a run. From the manifold the nitrogen passed through an electrically heated tube with an adjustable voltage supply to compensate for the temperature drops due to the Joule Thomson effect at the pressure reducing valve. The oxygen was used at smaller flowrates and was delivered at room temperature.

Gas flowrates were measured by means of rotameters supplied by the Rotameter Manufacturing Co. For oxygen a 7X rotameter and for nitrogen a 24X rotameter was used, both with Duralamin type A floats. Flowrates were regulated by needle valves down stream of the rotameters in such a way as to keep the pressure at the rotameters constant at $6{,}98 \times 10^4$ N/m^2. The pressure was read from a Bourdon gauge to within $0{,}15 \times 10^4$ N/m^2 and

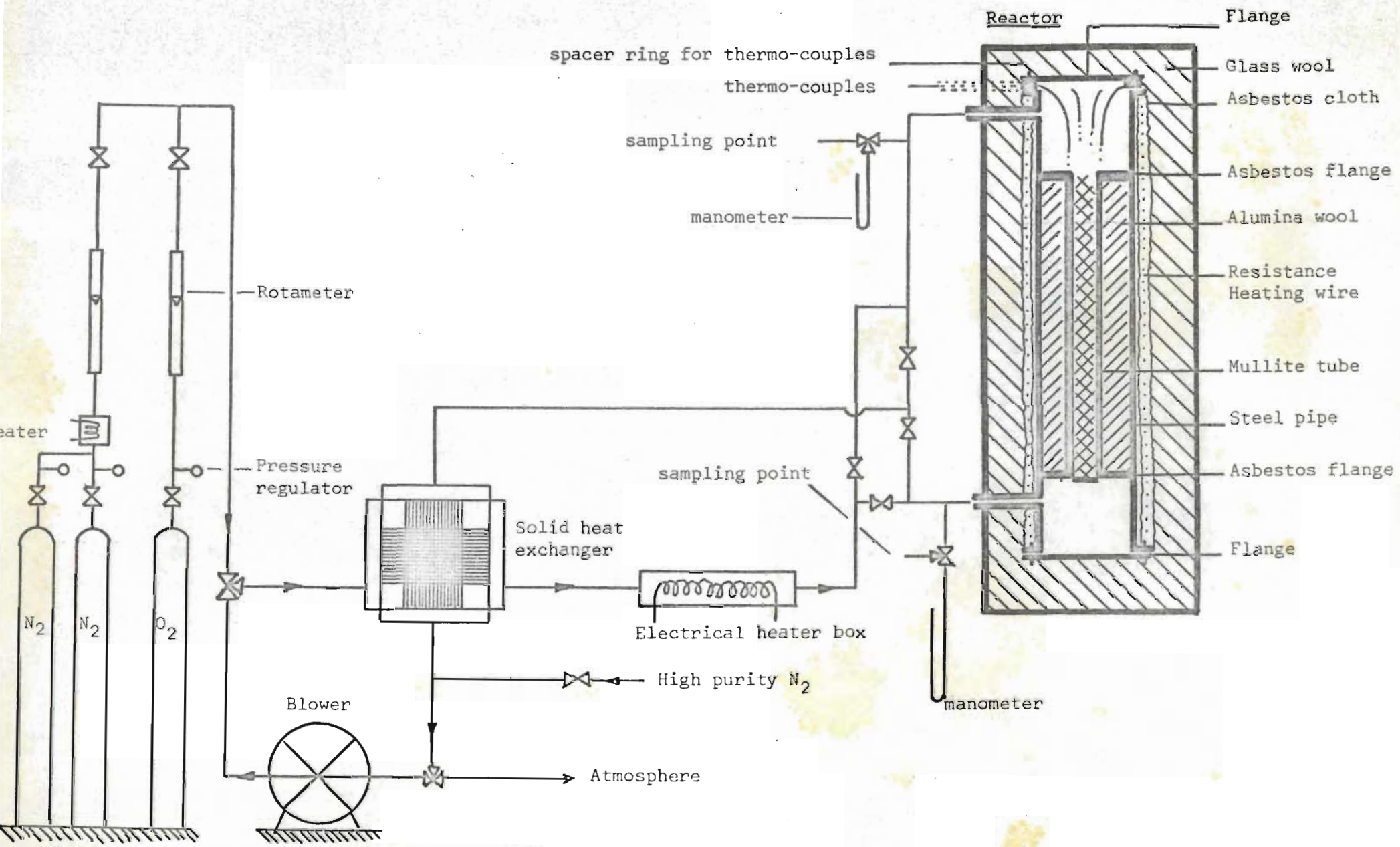

FIGURE 2.5 EXPERIMENTAL LAY-OUT

the temperature at the rotameters to within $0,5^{o}K$ by means of a mercury thermometer. Both gauge and thermometer were situated at the entrance to the rotameter. Flowrates were obtained for the conditions at the rotameter from calibration charts supplied by the manufacturer. At $6,98x10^{4}$ N/m^{2} they could range from $1,96x10^{-4}$ m^{3}/s to $1,96x10^{-3}$ m^{3}/s for nitrogen and from $0,84x10^{-5}$ m^{3}/s to $8,4x10^{-4}$ m^{3}/s for oxygen.

The feed gas was preheated by passing it first through a solid aluminium heat exchanger, the heat being obtained from the reactor outlet gas. It was then further heated in a gas heater box which was thermally insulated with fire brick covered with glass wool, and which contained 4 bar heaters 1,5 kW each. From the heater the gas passed through a system of valves into the reactor. The valves, as shown in figures 2.6 and 2.7, interconnected the gas lines to the top and bottom of the reactor in such a way that either could be used as an inlet or outlet and reversal of the direction of flow during a run was possible. From the reactor the outlet gas passed through the solid aluminium exchanger preheating the feed gas and then it was either exhausted to the atmosphere during regeneration or it was recycled by means of the blower during the heat up period. During regeneration the blower was isolated by means of two three way valves as shown.

The blower was a RN type oil-free rotary compressor manufactured by Reavel and Co., which delivered $3,58x10^{-3}$ m^{3}/s of free air at $3,5x10^{4}$ N/m^{2}. In order to protect it against excessive temperatures the gas fed to the blower was passed through a small water cooled tube and shell heat exchanger which kept the inlet temperature well within the safe working temperature range. This arrangement is shown in figure 2.7.

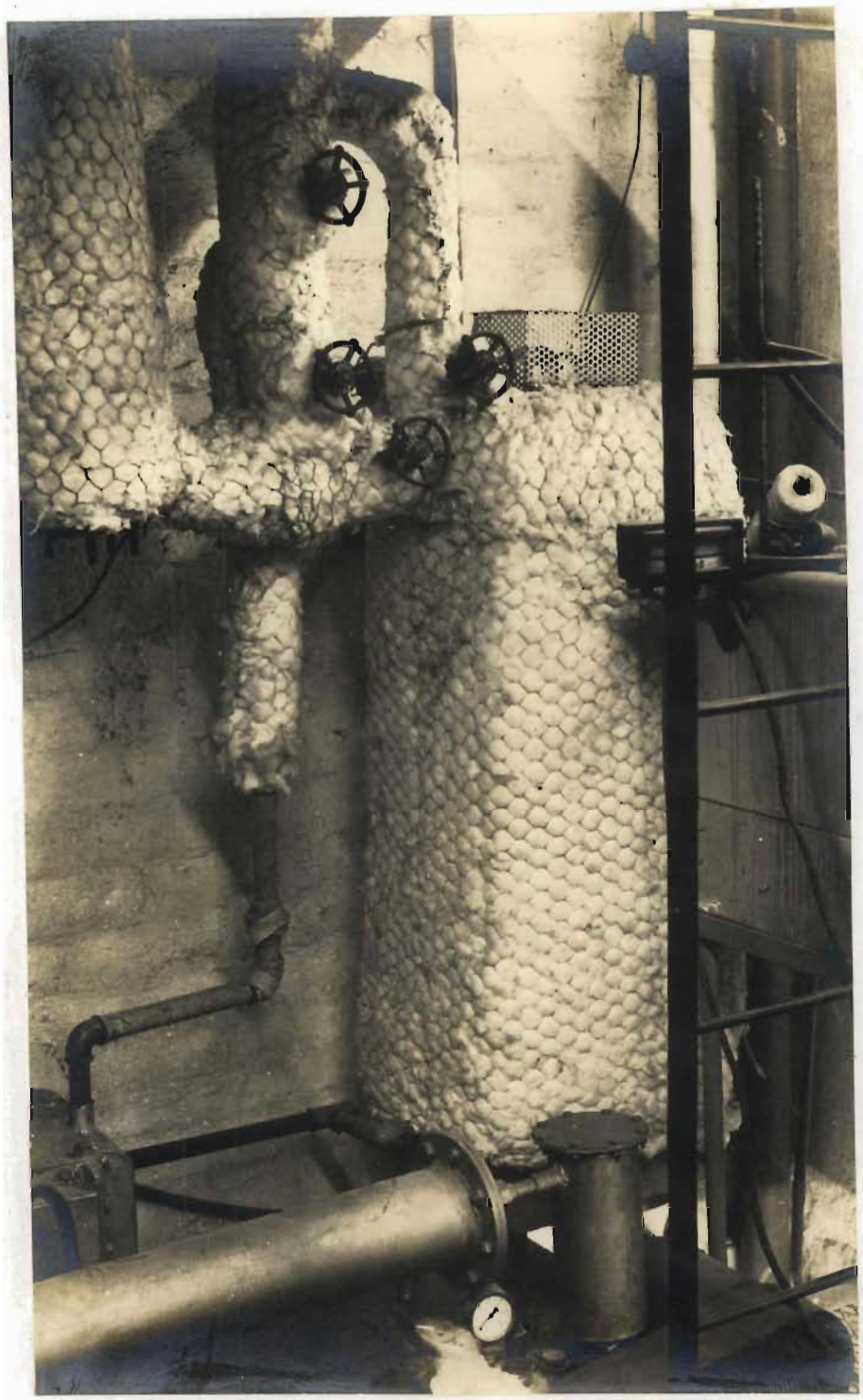

FIGURE 2.6 GAS HEATER AND INLET AND OUTLET VALVE ARRANGEMENT

(The bottom flange has been removed from the reactor.)

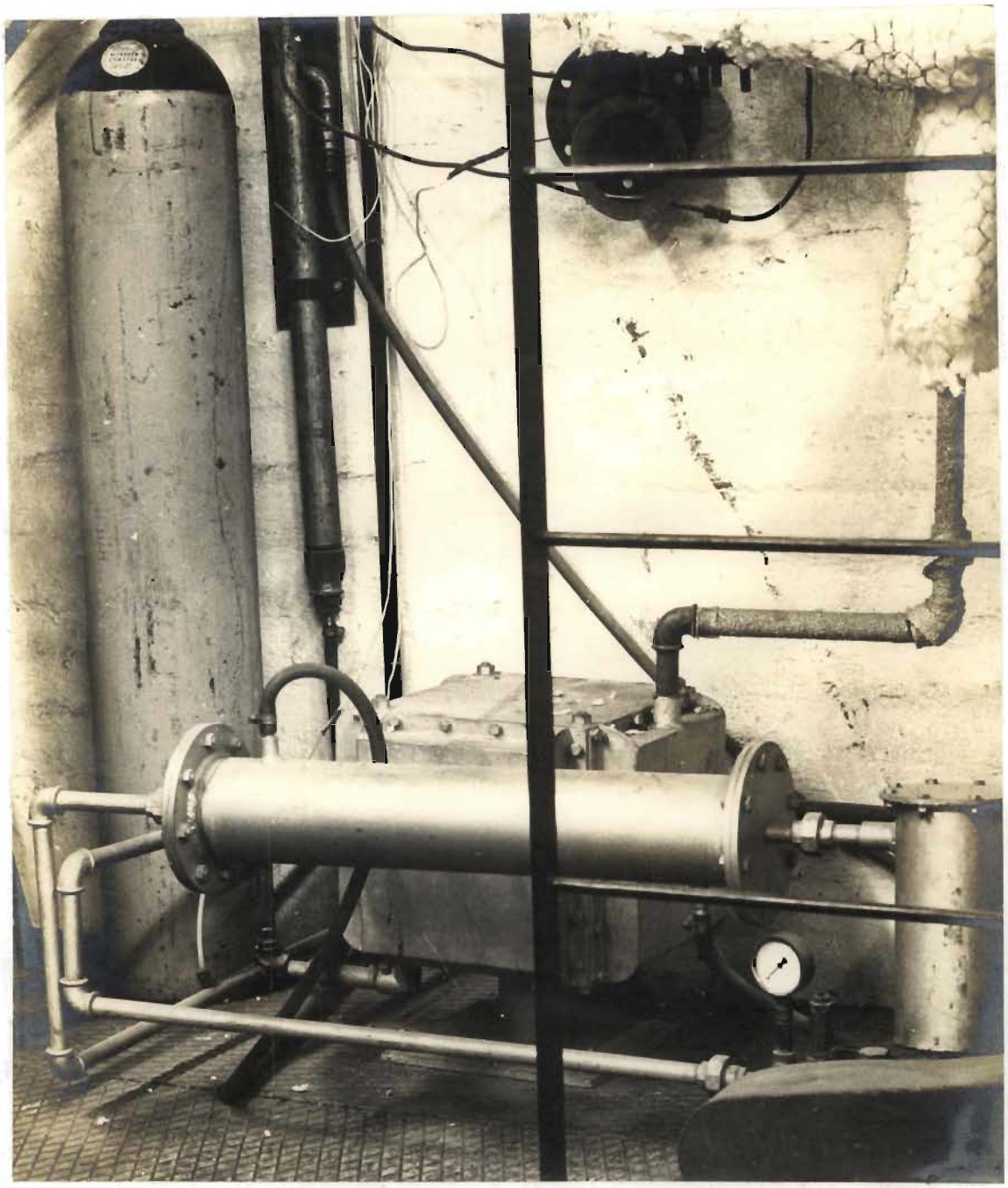

FIGURE 2.7 ALUMINIUM HEAT EXCHANGER AND BLOWER WITH TUBE AND SHELL HEAT EXCHANGER

All the gas lines between the gas heater and the reactor and the reactor and the solid heat exchanger were lagged, first with asbestos tape, and finally with glass wool. The asbestos tape served to protect the glass wool from too high temperatures. The gas line carrying the feed gas from the gas heater to the top of the reactor during reverse flow was resistance wire wound with asbestos cloth separating the wire from the pipe. The pipe would be electrically heated through an adjustable 1 KVA autotransformer during normal flow when it would be non-operational, to prevent cooling of the feed gas just after flow reversal. The gas lines on the cold side of the solid heat exchanger were not lagged.

Copper tubing, 6 mm in diameter was used to connect the in and outlet lines of the reactor to three-way valves, which could direct gas to gas sampling lines, or to manometers for pressure measurements. These tubes were partly jacketed for water cooling.

2.4 Temperature measurement and Recording.

Thermo-couples as described in section 2.2 were used to measure temperatures at the centre line of the reactor and at the inlet and outlet. The tolerance limits of accuracy reported for these thermo-couples were ±3 C^{o}below 400^{o}C and ±0,75% above 400 C. The temperatures were recorded on a CDC 1700 computer which was able to read and record with a resolution of about 0,5^{o}K, which was well within the possible error of the thermo-couples. All eight thermo-couples were sampled and their readings converted to temperatures every 15 seconds, within milliseconds of each other.

For monitoring purposes during the run, parallel leads were taken from the thermo-couples to a rotary switch by means of which one thermo-couple at a time could be continuously monitored on a Philips GM 6020 electronic millivoltmeter. The thermo-couple circuits were of very low impedance compared to those of the millivoltmeter and the CDC 1700. There was therefore no interference between the voltmeter and the computer.

Initially, for experiments IL1 and LI1 (for designation of runs and figure number see table 6.1), all the hot junctions of thermo-couples were connected by means of compensating cable to one common cold junction and they had one common lead to the analogue terminals of the CDC 1700. During experiment LI1 electrical equipment in the laboratory not associated with this experiment, was switched on and induced low frequency noise into the readings in the 32nd to 38th minute after the start of the regeneration period. The fluctuations were not excessive and hardly show up in the experimental temperature profile where only every eighth reading is plotted. After run LI1, the same problem occurred again in a much more severe form. It was put down to improper connections with the computer. The recording system was then changed to provide every hot junction with its own cold junction and individual screening from the thermo-couple to the analogue terminals of the CDC 1700. This completely solved the problem and all the other runs were all done with this improvement incorporated. The arrangement is shown in figure 2.8.

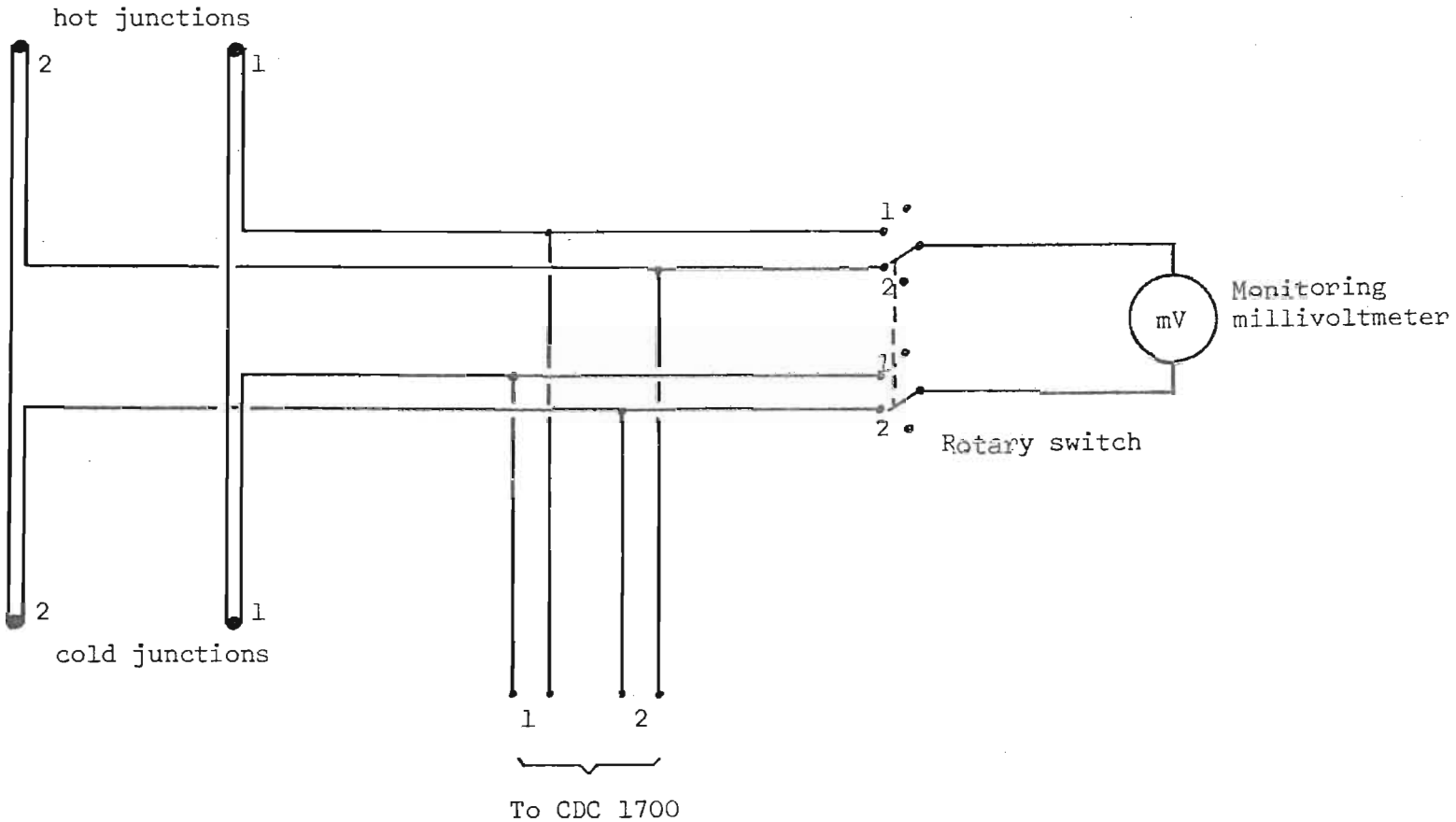

FIGURE 2.8 SCHEMATIC ARRANGEMENT OF THERMO-COUPLES

(only two shown)

2.5 Gas Analysis

The gas analysis was done using a gas chromatograph designed by Mr. Frank Fisher of African Explosives and Chemical Industries Research Department, Johannesburg.

The chromatograph was simple but functioned reasonably well. It contained two 6 mm copper tube columns, one, 25 cm long, packed with Poropak Q for the separation of CO_2 and one, 150 cm long, packed with Molecular Sieve 13X for the separation of O_2 and CO. No oven was required for these (permanent) gases and the whole assembly was housed in a wooden box.

The detector was a katharometer block using matched rhenium-tungsten resistance wire (type WX mount 9225 GOW-MAC) which were operated at 200 m.a. They were relatively insensitive to ambient temperature fluctuations although packing the box with alumina wool seemed to give a better base line. The output signal from the katharometer was generated from a Wheatstone bridge in which the resistance of the wires cooled by the gas stream leaving the one column was balanced against the resistance of the wire cooled by the stream leaving the other column. By proper timing of the injection of samples, which was done using a Hamilton gas syringe, it could be arranged that when sample gas flowed past one detector, carrier gas (helium) would flow past the other. With this arrangement CO_2 would be deflected in the opposite direction to that of CO and O_2. A diagrammatic sketch of the chromatograph and Wheatstone bridge is shown in figure 2.9.

When the gas chromatograph was checked for linearity of peak height response, a gas mixture with known concentrations of O_2, CO_2 and CO in

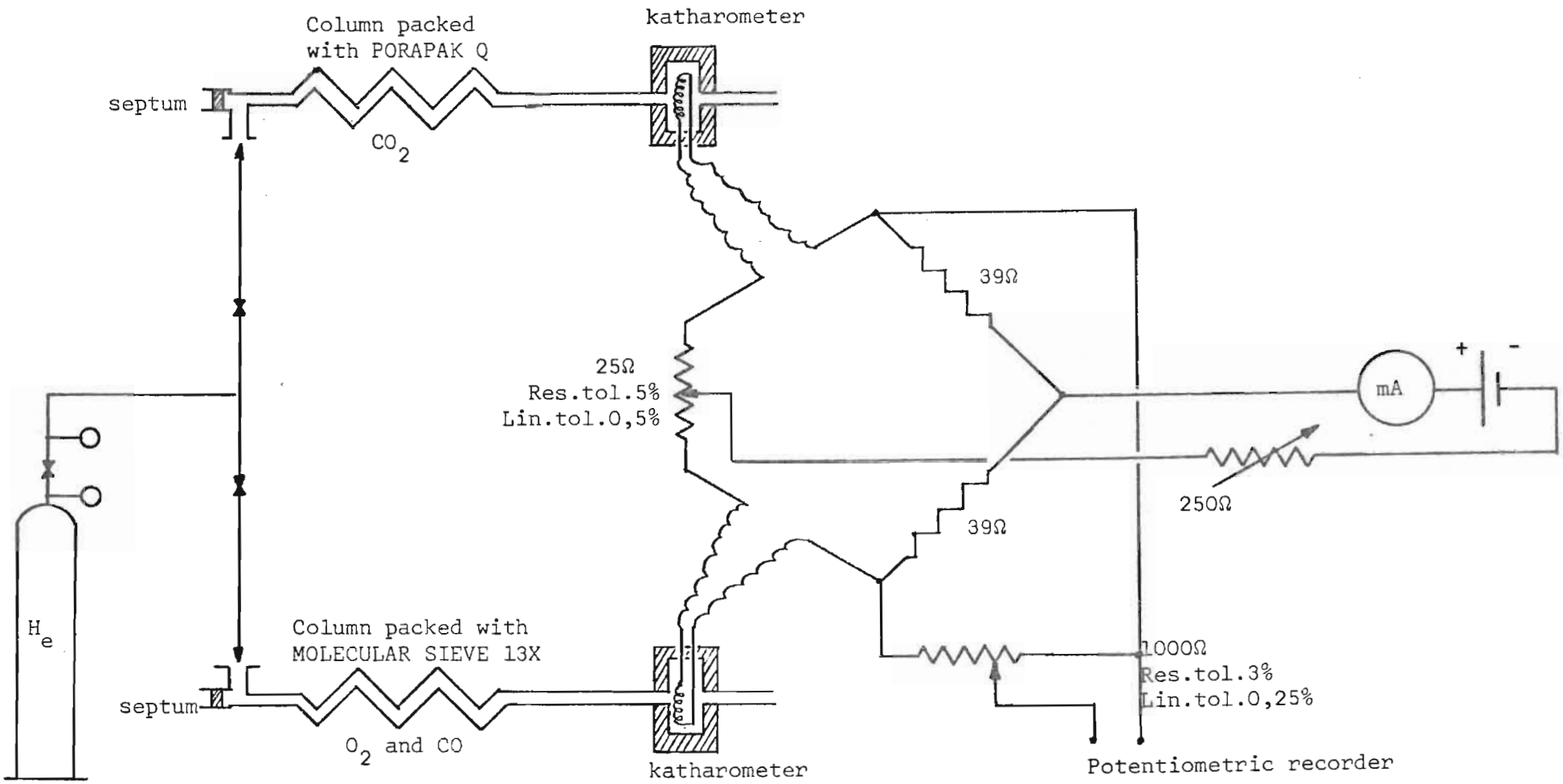

FIGURE 2.9 GAS CHROMATOGRAPH ARRANGEMENT

the concentration range of interest, was made up with high purity N_2, to calibrate the instrument. A known volume of the mixture was taken through a septum into a gas syringe with a Chaney adaptor, and diluted by drawing further high purity N_2 from a fast flowing stream out of a small tube. A specified total volume could thus be obtained of varying but known amounts of O_2, CO_2 and CO. Injecting this into the two columns of the gas chromatograph, the responses shown in figure 2.10 were obtained.

For oxygen the response was linear and a straight line could be drawn through the points to give a good fit. For CO and more specifically for CO_2, the points seemed to lie on slightly sigmoidal curves. However, straight lines drawn through the points gave fairly good fits except at low concentrations when the point values were about 20 - 25% below those of the line. During experimental runs low values of CO and CO_2 were obtained at the beginning and end of the regeneration period. The ratio CO/CO_2 would then on the average be about 1,0 to 1,4, for which ratio (in the low concentration range) the percentage errors in CO and CO_2 are similar. Whereas for O_2 absolute concentration values were required, only relative amounts of CO and CO_2 are needed. On dividing the concentration of CO by that of CO_2, because the percentage error is similar, the error in the ratio will be much smaller than that for the individual CO and CO_2 concentrations.

When calibrating the gas chromatograph, considerable savings in time and effort were achieved by making use of the virtual linear behaviour of both the O_2 concentration and the CO/CO_2 ratio, with respect to peak heights. Assuming linear response for all three gases a response factor

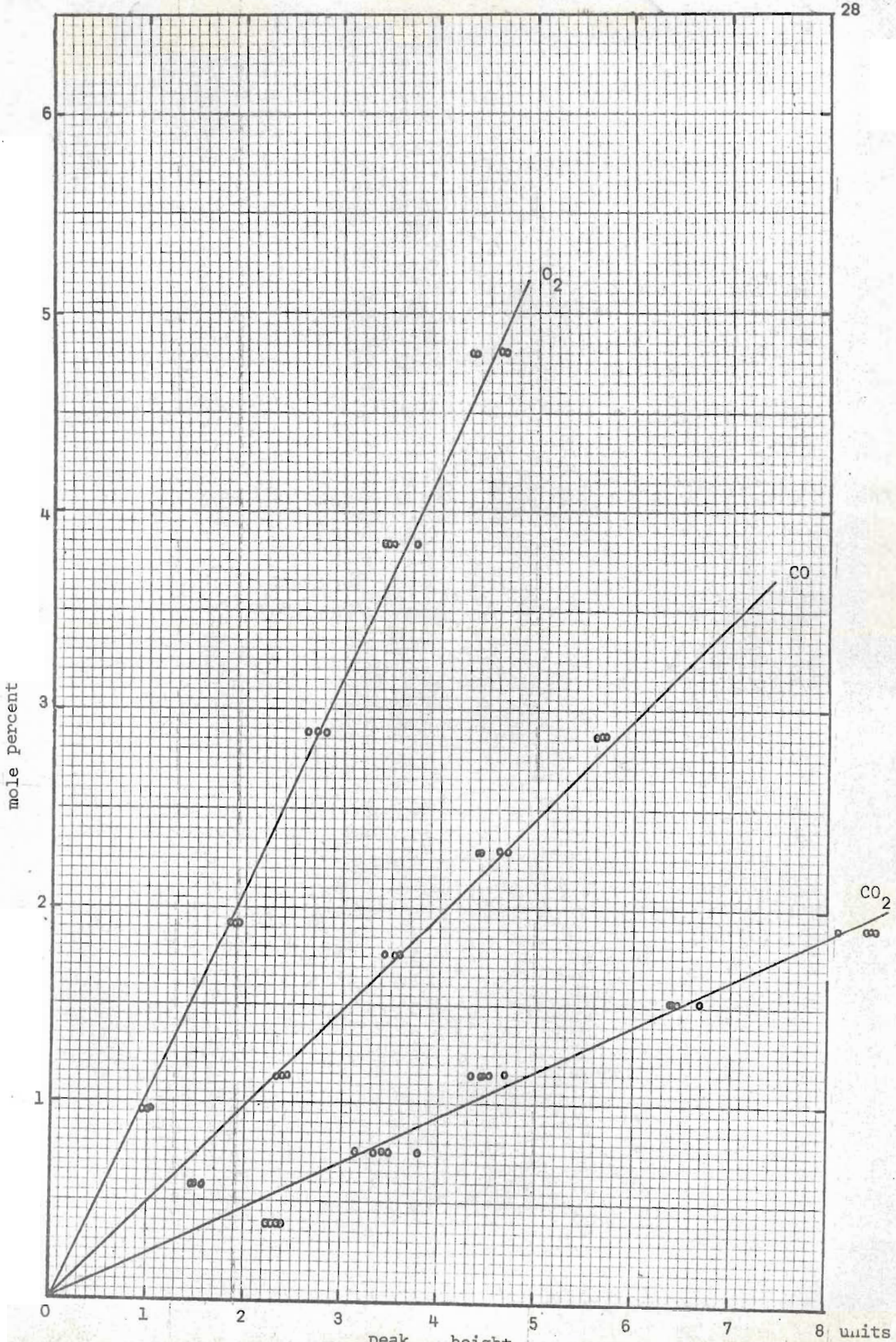
O_2
CO
CO_2
mole percent
peak height
units
0
1
2
3
4
5
6
7
8

could be obtained from single concentration values using a specially made up and bottled gas mixture containing 2,87 ± 0,04% O_2 and 1,15 ± 0,03% CO_2 and 0,98 ± 0,03% CO. The mean response of 5 to 8 samples of this standard gas would be used to convert peak heights to concentrations. Part of the chromatogram obtained for run LL, which was typical, is shown in figure 2.11.

2.6 Preparation and Analysis of Carbonised Catalyst

2.6.1 Preparation of catalyst.

Carbonised pellets were obtained by soaking the catalyst in an aqueous sucrose solution and thermally cracking the sugar to a coke which Dart and Öblad (1949) and Johnson (1956) report to have the approximate composition of $CH_{0,5}$. The pellets were prepared as follows.

Approximately 4 kg of 6,4 mm x 6,4 mm cylindrical Aerocat AAA, high alumina catalyst was evacuated in a 20 l suction flask for about 20 minutes. The sucrose was then slowly added through a separating funnel, without releasing the vacuum. The vacuum was maintained for another 10 minutes while the flask was rocked to dislodge any bubbles adhering to the pellets. In order to force the solution into the pellets,the vacuum was released and reapplied till the solution boiled gently. Rocking the flask occasionally, the vacuum was then maintained for another 5 to 10 minutes. This process was repeated three times. The catalyst absorbs just less than half its weight in water and when cracking sugar, only about half the carbon remains in the coke. From this the approximate sucrose concentration needed for a particular final carbon concentration could be estimated.

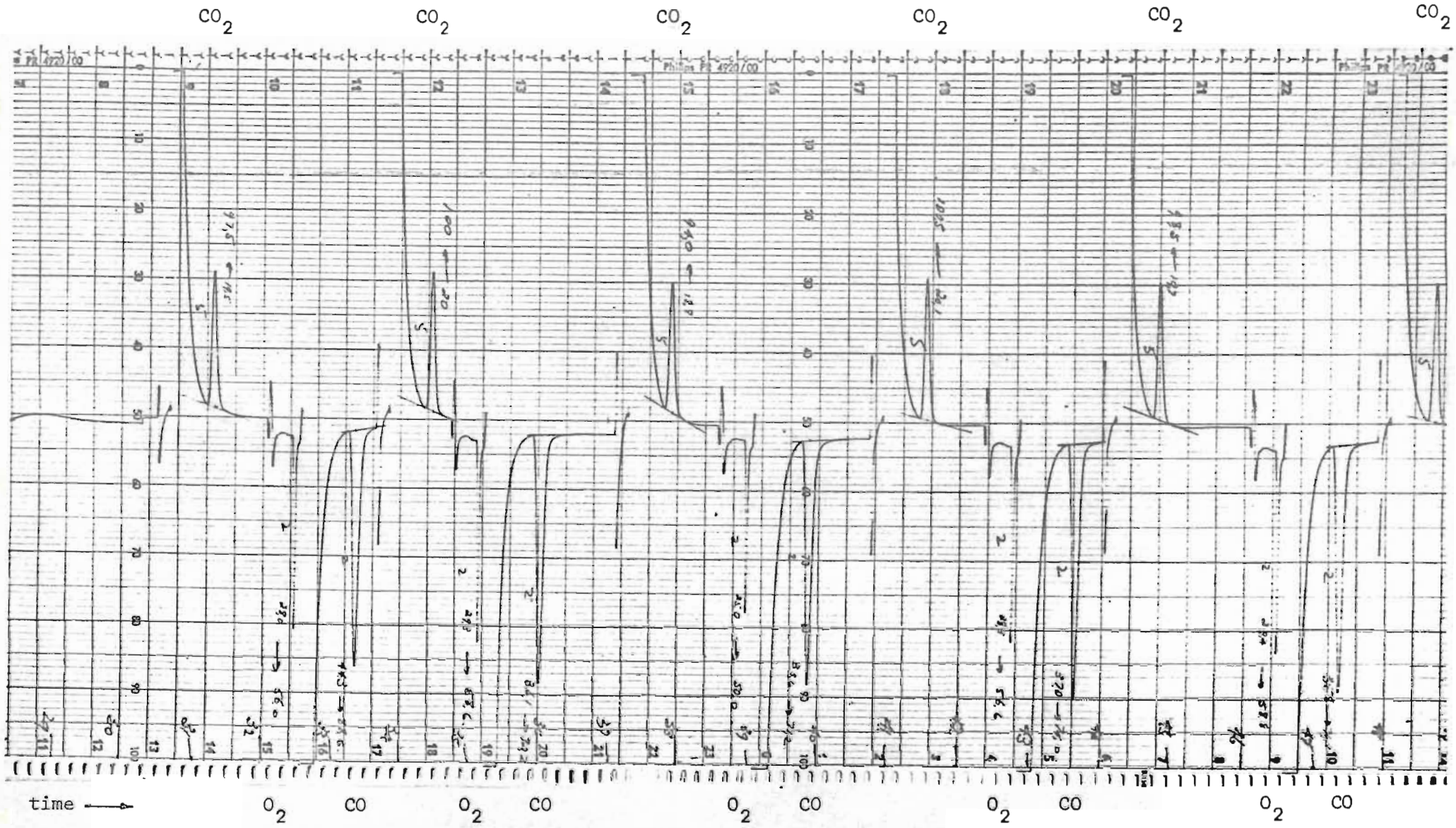

FIGURE 2.11 PART OF CHROMATOGRAMS FOR RUN LL

In order to crack the sugar, first the excess solution was removed from the soaked pellets on a vibrating screen. The pellets were then charged into a container in which the sucrose was to be cracked. This container consisted of a rectangular sheet metal box 0,37 m x 0,16 m x 0,12 m, with a lid on one of the ends. The closed end was threaded to take a 6,4 mm pipe through which high purity nitrogen could be fed to the box. The charged container was first flushed with high purity nitrogen and then heated in a muffle furnace to about 550^{o}K and kept at that temperature for about 2 hours. During this period all the moisture and most of the volatile cracking products were removed by a small stream of high purity nitrogen which passed through the charge and out of the container through a small hole in the lid. In order to reduce channeling in the charge, pairs of perforated plates separated by about 3 mm were placed in the container at 0,12 m intervals. Finally, maintaining the stream of nitrogen, the charge was heated to 755^{o}K where it was kept overnight to complete the cracking, after which it was cooled.

To maintain fairly uniform carbon concentrations for a number of regeneration experiments, several of these charges were combined and thoroughly mixed by passing them ten times through a sample splitter, recombining the lots so obtained each time. Any excess carbon on the surface of the pellets due to excess moisture on the outside was thereby loosened through attrition and then continuously removed by blowing an air stream around the pellets as they dropped from the sample splitter.

2.6.2 Analysis of the catalyst.

The carbonised catalyst was analysed for carbon as follows :-

Approximately 0,5 g of a 200g finely ground representative sample of the catalyst pellets was placed in a porcelain boat in a combustion tube, which was then heated to about 1200°K. CO_2 free air was slowly passed over the sample and any CO produced converted to CO_2 over some heated platinised asbestos. The CO_2 was then absorbed in a 0,1 N Ba $(OH)_2$ solution in a wash bottle with a fritted glass sparger. A second wash bottle was put in series with the first, but, at small gas flow-rates, the absorption of CO_2 in the first bottle would be complete. The amount of CO_2 absorbed was found by back titrating with 0,3 N HCl solution against phenolpthalein indicator and comparing this with the titration figure for a blank sample of Ba $(OH)_2$.

The carbon concentration in percentage by weight was then calculated from

$$\%\ {}^{w}/_{w} = \frac{6\ (V_B - V_S)\ N \times 10^5}{W_S}$$

where V_B = cm^3 of acid used to titrate blank

V_S = cm^3 of acid used to titrate sample

N = normality of acid

W_S = weight of sample

For the two lots of carbonised pellets used the analysis, repeated several times, gave 6,89 ± 0,06 kg carbon/kg of catalyst and 4,80 ± 0,03 kg carbon/kg of catalyst respectively.

2.7 Experimental Procedure

For an experimental run the reactor first had to be heated to the required temperature after which nitrogen containing the required amount

of O_2 would be passed into the reactor for the regeneration run proper. The following is a more detailed account of the experimental procedure used.

2.7.1 Preparation.

After the reactor has been charged, the gas chromatograph is switched on and the carrier gas and resistance wire current are properly adjusted. The cold junctions of the thermo-couples are immersed in an ice water mixture in a thermosflask. The real time program to record the temperatures on the CDC 1700 is started. The cooling water flowrates for the heat exchanger associated with the blower and the jackets of the sampling lines are adjusted. The three way valves are adjusted for recycling of the gas, and the inlet valves of the reactor in such a way as to give normal i.e. upward flow.

2.7.2 Preheat period.

Before the top flange is bolted onto the reactor, the blower is started and the system is flushed with high purity nitrogen which enters the gas stream at the blower inlet. After a few minutes the N_2 stream is reduced to a small purge and the top flange is bolted onto the reactor and covered with alumina wool insulating material. The heater elements in the gas heater and those around the steel pipe jacket are switched on. The autotransformers are adjusted to give the proper jacket temperature. A small purge of high purity nitrogen is maintained to give a positive pressure at the top or downstream manometer. This is to counteract any small leaks that may exist particularly in the solid heat exchanger.

The temperatures are monitored on the millivoltmeter while they rise, till the thermo-couples indicate that approximately 60% of the bed is at a temperature above the nominal base temperature at which the experiment is to be performed. The gas heater elements are then switched off till the inlet gas temperature has dropped to the required nominal base temperature after which this is maintained by manually switching the elements on or off as required. When the temperature range indicated by the different thermo-couples is no more than about $5^{o}K$ for the bed, the blower is stopped and the heaters in the gas stream switched off and the three-way valves set for normal flow conditions.

The pressure regulators on the nitrogen and oxygen supply are approximately adjusted during the heat up period. The nitrogen flow is now adjusted to give the correct reading for the particular temperature condition and pressure setting of $6,89 \times 10^{4}$ N/m^{2} at which the rotameter must be maintained. The heaters are switched on again.

The regeneration run proper is now started by the introduction of oxygen into the nitrogen stream. The oxygen flowrate is adjusted in the same way as the nitrogen flow. The pressure gauge at the rotameter is adjusted to $6,89 \times 10^{4}$ N/m^{2} while the flow is adjusted to give the proper rotameter reading for the temperature of the gas.

2.7.3 Regeneration period.

As the oxygen flowrate is set, the potentiometric recorder for the gas chromatograph is started and a binary input to the CDC 1700 to record the starting time of the regeneration period, is closed. The inlet temperatures and flowrates are checked and readjusted if necessary by

means of heat input to the gas heater and the valves in the gas supply lines.

The three-way valve in the outlet sampling line is adjusted to give a steady flow of reactor outlet gas. After a minute samples are taken by means of a gas syringe directly from the outlet of the sample line and they are alternately injected in the gas chromatograph column for CO_2 and into the column for O_2 and CO analysis. While waiting for an analysis to be completed before the next sample can be injected into the other column, the inlet gas temperature is continuously monitored and adjusted by switching gas heater elements on or off as required. The nitrogen and oxygen stream flowrates and pressures are continuously checked and adjusted to compensate for small drifts in the pressure drops across the bed. These drifts are due to viscosity variations in the gas in the reactor caused by the changing reactor temperatures. The pressures at the inlet and outlet of the reactor are occasionally recorded to provide an average pressure drop across the reactor for simulation purposes.

2.7.4 Flow reversal.

The sampling valve at the outlet is closed. The flow reversal is then performed by opening the closed and closing the open valves in the feed lines. The new outlet sampling valve is opened and set for a steady flow of outlet gas. The inlet temperatures and flowrates are monitored and adjusted as before. The outlet gas is sampled as before flow reversal.

2.7.5 Termination of a run.

The real time temperature recording program is stopped. The inlet sampling valve is opened and set for a steady flow. After a minute the inlet gas is analysed and the mean of about 5 samples is used as inlet gas oxygen concentration. The heaters are switched off and the gas flows and cooling water flows are stopped.

The gas chromatograph is calibrated using a standard gas mixture.

The recorded temperatures are printed for a permanent record, plotted on a Calcomp plotter and stored onto magnetic disc for later comparison with simulated data.

2.8 Some Comments on the Recorded Temperatures

During charging, the unprotected hot junctions of the thermo-couples in the bed were susceptible to breakage. One faulty thermo-couple was allowed per run. The sudden fall in temperature on the curve for the 0,559m point in run LH was due to thermo-couple malfunction. Because the bottom and top flanges were not heated by resistance wire, these acted as heat sinks for the gas spaces below and above the reactor bed proper. The temperature of the gas in these gas spaces, which act as mixing cells, would be considerably lower than the gas entering. The temperature of the gas leaving these cells would be closer to that in the cells. Because of this the outlet thermo-couple would indicate a temperature very much lower than that at the outlet of the bed. It was therefore not plotted with the temperature profiles. On flow reversal the role of the top and bottom thermo-couples would be reversed and

the top thermo-couple temperature was plotted rather than that of the bottom thermo-couple.

From the foregoing one might expect that the measured inlet temperature would be equal to or slightly higher than the temperature at the entrance of the bed. During heat up, however, the thermo-couple 5 cm from the entrance indicated a temperature a few degrees higher than that indicated by the inlet. When maintaining a constant inlet temperature the inlet thermo-couple indicated $2\pm2^{o}K$ below that at the 5 cm mark. The off-centre position of the bottom thermo-couples and imperfect gas mixing are probably the causes for this small error. Because the error was so small unadjusted inlet values were used for the simulations. The same temperature deviations were noticed for the top thermo-couple. The error was more exaggerated and was either positive or negative. Here the distance between the bed and thermo-couple was greater and mixing was not reproducible as the thermo-couples passing through the gas space would be bent into different positions in between runs during charging and also when removed for repairs.

While changing from preheating to regeneration, some time was invariably lost during which the gas in the gas feed lines and in the space below the entrace would cool. This caused initial differences between the inlet temperature and the required inlet temperature for regeneration. This was not serious since the recorded inlet temperatures were used as the boundary conditions for the simulation of a run.

Run HI, was stopped just after flow reversal by a power failure.

CHAPTER 3

THEORY I: DERIVATION OF A MATHEMATICAL MODEL.

3.1 Introduction

A mathematical model to describe any chemical reactor is obtained as a set of differential equations, by applying the principles of conservation of mass and energy to infinitesimal volume elements. In this case two sets of differential equations are obtained; one for phenomena taking place inside the pellet and one for the bed as a whole. The two sets are related through rates of mass and heat transfer at the pellet surface. In deriving these sets of differential equations several problems are encountered and the following points may be made.

A basic problem is with the differential volume element approach. For the pellet equations uniform surface conditions are assumed i.e. uniform gas phase conditions in the bed volume associated with a single pellet. However, for the equations describing the bed, variables are assumed to vary continuously with distance along the bed. This assumption will be poor in cases where a narrow reaction zone develops in the bed and gradients are steep. Further discussion of the implications of this approach as related to the results obtained, is given in Chapter 6.

The sets of partial differential equations obtained are highly coupled and made more non-linear through the temperature dependence of various physical constants. The complexity of the model precludes analytical solutions and a numerical iterative solution is to be used. Some parameters used for a specific integration may be functions of the variable

to be obtained by the integration. Such parameters are calculated before the integration and updated afterwards. Normally the average value of the parameter over the range is then used to reintegrate to obtain "corrected" values of the variable. With this in mind the present mathematical model has been derived.

3.2 Derivation of a Model for a Single Pellet

The following processes play a role in determining the overall rate of combustion of coke in a single pellet.

(i) the rate of combustion of coke with oxygen,

(ii) the rate of diffusion of oxygen from the gas phase through the gas film to the surface of the pellet,

(iii) the rate of diffusion of oxygen from the surface to the coke and of combustion products from the coke to the surface,

(iv) rate of heat transfer in the pellet,

(v) rate of heat transfer from the surface of the pellet to the bulk gas phase.

It was shown by Aris (1957) that if the characteristic dimension of a particle is given by V/S where V is the volume and S is the surface area of the particle, then the isothermal effectiveness of a first order irreversible reaction is virtually independent of the particle shape. It will be argued in section 3.2.4 that at any time the temperature gradients in the pellet are small. It will also be shown in section 3.2.2 that a pseudo steady state with respect to oxygen may be assumed. If at the same time it is assumed that the change in coke concentration with respect to time is small, then at any instant a first order isothermal reaction may be assumed. This suggests the simplification of

assuming spherical rather than cylindrical geometry to represent cylindrical pellets. Bowman (1955) verified the applicability of this assumption by his experiments on the combustion of coke in single pellets. For a cylinder with length equal to the diameter the V/S ratio is identical to that of a sphere. Hence in developing the model, a cylinder will be replaced by a sphere of equivalent diameter. Hence rather than use a two dimensional model to describe a finite cylinder, in developing the model, the finite cylinder is replaced by a sphere of equivalent diameter.

In deriving the model for a pellet a homogeneous pore structure is assumed and a distributed parameter model is chosen rather than the shrinking core model (see section 3.2.2).

3.2.1 The intrinsic rate of reaction.

The intrinsic rate of reaction has been derived in section A1.4 and may be rewritten as

$$\exp\left(k_o - \frac{E}{R'T_s}\right)\left(\frac{y_g P}{R'T_s}\right)^{m}(C)^{n} \quad \text{kg mole C/m}^3\text{s} \qquad (3.1)$$

3.2.2 Oxygen balance in pellet.

Assuming an isothermal pellet (see section 3.2.4) an oxygen balance over a differential volume of a spherical pellet gives

$$\frac{1}{r^2}\frac{\partial}{\partial r}\left(Der^2\frac{\partial Y}{\partial r}\right) = \frac{\exp\left(k_o - \frac{E}{R'T_s}\right)\left(\frac{Yy_g P}{R'T_s}\right)^{m} C^{n}\left(R_p^2 + \varepsilon_p R_p^2\right)}{N\, y_g\, C'}\frac{\partial Y}{\partial t}$$

Bischoff (1963,1965) showed that for spherical pellets with mass transfer and diffusion rate controlled gas solid reactions the pseudo steady state is valid in the initial stages of combustion. Luss (1968) showed that this is true even under time dependent ambient conditions for all but the

very final stages of combustion in a pellet. In our case the rate is not limited only by diffusion control but reaction rate control is also included, which reduces the overall rate of reaction. The accumulation of oxygen in the pores is negligible compared with the rate at which oxygen is consumed by the reaction. The last term on the right hand side of the above equation may therefore be neglected and a pseudo steady state may be assumed.

As shown in Chapter 5 the diffusion mechanism may be represented by a Knudsen type expression. The isothermal Knudsen diffusion coefficient De which is proportional to pore diameter, may be assumed constant and independent of carbon concentration.

Hence the above expression reduces to:

$$\frac{1}{r^2}\ \frac{\partial}{\partial r}\left(r^2\ \frac{\partial Y}{\partial r} \right) = \frac{\exp\left(k_o - \frac{E}{R'T_s}\right)\left(\frac{Yy_g P}{R'T_s}\right)^m C^n\ Rp^2}{De\ N\ y_g\ C'} \qquad (3.2)$$

Boundary conditions are obtained from the symmetry at the centre of the pellet where

$$\text{at}\quad r = 0: \quad \frac{\partial Y}{\partial r} = 0 \qquad (3.3)$$

and by equating the rates at which oxygen diffuses through the film around the pellet and at which it diffuses from the surface into the pellet:

$$\text{at } r = 1: \ 4\pi Rp^2\ De\ C'\ \frac{\partial y_p}{\partial R/_{Rp}} = -k_g\ 4\pi Rp^2\ (y_{p/_{Rp}} - y_g) \qquad (3.4a)$$

$$\therefore \text{ at } r = 1: \ \frac{\partial Y}{\partial r} = \frac{k_g\ Rp}{De\ C'}\ (1 - Y) \qquad (3.4)$$

In figure 3.1 pellets are shown which were regenerated to different extents at different temperatures. The pellets are broken in half and

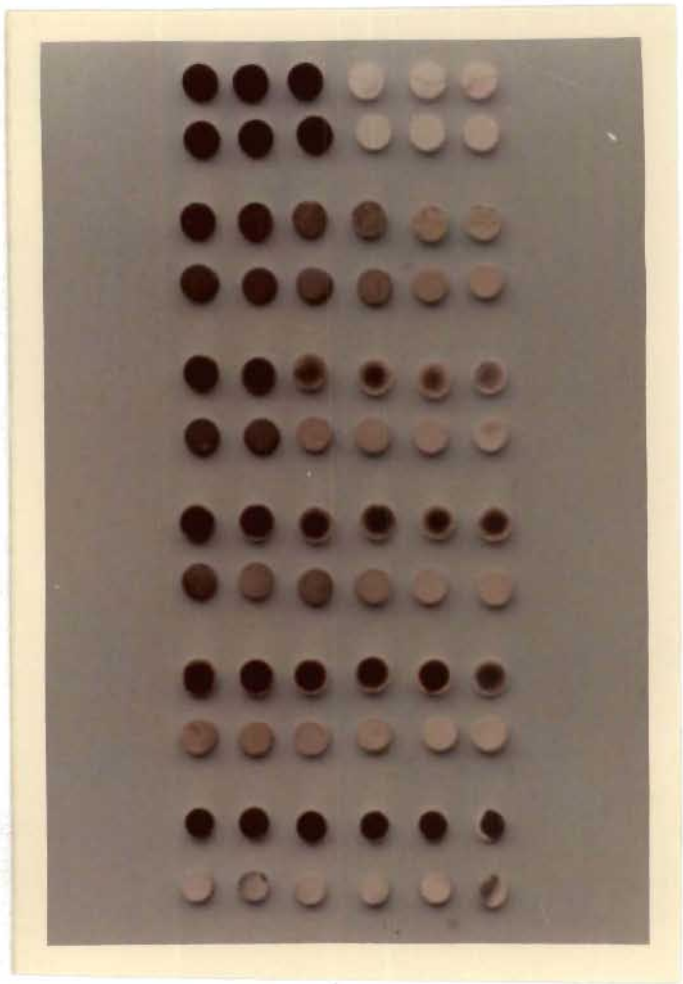

FIGURE 3.1 THE EFFECT OF TEMPERATURE ON CARBON PROFILES DURING REGENERATION.

Pellets were broken in half. In every double row the broken face is shown in the top and the outside surface in the lower row.

the top row of every double row shows the broken face i.e. a cross section through the pellet. The lower row shows the outside surface. In the top double row fresh and carbonised pellets are shown. For every other double row the degree of carbon removal increases from left to right. In the second double row carbon was removed at a temperature of 750°K or slightly higher. In the penultimate double row, the carbon was removed at about 1000°K. In the very last double row pellets are shown which were regenerated in air, when for a short time the thermocouple readings were well off the calibration curve which goes up to 1600°K. Extrapolation indicated temperatures in excess of 2000°K. As can be seen these pellets shrank considerably and apparently they lost their porous structure because further removal of carbon proved impossible.

Visual observation of the pellets after regeneration always indicates some diffuse zone in which the reaction took place. This confirmed observations made by Weisz and Goodwin (1963) and Strijbos (1973) who indicate that reaction rate controls below 750°K and diffusion controls above about 930°K, with a transition region between these two limits. A shrinking core or shell progressive model as used by Olson, Luss and Amundson (1968) is therefore not applicable in this range. A sharp interface, unreacted core model with a finite thickness reaction zone and linear concentration profiles in this zone was used by Shettiger (1972). Also this model does not give the profiles as shown in figure 3.1 for 750°K.

The distributed parameter model as derived above, can be used to simulate both reaction rate controlled and diffusion rate controlled mechanisms, provided the reaction rate is not so high as to give a pure

shrinking core.

A numerical form of the distributed parameter model is similar to that which Ausman and Watson (1962) and Ishida and Wen (1968) solved analytically for isothermal pellets and zero order reaction with respect to carbon. Apart from the disadvantage of speed, it has the advantage over an analytical solution that it can cope with parameters which change with time and it is not restricted to a specific order of reaction with respect to either carbon or oxygen. Provided the reaction is not zero order with respect to carbon, it need not differentiate between the reaction zone and the diffusion zone because the diffusion zone is the limiting case of the reaction zone when the reaction rate has approached zero. This is a definite advantage for a finite difference predictor-corrector scheme where tracking the interface between the two zones is difficult. As the temperature rises, the finite thickness zone model and eventually the shrinking core model become more applicable. However provided a fine enough grid spacing is used at which conditions are computed, the distributed parameter model is always better than the finite thickness zone model, except for computation speed. This is because it does not limit the model to linear concentration profiles. In the limit the distributed model can only approach the shrinking core model. From the visual observations of the pellets, even at $1000^{o}K$ a slight fuzziness separating the carbonised and decarbonised zones is apparent, so that the finite zone or better still the distributed model should be applicable.

3.2.3 Coke balance in pellet.

From the intrinsic rate expression, equation (3.1), at any point in the pellet at any temperature Ts, the rate at which the coke is consumed is

given by

$$\frac{\partial C}{\partial t} = \exp\left(k_o - \frac{E}{R'Ts}\right)\left(\frac{y_p P}{R'Ts}\right)^m C^n$$

Defining $c = C/Co$ where Co is the initial average carbon concentration, the above expression reduces to

$$\frac{\partial c}{\partial t} = \frac{\exp\left(k_o - \frac{E}{R'Ts}\right)\left(\frac{Y y_g P}{R'Ts}\right)^m (c\,Co)^n}{Co} \qquad (3.5)$$

with boundary condition

at $t = 0$, $c = 1$ (3.6)

if the initial carbon concentration is uniform right through the pellet. Otherwise if the initial carbon profile is not uniform

$$t = 0, \qquad c_o(r) = \frac{C(r,o)}{Co}$$

3.2.4 Temperature profile in pellet

At practically constant pressure a heat balance is equivalent to an enthalpy balance. Through the pseudo steady state assumption for the diffusion of oxygen in the pellet, a stoichiometric relationship between oxygen and combustion products is maintained. Also the heat capacity of the oxygen more or less equals the heat capacity of the reaction products so that the nett contribution of heat due to mass transfer into and out of an elemental volume of pellet is negligible (see also section 3.3.3 for this effect at the pellet boundary). For a heat balance in an elemental shell in a pellet we therefore only need to consider the heat produced by reaction, the heat transferred by conduction and the heat accumulated in the element. The total heat accumulated is due to the heat capacity of the catalyst, the carbon and the gas in the pores. The density of the gas phase is very small compared with that of the solids

and its capacity may therefore be neglected. The carbon is but a small fraction of the total carbonised catalyst weight and it has a specific heat similar to that of the catalyst. No great error is therefore introduced by treating the charred catalyst as fresh catalyst for purposes of calculating its heat capacity. With this assumption the elemental shell heat balance leads to

$$\frac{1}{r^2}\ \frac{\partial}{\partial r}\left(k_s r^2 \frac{\partial Ts}{\partial r} \right) = -(-\Delta H) Rp^2 \exp\left(k_o - \frac{E}{R'Ts} \right)^m \left(\frac{Yy_g P}{R'Ts} \right)^m C^n + \rho_s c_s Rp^2 \frac{\partial Ts}{\partial t} \qquad (3.7)$$

which is similar to the expression obtained in section 3.2.2 for the oxygen profile in the pellet.

It is proposed to assume Ts to be uniform in a particular pellet. This assumption makes the numerical solution much more economic both with respect to computer time and core space. In order to check the validity of this assumption one needs to show that the temperature gradient within the pellet is relatively small or that the temperature difference between any two points in the pellet is small. Several workers, Prater (1958), Wei (1966), Luss and Amundson (1969) and Lee and Luss (1969), have proposed methods for estimating temperature differences between the centre and the surface of a pellet and between the pellet surface and the surrounding gas, Carberry (1966). Wei deals with the transient case and Luss and Amundson have their calculations based on the shrinking core model. In this investigation visual examination of the partly regenerated pellets (figure 3.1), shows both the diffusion and the reaction mechanism to contribute to the overall scheme.

The combustion of carbon in a particular pellet is slow compared with the rise in temperature. This temperature rise is largely due to preheating

by hot gases from the upstream part of the bed rather than due to reaction in the pellet. Assuming that 0,4 of the carbon burns to CO_2 (a low but typical estimate) for a pellet with an initial carbon concentration of 4,8% it may be shown that the ratio heat produced per heat accumulated for such a pellet is about 1030/ΔT. Assuming a temperature rise due to reaction in the pellet itself, of about 50°K, this ratio would be about 20. If more carbon burned to CO_2 and for higher carbon contents this ratio would be higher. Therefore the assumption of pseudo steady state for the energy balance although probably not quite as good as for the oxygen balance (section 3.2.2) appears to be acceptable. In that case equation (3.7) reduces to

$$\frac{1}{r^2}\ \frac{\partial}{\partial r}\left(k_s r^2 \frac{\partial Ts}{\partial r} \right) = - \exp\left(k_o - \frac{E}{R'Ts}\right)\left(\frac{Y\, y_g\, P}{R'Ts} \right)^{m\ n} C\ (-\Delta H)\ Rp^2 \qquad (3.8)$$

with boundary conditions

$$\text{at } r = 0 \qquad \frac{\partial Ts}{\partial r} = 0 \qquad (3.9)$$

$$\text{and at } R = Rp \qquad - 4\pi Rp^2\, k_s \frac{\partial Ts}{\partial R} = 4\pi Rp^2 h_a\ (Ts - Tg)$$

which gives at

$$r = 1 \qquad \frac{\partial Ts}{\partial r} = \frac{h_a\ Rp}{k_s}\ (\ Tg - Ts\ ) \qquad (3.10)$$

Combining steady state equations (3.2) and (3.8)

$$\frac{\partial}{\partial r}\left(k_s r^2 \frac{\partial Ts}{\partial r} \right) = N(\Delta H)\, y_g\, C'\, De\, \frac{\partial}{\partial r}\left(r^2 \frac{\partial Y}{\partial r} \right)$$

$$= N(\Delta H)\, DeC'\, \frac{\partial}{\partial r}\left(r^2\ \frac{\partial y_p}{\partial r} \right)$$

Assuming for the time being k_s, ΔH, N and De are the same for all parts of the pellet at any instant, then

$$\frac{\partial}{\partial r}\ r^2\, \frac{\partial}{\partial r}\ (k_s Ts - N\ De\ C'(\Delta H) y_p) = 0$$

may be integrated once and using the boundary conditions (3.3) and (3.9) gives

$$\frac{\partial}{\partial r}\left(k_s\, Ts - N(\Delta H)\, De\, C'\, y_p \right) = 0$$

Integrating again

$$k_s\, Ts - N\,(\Delta H)\, De\, C'\, y_p$$

is a constant anywhere in the pellet and equal to its value at the pellet surface. Hence,

$$Ts - Ts_{Rp} = \frac{N(-\Delta H)\, De\, C'}{k_s}\left(y_{p_{Rp}} - y_p\right)$$

where the subscript Rp indicates surface conditions. A maximum value for Ts, Tm is obtained when all the oxygen is consumed and y_p is reduced to zero.

$$Tm - Ts_{Rp} = \frac{N(-\Delta H)\, De\, C'}{k_s}\, y_{p_{Rp}} \qquad (3.11)$$

To determine certain upper temperature bounds for this model Lee and Luss (1969) used this relationship together with expressions derived from equations (3.4) and (3.10).

Defining $\phi = \dfrac{1}{4\pi Rp\, De\, (C' y_g)}\, \dfrac{dn}{dt}$

where $\dfrac{dn}{dt} = 4\pi Rp^2\, k_g\, (y_g - y_{g_{Rp}})$

is the rate of reaction per pellet as observed at the pellet surface boundary (equation (3.4)), then

$$(1 - Y_{Rp}) = \frac{\phi}{M} \qquad (3.12)$$

where $M = \dfrac{k_g\, Rp}{De\, C'}$ is the Sherwood number.

Also for the total heat transfer at the pellet surface

$$De\, N\, (-\Delta H)\, C' \left.\frac{\partial y_p}{\partial R}\right|_{Rp} = h_a\, (Ts_{Rp} - Tg)$$

substituting for $\left.\frac{C' \partial y_p}{\partial R}\right|_{Rp}$ from equation (3.4), defining

$\beta = \frac{N(-\Delta H)\ De\ C' y_g}{k_s\ Tg}$ and noting that the Nusselt number for heat transfer $H = \frac{h_a\ Rp}{k_s}$, then

$$\frac{Ts_{Rp} - Tg}{Tg} = \frac{\beta}{H}\phi \qquad (3.13)$$

Substituting β into (3.11) and adding $\frac{Tm - Ts_{Rp}}{Tg}$ so obtained to equation (3.13).

$$\frac{Tm - Tg}{Tg} = \beta\{1 + \phi(\frac{1}{H} - \frac{1}{M})\} \qquad (3.14)$$

Using the expressions for physical constants as developed in this work H and M can be calculated. Then from the numerical model the computed Y_{Rp} values may be used in equation (3.12) to compute ϕ. At a temperature of $778^{o}K$ an oxygen concentration of 4%, a carbon concentration of 4% and using the above equations, it was found that

$$Tm - Ts_{Rp} < 28,7^{o}K$$

$$Ts_{Rp} - Tg < 4,3^{o}K$$

These figures compare well with the experimental results obtained by Shettiger (1972) for single spheres 1,25 cm. in diameter. His temperatures differences between gas and solid were up to $35^{o}K$ for particles containing up to 1,5% of coke. However the particles had twice the diameter of the particles used in the present work and the oxygen concentration in the gas phase was that of air as compared with up to about 4% for this work, so that smaller temperature differences may be expected for this work. Similar results were obtained by Ishida and Shirai (1969). Their

temperature differences were somewhat larger but their conditions more extreme: 2,3 - 3,7 cm. diameters, 12 - 28% carbon and air.

The upper bounds for temperature differences in the pellet and especially between the pellet surface and the gas phase are quite low. Using the model, assuming uniform temperature in the pellet, the interphase temperature difference only partially approaches the upper bound at the entrance of the bed during the initial stages of regeneration when both carbon and oxygen concentrations are high. Normally the interphase temperature differences are less than $1^{\circ}K$. This is because the oxygen concentration in the pellet does not fall to zero due to reaction rate control. At high temperatures the reaction rate controls less and the oxygen concentration may drop close to zero. However, this only occurs in parts of the bed where most of the oxygen has been consumed and the gas phase oxygen concentration is low. Under these conditions the upper bound is much lower anyway so that the actual temperature difference remains small.

The mechanisms which prevent a close approach of the upper bound for the interphase temperature difference or which lower this upper bound when closely approached, also operate for the intraphase temperature difference. It may be safely assumed that the temperature difference between the maximum temperature in the pellet and the surface temperature is normally well below $10^{\circ}K$ in which case the uniform pellet temperature assumption is good.

Another indication that an isothermal pellet may be assumed is obtained when inspecting data published by Satterfield (1970) for non-isothermal effectiveness factors for first order reactions in spheres. The effectiveness factor is defined as the ratio of the actual rate of reaction in a particle to that which would occur if the pellet interior were all exposed to the reactant at the same concentration and temperature as that at

the pellet surface. Two parameters may be introduced. $\gamma = E/R'Ts$, giving an indication of the sensitivity of the reaction rate to temperature, and the heat generation function β which has been defined above. Using regeneration conditions that will tend to give extreme non-isothermal conditions in pellets it is found that β is always smaller than 0,04 and γ never greater than 25 (which is equivalent to $E = 1{,}57 \times 10^8$ J/kg mol). On inspection of the published data it appears that for the given conditions the effectiveness curve does not appreciably differ from the curve obtained for $\beta = 0$ which is for isothermal conditions.

From the above it is clear that the assumption of an isothermal pellet is acceptable and the assumption that at any instant k_s, $(-\Delta H)$, N and De are the same for all parts of a pellet is in order for calculating the upper bounds for interphase and intraphase temperature differences.

3.3 Derivation of a Model for the Bed

In deriving a mathematical model for the bed, the bed is treated as non-adiabatic and non-isothermal. This conforms to the experimental reactor used in this investigation. The heat generated is lost through the gas leaving the reactor and by conduction through the walls. It is assumed that no heat is lost by conduction through the ends of the reactor.

Limitations on computer size and speed make it necessary to assume a one dimensional model, i.e. that there are no radial gradients in the bed. Schwartz and Smith (1953) show that one cannot expect a flat velocity profile across a bed with a tube to particle diameter ratio below 10, whereas our reactor has a ratio of 8. However Froment (1967)

when he reviews mixing indicates that radial mixing is normally several times greater than axial mixing and plug flow with respect to mass effects is probably not too bad an assumption. For radial heat transfer the above assumption is equivalent to assuming negligible resistance to heat transfer in the reactor compared with the resistance to heat flow at the wall. It will be shown in section A2.3.3 that the overall resistance to heat transfer through the wall is in fact normally several times greater than the resistance to radial flow of heat in the bed. Most of this resistance lies within the insulation around the reactor wall, so that one should include the heat capacity of the walls with the heat capacity of the bed for a one dimensional model. It was found (section A2.1.2) that the heat capacity of the tube is about 1,3 times the heat capacity of the solid phase in the reactor.

Since for the numerical solution an iterative procedure is to be used, and the simulated solid and gaseous temperatures do not differ much, it is not critical whether heat losses through the wall should be considered in the heat balance for the gas or solid phases or both. For convenience it is considered in the heat balance for the solid phase.

It was found that the pressure drop across the bed is small compared with the average operating pressure even for the higher flow rates. By assuming a constant pressure throughout no momentum balance need be made.

3.3.1 Overall rate of reaction with respect to the bed.

Assuming pseudo steady state for the oxygen profile in the pellet, the overall rate of reaction for a pellet, in terms of oxygen consumed, is obtained by considering the amount of oxygen diffusing across the film around each pellet. This rate as given by the right hand side of

equation (3.4a), is

$$- k_g \, 4\pi Rp^2 \, (y_{p,Rp} - y_g)$$

$$= k_g \, 4\pi Rp^2 \, y_o \, Yg \, (1 - Y_{r=1}) \quad \text{kg mole } O_2/s \text{ per pellet.}$$

By considering the volume of bed per single pellet, the overall rate of reaction, R*, with respect to bed volume is

$$R^* = \frac{3(1-\varepsilon)}{Rp} \; k_g \, y_o \, Yg \, (1 - Y_{r=1}) \quad \text{kg mole } O_2/(m^3 s) \tag{3.15}$$

3.3.2 Gas phase oxygen balance.

A balance of oxygen in the gas phase for a differential volume of thickness Δz in the bed, should consider convective flow, axial mixing, loss to catalyst and the accumulation in the element. Since the fraction of oxygen in the feed gas is normally small the mass flow rate and average molecular weight of the gas phase may be assumed constant (see section A3.2). This, with the differential mass balance for oxygen leads to

$$\frac{G}{MgL} \frac{\partial y_g}{\partial z} - \frac{\varepsilon}{L^2} \frac{\partial}{\partial z} \left\{ Dz \frac{\partial (C' y_g)}{\partial z} \right\} + R^* = \frac{\varepsilon \partial (C' y_g)}{\partial t}$$

Unless the flow rate is very small G/(MgL) is much greater than $\varepsilon C'$. Also for the range of Reynold Numbers involved in this work, the axial mixing coefficient is much smaller than 1,0 when expressed in the units used here. It follows therefore that the axial mixing and accumulation terms may be neglected. Hence the equation reduces to

$$\frac{\partial y_g}{\partial z} = - \frac{L \, Mg \, R^*}{G}$$

or

$$\frac{\partial Yg}{\partial z} = - \frac{L \, Mg \, R^*}{G \, y_o} \tag{3.16}$$

with the boundary condition at

$$z = 0, \; Yo = 1 \tag{3.17}$$

if the inlet oxygen concentration is constant and equal to y_o throughout. Otherwise if the oxygen concentration in the feed gas varies with time, at

$$z = o, \quad Yo(t) = \frac{y_o(t)}{y_o} \tag{3.18}$$

3.3.3 Gas phase temperature profile.

Olson (1962 - page 225) shows that for combustion of carbon in packed beds, heat transferred through axial diffusion of mass in the gas phase, even in extreme cases would be less than 0,0027 of the heat transferred convectively. This contribution is therefore ignored. He also showed that the nett heat exchange due to differences in heat contents between reagent diffusing into the catalyst and products diffusing out of the catalyst, would almost always be less than 0,0087 of the heat convectively transferred. This contribution was therefore also ignored. Subsequent inclusion of this effect in the numerical model showed its effect on the temperature profiles after several minutes of simulated time only in the fourth significant figure. Carberry and Wendel (1963) found that normally axial diffusion of heat is small in the gas phase. For convenience sake it's effect was therefore included in the derivation of an expression for conduction of heat in the solid phase (section 3.3.4). Neglecting also the minor effects of potential and kinetic energy, then one only has to consider the convective heat transfer, the heat from the catalyst and the heat accumulated in the gas phase. Hence for a differential bed element of thickness ΔZ a differential energy balance at a constant and low pressure, assuming the mass flow and the specific heat constant, gives

$$- G \; c_g \frac{\partial Tg}{\partial z} + h_v \, (Ts - Tg) = \rho_g \; \varepsilon c_g \frac{\partial Tg}{\partial t}$$

Since ρ_g c is very small compared with G we may neglect the accumulation term. Putting z = Z/L the equation further reduces to

$$\frac{\partial Tg}{\partial z} = \frac{L\ h_v}{G\ c_g} (Ts - Tg) \tag{3.19}$$

with the boundary condition at the inlet where

$$z = o \qquad Tg = To\ (t) \tag{3.20}$$

3.3.4 Solid phase temperature profile.

In order to keep the model realistic with respect to available computer size and speed, a uniform solid temperature, Ts, was assumed in the individual pellets (see section 3.2.4). Also a one dimensional model was assumed for the bed so that variables are only functions of time and distance along the bed and, where applicable, of radial position in the pellet. This is equivalent to assuming a homogeneous solid phase in which Ts is continuous in z (see section 3.1). From the assumption of pseudo steady state for the oxygen balance in the pellet (section 3.2.2), it follows that the combustion rate may be equated to the rate at which oxygen diffuses from the gas phase to the pellet, i.e. R*. Also the amount of catalyst in the solid phase is much greater than any carbon and very much greater than any gas present within the catalyst. Since the specific heats are all similar the heat capacity of the solid may be evaluated by lumping carbon and gas with the catalyst. Hence for the energy balance for the solid phase in a differential bed element of thickness ΔZ, one considers the heat generated by combustion, the heat transferred through the film separating the gas phase from the solid phase, the heat lost through the walls, the heat transferred by conduction in the solid phase and the accumulation of heat in the solid phase. Letting parameters be constant between narrow limits of integration,

this leads to

$$\frac{\partial Ts}{\partial t} = \frac{N(-\Delta H)R^*}{\rho_b c_e} - \frac{h_v}{\rho_b c_e}(Ts - Tg) - \frac{4U}{D\rho_b c_e}(Ts - Tw) + \frac{k}{L^2 \rho_b c_e}\frac{\partial^2 Ts}{\partial z^2} \qquad (3.21)$$

Since no heat is lost by conduction through the ends of the reactor the boundary conditions at in and outlet are

$$z = 0 \qquad \frac{\partial Ts}{\partial z} = 0 \qquad (3.22)$$

$$z = 1 \qquad \frac{\partial Ts}{\partial z} = 0 \qquad (3.23)$$

The initial boundary condition is at

$$t = 0 \qquad Ts = Ts(0,z) \qquad (3.24)$$

3.4 Expressions used in Material and Heat Balances

3.4.1 Consumption of oxygen.

At any time the total oxygen consumed is the difference between the oxygen entering the bed and the oxygen leaving the bed plus the oxygen accumulated in the bed. Hence the oxygen consumed, MO, is given by

$$MO = \int_o^t y_g(t,o)G\ A\ dt - \int_o^t y_g(t,L)G\ A\ dt - \int_o^L \rho_g\ \varepsilon\ A\ y_g\ (Z)\ dZ$$

since $\varepsilon\rho_g$ is much smaller than G the last term may be neglected. Hence for $y_g = Yg\ y_o$

$$MO = \int_o^t \{Yo - Yg(t)\}\ y_o\ G\ A\ dt \qquad (3.25)$$

3.4.2 Removal of coke.

MC, the total carbon removed at any time is the difference between MCO, the original carbon content of the bed and MCR, the carbon content at

that time. The total carbon content of a pellet at any time is

$$\int_o^{Rp} 4\pi R^2 \, C\,(t,Z,R)\, dR$$

and the average concentration of carbon in a pellet at Z is

$$\int_o^{Rp} \frac{3R^2}{Rp^3} C\,(t,Z,R)\, dR$$

Hence $$MCP = \int_o^L (1-\varepsilon)A \int_o^{Rp} \frac{3R^2}{Rp^3} C\,(t,Z,R)\, dR\, dZ$$

substituting $Z = zL$, $R = rRp$ and $C = cCo$

$$MCP = 3\,A\,L\,Co\,(1-\varepsilon) \int_o^1 \int_o^1 r^2\, c\,(t,z,r)\, dr\, dz \qquad (3.26)$$

which at $t = o$ gives

$$MCO = 3\,A\,L\,Co\,(1-\varepsilon) \int_o^1 \int_o^1 r^2 c\,(o,z,r)\, dr\, dz \qquad (3.27)$$

Then $$MC = MCO - MCP \qquad (3.28)$$

3.4.3 Heat generated.

At any time the total heat generated equals the sum of HG, the nett heat that has left the reactor through the gas phase up to time t, HA, the nett heat accumulated in the bed at that time and HW, the heat lost through the walls of the reactor up to that time.

$$HG = \int_o^t GA \left\{ \int_o^{Tg(t,L)} c_g\, dTg - \int_o^{Tg(t,o)} c_g\, dTg \right\} dt \qquad (3.29)$$

$$HA = \int_o^L A\rho_b \left\{ \int_o^{Ts(t,z)} c_s\, dTs - \int_o^{Ts(o,z)} c_s\, dTs \right\} dZ$$

$$= \int_o^1 AL\rho_b \left\{ \int_o^{Ts(t,z)} c_s\, dTs - \int_o^{Ts(o,z)} c_s\, dTs \right\} dz \qquad (3.30)$$

$$HW = \int_0^t U\pi D \int_0^L \{Ts(t,Z) - Tw\}\, dZ\, dt$$

$$= \int_0^t U\pi DL \int_0^1 \{Ts(t,z) - Tw\}\, dz\, dt \qquad (3.31)$$

3.5 Dimensional Analysis

The basic differential expressions used are given by equations (3.2), (3.5), (3.19) and (3.21). Writing these kind of expressions in a dimensionless form, and using a suitable choice of dimensionless variables, dimensionless responses normally depend only on a limited number of dimensionless combinations of the various parameters. In this way the problem of generating responses to different variables is reduced considerably and the simulated profiles can be made more generally useful.

For our system two such dimensionless schemes were derived. In both cases the contribution of axial conduction of heat in the solid phase to the differential equation describing the behaviour of the solid temperature was ignored. It will be shown in Chapter 6, that its contribution was negligible.

For both schemes the dimensionless temperature $\overline{T}$ was defined as T/To where To is the nominal base temperature equal to the inlet temperature at time is zero.

Scheme A.

Defining dimensionless distance $\overline{z} = \left(\frac{h_v(0)}{Gc_g(0)}\right) z$

and dimensionless time $\overline{t} = \left(\frac{h_v(0)}{\rho_b(0)c_e(0)}\right) t$

where the argument (0) indicates conditions at To, the system of differential equations reduces to:

$$\frac{1}{r^2}\ \frac{\partial}{\partial r}\left(r^2\frac{\partial Y}{\partial r}\right) = a_1 \exp\left(k_o - a_2/\overline{T}s\right) Yc$$

$$\frac{\partial c}{\partial t} = a_3 \exp\left(k_o - a_2/\overline{T}s\right) \frac{YgYc}{\overline{T}s}$$

$$\frac{\partial \bar{T}g}{\partial \bar{z}} = a_4 \, (\bar{T}s - \bar{T}g)$$

$$\frac{\partial Y}{\partial \bar{z}} = a_5 \, Yg \, (1 - Y_{Rp})$$

$$\frac{\partial \bar{T}s}{\partial \bar{t}} = a_6 \, Yg \, (1 - Y_{Rp}) - a_7 \, (\bar{T} - \bar{T}g) - a_8 \, (\bar{T}s - \bar{T}w)$$

where

$$a_1 = \frac{Rp^2 Co}{N(T) De(T)}$$

$$a_2 = \frac{E}{R'To}$$

$$a_3 = \frac{y_o P \rho_b(0) c_e(0)}{R'To \; h_v(0)}$$

$$a_4 = \frac{h_v(T) c_g(0)}{h_v(0) c_g(0)}$$

$$a_5 = 4\pi Rp^2 Mg \; \frac{c_g(0) k_g(T)}{h_v(0)}$$

$$a_6 = \frac{4\pi Rp^2 y_o \{-\Delta H(T)\} N(T) \; \rho_b(0) \; c_e(0) \; k_g(T)}{To \quad \rho_b(T) \; c_e(T) \; h_v(0)}$$

$$a_7 = \frac{h_v(T) \; \rho_b(0) \; c_e(0)}{h_v(0) \; \rho_b(T) \; c_e(T)}$$

$$a_8 = \frac{4U \quad \rho_b(0) \; c_e(0)}{D \quad \rho_b(T) \; c_e(T) \; h_v(0)}$$

Scheme B

Defining dimensionless distance $\bar{z} = \left(\frac{Mg}{Gy_o} \; R^*(0) \right) z$

and dimensionless time $\bar{t} = \frac{N(0)\{-\Delta H(0)\} \; R^*(0)}{\rho_b(0) \; c_e(0)}$

and dimensionless overall rate $\bar{R}^* = R^*/R^*(0)$

where $R^*(0) = 4\pi Rp^2 \, k_g(0) \, y_o \, (1 - Y_{Rp})$

is the rate at the entrance of the reactor at time is zero, and the argument (0) indicates conditions at To, then

$$\frac{1}{r^2} \frac{\partial}{\partial r} \left(r^2 \frac{\partial Y}{\partial r} \right) = a_1 \exp (k_o - a_2/\bar{T}s) \, Yc$$

$$\frac{\partial c}{\partial \bar{t}} = a_3 \exp (k_o - a_2/\bar{T}s) \, \frac{YgYc}{\bar{T}s}$$

$$\frac{\partial \bar{T}g}{\partial \bar{z}} = a_4 (\bar{T} - \bar{T}g)$$

$$\frac{\partial Yg}{\partial \bar{z}} = \bar{R}^*$$

$$\frac{\partial \bar{T}s}{\partial \bar{t}} = a_5 R^* - a_6 (\bar{T}s - \bar{T}g) - a_7 (\bar{T}s - \bar{T}w)$$

where $a_1 = \dfrac{Rp^2 \, Co}{N(T) \, De(T)}$

$$a_2 = \frac{E}{R'To}$$

$$a_3 = \frac{y_o P \, \rho_b(0) c_e(0)}{R'To \, N(0) \, \{-\Delta H(0)\} \, R^*(0)}$$

$$a_4 = \frac{h_v(T) \, y_o}{Mg \, R^*(0) \, c_g(T)}$$

$$a_5 = \frac{N(T) \, \{-\Delta H(T)\} \, \rho_b(0) \, c_e(0)}{N(0) \, \{-\Delta H(0)\} \, \rho_b(T) \, c_e(T) \, To}$$

$$a_6 = \frac{h_v(T) \quad \rho_b(0) \quad c_e(0)}{N(0) \, \{-\Delta H(0)\} \, \rho_b(T) \, c_e(T) \, R^*(0)}$$

$$a_7 = \frac{4U \qquad \rho_b(0) \, c_e(0)}{DN(0) \, \{-\Delta H(0)\} \, R^*(0) \, \rho_b(T) \, c_e(T)}$$

Most of the important variables appear in several groups. Consequently it is not possible to produce one simulation that will be valid for all

values of any one of these variables by merely holding one dimensionless group constant. Scheme B is not likely to be particularly useful in practice because of the difficulty in evaluating $R^*(0)$. Since, however, $R^*(0)$ should be independent of flowrate (film diffusion is not controlling), scheme B would indicate that the ratio L/G might be useful for correlating profiles at different positions and different flowrates. G does however also occur through h_v in groups a_4 and a_6 in this scheme. Since h_v depends on the square root of G, scheme A would indicate that $L/G^{\frac{1}{2}}$ might be useful for correlating purposes. Again G occurs in groups a_3 and a_8 of scheme A through h_v.

CHAPTER 4

THEORY II NUMERICAL MODEL

4.1 Introduction

The system of partial differential equations derived in Chapter 3 is highly non-linear and coupled. The variables are uncoupled by integrating every dependent variable individually while keeping the others constant. Non linearities are taken care of by keeping parameters which may be functions of the variables to be integrated, constant between limits of integration. The results are then used to up-date the parameters and the process is reiterated till a predetermined degree of convergence is obtained.

Before the equations derived can be used in a numerical scheme, they must be rewritten in a form amenable to numerical solution. For this purpose, in general derivatives may be written as:

$$\frac{dX(n)}{dx} = \frac{X(n+1) - X(n-1)}{2\Delta x} \tag{4.1}$$

$$\frac{d^2X(n)}{dx} = \frac{X(n+1) - 2X(n) + X(n-1)}{(\Delta x)^2} \tag{4.2}$$

and integrals may be written as

$$\int_{X_1}^{X_1+\Delta x} f(x)\,dx = f(n_1)\Delta x \tag{4.3}$$

or

$$\int_{X_1}^{X_1+\Delta x} f(x)\,dx = \{\frac{f(n_1) + f(n_1 + \Delta x)}{2}\}\,\Delta x \tag{4.4}$$

or

$$\int_{X_1}^{X_1+2\Delta x} f(x)\,dx = 2f(x_1 + \Delta x)\Delta x \tag{4.5}$$

For the sake of readability any dependent variable used in a numerical scheme in the following sections, will be subscripted only with respect to the independent variable with respect to which it is differentiated or integrated. To prevent confusion, time, axial position and radial position on the numerical grid are indicated by indexes i,j and k respectively so that a point (t,z,r) equivalent to {(i-1)Δt, (j-1)Δz, (k-1)Δr} will be denoted simply by subscripts (i,j,k). Indexes j and k have finite ranges from 1 to J and K respectively whereas i has a semi-infinite range starting at 1.

4.2 Pellet Oxygen Profile

Substituting equations (4.1) and (4.2) into equation (3.2) gives for the oxygen profile in a pellet for all times and axial positions, i.e. for all i's and j's

$$\frac{Y_{k+1} - 2Y_k + Y_{k-1}}{(\Delta r)^2} + \frac{2}{r}\left\{\frac{Y_{k+1} - Y_{k-1}}{2\Delta r}\right\} = \frac{Al_k\, Y_k}{(\Delta r)^2}$$

when $Al_k = \dfrac{(Rp\Delta r)\, P^m\, y_o^{m-1}\, Co^n}{De\, C'\, N} \exp\left(k_o - \dfrac{E}{R'Ts}\right)\left(\dfrac{Y_k\, Y_g}{R'Ts}\right)^{m-1} C^n$

is a function in t,z and r, which is treated as a constant parameter for integration of the above equation between grid points. By making Al a function of Y, as above, the equation is linearised. It may be rewritten as

$$Y_{k-1}\left(1 - \frac{\Delta r}{r}\right) + Y_k\left(-2 - Al_k\right) + Y_{k+1}\left(1 + \frac{\Delta r}{r}\right) = 0$$

$$\text{for } k = 2,.., K-1 \qquad (4.6)$$

For k = 1 at r = o, from equations (3.3) and (4.1)

$$Y_2 = Y_o$$

Substituting this into the general expression equation (4.6) with k=1

$$Y_1 (-2 - Al_1) + 2Y_2 = o \qquad (4.7)$$

For k=K at r=1, from equations (3.4) and (4.1)

$$Y_{K+1} - Y_{K-1} = 2A2_K (1 - Y_K)$$

where $A2 = \frac{k_g Rp \Delta r}{De\ C'}$

is a parameter which is a function of t and z. This is also kept constant on integrating between grid points. Substituting the above into the general expression, equation (4.6) with k=K gives

$$Y_{K-1} + Y_K \{-1 - \frac{Al_k}{2} - (1 + \Delta r)\ A2_K\} = - (1 + \Delta r)\ A2_K \qquad (4.8)$$

Equations (4.6), (4.7) and (4.8) form a set of K simultaneous equations which are linearised by keeping Al and A2 constant during iterations and updating them between iterations. This set of equations, the coefficients of which form a tridiagonal matrix, may be solved by the Thomas Algorithm as described by Ralston and Wilf (1960), that is by forward elimination followed by backward substitution as in subroutine SY (section A4.4)

4.3 Pellet Carbon Profile

In order to obtain the pellet carbon profile at all radial positions, r, and axial positions z, integrate equation (3.5) with respect to time t, using equations (4.4) and (4.5). Then

$$c_{i+1} = c_{i-1} - 2A3_i \Delta t \qquad i = 2,2,.... \qquad (4.9)$$

and

$$c_{i+1} = c_i - \tfrac{1}{2} (A3_{i+1} + A3_i) \Delta t \quad i = 2,3... \qquad (4.10)$$

where $A3_i = \exp\left(k_o - \frac{E}{R'Ts}\right)\left(\frac{Y\ Yg\ y_o\ P}{R'Ts}\right)^m\ Co^{n-1}\ c^n$

is a parameter which is evaluated at i and is a function of t,z and r. By making A3 a function of c the above equation is linearised when A3 is kept constant when integrating between gridpoints. Using equation (4.6) with equation (3.6) gives

$$c_2 = c_i - A3_1\ \Delta t \qquad (4.9a)$$

Equation (4.9) is used when the value of c_{i+1} has to be "predicted" for the next time increment. It is used in subroutine SCP (section A4.1). Equation (4.9a) is a special case of (4.9) and is used at the start of the simulation during the first time interval. Equation (4.10) is used in subroutine SCC (section A4.2) to correct estimates of c_{i+1}. It makes use of the estimated value of c_{i+1} to calculate the derivative needed for this.

Although equation (3.5) could have been integrated analytically, the form of the analytic solution depends on the value of n. As integrated above it is independent of the value of n.

4.4 Gas Phase Oxygen Profile in Bed

Combining equations (3.15) and (3.16)

$$\frac{\partial Yg}{\partial z} = A4\ Yg$$

where $A4 = \frac{3\ L}{RpG}(1-\varepsilon)\ Mg\ k_g\ (Y_{r=1} - 1)$

is a function of t and z, which is treated as a constant for integration between grid points. This integration may be done analytically to give for all i

$$Yg_{j+1} = Yg_j \exp\left\{(A4_{j+1} + A4_j)\ \frac{\Delta z}{z}\right\} \ldots\ j = 2,..,J \qquad (4.11)$$

and from equation (3.17) and (3.18)

$$Yg_1 = 1, \text{ or more generally}$$

$$Yg_1 = Yo(t) \tag{4.12}$$

These expressions are used to calculate the Yg profile in subroutine SYG (section A4.3)

4.5 Gas Phase Temperature Profile in Bed

In order to derive a numerical expression for the gas phase temperature profile one could integrate equation (3.19) analytically if during integration $Lh_v/(Gc_g)$, which is a function of Tg, could be kept constant. It was found that for stable integration the limits of integration had to be much closer than that provided by Δz used for the other variables which are integrated with respect to z. Also a local iterative procedure had to be used to update h_v during integration. In terms of the overall energy balance check incorporated in the numerical simulation, it was found that best results were obtained by subdividing Δz till a simpler iterative Euler numerical integration scheme could be used. This also meant a saving in computer time since the analytical integration involves exponentiation. Hence combining equations (3.19) with (4.3) and (4.4) and using M subdivisions of Δz then for all i

$$Tg_{j'+1} = Tg_{j'} + A5_{j'}\,\Delta z' \qquad j' = 2,..,J' \tag{4.13}$$

$$\text{and} \quad Tg_{j'+1} = Tg_{j'} + (A5_{j'+1} + A5_{j'})\frac{\Delta z'}{2} \qquad j' = 2,..,J' \tag{4.14}$$

$$\text{where} \quad A5_{j'} = \frac{Lh_{v_{j'}}}{Gc_{g_{j'}}}\,(Ts_{j'} - Tg_{j'})$$

is a parameter which is a function of t and z. It is kept constant during integration between grid points.

M = number of subdivisions

$\Delta z'$ = $\Delta z/M$

j' = index indicating axial bed position on the mesh with increments $\Delta z'$

J' = (J-1)M+1, the upper limit of the range of index j'.

Also at z = o, when j = j' = 1 from equation (3.20)

$$Tg = To(t) \tag{4.15}$$

Values of $A5_{j'}$ and $Ts_{j'}$, intermediates to values of A5 and Ts calculated and stored for the normal Δz grid, are calculated by a five point Lagrangian interpolation scheme. In subroutine STG (section A4.7) these values are used in equation (4.13) to estimate $Tg_{j'+1}$ and after updating $A5_{j'+1}$ this value is used in equation (4.14) to update $Tg_{j'+1}$.

4.6 Solid Phase Temperature Profile in Bed

In equation (3.21) Ts varies with both time and axial bed position. Rewriting the equation

$$\frac{\partial Ts}{\partial t} = A6 + A7.Ts + A8 \frac{\partial^2 Ts}{\partial z^2} \tag{4.16}$$

where $A6 = (N(-\Delta H)R^* + h_v Tg + \frac{4UTw}{D}) / (\rho_b c_e)$

$$A7 = -(h_v + \frac{4U}{D}) / (\rho_b c_e)$$

$$A8 = k/(\rho_b c_e L^2)$$

A6, A7 and A8 are all parameters which are functions of time and

axial bed position. They are kept constant during integration and updated in between iterations.

When Ts is a function of z and t we may define at $i + \theta$ between i and i+1

$$Ts_{i+\theta,j} = \theta Ts_{i+1,j} + (1-\theta)\, Ts_{i,j} \qquad (4.17)$$

where θ is an interpolation factor so that $0 \leq \theta \leq 1$. Comparing this with equations (4.1) and (4.2) the derivatives of Ts may now be rewritten as

$$\frac{d}{dt} Ts_{i+\theta,j} = \frac{Ts_{i+1,j} - Ts_{i,j}}{\Delta t}$$

and $$\frac{d}{dz} Ts_{i+\theta,j} = \frac{Ts_{i+\theta,j+1} - Ts_{i+\theta,j-1}}{\Delta z} \quad \text{etc.}$$

Substituting these expressions into equation (4.16)

$$\frac{Ts_{i+1,j} - Ts_{i,j}}{\Delta t} = A6 + A7.Ts_{i+\theta,j} + \frac{A8}{(\Delta z)^2} (Ts_{i+\theta,j+1} - 2Ts_{i+\theta,j} + Ts_{i+\theta,j-1})$$

where A6, A7 and A8 are to be evaluated at (i+θ,j) as in equation (4.17). Defining

$$\Delta Ts_{i,j} = Ts_{i+1,j} - Ts_{i,j} \qquad (4.17a)$$

and noting that

$$Ts_{i+\theta,j} = \theta.\Delta Ts_{i,j} + Ts_{i,j}$$

the above equation may be rewritten and rearranged as

$$A9.\theta.\Delta Ts_{i,j-1} + (1 + A10.\theta)\, \Delta Ts_{i,j} + A9.\theta.\, \Delta Ts_{i,j-1}$$

$$= A11 - A9.Ts_{i,j-1} - A10.Ts_{i,j} - A9.Ts_{i,j+1} \qquad j=2,..,J-1 \qquad (4.18)$$

where $A9 = -A8 \frac{\Delta t}{(\Delta z)^2}$

$$A10 = 2A8 \frac{\Delta t}{(\Delta z)^2} - A7.\Delta t$$

and $A11 = A6.\Delta t$

at $z = o$ where $j = 1$ from equations (3.22) and (4.1)

$$Ts_{i,o} = Ts_{i,2}$$

and $$\Delta Ts_{i,o} = \Delta Ts_{i,2}$$

Substituting this into equation (4.18) where $j = 1$

$$(1 + A10.\theta)\Delta Ts_{i,1} + 2A9.\theta.\Delta Ts_2 = A11 - A10\ Ts_{i,1} - 2A9.Ts_{i2} \qquad (4.19)$$

As for z=1 when j=J, from equations (3.23), (4.1) and (4.18)

$$2A9.\theta.\Delta Ts_{i,J-1} + (1 + A10.\theta)\Delta Ts_{i,J} = A11 - 2A9.Ts_{i,J-1} - A10\ Ts_{i,J} \qquad (4.20)$$

Equations (4.19), (4.18) and (4.20) form a set of J simultaneous equations in ΔTs which on solving and substituting into equation (4.17) give the required Ts vector. A set of ΔTs rather than Ts was derived to improve the precision of the final Ts vector by 2 to 3 orders since ΔTs is often but a small fraction of Ts. This extra precision was needed to prevent stability problems.

As for the carbon and gas phase oxygen profiles, two expressions are required. One to estimate or predict, and one to correct these estimated values. By putting θ=o, the terms on the left hand sides of equations (4.19), (4.18) and (4.20) containing θ vanish and explicit

equations are obtained which can be used to predict $Ts_{i+1,j}$ from $Ts_{i,j}$. This is done in subroutine STSP (section A4.5). By putting $0<\theta\leq 1$, the above mentioned equations form a set of simultaneous implicit equations in Ts. As for the pellet oxygen profile, the solid temperature profile is obtained by use of the Thomas Algorithm for tri-diagonal matrices. Ralston and Wilf (1960 - page 135) state that if $\frac{1}{2}\leq\theta\leq 1$, the solution is stable. This implicit scheme can, therefore, be used to correct the predicted values obtained using the explicit scheme. When $\theta=\frac{1}{2}$ the scheme reduces to the well known Crank-Nicholson method. The correction scheme using the Thomas Algorithm is used in subroutine STSC (section A4.6)

4.7 Material and Heat Balances

4.7.1 Total oxygen consumed.

To obtain the total oxygen consumed up to time (I-1) t, from equation (3.25)

$$MO = A12 \sum_{i=2}^{I} (Yg_{i,} - Yg_{i,J}) \qquad (4.21)$$

where $A12 = y_o$ G A Δt is a parameter independent of time or position. Since the time intervals are small, the trapezoidal rule for integration is used, but instead of using $\frac{\Delta t}{2}$ (first ordinate + last ordinate), the first ordinate is ignored and (Δt)x(last ordinate) is used. This way, very conveniently, at time (I-1)Δt, the integral is obtained by adding (Δt)x(last ordinate) to the value of the integral obtained at time (I-2)Δt. The error involved tends to zero after a relatively small number of intervals. MO is calculated in subroutine SHMAC (section A4.8)

4.7.2 Total coke removed.

The carbon present at any time is found from equation (3.26') as follows. The integration with respect to r is performed using Durand's rule (Perry, 1950 - page 90) which is a more accurate form of the trapezoidal rule.

$$\int_o^1 r^2 c\ (t,z,r)\ dt = \int_o^1 r_k^{\ 2}\ c_{i,j,k}\ dr = Q_{i,j}$$

on applying Durand's rule and noting that $r_1^{\ 2}\ c_{i,j,1} = 0$

gives

$$Q_{i,j} = (\Delta r)^3 \left[0{,}4\ (K-1)^2\ c_{i,j,k} + 1{,}1\ \{c_{i,j,2} + (K-2)^2\ c_{i,j,K-1}\} + \sum_{k=3}^{K-2} (k-1)^2\ c_{i,j,k} \right] \qquad (4.21a)$$

If $\int_o^1 \int_o^1 r^2 c(t,z,r)\ dr\ dz = \int_o^1 Q_{i,j}\ dz = Q_i^{\ 1}$

then on applying Durand's rule to integrate with respect to z, gives

$$Q_i^{\ 1} = \left[0{,}4\ (Q_1 + Q_J) + 1{,}1\ (Q_2 + Q_{J-1}) + \sum_{j=3}^{J-2} Q_j \right] \Delta z$$

so that $MCP = A13\ Q_i^{\ 1}$ (4.22)

where A13 = 3 A L Co (1-ε) is a parameter independent of time and position. From the above at t = o

$$MCO = A13\ Q_o^{\ 1} \qquad (4.23)$$

and the carbon removed is

$$MC = MCO - MCP \qquad (4.24)$$

MCO and MCP are calculated in subroutine SHMIN and MC in SBAL (sections A4.9 and A4.10).

4.7.3 Total heat generated.

The integral $\int_o^T c_g \, dT$ appearing in equation (3.29) where c_g is a linear function of T, say a + bT, becomes

$$\int_o^T c_g \, dT = \int_o^T (a + bT) \, dT$$

$$= 0{,}5 \{c_g(o) + c_g(T)\} T$$

so that the sensible heat lost in the gas stream up to time (I-1)Δt can be obtained from equation (3.29) as

$$HG = A14 \sum_{i=2}^{I} \left[\{c_g(o) + c_g(Tg_{i,J})\} Tg_{i,J} - \{c_g(o) + c_g(Tg_{i,o})\} Tg_{i,o} \right] \quad (4.25)$$

where A14 = 0,5 AGΔt is a parameter independent of time and axial position. As for the total oxygen consumed (see section 4.7.1) a modified trapezoidal rule is used. Again the error involved is small after relatively few intervals. HG is calculated in subroutine SHMAC (section A4.8).

The heat accumulated in the bed at any time, (i-1)Δt, may be obtained from equation (3.30). The integral $\int c_s \, dT$ is obtained as above. The second term need only be evaluated once. Durand's rule is used to integrate with respect to z. The second term is then given by

$$HAO = A16 \Big(0{,}4 \left[\{c_s(o) + c_s(Ts_{1,1})\} Ts_{1,1} + \{c_s(o) + c_s(Ts_{1,J})\} Ts_{1,J} \right]$$
$$+ 1{,}1 \left[\{c_s(o) + c_s(Ts_{1,2})\} Ts_{1,2} + \{c_s(o) + c_s(Ts_{1,J-1})\} Ts_{1,J-1} \right]$$
$$+ \sum_{j=3}^{J-2} \{c_s(o) + c_s(Ts_{1,j})\} Ts_{1,j} \Big) \quad (4.26)$$

and

$$HAP=A16\left(0{,}4\left[\{c_s(o)+c_s\,(Ts_{i,1})\}\,Ts_{i,1}+\{c_s(o)+c_s\,(Ts_{i,J})\}\,Ts_{i,J}\right]\right.$$
$$+1{,}1\left[\{c_s(o)+c_s\,(Ts_{i,2})\}\,Ts_{i,2}+\{c_s(o)+c_s\,(Ts_{i,J})\}\,Ts_{i,J-1}\right]$$
$$\left.+\sum_{j=3}^{J-2}\{c_s(o)+c_s\,(Ts_{i,j})\}\,Ts_{i,j}\right) \qquad (4.27)$$

and $HA = HAP - HAO$ (4.27a)

where $A16 = 0{,}5\ A\ L\ \rho_b \Delta z$ is a time and axial position independent parameter. HAP and HAO are calculated in subroutine SHMIN (section A4.9).

The rate of loss of heat through the walls of the reactor at any time $(I-1)\Delta t$ may be obtained from equation (3.31).

If $\int_o^1 \{Ts_{i,j} - Tw_j\}\,dz = Q_i$ (say)

then on using Durand's rule

$$Q_i=0{,}4\,(Ts_{i,1}+Ts_{i,J}-Tw_1-Tw_J)+1{,}1(Ts_{i,2}+Ts_{i,J-1}-Tw_2-Tw_{J-1})$$
$$+\sum_{j=3}^{J-2}(Ts_{i,j}-Tw_j)$$

Again for integrating numerically with respect to time in order to evaluate the heat lost up to time $(I-1)\Delta t$, the modified trapezoidal rule is used as for the total oxygen consumed (see section 4.7.1). Hence

$$HW = A15 \sum_{i=2}^{I} Q_i \qquad (4.28)$$

where $A15 = U\pi D\ L\ \Delta z\ \Delta t$ is a constant parameter independent of time and position. HW is calculated in subroutine SHMAC (section A4.8). Now total heat generated then at any time is calculated as

$$HT = HG + HW + HA \qquad (4.29)$$

in subroutine SBAL (section A4.10).

4.7.4 Checks by material and heat balances.

If x, the fraction of carbon converted to CO_2, and ΔH, the heat of reaction are constant, an overall material and heat balance can be performed without differentiating between points in the reactor. The total carbon removed as given by equation (4.24) is then directly related to the total oxygen consumed (equation (4.21)) according to equation (A1.3) (section A1.3). Also the total heat generated by the system given by equation (4.29) is directly related to the carbon removed through the heat of reaction as given in equation (A1.4) (section A1.3). For conditions of constant x and ΔH, therefore, material and heat balances provide explicit checks on the validity and stability of the numerical procedure.

When x and ΔH are not constant but functions of a varying temperature, a check like the one above is impossible. However, an average or overall value of x, $\bar{x}$, for the whole of the reactor up to a certain instant may be calculated either by comparing the amounts of oxygen and carbon consumed or by comparing the heat generated with the amount of carbon removed. $\bar{x}_M$, the value of $\bar{x}$ based on the material balance may be calculated from equation (A1.3)

$$\bar{x}_M = 2 \left(\frac{MO}{MC} - 0{,}632 \right) \qquad (4.30)$$

$\bar{x}_H$, based on the heat balance may be calculated from equation (A1.4),

$$\bar{x}_H = \left(\frac{HT}{MC} - 1{,}97\times10^8 \right)/2{,}83\times10^8 \qquad (4.31)$$

Defining $XR = \bar{x}_M/\bar{x}_H$, (4.32)

the closeness of $\bar{x}_M$ to $\bar{x}_H$, or the closeness of XR to unity, gives implicitly an indication of the accuracy of the material and heat

balances. $\bar{x}_M$, $\bar{x}_H$ and XR are calculated in subroutine SBAL (section A5.10).

4.7.5 Fraction "x" in the outlet gas.

Experimentally q' the ratio CO/CO_2 in the outlet gas at any instant, can be obtained from the outlet gas analysis and may be used to check the model and model parameters. q' is related to x', the instantaneous value of x in the outlet gas, i.e. $CO_2/(CO_2 + CO)$ by equation (A1.1) as follows

$$q' = (1-x')/x'$$

x' is obtained from the material and heat balances as follows. Using $\bar{x} = \frac{1}{2}(\bar{x}_M + \bar{x}_H)$ at time is t_i

$$\bar{x}_i = \left.\frac{\Sigma CO_2}{MC}\right|_i = \frac{\text{total } CO_2 \text{ produced up to } t_i}{\text{total C removed up to } t_i}$$

$$\simeq \frac{\text{total } CO_2 \text{ left by outlet gas up to } t_i}{\text{total C removed up to } t_i}$$

Since the mean residence time of gas in the reactor is less than a second and the gaseous hold up is very small compared with the solid content of the bed, this approximation is good except for very small values of time. Similarly at time t_{i-1}

$$\bar{x}_{i-1} = \left.\frac{\Sigma CO_2}{MC}\right|_{i-1}$$

Now $$x'_{i-\frac{1}{2}} = \frac{CO_2 \text{ leaving reactor during interval between } t_{i-1} \text{ and } t_i}{C \text{ removed during the interval between } t_{i-1} \text{ and } t_i}$$

$$= \frac{\bar{x}_i MC_i - \bar{x}_{i-1} MC_{i-1}}{MC_i - MC_{i-1}} \qquad (4.33)$$

x' is calculated in subroutine SBAL (section A4.10).

4.8 Reversal of Direction of Gas Flow

To program the reversal of the direction of gas flow, the boundary conditions of Yg and Tg have to be changed and the integration has to proceed from z=1 to z=o rather than from z=o to z=1. Equivalent to this is to invert all the profiles with respect to z in which case the boundaries and numerical procedure remain unchanged. The physical analogy to this is rather than to reverse the flowrate, the reactor is rotated between the inlet and outlet, so that what used to be inlet is outlet and vice versa.

In subroutine SREV (section A4.11) this inversion is performed for individual variables. For the recording of numerical profiles it is required to change the printing or storing order of variable values at different points in the reactor, as well. This is not shown.

4.9 Outline of Numerical Procedure and Logic Diagram

Because of the small capacity of the gas phase with respect to both heat and mass, the Tg, Y and Yg profiles are assumed at pseudo steady state and for any of these to be calculated, needed is only a knowledge of the other variables at that particular time. The C and Ts profiles however, are integrated with respect to time and for their computation require past values of the variables and parameters involved. Because carbon is removed irreversibly and the solid phase has an appreciable heat capacity, a pseudo steady state cannot be assumed for the variables C and Ts.

The system consists of some highly coupled partial differential equations and is highly non linear. An iterative procedure is therefore

used. When complete profiles are available for all the variables and parameters at $i\Delta t$, derivatives at $i\Delta t$ are computed to estimate or predict Ts and C profiles at $(i+1)\Delta t$. These values and the best (latest) values of the other variables and parameters are then used to compute Tg, Y and Yg profiles at $(i+1)\Delta t$. The profiles calculated at $(i+1)\Delta t$ may then be used to calculate the derivatives at any point in the interval between $i\Delta t$ and $(i+1)\Delta t$ and these are used to recalculate Ts and C. From these corrected values, Tg, Y and Yg at $(i+1)\Delta t$ may be recalculated to correspond to the corrected values. The correction process may be repeated till some measure of convergence has been attained. At any stage, parameters dependent on one or more variables are evaluated prior to use, from the current values of the variables. Successive correction cycles then allow both variables and parameters to converge to a steady value.

Because a pseudo steady state has been assumed for Tg, the initial boundary need not be defined for the computation of the Tg profile. It needs to be defined however for calculating parameters dependent on Tg.

Due to the pseudo steady state assumption for the Yg and Y profiles, initial profiles for Y and Yg cannot be inferred from the initial boundary condition that the oxygen concentration in the inlet gas stream changes from zero to a finite value at zero time. These initial profiles have to be computed. To compute Y profiles from equations (4.6), (4.7) and (4.8) the parameter Al needs to be calculated first. In general Al is a function of Yg. However Yg is not known at zero time and Yg can only be calculated when the Y profiles at the surface of the pellets are known.

Considering the expression for Al it appears that Al is independent of Yg when m=1, i.e. when the combustion reaction is first order with respect to oxygen. Initial profiles of Y and Yg can therefore be obtained as follows: The initial Y profile is computed for m=1. Then the initial Yg profile is computed and this is used to recalculate Y with m=m. The process is repeated till the initial Y and Yg profiles have converged for m=m.

At any time only the current variables and parameters and those of the previous predictor-corrector cycle are required to correct the current or predict the next set of variables and parameters. Only three sets of variables and parameters need therefore be stored. Core saving is achieved by resetting indices of subscripted variables after every prediction cycle.

The following is a description of the functions of some of the blocks in the logic diagram, figure 4.1. Subroutines referred to here, by names starting with S, are given with their associated function subprograms in Appendix 5. No rigorous attempt is made here to show how certain recurring groups in parameters may be stored to cut down on computing time.

Block B. Initial profiles are set up. For Tg, Ts and C the initial boundary conditions are used. (equations (3.20), (3.24) and 3.6))

Block C. The initial Y profiles are computed by subroutine SY with m=1 after which m is redefined to its original value.

Blocks D and E. Initial Yg and Y profiles are calculated and recalculated for m=m in block D till the convergence criteria are satisfied

In block E.

Block F. The first predictions are made for time equal to Δt. $Yg_{2,1}$ is set to Yo_2 and MC set to 0.0.

Block G. $Tg_{2,j}$, $Yg_{2,j}$ and $Y_{2,j,k}$ profiles are computed using current values of parameters needed.

Block H. After the first prediction 20 corrector cycles are normally used. After flow reversal 4 or 5 cycles are used. Otherwise 2 or 3 cycles are sufficient for convergence. More cycles are required when perturbations are encountered, i.e. at the start and with flow reversals.

Block I. Current values of $Ts_{2,j}$ and $C_{2,j,k}$ are corrected using current updated parameter values.

Block J. HW, HG and MO, which are quantities summed in time, are updated to include contributions from the last time interval.

Block L. Computes MCP and HA, the carbon and heat content of the reactor in subroutine SHMIN, and uses these to do overall heat and material balances in subroutine SBAL for implicit checks (see section 4.7.4).

Block M. Stores and/or prints profiles of variables and results from heat and mass balances. It takes care of the order of the profiles if flow reversal has occurred.

Block Q. Time is updated and $C_{3,j,k}$ and $Ts_{3,j,k}$ are predicted for the new time.

Block R. Indexes are reset to save core space.

Block S. Redefines or updates the inlet values $Tg_{2,1}$ and $Yg_{2,1}$ for the inlet gas if there is a change. The values are obtained by means of a five point Lagrangian interpolation of known feed gas values.

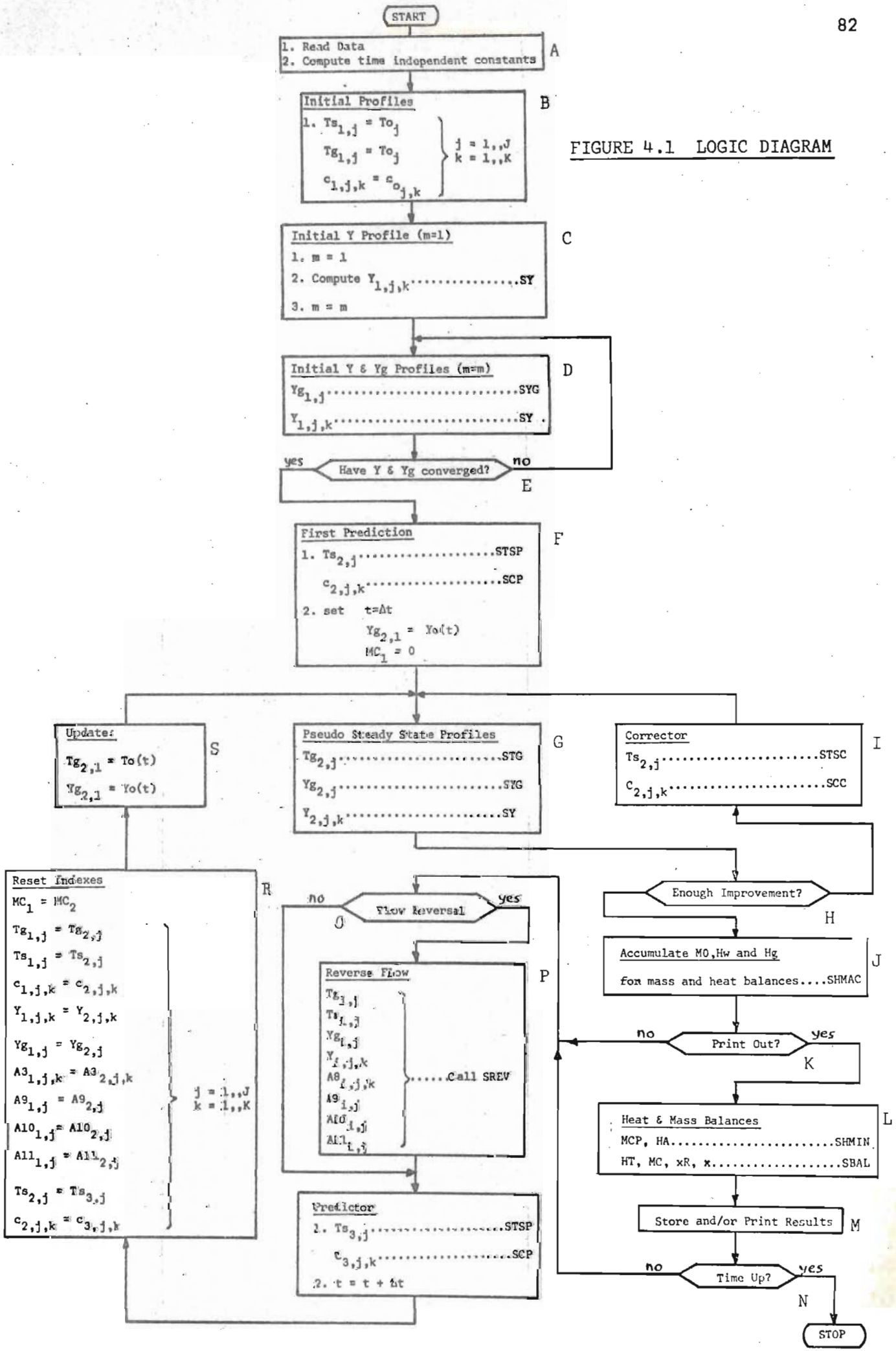

FIGURE 4.1 LOGIC DIAGRAM

CHAPTER 5

DIFFUSION IN A PELLET

5.1 Introduction

Normally for the regeneration of charred catalyst pellets, the shell progressive or shrinking core model is used, where the reaction rate is assumed not to contribute to the overall rate appreciably. From the initial experimental results obtained (section 3.2.2) during regeneration of the bed, it was found that both the reaction rate and the diffusion rate contributed to the overall rate as controlling mechanisms. The magnitude of both the reation rate parameters and the diffusion coefficients determine which of the two mechanisms do play a significant role. Although parameters for the two mechanisms could be inferred from the experimental results for the bed by regression analysis, for a complex model as used, it is much better to obtain these parameters, where possible, from independent experiments. This is fairly easily achieved for the diffusivity of oxygen in the pellets.

5.2 Overall Diffusivity

The diffusivity of a gas in porous pellets is in general due to a combination of Knudsen and molecular or bulk diffusion, i.e. gaseous molecules may diffuse both due to collision with pore walls and due to collisions with each other. For binary gas diffusion in a porous solid at constant total pressure Satterfield (1970) reports as the most useful model

$$N_1^o = \frac{-D_{12} \frac{dC_1}{dx} + y_1 (N_1^o + N_2^o)}{1 + D_{12}/D_{K1}} \qquad (5.1)$$

where N_1 and N_2 are the fluxes of components 1 and 2 (kg mol/(m^2s))

D_{12} = bulk diffusion coefficient of species 1 in a mixture of 1 and 2 (m^2/s)

D_{K1} = Knudsen diffusion coefficient for species 1 (m^2/s)

y = mole fraction

x = distance in the direction of diffusion (m)

c = concentration (kg mol/m^3)

superscript o indicates that there is no D'Arcy flow resulting from pressure gradients and no surface diffusion.

For equimolal counter diffusion this reduces to

$$N_1 = - D \frac{dc_1}{dx}$$

where $\frac{1}{D} = \frac{1}{D_{12}} + \frac{1}{D_{K1}}$, the so-called Bosanquet interpolation formula.

Taking into account the voidage and pore structure of the pellets, effective properties are obtained when

$$D_e = \frac{\varepsilon}{\tau} D \quad , \quad D_{12,e} = \frac{\varepsilon}{\tau} D_{12} \quad \text{and} \quad D_{K1,e} = \frac{\varepsilon}{\tau} D_{K1}$$

where ε = voidage fraction of the porous solid

τ = tortuosity factor for the porous solid,

then D_e, the effective overall diffusivity is given by

$$\frac{1}{D_e} = \frac{1}{D_{12,e}} + \frac{1}{D_{K1,e}} \tag{5.2}$$

The effective bulk diffusivity can be calculated with fair accuracy as done in section 5.4. For pellets with a simple and well known pore structure $D_{K,e}$ may be calculated from

$$D_{K,e} = 0{,}9700 \frac{\varepsilon}{\tau} \hat{r} \sqrt{\frac{T}{M}} \quad m^2/s \tag{5.3}$$

when $\hat{r}$ = pore radius

M = molecular weight.

For an unknown pore structure D_K has to be obtained experimentally.

5.3 Determination of the Knudsen Diffusion Coefficient

Gunn (1967) modified equation (5.1) to include D'Arcy flow. This Balder and Petersen (1968) used to obtain for a single component in a porous pellet

$$N_1 = - \left(D_{Kl,e} + \frac{C_0}{\mu} P\right) \frac{1}{R'T} \frac{dP}{dx}$$

where $\frac{C_0}{\mu}$ = D'Arcy flow parameter ($m^3 s/kg$)

P = pressure ($kg/(m^2 s)$)

R' = gas constant

T = temperature (K)

Integrating over the pellet length L

$$\frac{N_1 R'TL}{\Delta P} = D_{Kl,e} + \frac{C_0}{\mu} \overline{P} \qquad (5.4)$$

where ΔP = pressure drop across the pellet

$\overline{P}$ = average pressure in the pellet.

Plotting $\overline{P}$ vs the right hand side of equation (5.4) should give a straight line with at P=0 the intercept equal to $D_{Kl,e}$ the effective Knudsen diffusion coefficient.

5.3.1 Experimental determination of $D_{Kl,e}$

Permeability experiments similar to those done by Balder and Petersen (1968) were performed on several pellets both carbonised and uncarbonised.

Fresh pellets were heated to 480°C and kept at that temperature overnight so as to have the same temperature history for the fresh pellets as for the carbonised pellets. The pellets were then cemented into brass sleeves using Araldite, an epoxy cement. The two flat surfaces were finally faced off to remove Araldite covering the ends of the cylindrical pellets.

Microscopic examination of the faced off pellets in their sleeves, indicated good sealing by the cement. The Araldite appeared not to have penetrated the pellets to any extent. Pellet diameters were obtained from the finished sleeved pellets using a travelling microscope. Care was taken to exclude parts of the pellet penetrated by the Araldite. The mean of several readings on both sides was used.

Prior to a permeability experiment, the sleeved pellets were evacuated for four hours. It was then fitted inside the sleeve holder of the permeability apparatus as shown in figure (5.1). During a run, a purge was allowed on the upstream side to remove any impurities and give a quicker response to any pressure changes applied. The apparatus as designed only allowed for average pressures greater than atmospheric. Flow measurements were made for pressure drops across the pellet ranging from about 100 mm to 1300 mm Hg. The results obtained for oxygen are shown in figure (5.2). The straight lines were obtained by linear regression. Experimental points are only shown for some of the plots with the higher standard deviations. The results are tabulated in table (5.1).

The ranges of $D_{K,e}$ for the two types of pellets are considerable. They also overlap considerably. This is not surprising for these industrial catalysts. For this work the mean for the two types of pellets was used, i.e.

$$D_{K,e} = 2{,}87\times10^{-7}\sqrt{T} \pm 44\% \quad m^2/s$$

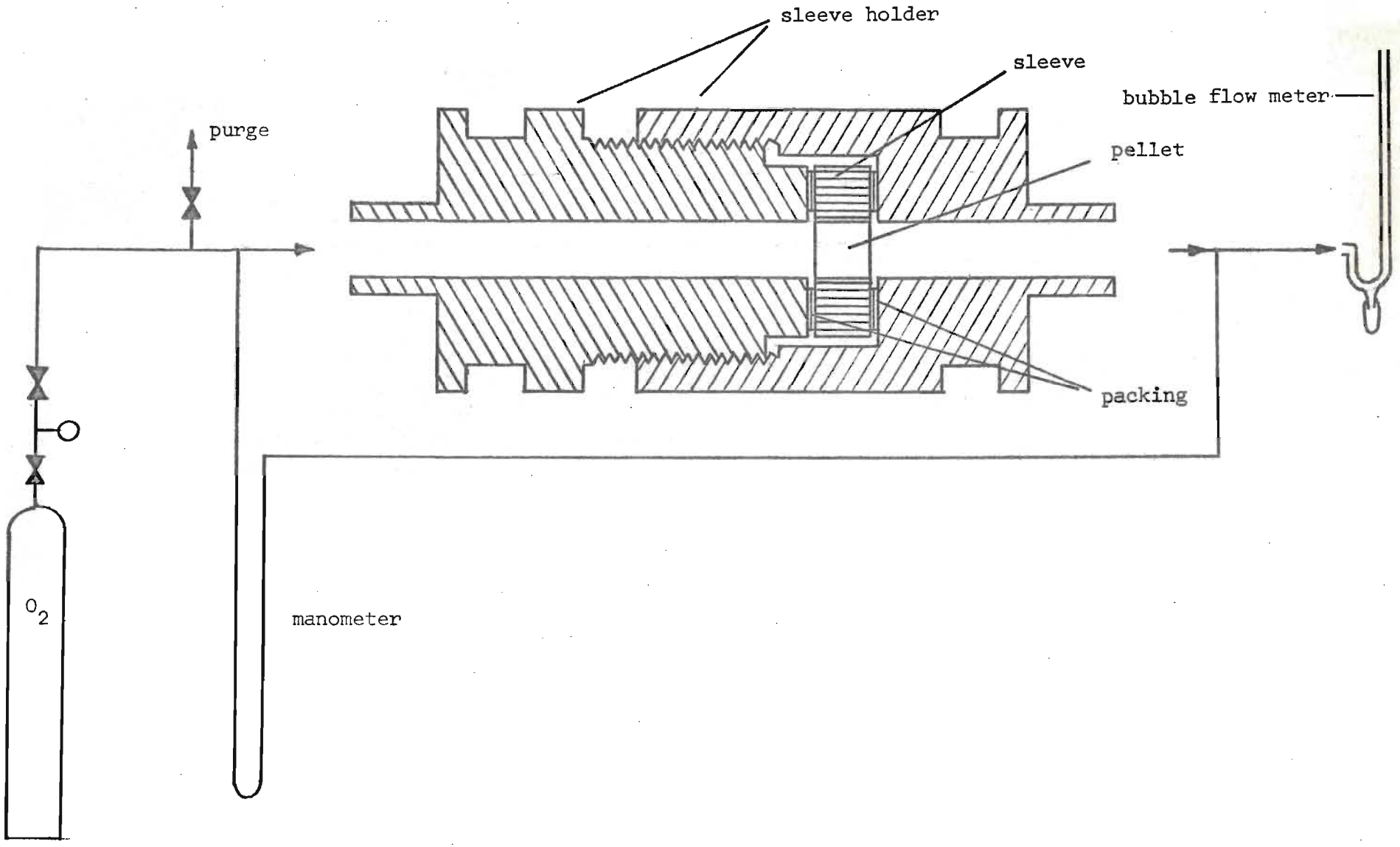

FIGURE 5.1 SCHEMATIC ARRANGEMENT FOR DETERMINATION OF PERMEABILITIES

FIGURE 5.2 RESULTS FROM PERMEABILITY TESTS FOR DETERMINATION OF $D_{K,e}$

$\frac{N_1 R'TL}{\Delta P}$ vs $\overline{P}$,

——— fresh pellets

– – – – carbonised pellets

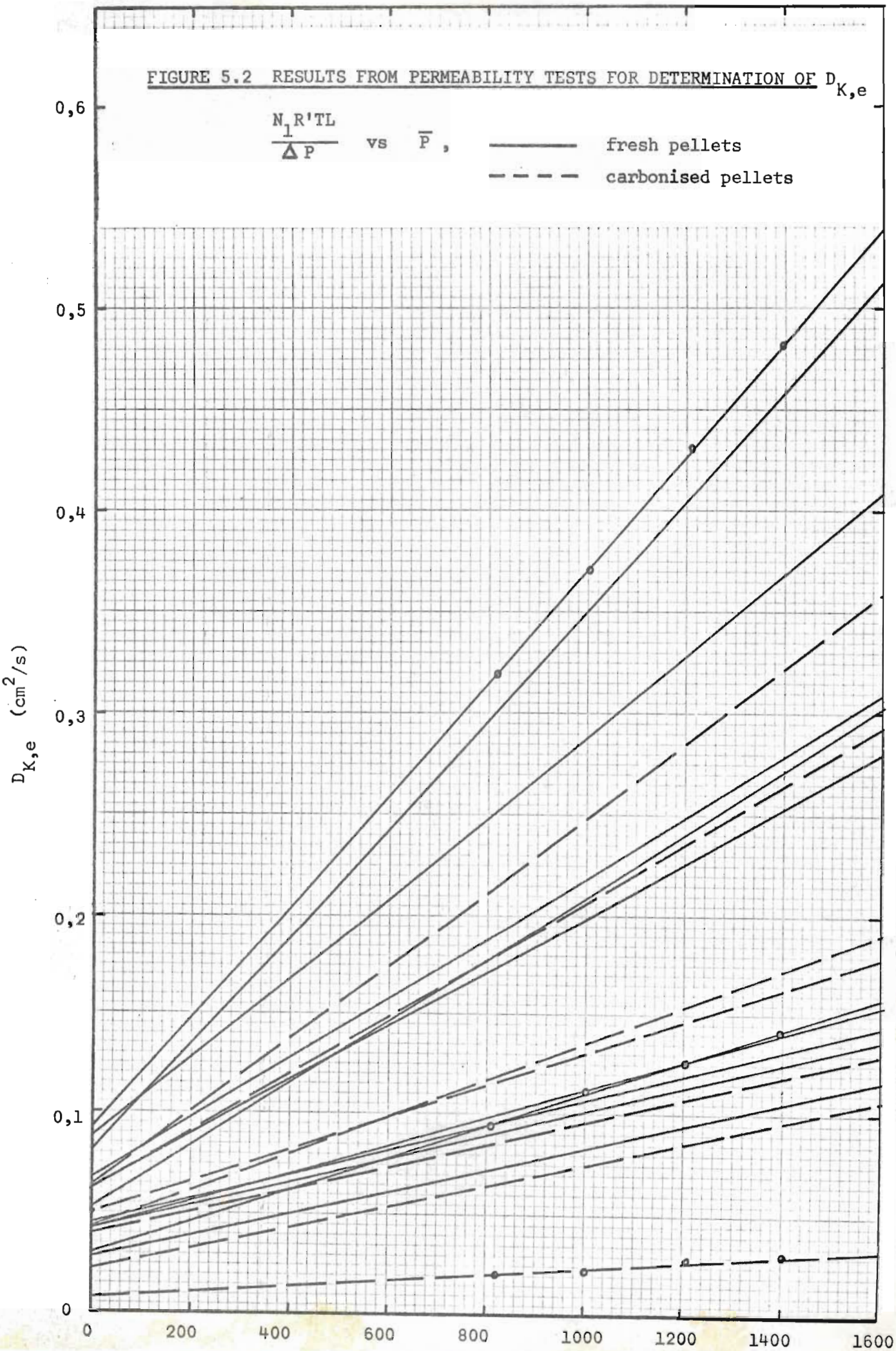

TABLE 5.1 KNUDSEN DIFFUSIVITIES.

$$D_{K,e} = K_D \cdot \sqrt{T}$$

Pellet	Temperature ^oK	Un/ Carbonised	$D_{K,e}$ cm^2s^{-1}	$K_D \times 10^2$ $cm^2s^{-1}T^{-\frac{1}{2}}$	Standard Deviation %
A	295	FRESH	0,063	0,365	2,17
B	298	"	0,081	0,468	2,05
C	298	"	0,088	0,511	2,25
D	298	"	0,028	0,164	6,41
E	298	"	0,030	0,173	4,67
F	298	"	0,068	0,385	2,29
G	296	"	0,045	0,260	1,24
H	295	"	0,042	0,244	0,88
I	296	"	0,093	0,539	3,21
J	295	"	0,042	0,242	0,72
K	295	"	0,053	0,308	3,15
			Mean	0,332±40%	
L	297	CARBONISED	0,040	0,232	3,21
M	297	"	0,065	0,378	2,00
N	298	"	0,044	0,253	3,20
O	299	"	0,050	0,290	2,86
P	296	"	0,022	0,127	3,67
Q	296	"	0,063	0,365	0,79
R	295	"	0,007	0,0423	14,2
			Mean	0,241±50%	

5.4 Bulk Diffusion Coefficient

Using data and methods based on the Lennard Jones potentials, the bulk diffusion coefficients, D_{12}, for common gases may be calculated with a better than 8% accuracy - Satterfield (1970).

The effective bulk diffusion coefficient is then

$$D_{12,e} = \frac{\varepsilon}{\tau} D_{12}$$

where ε, the void fraction for the pellet is 0,515 (Appendix 3.1). For τ a value of 2 is assumed. This figure is probably a bit low when compared with those reported by Satterfield on silica-alumina catalyst. A low figure will tend to increase the contribution by $D_{12,e}$ to the overall effective diffusion coefficient, but this effect will be shown to be small. Hence

$$D_{12,e} = D_{12}/4$$

It may then be shown that for a pressure of 1 atmosphere in the range of 500 to 800°K

$$4{,}50 < D_{O_2\text{-}N_2,e} < 9{,}91 \text{ cm}^2/\text{s}$$

$$3{,}55 < D_{O_2\text{-}CO_2,e} < 7{,}98$$

$$4{,}46 < D_{O_2\text{-}CO,e} < 9{,}75$$

$$4{,}40 < D_{O_2\text{-}H_2O,e} < 10{,}39$$

Now for a mixture of gases

$$D_{1m} = (1-y_1)\left(\sum_{j=2}^{n} \frac{y_j}{D_{1j}}\right)^{-1}$$

Since the diffusivity of oxygen in the different binary gas mixtures does not change appreciably and the gas mixture in the reactor has

nitrogen as its main component (+94%), it is found that $D_{lm,e}$ can be approximated by $D_{O_2\text{-}N_2,e}$.

5.5 Effective Diffusion Coefficient

Substituting the values obtained for effective Knudsen and bulk diffusion into equation (5.2) it is found that for the reaction conditions in the porous pellet, Knudsen diffusion is the major contributor to the overall effective diffusion coefficient. The effect of bulk diffusion on the overall diffusion coefficient ranges from about $1\frac{1}{2}$% at $500^{o}K$ to 1% at $800^{o}K$. In terms of equation (5.3), the expression for Knudsen diffusion, the experimental values indicate a mean pore diameter of about $1300\mathring{A}$. This is still considerably less than the length of the mean free path which for a typical gas molecule at atmospheric pressure and $750^{o}K$ is about $1600\mathring{A}$ (Hirschfelder et.al.1964). This indicates that Knudsen diffusion prevails. The effect of bulk diffusion is much smaller than the variations obtained in $D_{K,e}$. Incorporating it however, gives an overall effective diffusion coefficient

$$D_e = 2{,}8\times10^{-7}\sqrt{T}\ \ m^2/s.$$

5.6 Effective Diffusivity, Average Pore Size and Carbon Concentration

Assuming long narrow and straight pores, circular in cross section and considering only the curved surface, it may be shown that

$$\hat{r} = \frac{2\varepsilon_p}{\rho_p S}$$

Using a full B.E.T. method with nitrogen as an absorbent, the following data was obtained for S by Finkelstein (1969) for the catalyst used.

Fresh catalyst	289	m^2/g
Carbonised catalyst	235	m^2/g
Partly regenerated catalyst	262	m^2/g

The coefficient of variation was thought to be better than 3%. Using experimental values from section A3.1 this gives for fresh catalyst an average pore diameter of about 70Å. This compares badly with the 1300Å obtained from Knudsen diffusivities.

Porous catalyst pellets of the type used, are manufactured by compressing ground porous materials. This tends to give the catalyst pellets a pore size distribution with two distinct peaks. The smaller pores, less than say 200Å in diameter provide most of the internal surface area and the bigger pores which have diameters up to two orders bigger than the smaller ones, provide most of the cross sectional area for flow through the pellet. Most of the distance a gas molecule has to traverse to reach an active site, may be covered in the bigger pores. The effective diffusivities should therefore be associated with these bigger pores and the smaller pores with the B.E.T. results.

If the char consisted purely of cubical carbon atoms, then the thickness of a monolayer of the coke would be given by

$$\left(\frac{Mc}{\rho_c N_A v} \right)^{1/3}$$

Weast (1968-1969) reports a density of 1,8 - 2,1 g/cm^3 for amorphous carbon and 2,25 for graphite. These figures give a monolayer thickness of roughly 2Å. For S=235 m^2/g and assuming a monolayer of carbon, about half the available surface in the pellet would be covered for a carbon concentration of 5% by weight. However Hill (1972) indicates that the char is very much more complex than a monomolecular layer of carbon atoms

and Hall and Rase (1963) indicate that carbon deposits in particles rather than in layers. This indicates that pore blockages might occur. The experimental diffusivities in fresh and carbonised pellets do indicate that this does take place, however the effect is fairly small compared with the variations found for the fresh pellets and the effect has been ignored for this work.

CHAPTER 6

RESULTS AND DISCUSSION

In this chapter the results from the model will be dealt with first. The information obtained from the model will then be used to interpret the experimental results and show the validity of the model. The model will then be compared with existing models.

6.1 Computed Temperature Profiles

6.1.1 Introduction and the standard case.

Any model proposed for the regeneration of carbonised catalyst pellets is most conveniently evaluated for applicability by comparing the temperature profiles it predicts with those obtained experimentally. Not only is temperature an easily measured variable, it is also the most important one from a control point of view. Too high a temperature will permanently destroy the catalyst. It is also well known, and it will be shown again, that at too low temperatures the regeneration process is very slow and requires inconveniently long times. Most comparisons will therefore be done on a basis of temperature profiles. Unless otherwise specified in the remainder of this chapter, whenever reference is made to a temperature, this reference will be to gas temperatures. Gas temperature is also the one measured experimentally. According to the computed results, gas and solid temperatures normally differed by less than $10^{o}K$.

In order to demonstrate the effect of different parameters and

operational conditions a standard case is defined. This standard case is approximately the average condition used in the experimental program and uses the physical constants and expressions obtained in the appendices.

P - pressure - 1,057 N/m^2

Rp - pellet radius - 3,175 mm

L - reactor length - 0,914 m

D - diameter of reactor tube - 0,050 m

G - gas flowrate - 0,949 $kg/(m^2 s)$

To - inlet gas, initial bed and reactor jacket temperature - 783°K

y_o - oxygen mole fraction in inlet gas - 0,025

c_{wo} - initial weight fraction of carbon in pellet - 0,069

k - apparent thermal conductivity of the solid phase. Assumed zero.

U - overall wall heat transfer coefficient- 8,84 $W/(m^2 K)$

h_a - film heat transfer coefficient - $0{,}2638 \left(\frac{GT}{\varepsilon Rp} \right)^{\frac{1}{2}}$ $W/(m^2 K)$

k_g - film mass transfer coefficients for oxygen - $2{,}161 \times 10^{-5} \left(\frac{G}{\varepsilon Rp} \right)^{\frac{1}{2}} Tg^{1/3}$ kg mol/$m^2 s$.

c_e - effective specific heat of solid phase - $1{,}958 \times 10^3 + 0{,}782\ Ts$ J/(kg K)

c_g - specific heat of gas phase - $0{,}9181 \times 10^3 + 0{,}2721\ Tg$ J/(kg K)

Mg - molecular weight of inlet gas = $32\ y_o + (1-y_o)28$ kg/kg mol

ε - bed void fraction - 0,395

m - order of combustion reaction with respect to oxygen - 1

n - order of combustion reaction with respect to carbon - 1

k_o - natural log of pre-exponential factor - 9,53

E - activation energy - $0{,}785 \times 10^8$ J/(kg mol)

$(-\Delta H)$ - heat of combustion - $1{,}97 \times 10^8 + 2{,}83 \times 10^8 x$ J/(kg K)

x - fraction of carbon burned to CO_2 = 1/(1+q)

q - ratio of CO to CO_2 produced - Fq exp (7,83 - 6241/T)

F_q - factor determining the level of CO to CO_2 produced - 1,0

ΔZ - increment along length of reactor - 0,0254 m

ΔR - radial increment in pellet - $3{,}53 \times 10^{-4}$ m

Δt - time increment - 10 s

NOCC - number of correction cycles - 2

Unless otherwise specified these are the values used for computed results.

The gas temperature profiles obtained for standard conditions are shown in figure 6.1. A temperature peak is produced which increases in height as it moves down the bed. In this as well as in all other simulations, profiles are calculated using a time increment of 10 seconds, but the results are recorded and plotted at intervals of 30 seconds for high and intermediate flowrates, and at intervals of 60 seconds for low flowrates.

The internal consistency of the model as demonstrated by the computed material and energy balances will be dealt with in section 6.3. The effect of assuming zero axial conduction and the stability of the numerical solution to changing increments in space and time are discussed in section 6.4.

6.1.2 The effect of the reaction rate parameters k_o and E

The effect of varying k_o, the natural log of the frequency factor, on the gas temperature profiles at different positions in the bed, is shown

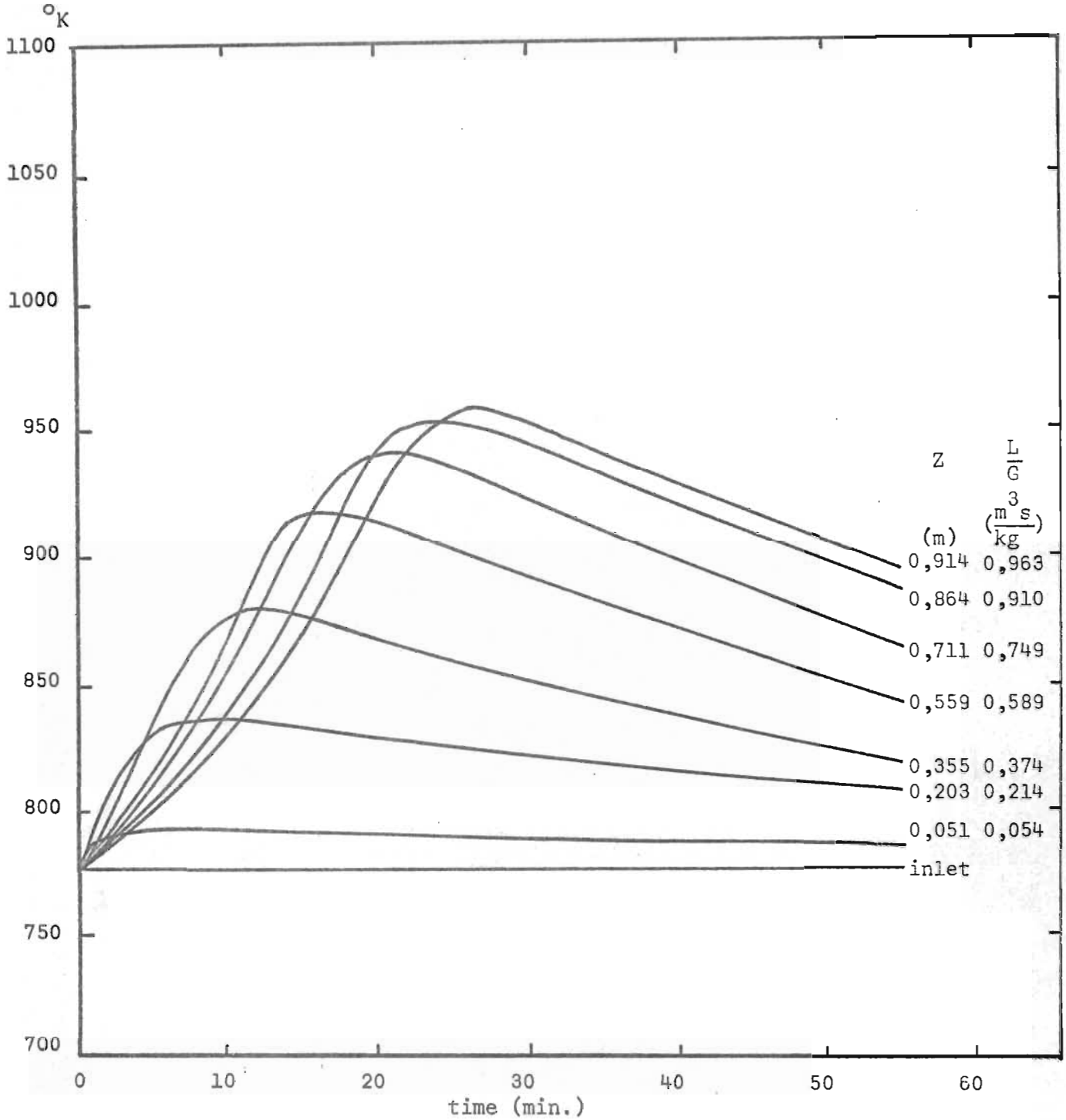

FIGURE 6.1 TEMPERATURE PROFILES FOR STANDARD CONDITIONS.

in figure 6.2. Increasing k_o, the general activity increases, the peaks become steeper and the peak heights at 0,355m become greater relative to that at 0,914m.

The effect of varying E, the activation energy is shown in figure 6.3. In order to maintain the same degree of activity in the different simulations, k_o has to be changed in sympathy with E. For purposes of demonstrating the effect of E, k_o was adjusted so as to give the same temperature peak height at the outlet of the bed.

The effect of temperature changes on the reaction rate is increased with increasing values of E. Since higher reaction rates produce higher temperatures, the effect of temperatures become "auto catalytic". This is readily understood from the form of the Arrhenius reaction rate expression. At low values of E the temperature effect is weak and the activity is fairly uniform throughout the reactor and depends mainly on the concentrations of oxygen and carbon. At higher values of E, the temperature effect on the activity in the bed is stronger and this will exaggerate the temperature rise. In terms of the comparison, using the outlet temperature peak height as a standard, this gives rise to two effects. The higher the value of E used, the higher the temperature level required for the reaction to start and once started, the higher the rate at which the reaction rate increases. Expressed differently, higher E's give steeper temperature peaks and a greater spread of the relative peak heights occurring at different points in the reactor. These effects are very much more pronounced than similar effects obtained when varying k_o alone. The combined effect of k_o and E affects mainly the relative peak heights at different points in the reactor, and it affects the shape of the curves. k_o (adjusted for the level of the activation energy) affects the average activity of the reactor.

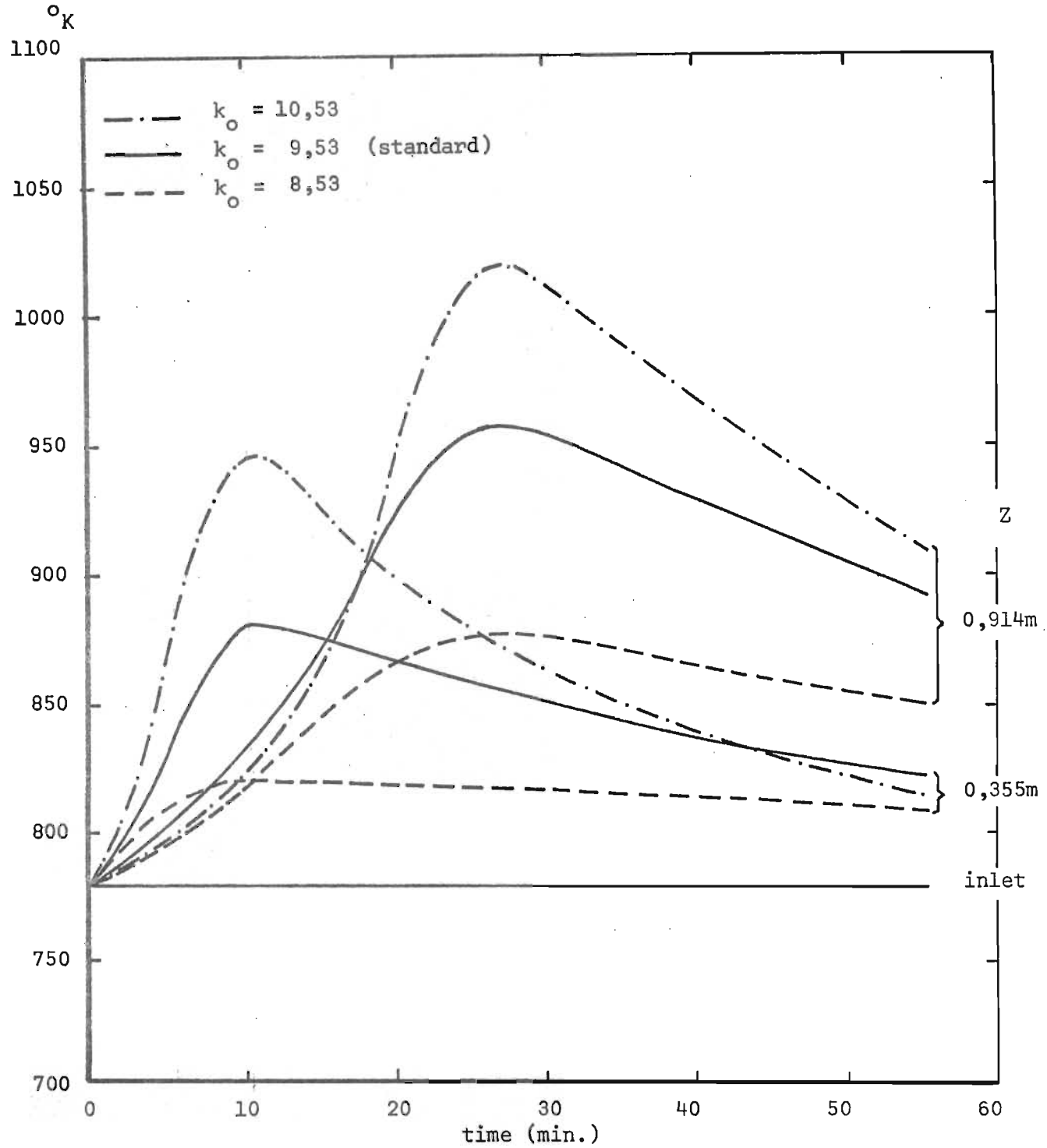

FIGURE 6.2 TEMPERATURE PROFILES FOR VARIOUS FREQUENCY FACTORS

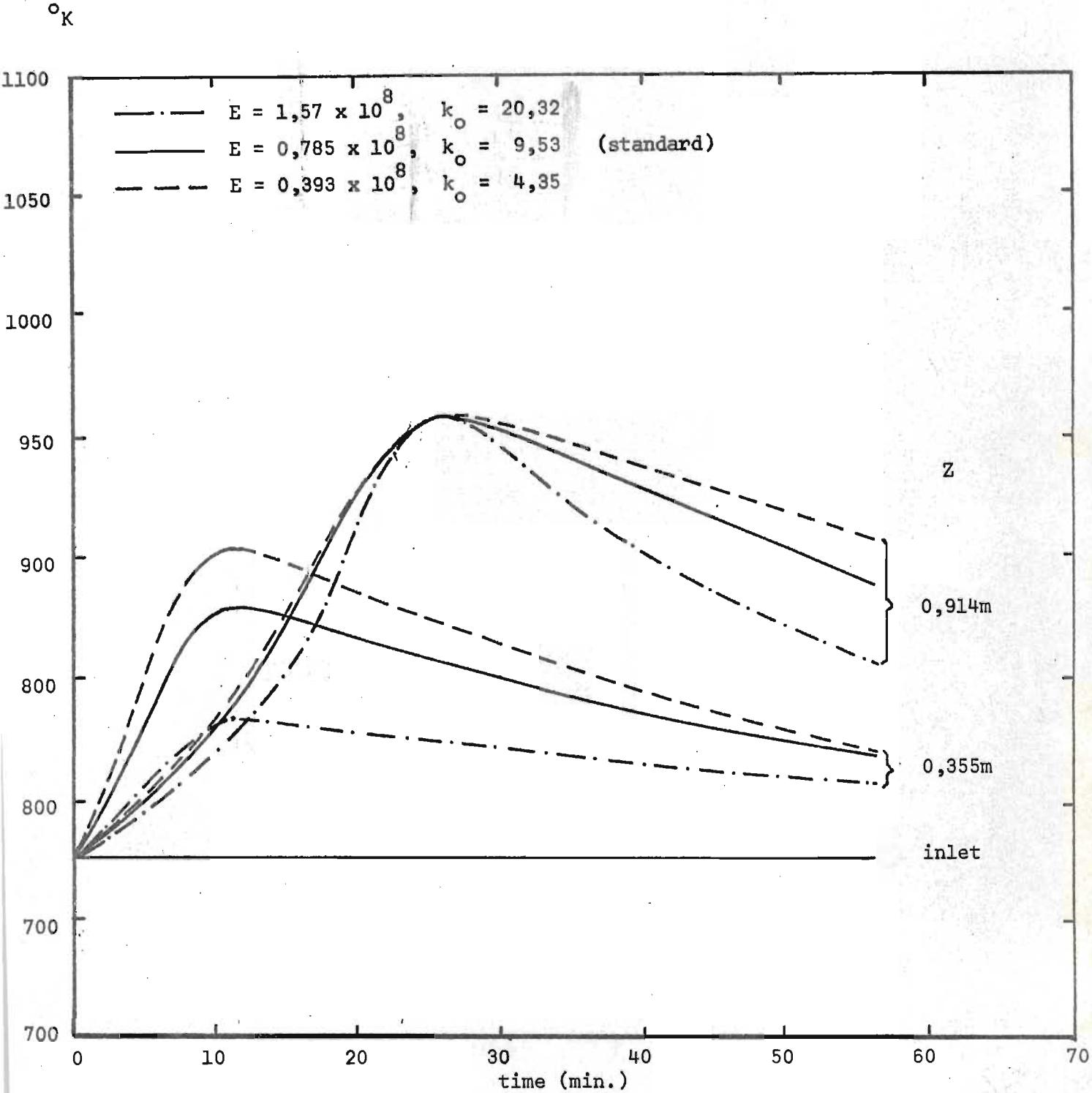

FIGURE 6.3 TEMPERATURE PROFILES FOR VARIOUS ACTIVATION ENERGIES

Although any reaction rate can be obtained by an infinite number of combinations of k_o and E, rates at different temperatures or as in our model, a specific relative peak height for two points in the bed, is uniquely defined by only one combination of k_o and E, provided no other variables could have an effect on relative peak heights.

These are important considerations when computed and experimentally obtained temperature profiles are compared. If the model is applicable then the shape of the experimental curve and the relative peak heights at different points in the reactor should be criteria to be used in evaluating the values of k_o and E appropriate to the conditions in the reactor.

At stationary state when a completely developed burning zone moves down the bed, the peak height will be constant and relative peak heights cannot be used. Plotting temperature profiles as functions of distance moved in the reactor, then produces curves, from the trailing edge of which, values of k_o and E might be inferred.

6.1.3 The effect of the relative production of CO and CO_2 (q)

The heats of reaction of the combustion of carbon to CO_2 and that to CO, differ considerably. Depending on the relative rates of production of CO and CO_2 in the reactor, more or less heat is produced and higher or lower temperature profiles may be expected. In this work q, the relative rate of CO and CO_2 produced, is given in section A1.2 as

$$q = Fq \exp (7{,}830 - 6241/Ts)$$

where Fq normally has a value of 1,0. Levels of q may be changed through Fq. The effect of varying levels of CO/CO_2 production is shown

in figure 6.4.

On changing Fq from 0,5 to 1,5, the relative peak height, and the shapes of the temperature profiles are hardly affected. For the considerable change in Fq, the temperature changes are relatively small. Fq has an effect on the temperature profiles similar to that of k_o but to a much smaller degree.

6.1.4 The effect of overall wall heat transfer coefficient (U)

The rate at which heat is being lost through the wall, is going to influence the temperature levels attained in the bed. The effect of varying values of the overall wall heat transfer coefficient, U, is shown in figure 6.5.

The effect of U on the shape of the temperature profiles and on the relative peak heights between points in the reactor at 0,355m and 0,914m is relatively small. U depends mainly on the thermal conductivity of the insulating alumina wool around the reactor. The range through which U varies in figure 6.5, is much greater than the error in data on alumina wool as provided by the manufacturers, is likely to be. U is therefore likely to be a parameter of minor importance when comparing predicted with experimental temperature profiles.

6.1.5 The effect of flowrate, G, and the ratios $L/G^{\frac{1}{2}}$ and L/G

The effect of different flowrates on the gas temperature profiles, is shown in figure 6.6. As the flowrate increases the temperatures in the bed rise quicker but not to the same extent. In the case of the lower flowrate, the stationary state temperature has practically been reached at z = 0,914m.

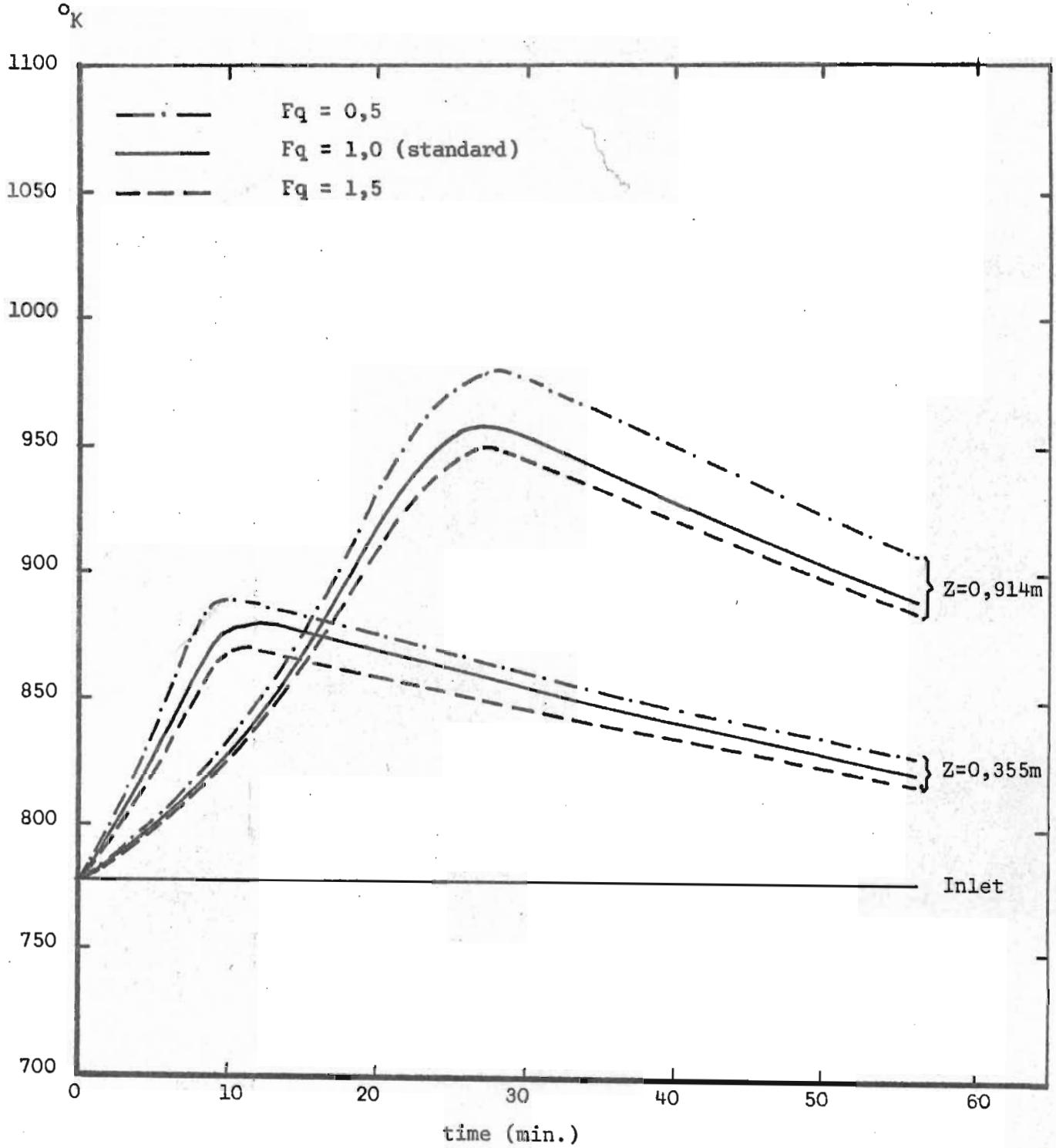

FIGURE 6.4 TEMPERATURE PROFILES FOR VARIOUS VALUES OF $\frac{CO}{CO_2}$ (Fq)

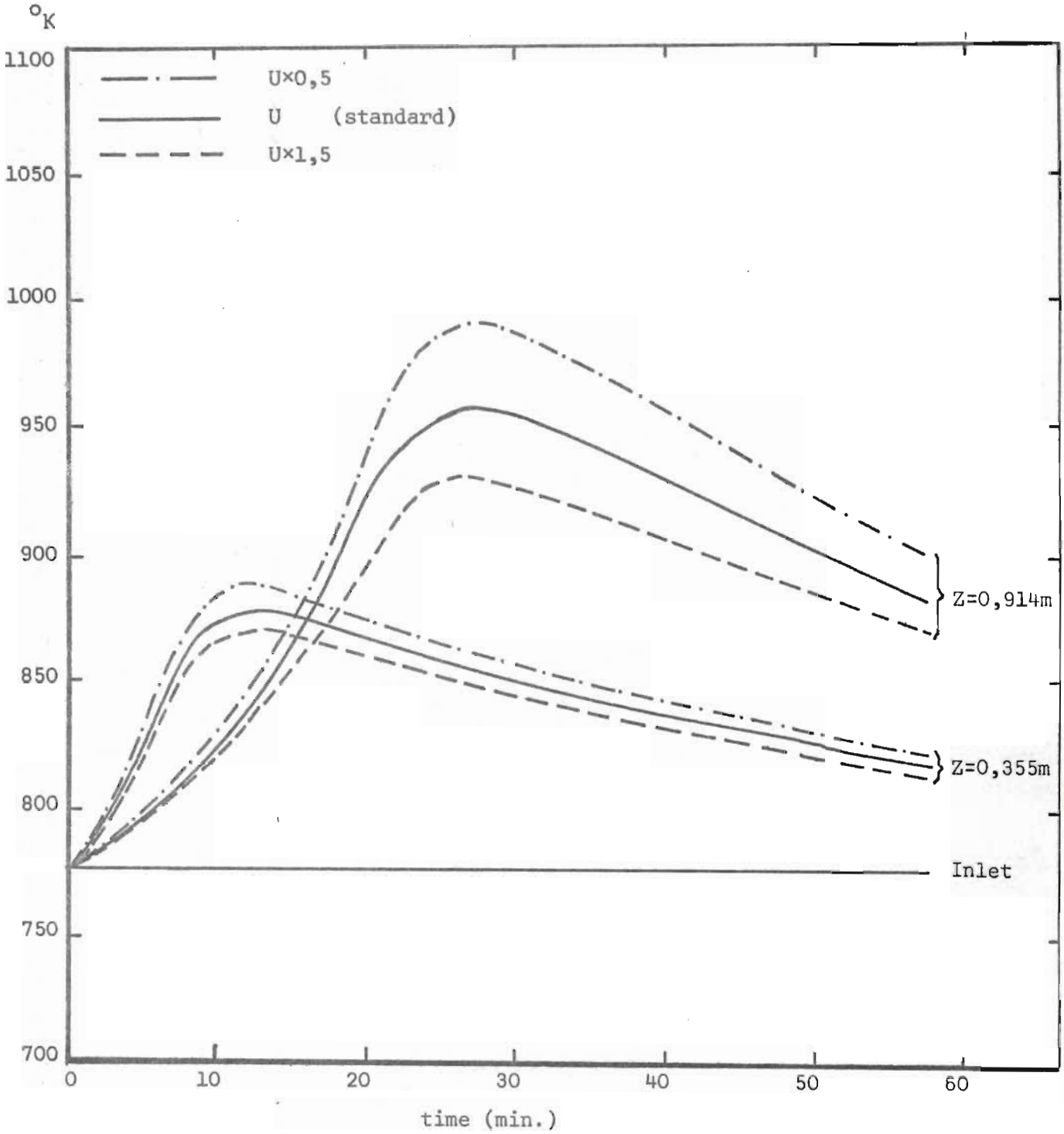

FIGURE 6.5 TEMPERATURE PROFILES FOR VARIOUS WALL HEAT TRANSFER COEFFICIENTS (U)

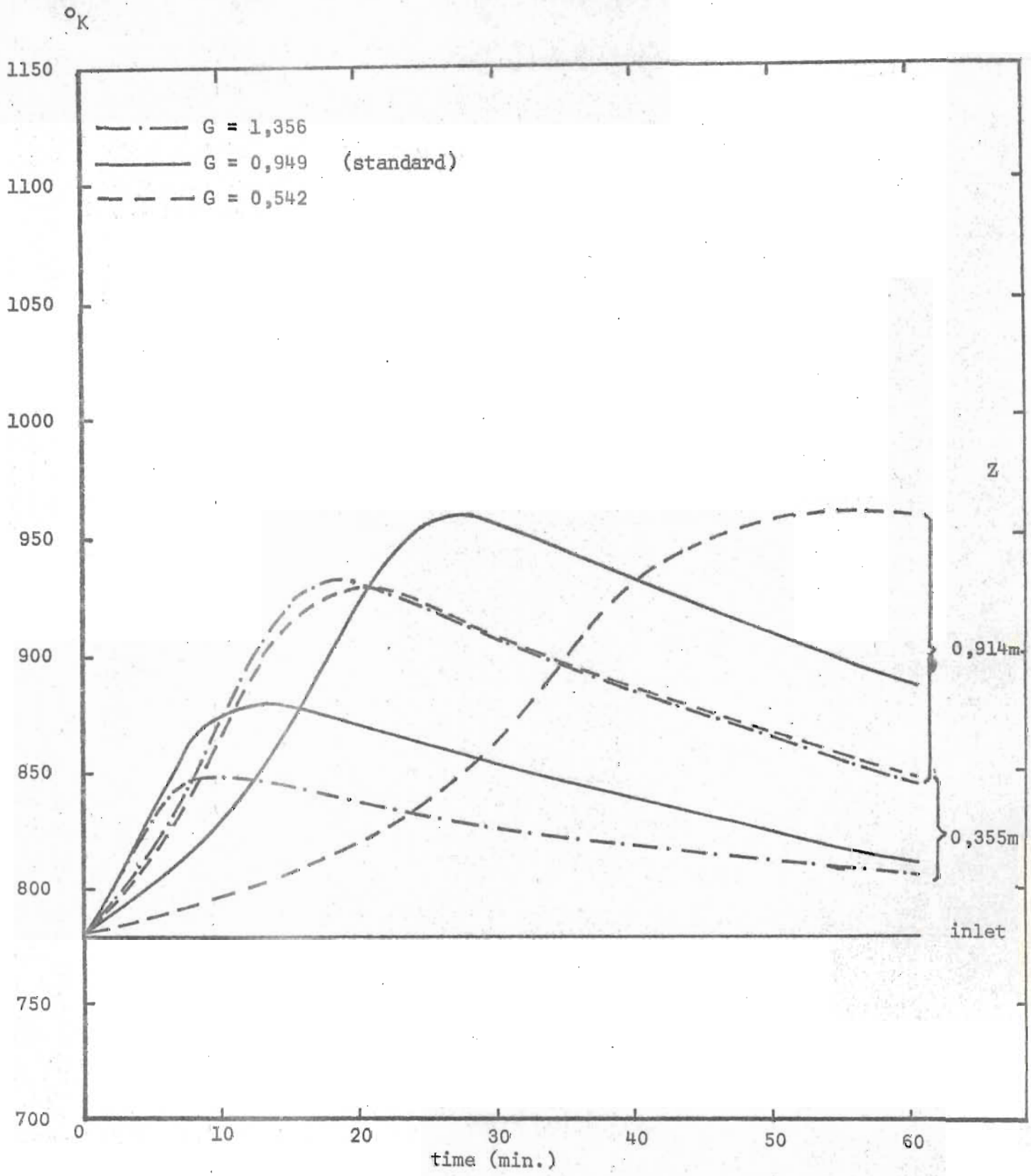

FIGURE 6.6 TEMPERATURE PROFILES FOR VARIOUS FLOWRATES (G)

In section 3.5, the dimensionless forms of the basic differential equations were considered. Two schemes were proposed in which $\bar{z}$, the dimensionless distance along the length of the bed was obtained as a function of $Z/G^{\frac{1}{2}}$ and Z/G respectively. Temperature profiles for various flowrates G, holding $L/G^{\frac{1}{2}}$ constant, are shown in figure 6.7. Holding $L/G^{\frac{1}{2}}$ constant does not give profiles invariant with G. Similar profiles with L/G constant instead, were found to be practically invariant with G. The simulated profiles were valid for all values of bed position Z, and gas flowrate G, over a substantial range. Provided the appropriate value of L/G is used, the profiles may be obtained from the standard curves given in figure 6.1. The maximum deviations from the standard curve for different flowrates and L/G less than 0,965 m^3s/kg, were found to be

Flowrate $kg/(m^2s)$	0,136	0,542	0,949	1,356	2,712
Max. deviation ^oK	17	4	standard	3	7

These results agree with the findings of Johnson (1956). He showed that when certain assumptions are made, the most important of which is probably that of a temperature independent reaction rate, then the inverse proportionality between the effects of gas flowrate and length of reactor is exact.

6.1.6 Adiabatic gas temperature profiles.

From a practical point of view, the important application of the model is for the adiabatic case. With this in mind the effect of different operational variables was computed. As standard adiabatic conditions those of the 'standard' case were chosen except for the overall wall

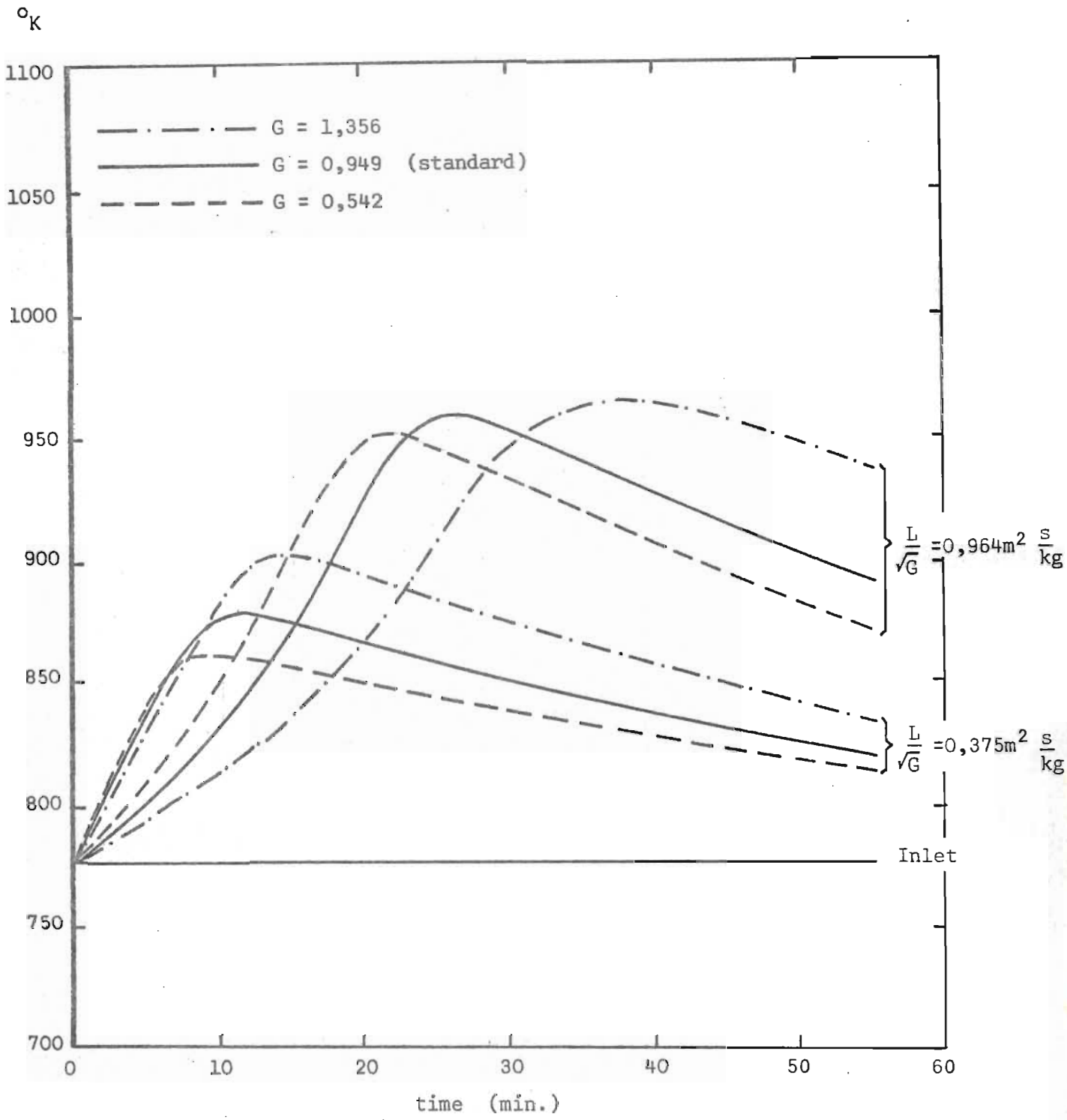

FIGURE 6.7 TEMPERATURE PROFILES FOR DIFFERENT FLOWRATES AND $L/\sqrt{G}$ RATIOS

heat transfer coefficient which was reduced to zero and the inlet oxygen concentration which was reduced from 2,5 to 2,0 % to compensate for the reduced heat losses. The gas temperature profiles obtained for standard adiabatic conditions are shown in figure 6.8 for different positions in the reactor and associated L/G ratios.

6.1.6.1 The effect of inlet gas temperature.

The effect of different inlet gas temperatures on the temperature profile 0,914m from the entrance of the bed is shown in figure 6.9. The initial bed temperature was taken equal to the inlet gas temperature.

As the inlet temperature is lowered, the general activity in the bed decreases till at an inlet temperature of 672^{o}K the maximum temperature rise achieved at 0,914m from the entrance is about one third of that obtained with an inlet temperature of 811^{o}K. The increase in activity with inlet temperature slows down at higher inlet temperatures, because at higher rates of combustion the oxygen supply to the bed becomes the limiting factor. Provided the bed is long enough or the flowrate small enough, temperatures will be able to build up in an adiabatic bed and some distance from the entrance, when the temperatures become high enough, the rate of combustion will depend only on the oxygen concentration in the inlet gas.

Compared with that of the inlet temperature, the effect of the initial bed temperature on the temperature profiles is small. As shown in section 3.2.4, the ratio of heat produced per heat accumulated in a pellet is of the order of 20 to 1. The effect of the initial temperature profile on the temperature profiles in the bed will therefore be important only in the initial stages of regeneration.

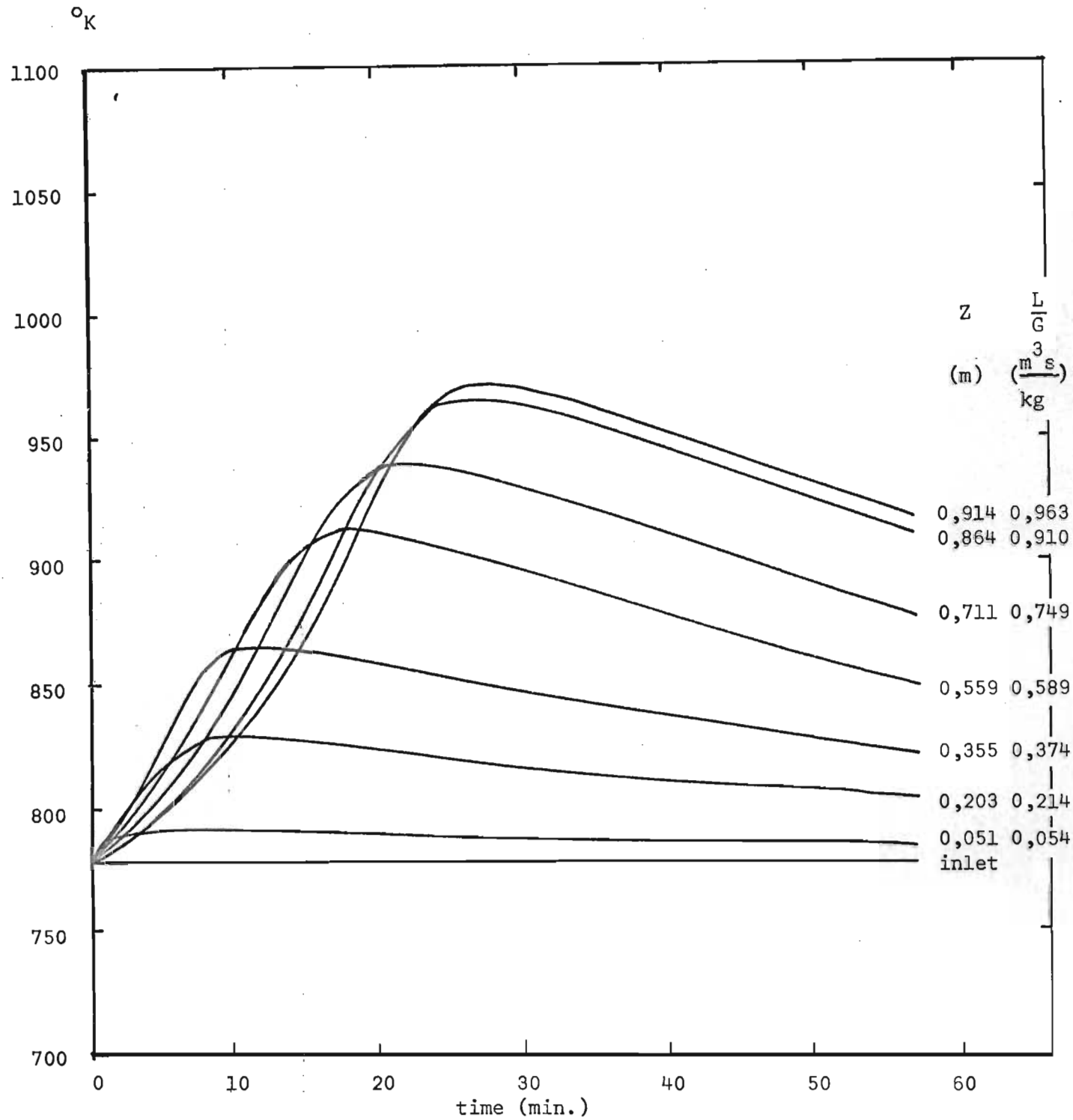

FIGURE 6.8 ADIABATIC TEMPERATURE PROFILES FOR STANDARD CONDITIONS (y_o =0,02)

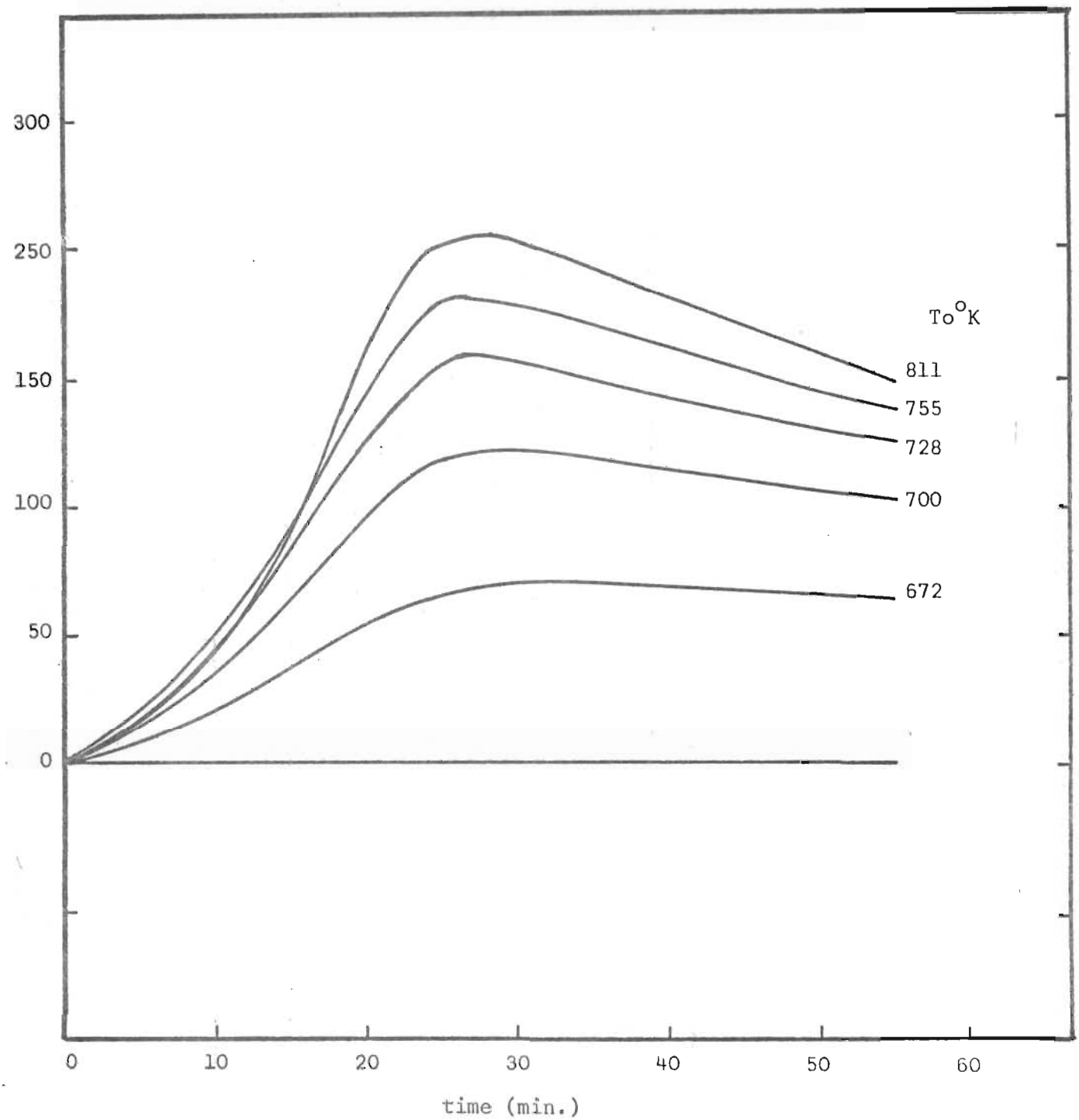

FIGURE 6.9 ADIABATIC TEMPERATURE PROFILES AT OUTLET OF THE BED (Z=0,914m) FOR VARIOUS INLET TEMPERATURES (To)

6.1.6.2 The effect of initial carbon concentration c_{wo}

The effect of different initial carbon concentration on the gas temperature profiles is shown in figure 6.10 for two points in the bed. The concentrations chosen were those used in the experimental program. As expected higher temperatures were obtained for higher carbon concentration.

6.1.6.3 The effect of inlet oxygen concentration.

The effect of different inlet oxygen concentrations is shown in figure 6.11 for a position 0,914m from the entrance of the bed. It shows typical first order behaviour of the general activity in the bed with inlet oxygen concentration, in that peak heights are approximately proportional to the inlet oxygen concentration.

By suitable control of the inlet oxygen concentration, it is possible to maintain the bed at a high level of activity without exceeding a certain arbitrary temperature level. Figure 6.12 shows the behaviour of the temperatures in the bed when the inlet oxygen is started at a high value in order to reach a high activity quickly; it is then reduced to prevent temperatures becoming too high and is then increased again as the temperatures drop, to maintain a high rate of combustion. The rate of combustion tends to decrease as the carbon is removed.

It is interesting to note the rate at which carbon is removed from different parts of the bed. Levels of carbon content in the bed as functions of bed position and time for the above simulation, were computed and shown in figure 6.13. It takes about 90 minutes to remove 90% of the carbon at the entrance, whereas it takes only 61 minutes halfway in the bed.

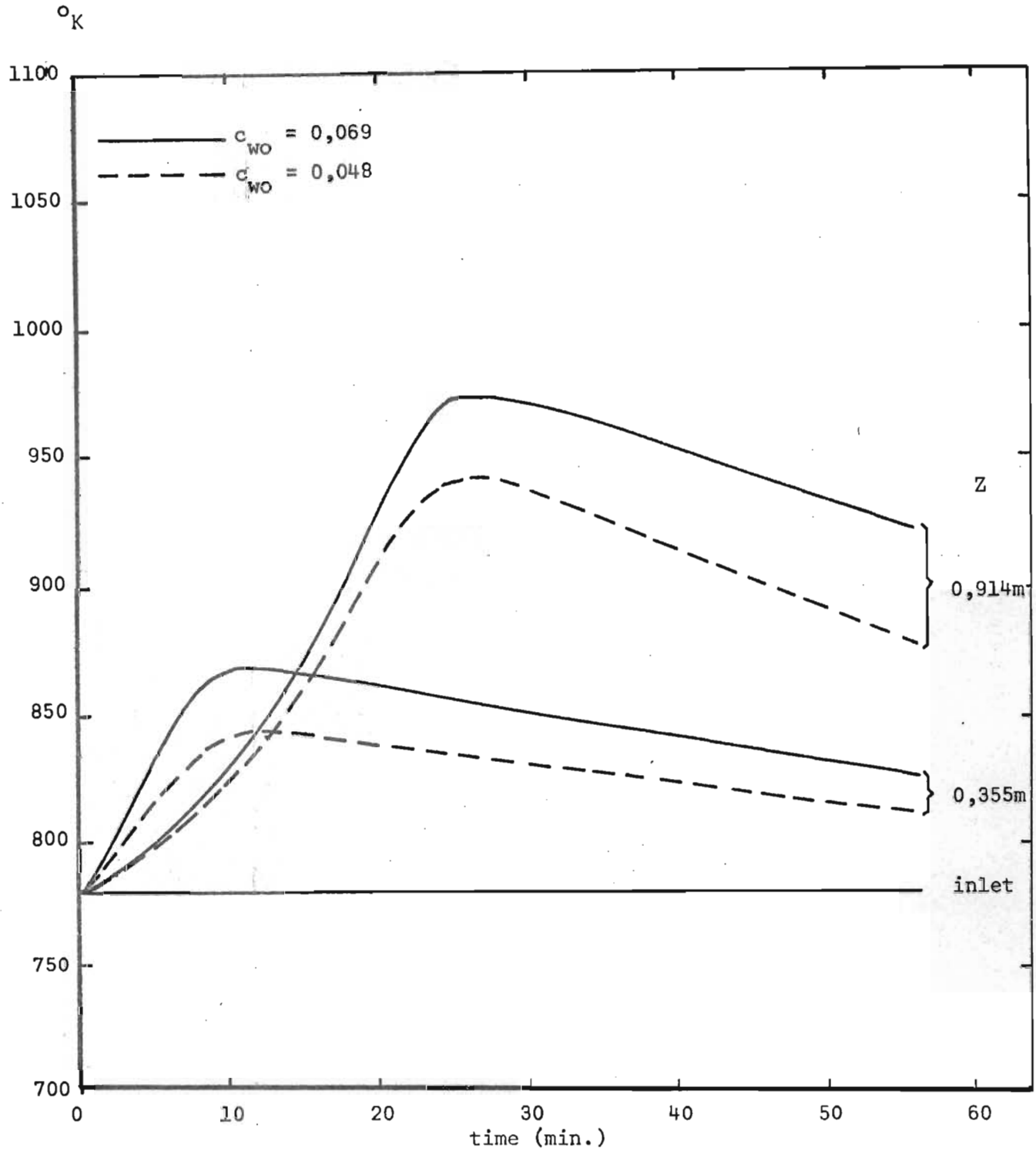

FIGURE 6.10 ADIABATIC TEMPERATURE PROFILES FOR VARIOUS INITIAL CARBON CONCENTRATIONS (c_{wo})

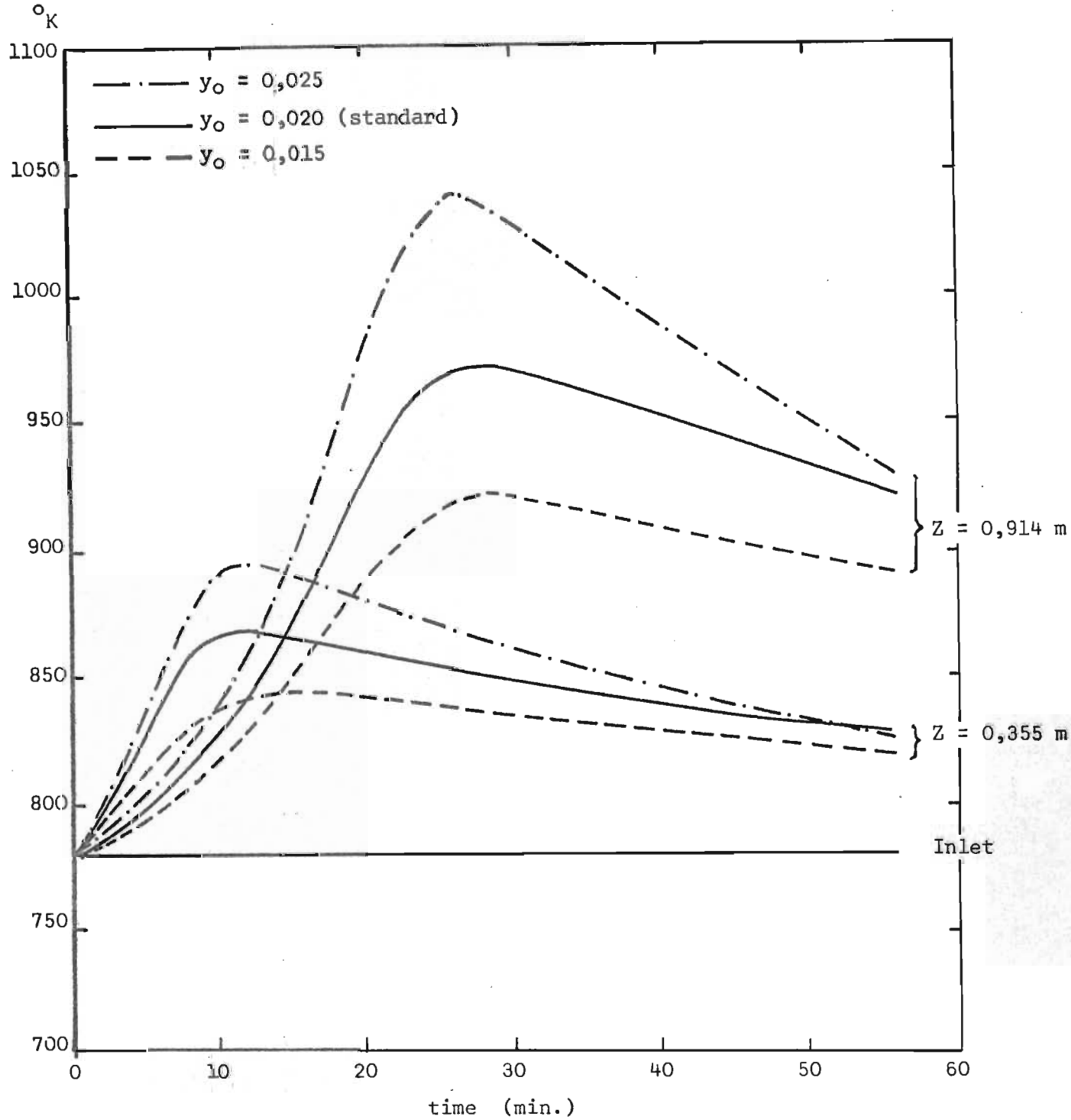

FIGURE 6.11 ADIABATIC TEMPERATURE PROFILES FOR VARIOUS INLET OXYGEN MOLE FRACTIONS (y_o)

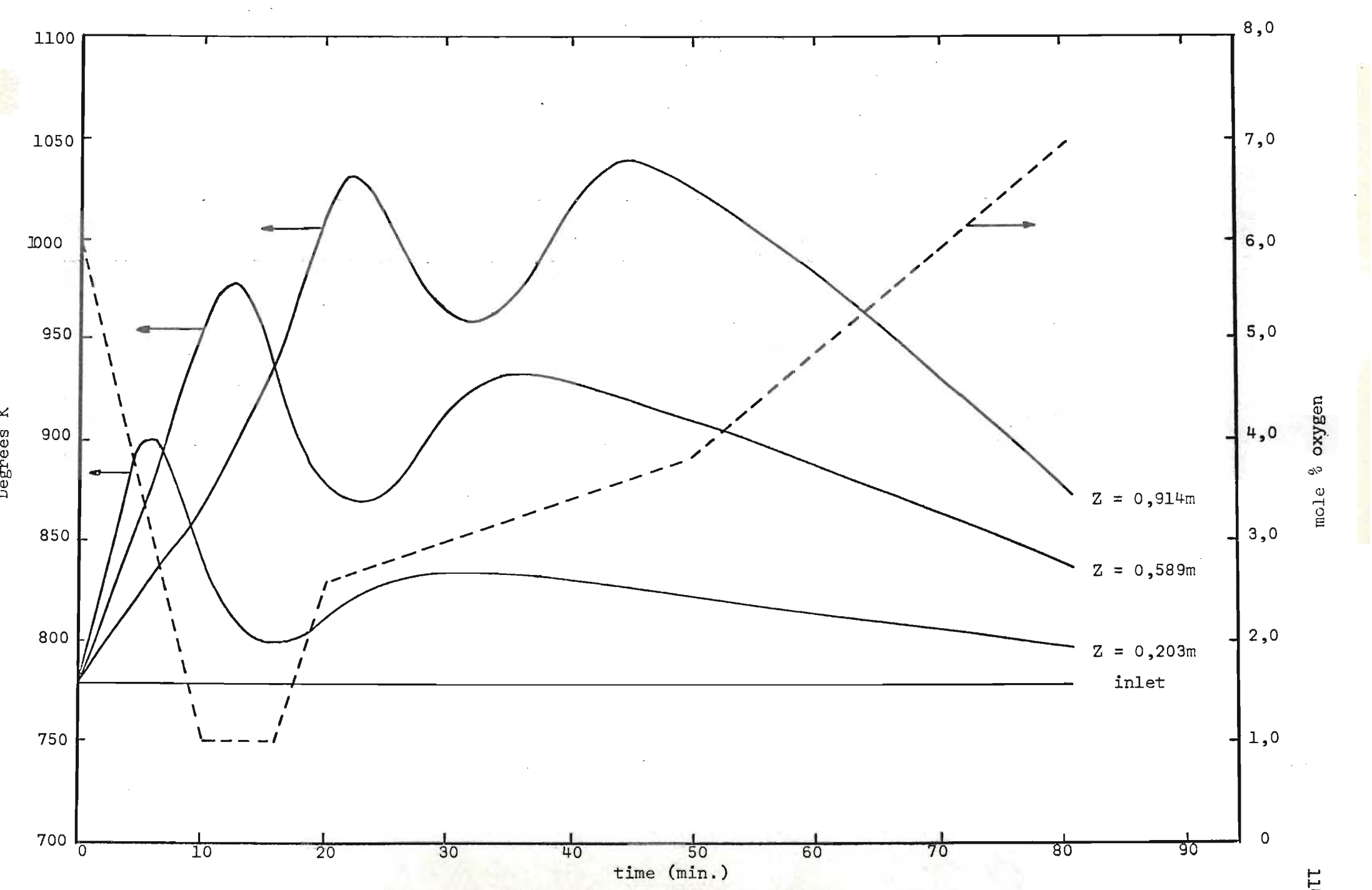

FIGURE 6.12 TEMPERATURE PROFILES FOR VARYING OXYGEN INLET CONCENTRATION

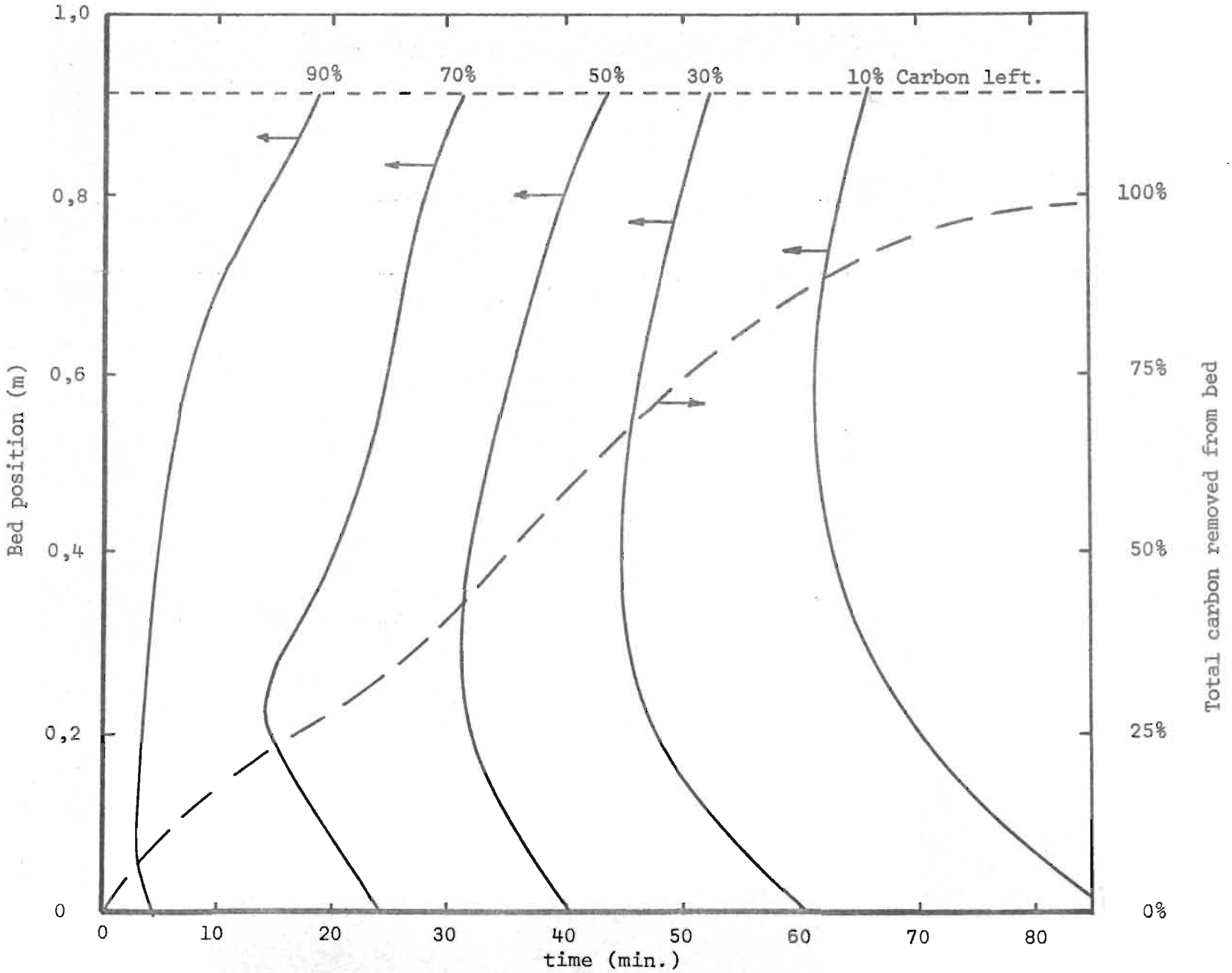

FIGURE 6.13 CARBON CONTENT IN THE BED AS A FUNCTION OF BED POSITION AND TIME

6.1.7 Stationary state temperature profiles.

In figure 6.14, the temperature profile computed for standard conditions are shown for a bed 2,82m long. This is three times the length of the bed used in our investigation. The locus of the peak height as it moves along the reactor length with time, is indicated by the dotted line. It passes through a slight peak before it settles at a stationary value. This is the same sort of behaviour, although in a less extreme form, as that predicted by Olson's model (1962) which is based on the shrinking core and diffusion controlled combustion of carbon. The initial peak is due to an initial combination of high oxygen concentration at the inlet and carbon concentration at or close to the surface of the pellets at the entrance of the bed, when diffusion is not yet controlling to the same extent as it will when stationary burning zone profiles have been developed.

Making use of the fact that temperature profiles are invariant with respect to distance along the bed or with flowrate provided the ratio L/G is kept constant, it follows from these curves that at standard conditions in our bed, the computed temperature peak will still be rising as it leaves the bed at the high flowrate of 1,356 kg/(m^2s). At the intermediate flowrate of 0,949 kg/(m^2s), the peak will almost have reached its peak at the outlet of the bed. For the low flowrate of 0,542 kg/(m^2s), the peak has practically reached the stationary peak height as it leaves the bed.

6.2 Flow Reversal and Regeneration Time

As already intimated in section 6.1.6.3, carbon is removed faster from parts of the bed where high temperatures maintain high reaction rates.

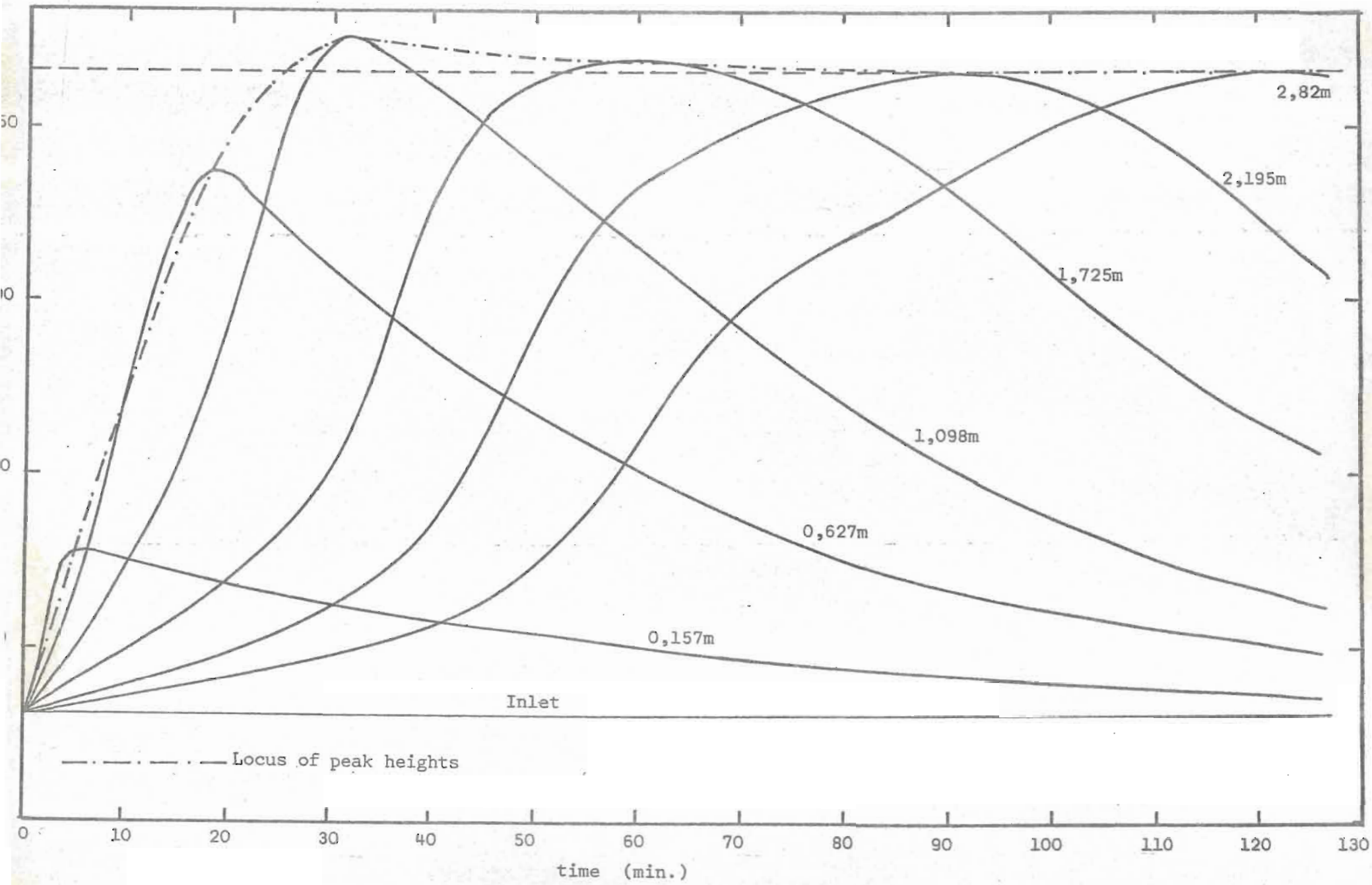

FIGURE 6.14 STATIONARY STEADY STATE FOR STANDARD RUN SHOWING INITIAL PEAK

Close to the entrance, where the temperature remains low and the combustion rate may therefore be slow, carbon is removed at a slower rate compared with the rest of the bed. When the reactor length to flowrate ratio is such that most parts of the bed are being regenerated simultaneously (i.e. for a relatively short bed or high flowrates, or both), this gives rise to the situation that after some time most of the remaining carbon left, is atthe entrance. High temperatures at the entrance would accelerate the carbon removal. This may be achieved by reversing the flowrate when the bed closer to the outlet is still at a fairly high temperature. The heat generated is then used to heat up what used to be the entrance, to increase the reaction rate.

The effect of flow reversal and reversal times on temperature profiles and rate of carbon removal was computed for the conditions that occurred in run HL1 (for designation of run see table 6.1). The computed temperature profiles are shown in composite figure 6.15 and the total carbon present curves for different reversal times as a function of time are shown in figure 6.16. As can be seen from the computed results, depending on the required degree of regeneration, there is a flow reversal time for which the regeneration time is a minimum, which may be up to 30% below normal regeneration time. The results of these computations are tabulated below.

	Time required for regeneration				
Reversal time (min.):	10	12,5	15	17,5	21,7
Degree of regeneration (%)					
80	16,5*	18,8	20,3	22,0	24,2
85	19,6*	20,3	21,8	24,0	27,2
90	23,4	22,3*	23,7	26,3	31,3
95	>33,0	33,0	28,0*	31,5	>33,0

* denotes minimum regeneration times.

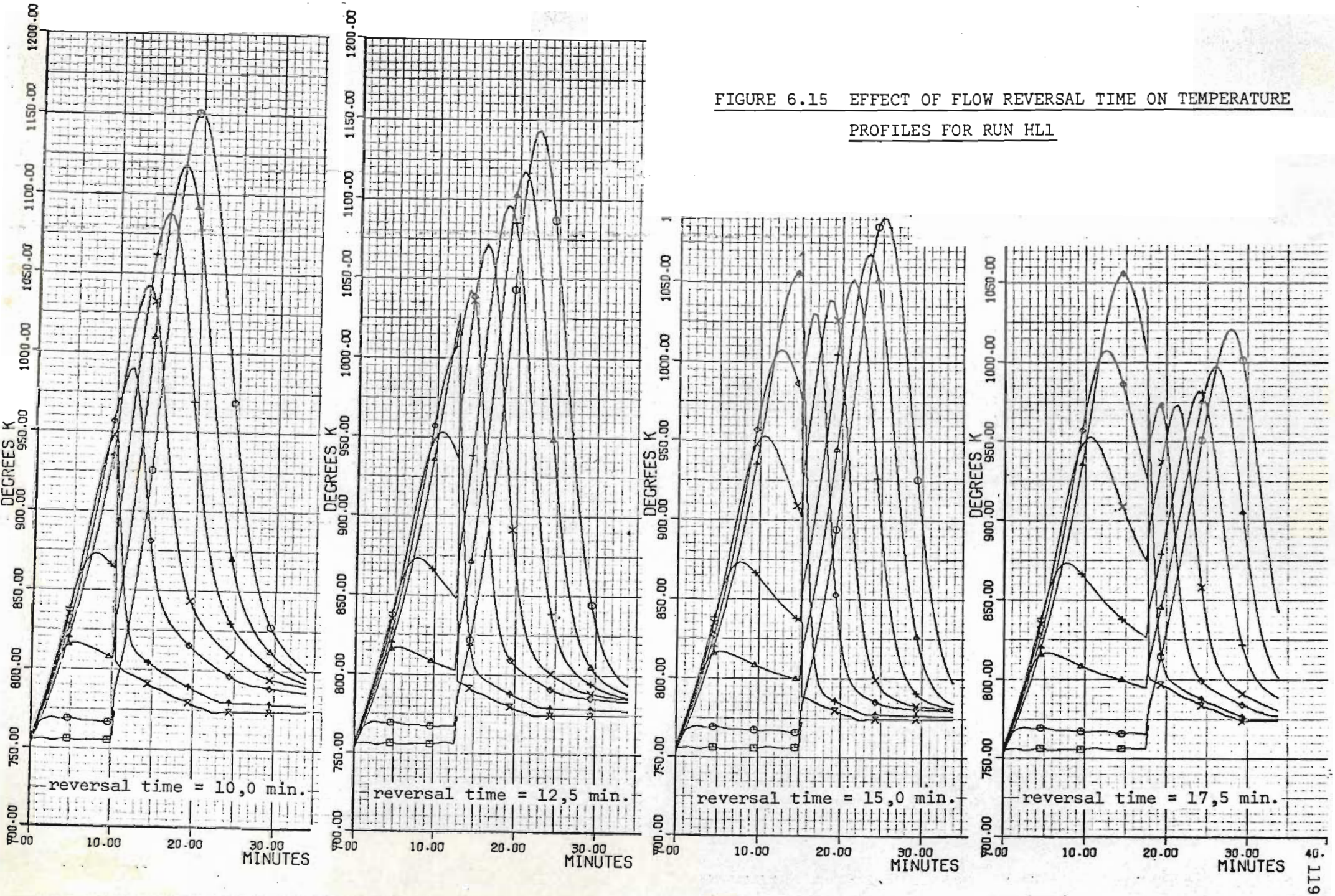

FIGURE 6.15 EFFECT OF FLOW REVERSAL TIME ON TEMPERATURE PROFILES FOR RUN HL1

FIGURE 6.16 FRACTION OF INITIAL CARBON LEFT IN BED FOR VARIOUS FLOW REVERSAL TIMES FOR RUN HL1

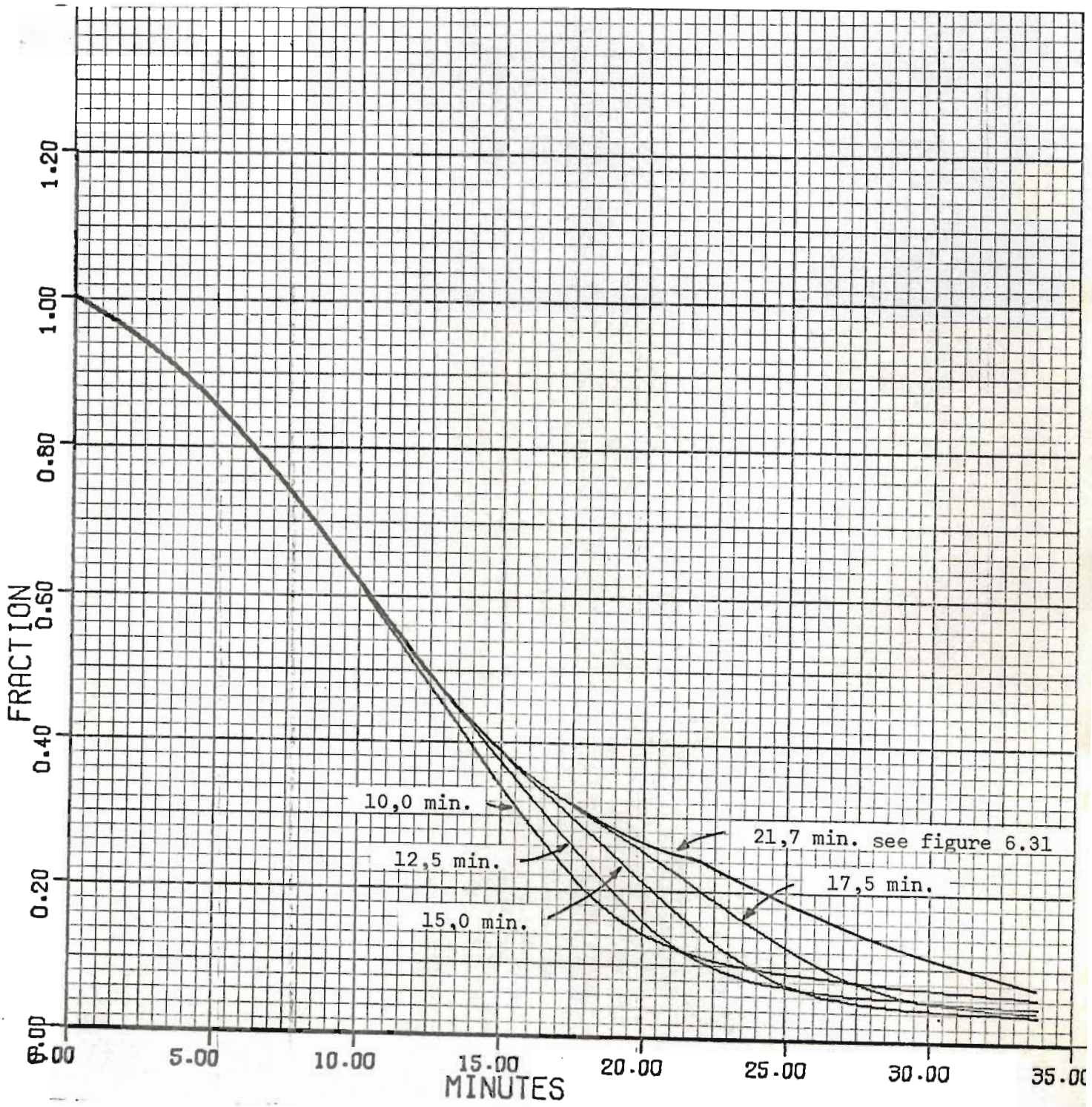

It appears that the optimum time for flow reversal, for run HL1 at least, is approximately when the temperature peak travelling in the bed, emerges from it. It should be noted that at that stage enough carbon was removed from the end of the bed so that on flow reversal no higher peaks developed at this end of the bed. In practice this is important, because this means that if a temperature peak travelling back into the bed after flow reversal, is going to rise beyond acceptable levels, this will not occur immediately and enough time should be available to take preventative action.

The concept of reversal of flow to reduce regeneration time is interesting when the practice at the South African Coal, Oil and Gas Corporation (SASOL) is considered. They have to regenerate three clay treatment beds stacked on top of each other and each just under one metre long. For regeneration purposes their normal practice is to treat the stack as a single bed and pass the same gas through all three beds. The regeneration time was about double the normal process time. In order to speed up regeneration, they were seriously considering regenerating the three beds individually by splitting the feed and introducing it to the reactor between the beds. With these shortened beds, provided high enough flowrates are used, reversal of flow should considerably reduce the overall regeneration time.

6.3 Material and Energy Balances

Material and energy balances were computed for all computed profiles. They have only been recorded, however, for those cases where actual experimental runs were simulated.

6.3.1 Total carbon present and the rate of its removal at any instant.

In the "A" part of figures 6.18 to 6.39 the computed total unconverted carbon still present, is shown for the relevant runs. Of more interest is the rate at which this carbon is removed. This is obtained quite simply by differentiating the curve for total carbon present with respect to time according to equation (4.1). The initial and final rate values cannot be computed in this way. A three point forward and a three point backward finite difference expression as used by Lapidus (1962) were used to calculate respectively the initial and final rate values from the total carbon present curve. For convenience of representation a normalised overall rate of carbon removal is plotted, which is obtained by dividing all the removal rate values by the largest value encountered for a specific simulated run.

For all the simulations, the computed overall rate of carbon removal shows a steady increase as the temperature in the bed rises and hence the temperature dependent reaction rate increases. After some time so much carbon has been removed however, that the rate which is also carbon concentration dependent, cannot be sustained and the overall rate of carbon removal decreases up till the time of flow reversal. At flow reversal, depending on the amount of carbon still left in the bed, the decrease in overall rate of carbon removal is arrested or when a fair amount of carbon is still present, the rate of removal may increase again quite considerably due to a combination of high temperatures and carbon and oxygen concentrations at what used to be the entrance of the bed.

At the onset of the regeneration period there is a slight break in the rising rate of carbon removal pattern. During the first time increment the calculated curve shows a drop from the initial value. For the second

and successive time increments the pattern is as described above. This anomaly occurs in the material balance rather than in the model itself because it is due to the manner in which the total carbon present in the bed at any time is calculated. Calculating the initial carbon present from the total bed volume, average bed density and uniform initial carbon concentration and comparing this with the initial carbon present computed by numerical integration of the carbon profile in the bed through the concave upward curve of r^2c in equation (3.25), it is found for simulation run II, that the integrated result was 0,51% low with 9 radial increments in the pellet. In the model, the initial value of the carbon present is found from the average bed condition whereas at all other times the carbon present has to be obtained by numerical integration. The error thus introduced during the first increment will show up as an increased rate of carbon removal. As regeneration proceeds and the (r^2c) curve becomes less concave, the error will decrease.

At flow reversal there is a similar spike in the carbon removal curve. This is similarly owing to the crude numerical approximations not being able to represent accurately the drastic changes in oxygen profiles and carbon removal rates that occur at flow reversal.

6.3.2 Yg_J, the oxygen concentration in the outlet gas as a fraction of that in the inlet.

These curves computed for the relevant runs, may be found in the "A" parts of figures 6.18 to 6.39. Roughly, the Yg_J curves are inversions of the overall rate of carbon removal curves. This is to be expected since the rate of oxygen consumption is directly proportional to the overall rate of combustion of carbon. The curves do not, however, contain the spurious peaks that occur in the overall rate of carbon removal

curves, because Yg_J comes directly from the model whereas the carbon removal rate curve depends on the material balance which is only approximate in the initial stages and at the time of flow reversal.

6.3.3 XR, the material and energy balance check parameter.

Except for an anomalous dip in the curves at the initial stages of the simulations, the XR curves, shown in the "A" parts of figures 6.18 to 6.39 for the relevant runs, are close to unity. For most of the simulated runs, XR is normally well within 1% of unity, indicating that the model is consistent with respect to material and energy balances.

The anomaly at the initial stages is due to the manner in which x_M and x_H are computed (section 4.7.4). During the initial period both x_M and x_H will be low due to the error in the evaluation of the initial overall rate of carbon removal. This error was described in section 6.3.1. Both x_M and x_H should be equally affected however, and the ratio XR should therefore be unchanged. The difference between the initial values of x_M and x_H is due to the way in which the trapezoidal rule for integration has been used during the first increment in time, to compute the oxygen consumed (section 4.7.1) and the heat lost through the outlet gas and through the reactor walls (section 4.7.3). For all three quantities the rate at the end of the initial time increment is used as a mean rate for that increment. Remembering that a pseudo steady state assumption was made for the oxygen profile in the gas phase, then for oxygen consumption, this is a fair assumption as the change in oxygen concentration in the outlet gas during the initial time increment is not great as indicated by the Yg_J curve. For the heat lost in the outlet gas and through the walls, this assumption is not so good, since at the

beginning of the initial time increment the rate of heat loss for both is zero. Due to the manner in which the material and energy balances have been calculated therefore, relatively more heat is lost, than the equivalent amount of oxygen consumed. This increases the value of x_H over that of x_M giving an XR ratio less than unity. As the errors become only small fractions of the total heat accounted for and the oxygen consumed after subsequent time increments, the error in XR will tend to zero. It should be noted that the error is not part of the model proper but of the material and energy balances which are used to check the internal consistency of the model.

During flow reversal, small changes are noticed in the XR ratios. As for the anomaly in the initial portion of the curve the error is owing to the rates of consumption of oxygen and heat loss through the outlet gas not changing to the same extent. The changes are so small however, that they are of no consequence within the overall picture.

6.3.4 x', the instantaneous fraction of carbon converted to CO_2 in the outlet gas.

The x' curves, computed for the relevant simulation runs may also be found in the "A" parts of figures 6.18 to 6.39.

Values for $x'_{i-\frac{1}{2}}$ are calculated from computed values of x_H and x_M as indicated in section 4.7.5. They are slightly offset when plotted, when they are treated as x'_i values. The error introduced in this manner is minimal. The initial value of x'_i cannot be found this way, but may be directly calculated from the expressions for x and q in section A1.2, assuming the nominal initial temperature to be uniform for the bed at time is zero.

Apart from an anomaly after the first increment the x' values decrease as the general temperature level in the bed increases and x' increases as the general temperature level in the bed drops. This is in accordance with the behaviour predicted by the expressions for x and q given in section A1.2.

The anomaly at the end of the first increment in time is due to the initial error in the evaluation of the total carbon present in the bed and the errors in the evaluation of the oxygen consumed and heat lost through the walls and through the outlet gas. The reasons for these errors have been dealt with in the previous sections. Since x' is obtained by a process of differentiation, the error will only show up when it is introduced. Similar to that of the overall rate of carbon removal, the x' curve has spurious peaks at the time of flow reversal. They are however more closely related to the small changes in the XR curves noticed at flow reversal time.

A small positive stepchange occurs in the x_M value at flow reversal. Although the change is small, e.g. for run II it is less than 2/3%, because the x' curve is obtained through a process of differentiation of the average value for x_M and x_H, it shows up as a spurious peak in the x' curve.

6.4 The Accuracy of the Model

6.4.1 Effect of computational parameters on the computed profiles.

For all the simulated runs the following computational parameters were used :

ΔZ = 0,0254 m (37 grid points)

$\Delta R = 3{,}53 \times 10^{-4}$ m (10 grid points)

Δt = 10 seconds.

Two correction cycles were used per prediction.

The numerical solution of the model was stable with respect to ΔZ, ΔR and Δt. The effect of changing these parameters was computed using the conditions for run II given in table 6.1. Halving ΔZ, the spatial increment along the bed length, the computed temperature profiles changed by less than $0{,}1^{\circ}K$. Halving Δt, the increment in time, the computed temperature profile changed by less than $1{,}4^{\circ}K$. Using 8 increments in R, the radial position in the pellet, instead of 9, tended to raise the temperature profiles but never more than $1{,}3^{\circ}K$. Using 4 correction cycles, gave temperature profiles within $1{,}4^{\circ}K$ of those obtained with 2 corrector cycles. Normally during an experimental run, temperatures would range through a few hundred degrees. The increments used in Z, R and t and the number of correction cycles used were therefore completely adequate for simulation purposes.

6.4.2 The effect of axial conduction.

The effect of axial conduction of heat in the bed on the computed temperature profiles was also investigated. It was found that on ignoring axial conduction for the conditions of run II, where the flowrate of $0{,}949$ kg/(m^2s) was used, that the change in temperature profiles, at any time, was never more than about $1^{\circ}K$. Since this change was accompanied by a saving in computer time of more than 9%, the axial conduction of heat was ignored for all the reported simulations.

6.5 Experimental Results

6.5.1 Experimental conditions.

The experimental conditions with respect to gas flowrate, initial carbon concentration, inlet oxygen concentration and the nominal base temperature, are given in table 6.1. The nominal base temperature is the average of the inlet temperatures and the initial temperatures of the bed. The conditions given in table 6.1 were also used in the model to simulate the experimental runs. Table 6.1 also gives the natural log of the frequency factor needed in the Arrhenius rate expression in the model, in order to get as close agreement between the experimental and simulated runs, as possible.

The name of a run is designated by two alphameric characters. The first indicates the gas flowrate used. H, I and L indicate high, intermediate or low flowrate respectively. The last alphameric character indicates the level of the nominal base temperature and is also H, I or L depending on whether the lebel is high, intermediate or low. If more than one run was performed at the same nominal flowrate and temperature, an extra numerical character is added at the end of the name. For some runs the correspondence between experimental and simulated temperature peak positions could be improved by adjusting the flowrate used in the simulation. The corrected flowrate used and the associated frequency factor are also tabled and these simulations are indicated by adding (C) to the name of the run.

A special run done at high flowrates but at an "ultra" low nominal temperature, was named HUL.

6.5.2 Experimental temperature profiles.

The temperature profiles for the runs tabulated in table 6.1 are plotted in the "B" parts of figures 6.17 to 6.39. Although temperatures were recorded at 15 second intervals, the experimental points are shown at 60 second intervals for the experiments done at intermediate and high gas flowrates and at 120 second intervals for the low flowrate experiments. It was done this way to prevent overlapping of plotted points and to keep the experimental plots legible. Since the experimental curves were very smooth there is no loss of information except for a slight loss at the peaks of the profiles where points are more widely spaced.

The decision as to when to reverse the flow was a fairly arbitrary one. Computed results (section 6.2) suggested that optimum reversal time is just after the temperature peak has travelled through the bed. On the other hand the tails of the temperature profiles during normal flow were useful for comparing the experimental with computed results. A compromise was made for most of the runs so that the experimental and computed results could be compared and the effect of reversal time could also be noted. For runs LI1, HL1, HI and HH1, however, the flow was reversed at a fairly late stage in the experiment. For runs IL2 and HL2, figures 6.26 and 6.33, the flow was reversed soon after the temperature peak had passed through the bed.

6.5.3 Experimental outlet oxygen concentration profiles.

These are given in the "A" parts of figures 6.18 to 6.39. The outlet gas concentration is expressed as a fraction of the inlet gas oxygen concentration.

TABLE 6.1 EXPERIMENTAL CONDITIONS, FREQUENCY FACTORS AND FIGURE NUMBERS

Run	Initial Carbon Wt. Fraction	Inlet O_2 Mol. Fraction	Nominal Base Temp. °K	Nominal		Corrected		Figure Number
				Flowrate $kg(m^2s)$	ln(frequency factor)	Flowrate $kg(m^2s)$	ln(frequency factor)	
LL	6,9	2,8	755	0,542	9,34			6.18
LL(C)	"	"	"			0,461	9,14	6.19
LI1	4,8	4,0	775	0,542	9,79	0,542	9,79	6.20
LI2	6,9	3,0	777	0,542	9,24			6.21
LI2(C)	"	"	"			0,407	8,94	6.22
LH	4,8	2,2	808	0,542	10,59			6.23
LH(C)	"	"	"			0,475	10,45	6.24
				Average	9,74 ± 0,62	Average	9,58 ± 0,70	
IL1	4,8	3,7	755	0,949	9,54	0,949	9,54	6.25
IL2	6,9	3,0	761	0,949	9,64			6.26
IL2(C)	"	"	"			0,773	9,44	6.27
II	6,9	2,9	785	0,949	9,49			6.28
II(C)	"	"	"			0,841	9,29	6.29
IH	4,8	3,0	808	0,949	9,74	0,949	9,74	6.30
				Average	9,60 ± 0,12	Average	9,50 ± 0,19	
HL1	4,8	6,7	755	1,356	9,29			6.31
HL1(C)	"	"	"			1,763	9,59	6.32
HL2	6,9	3,5	752	1,356	9,04			6.33
HL2(C)	"	"	"			1,017	8,74	6.34
HI	4,8	3,0	778	1,356	9,24	1,356	9,24	6.35
HH1	4,8	4,2	810	1,356	10,09			6.36
HH1(C)	"	"	"			1,559	10,19	6.37
HH2	6,9	2,8	808	1,356	9,34			6.38
HH2(C)	"	"	"			1,220	9,14	6.39
				Average	9,40 ± 0,40	Average	9,38 ± 0,55	
HUL	6,9	5,0	731	1,356				6.17

TABLE 6.2 Legend for Experimental and Simulated Temperature Profiles.

Temperature Profiles.

Experimental profiles are given by points and the associated simulated profiles are given by solid lines identified by the same points. (When confusion between an experimental point and a point identifying a line is possible, this occurs only when the two profiles are almost identical and confusion is not serious.)

- ⊡ - profile at the bottom of the bed
- ⊙ - profile 0,051 m above bottom of the bed
- △ - profile 0,203 m above bottom of the bed
- \+ - profile 0,356 m above bottom of the bed
- × - profile 0,559 m above bottom of the bed
- ◇ - profile 0,711 m above bottom of the bed
- ↑ - profile 0,864 m above bottom of the bed
- ⧖ - Profile 0,914 m above bottom of the bed (top of bed)

Fraction Curves.

Experimental points	Calculated curves	
	⊙	- total carbon present in the bed.
	△	- normalised rate of carbon removal
⊗	×	- outlet oxygen as a fraction of inlet oxygen concentration.
2	Z	- x', the instantaneous fraction of carbon burned to CO_2 in the outlet gas
	↑	- XR, $\bar{x}_M / \bar{x}_H$

- G - gas flowrate kg/(m^2s)
- C_o - initial carbon concentration in bed kgC/kg of catalyst
- Y_o - mole fraction of oxygen in the feed gas
- T_o - nominal feed gas temperature ^oK
- k_o - natural log of the pre-exponential factor.

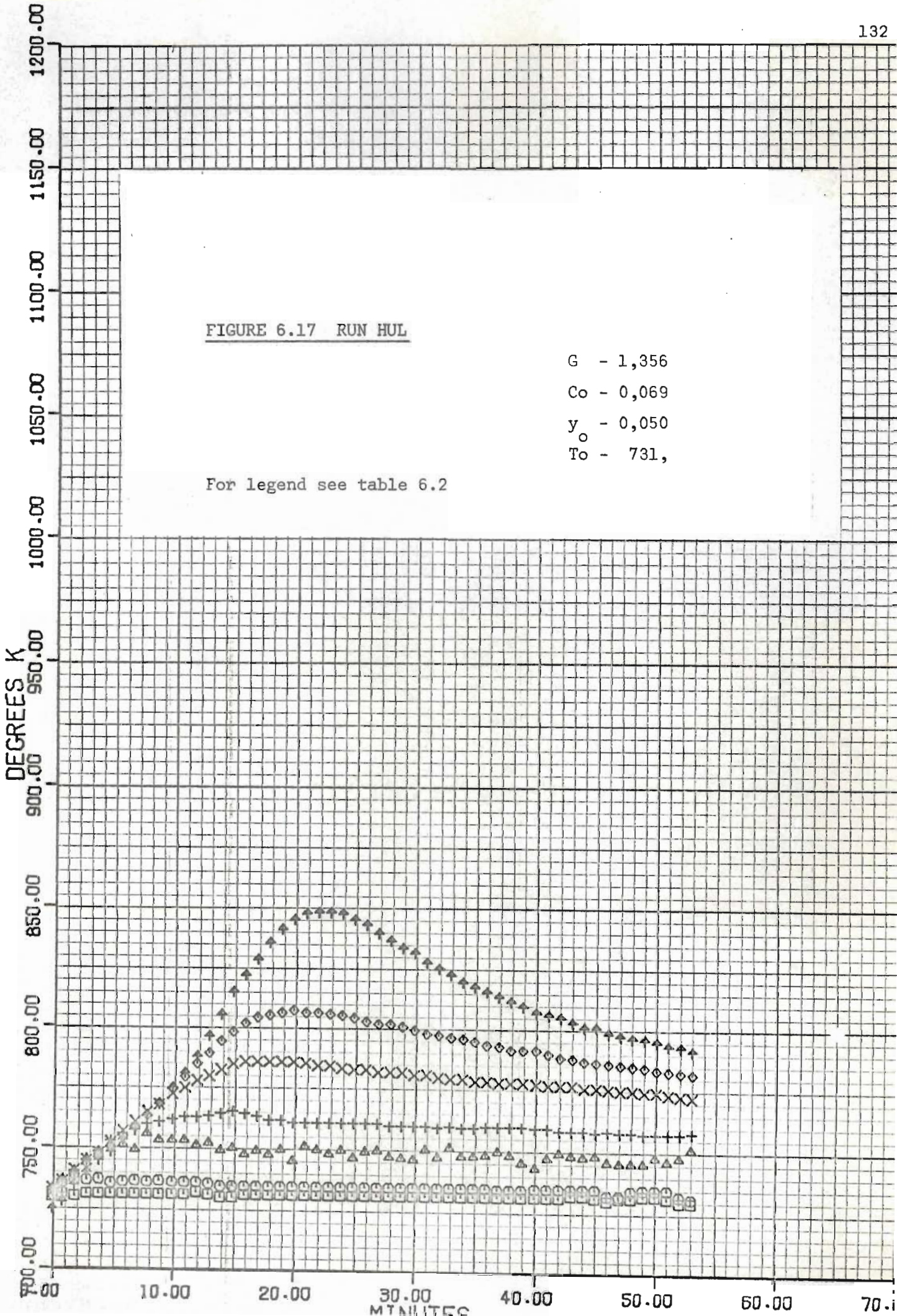

FIGURE 6.17 RUN HUL

G - 1,356

Co - 0,069

y_o - 0,050

To - 731,

For legend see table 6.2

FIGURE 6.18 RUN LL

G - 0,542

C_o - 0,069

y_o - 0,028

To - 755,

k_c - 9,34

For legend see table 6.2

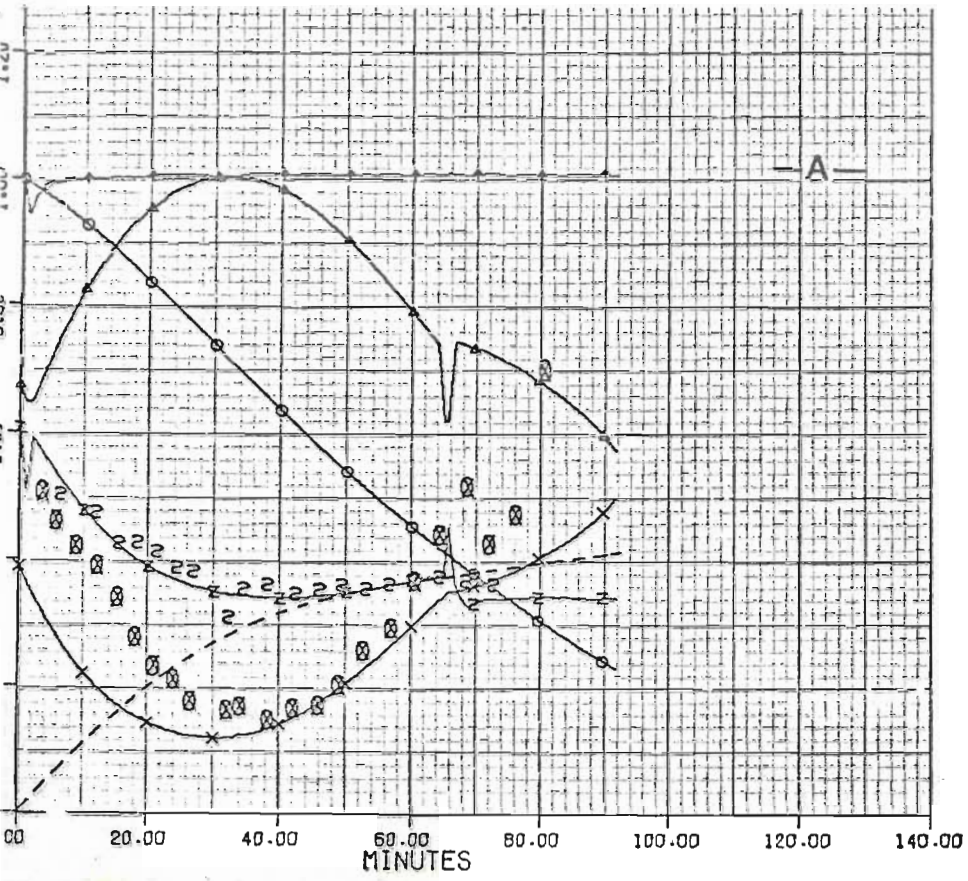

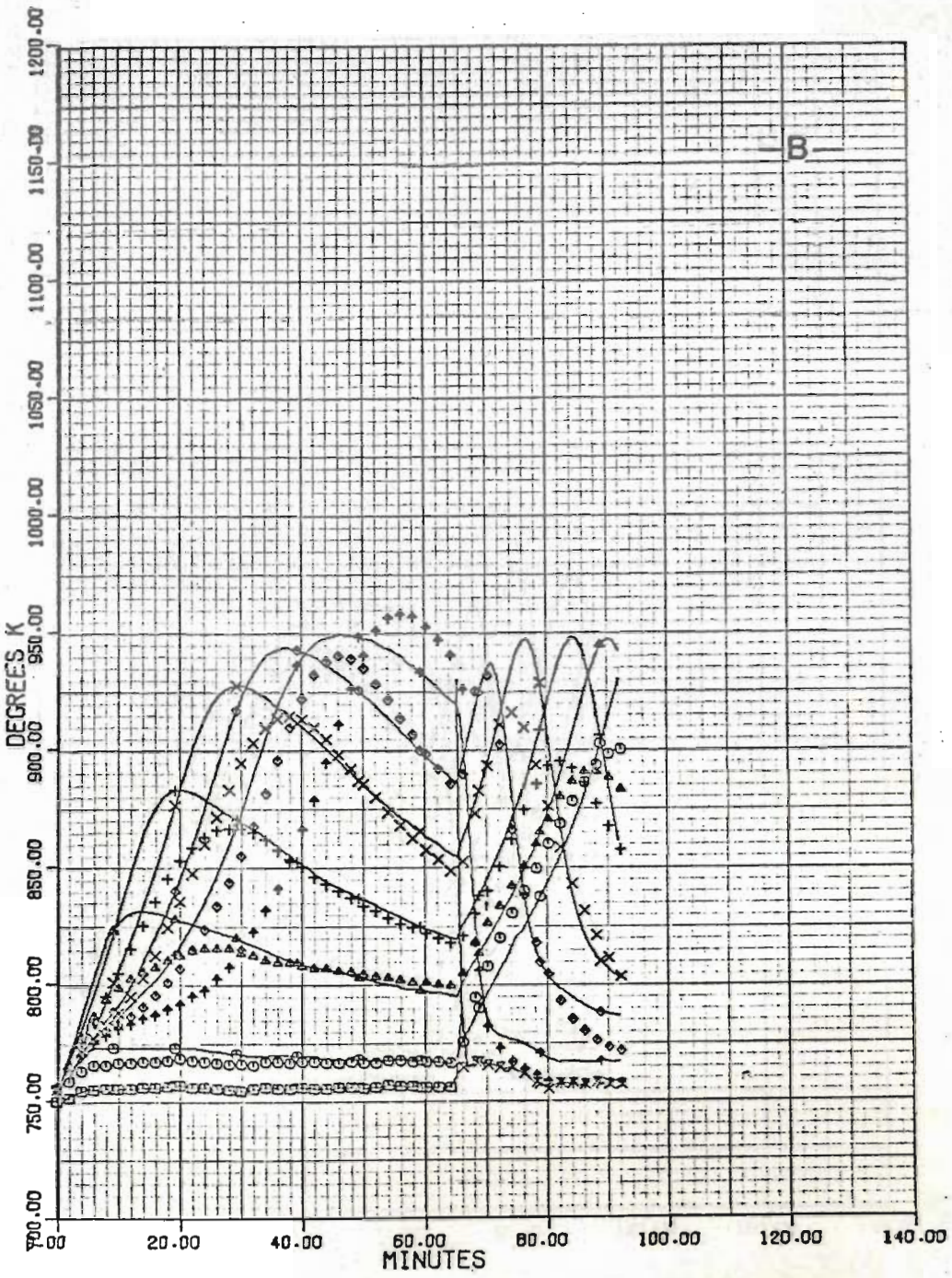

FIGURE 6.20 RUN LI1

G - 0,542

C_o - 0,048

y_o - 0,040

To - 775,

k_o - 9,79

For legend see table 6.2

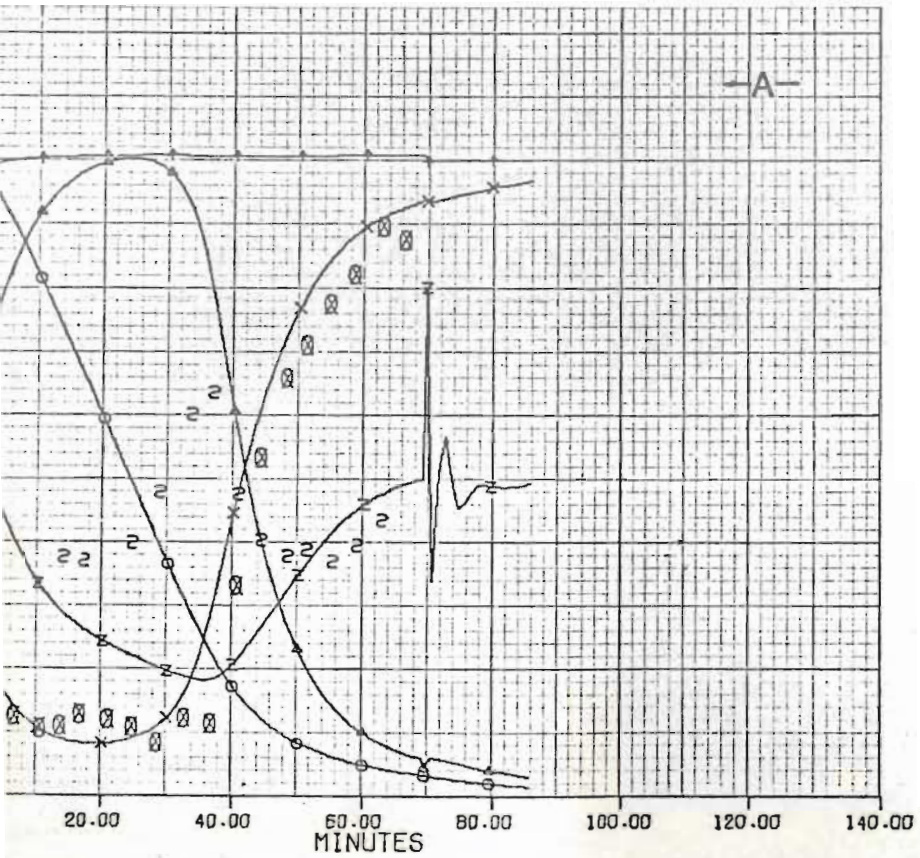

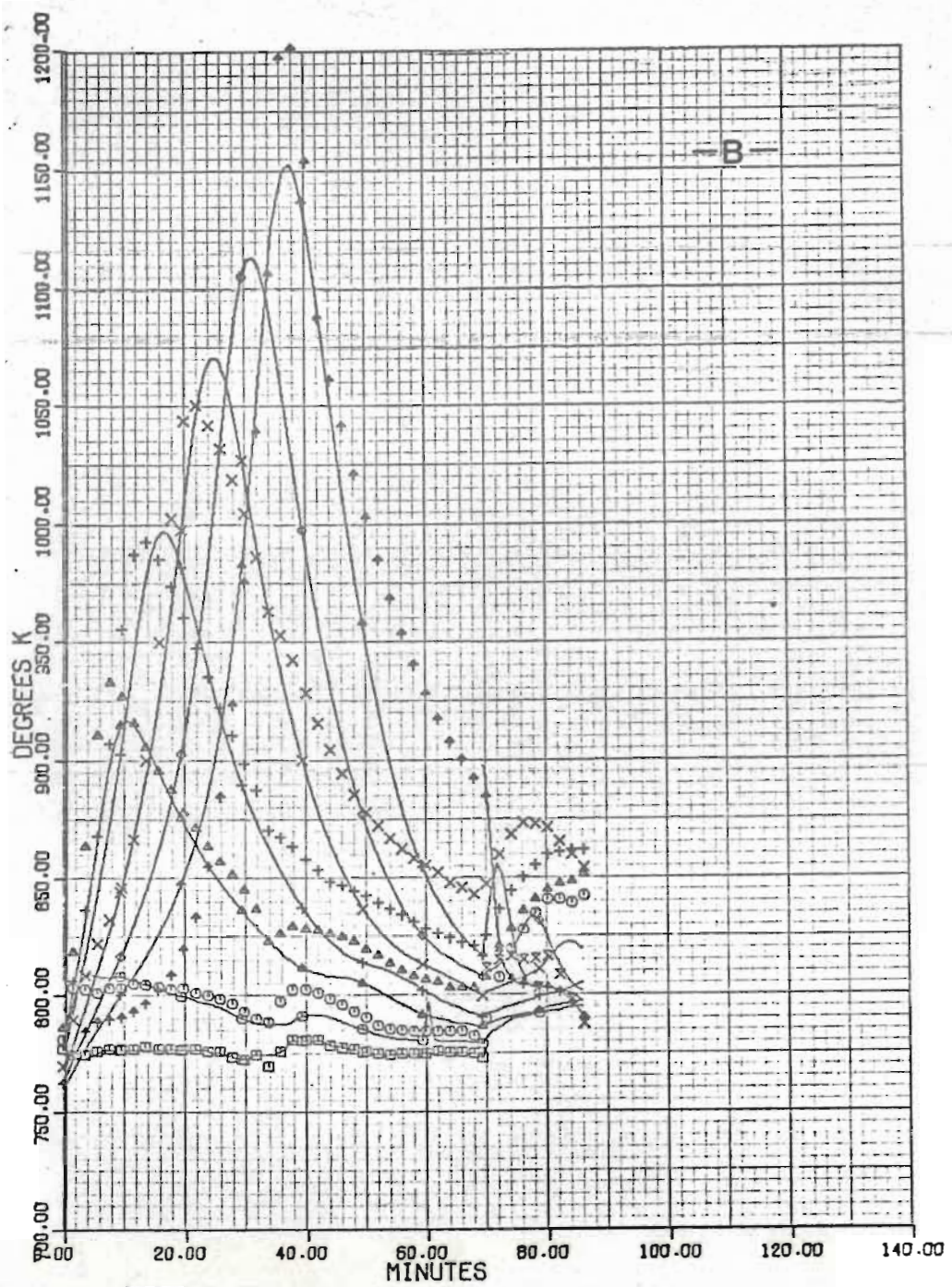

FIGURE 6.21 RUN LI2

G - 0,542

C_o - 0,069

y_o - 0,030

To - 777,

k_o - 9,24

For legend see table 6.2

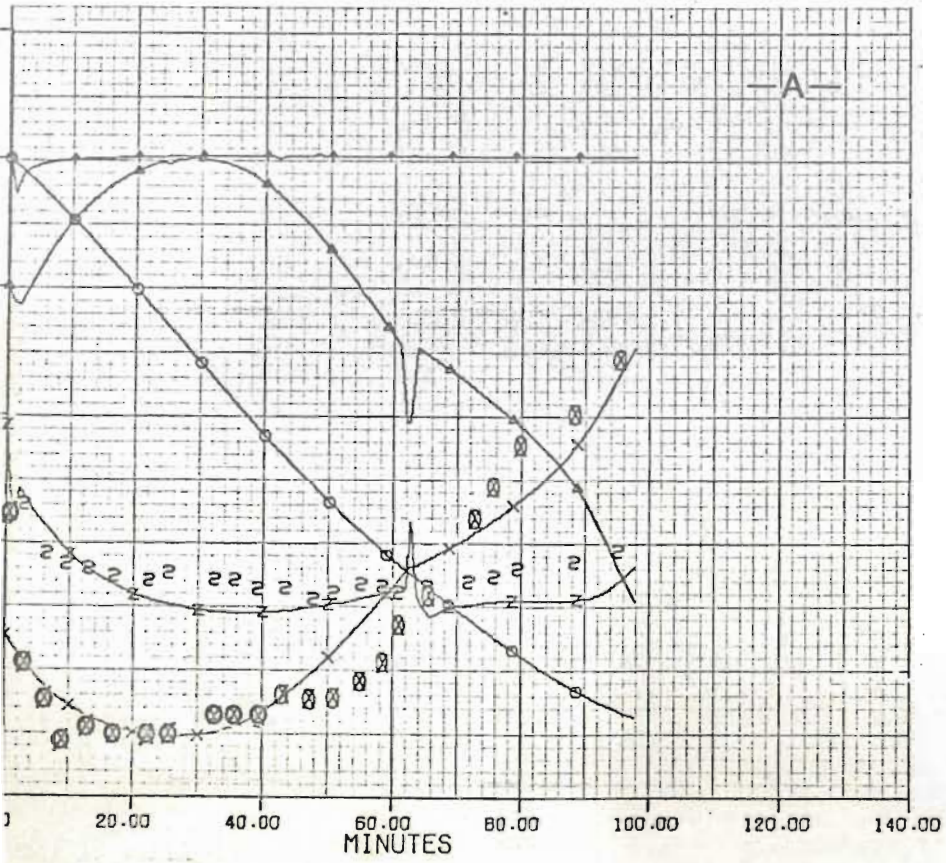

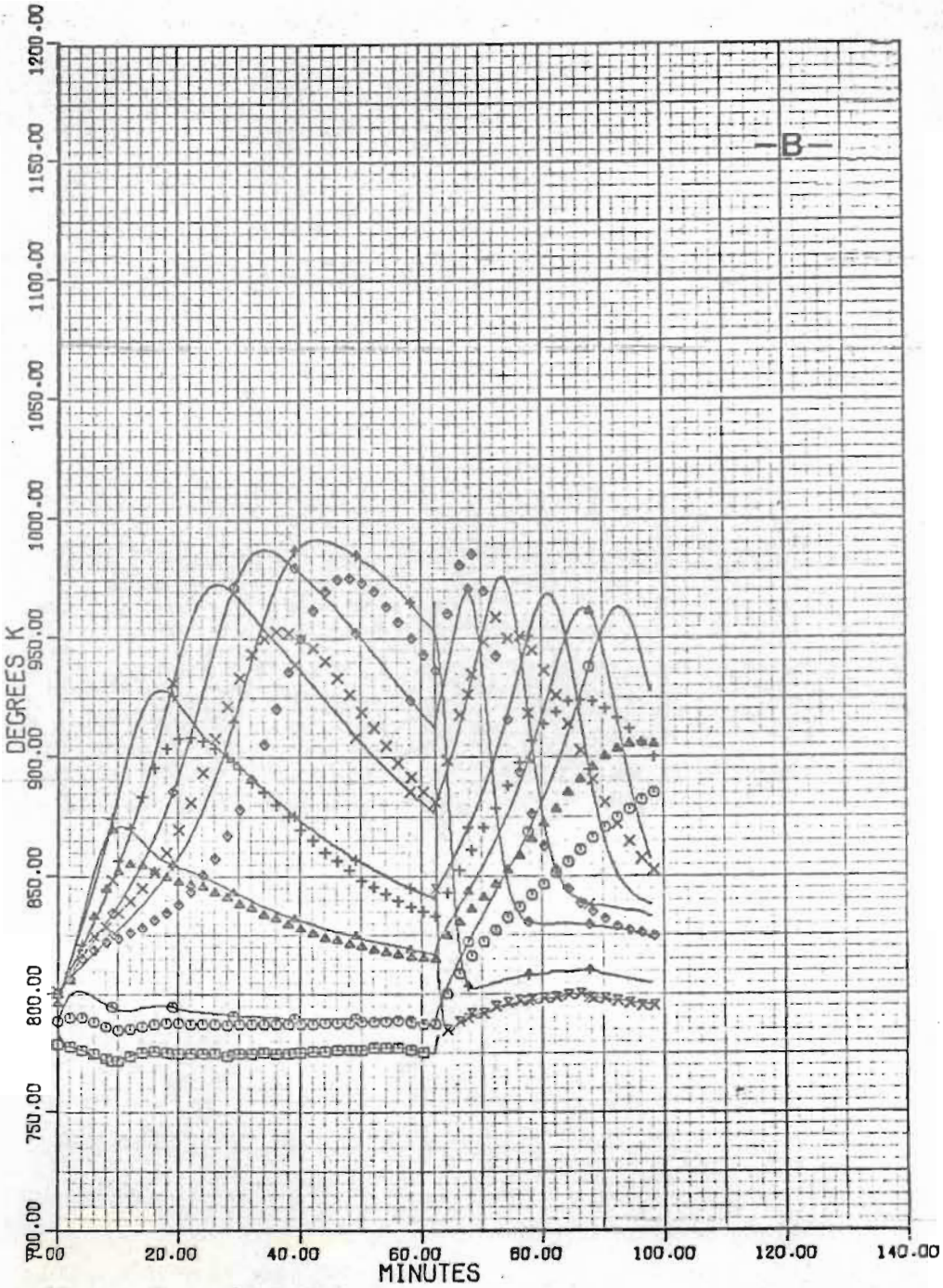

FIGURE 6.22 RUN LI2(C)

G - 0,407

Co - 0,069

y_o - 0,030

To - 777,

k_o - 8,94

For legend see table 6.2

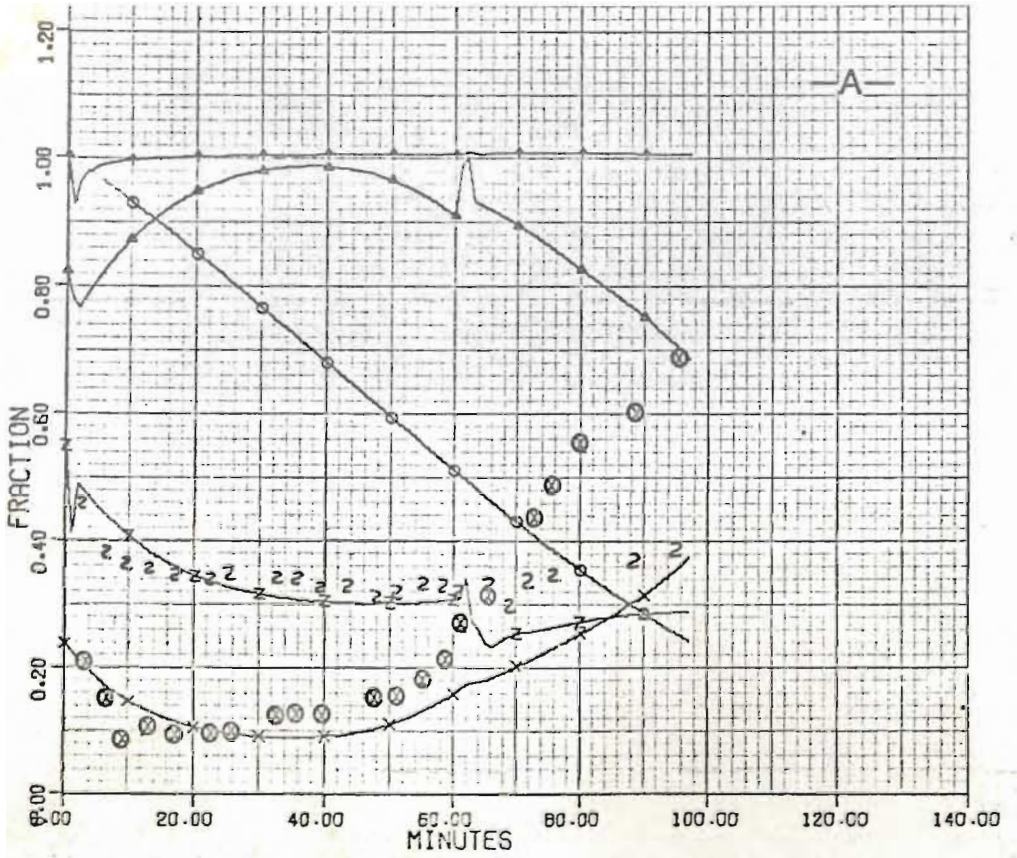

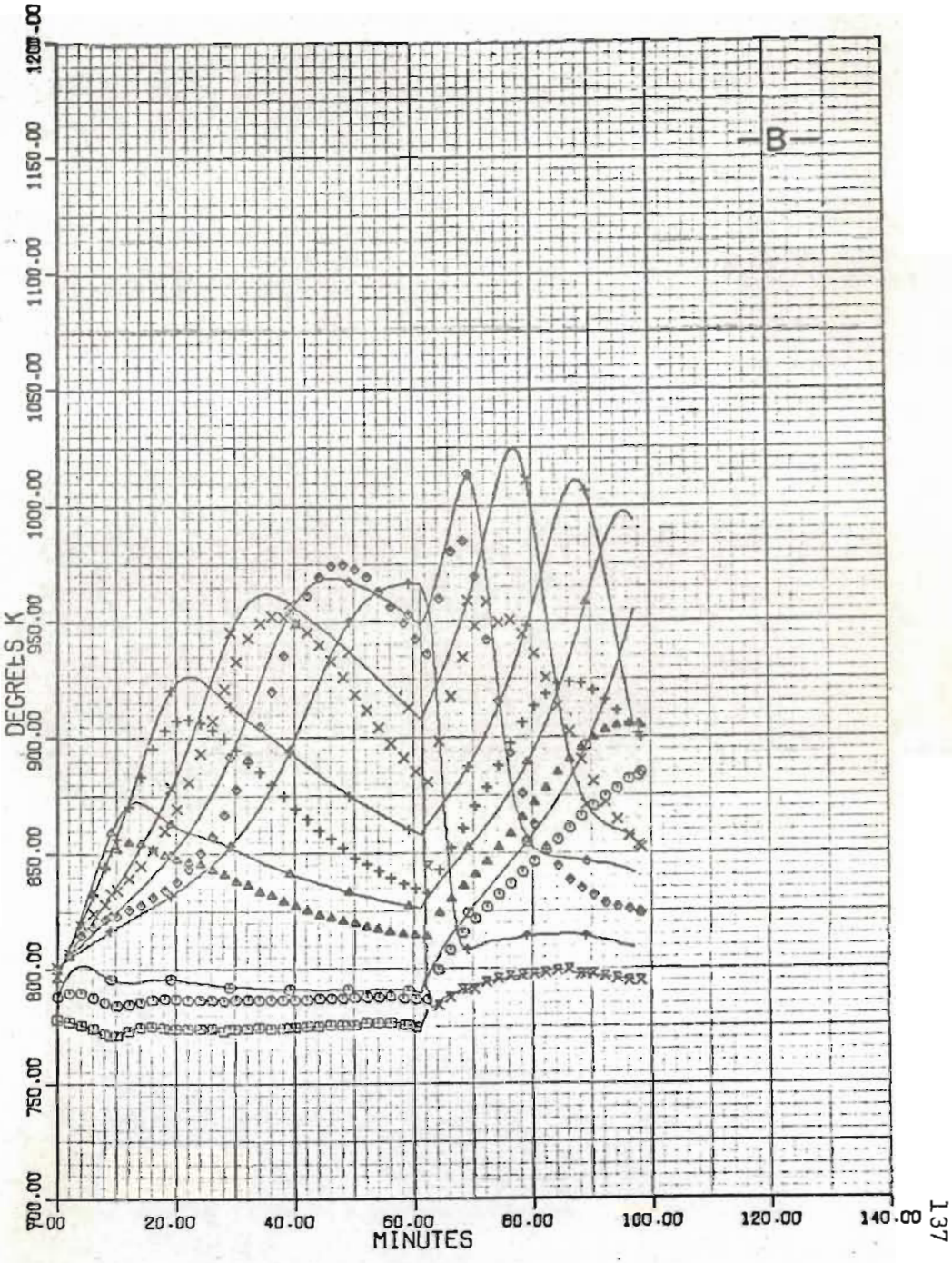

FIGURE 6.23 RUN LH

G - 0,542

Co - 0,048

y_o - 0,022

To - 808,

k_o - 10,59

For legend see table 6.2

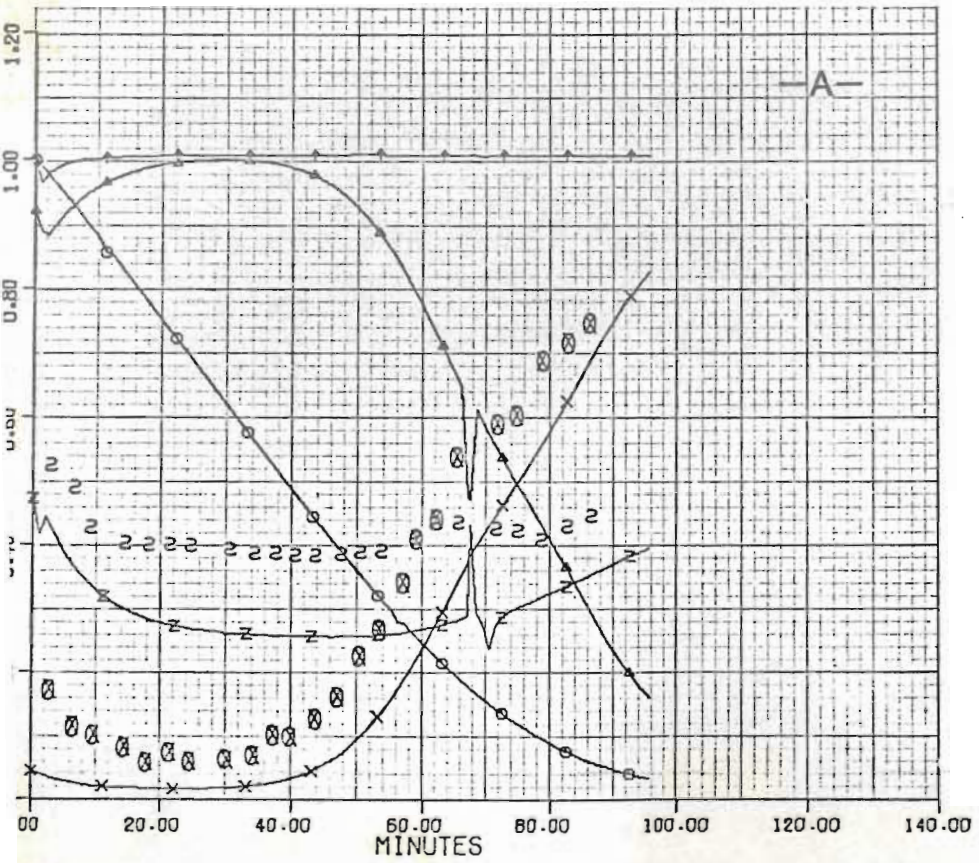

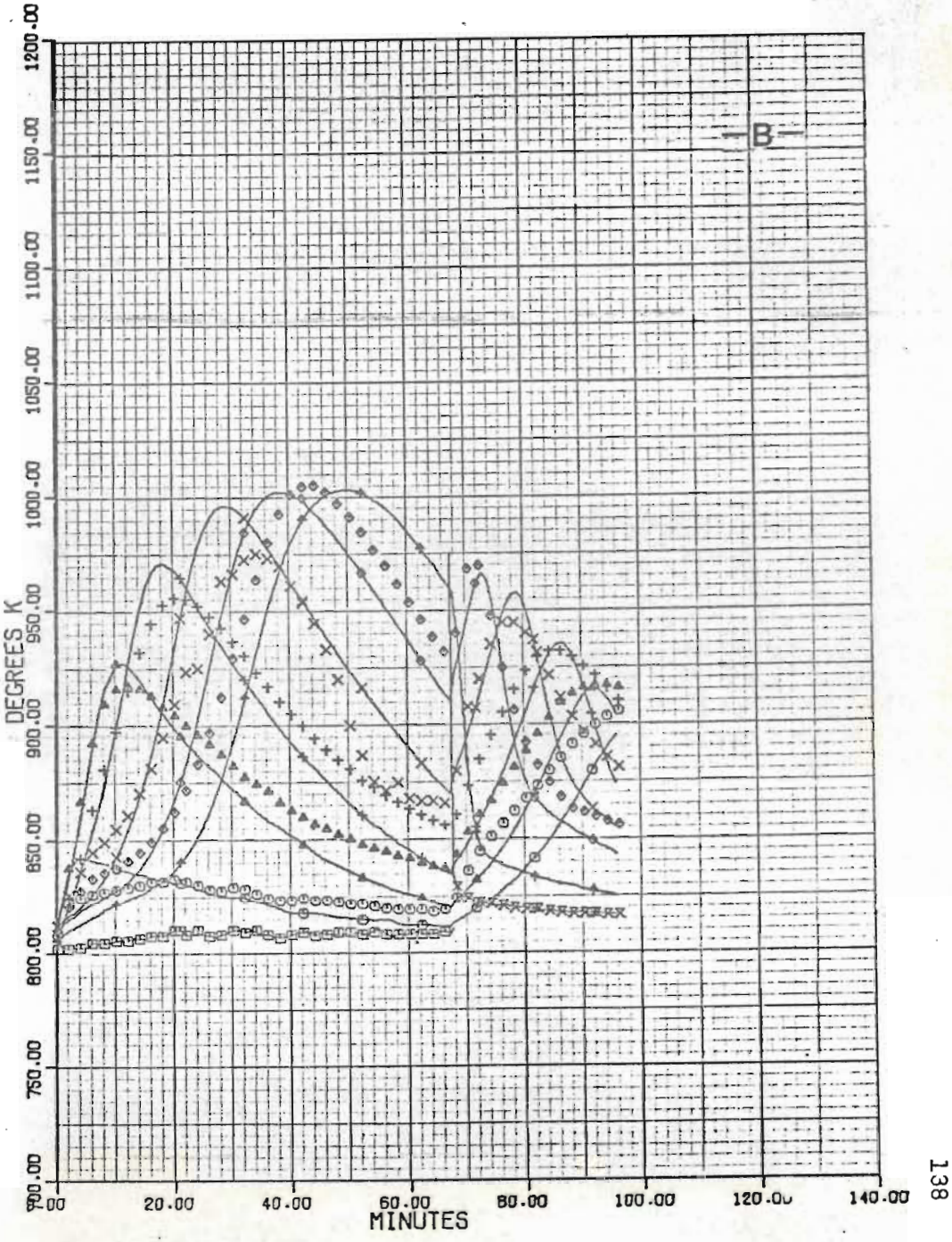

FIGURE 6.24 RUN LH(C)

G - 0,475

Co - 0,048

y_o - 0,022

To - 808,

k_o - 10,45

For legend see table 6.2

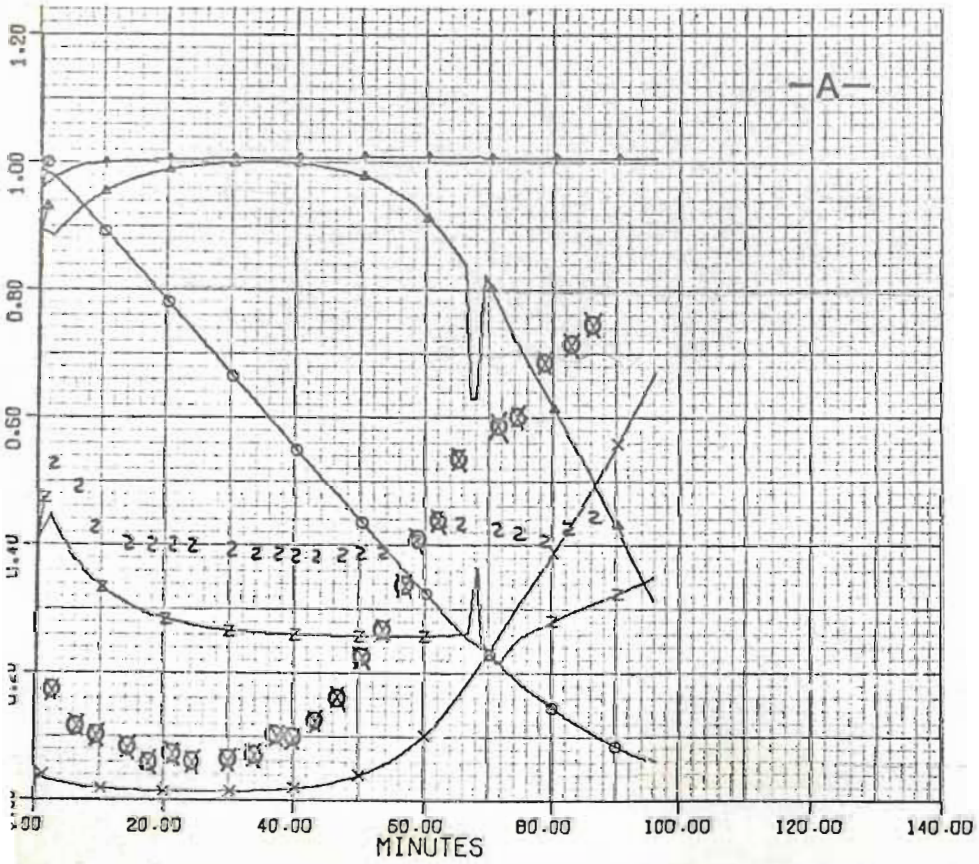

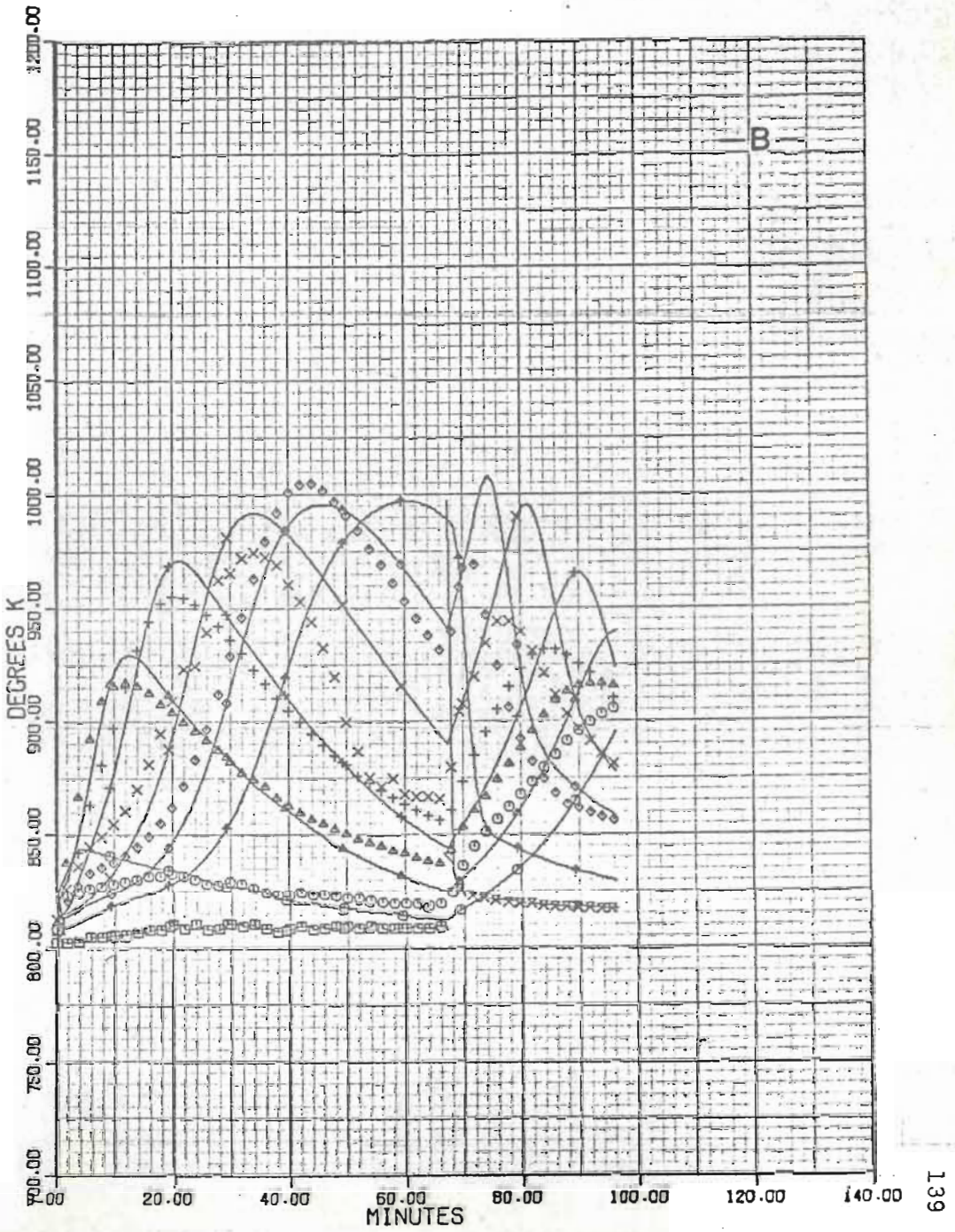

FIGURE 6.25 RUN IL1

G - 0,949

Co - 0,048

y_o - 0,037

To - 755,

k_o - 9,54

For legend see table 6.2

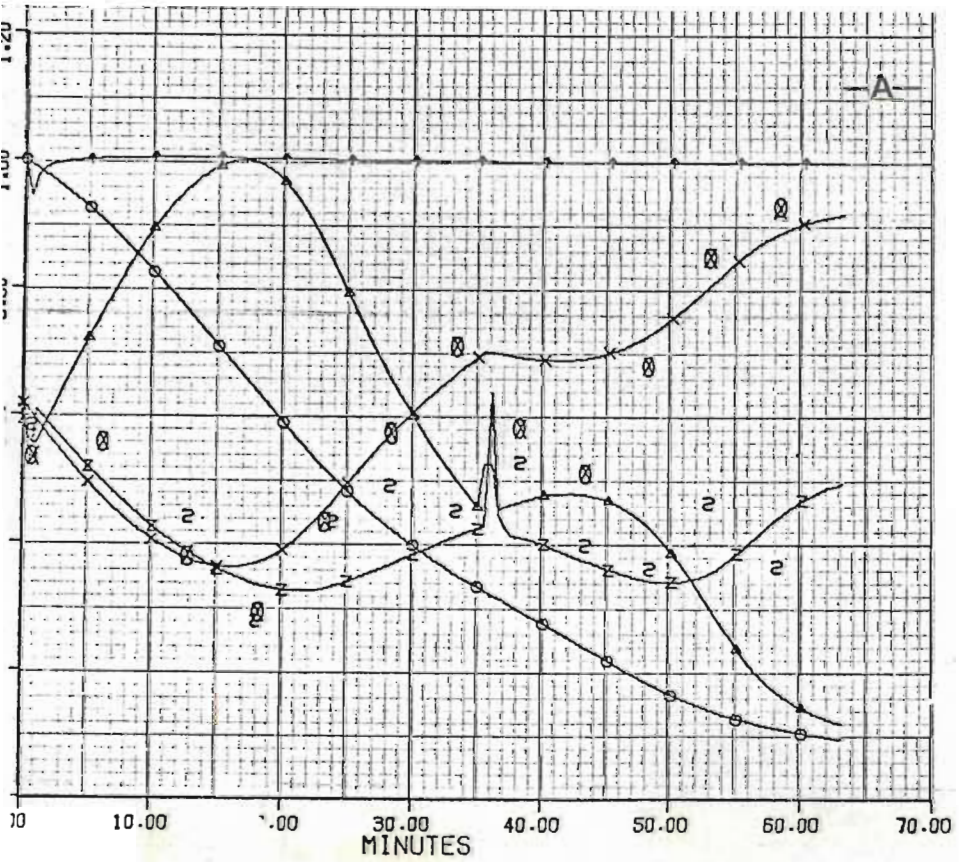

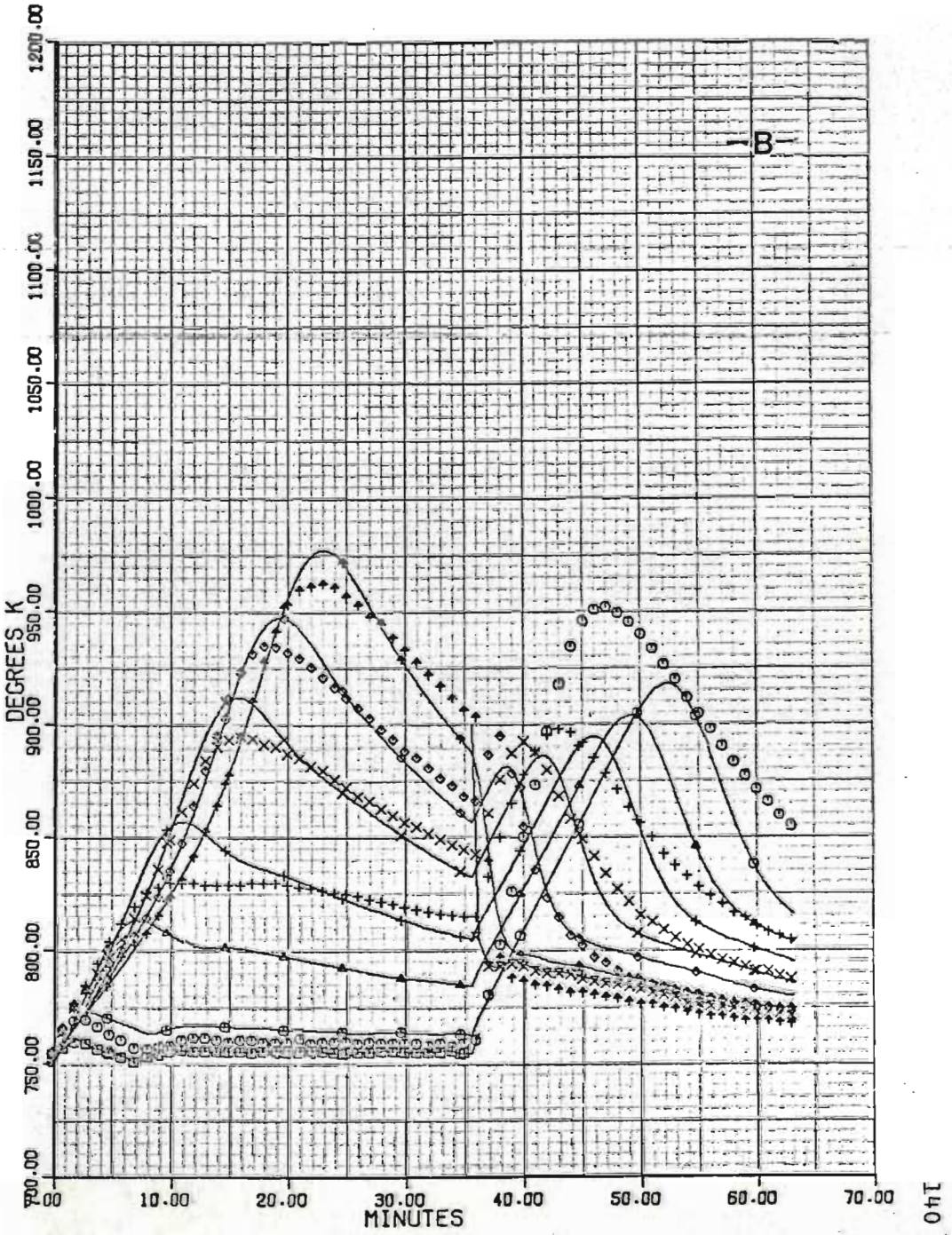

FIGURE 6.26 RUN IL2

G - 0,949

Co - 0,069

y_o - 0,030

To - 761,

k_o - 9,64

For legend see table 6.2

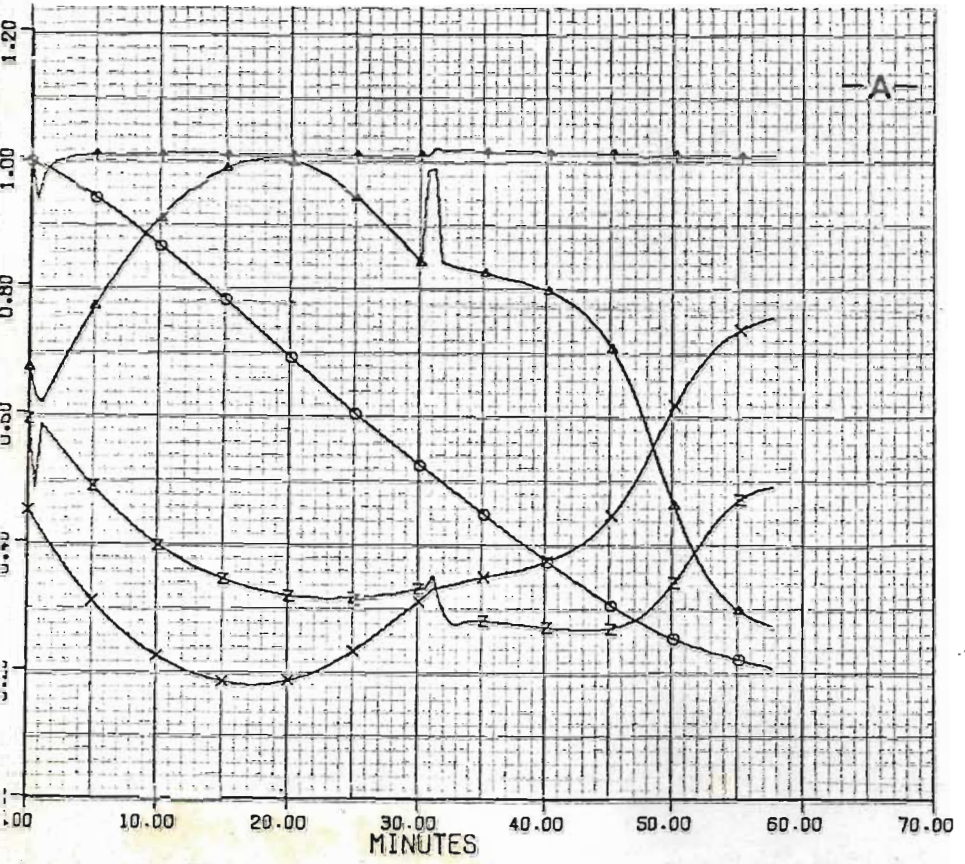

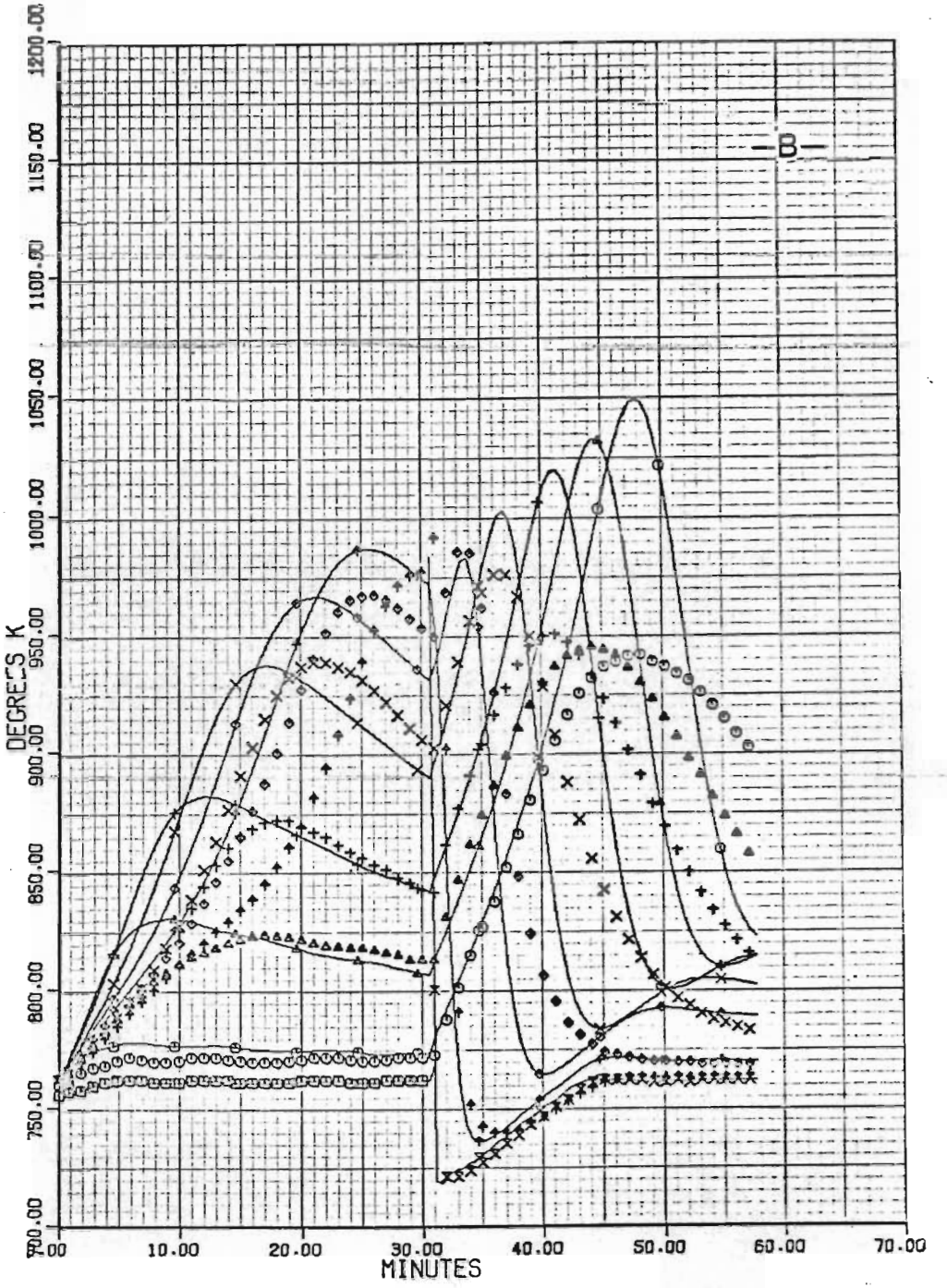

FIGURE 6.27 RUN IL2(C)

G - 0,773

C0 - 0,069

y_o - 0,030

To - 761,

k_o - 9,44

For legend see table 6.2

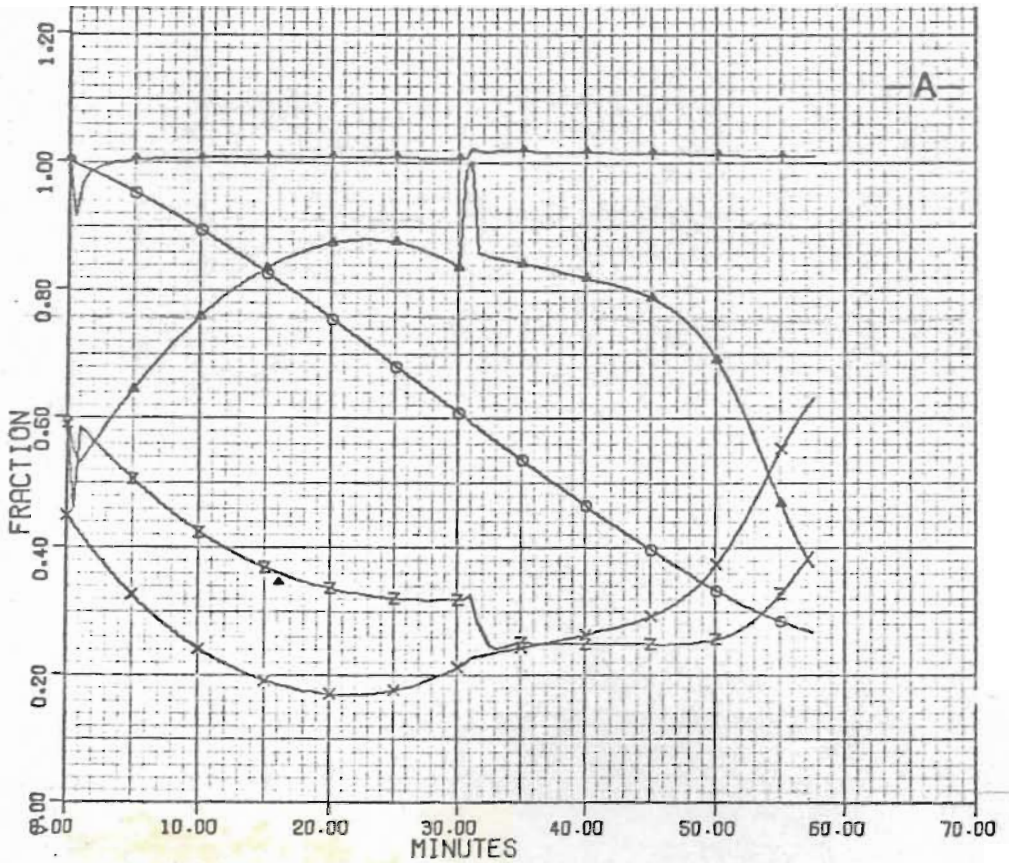

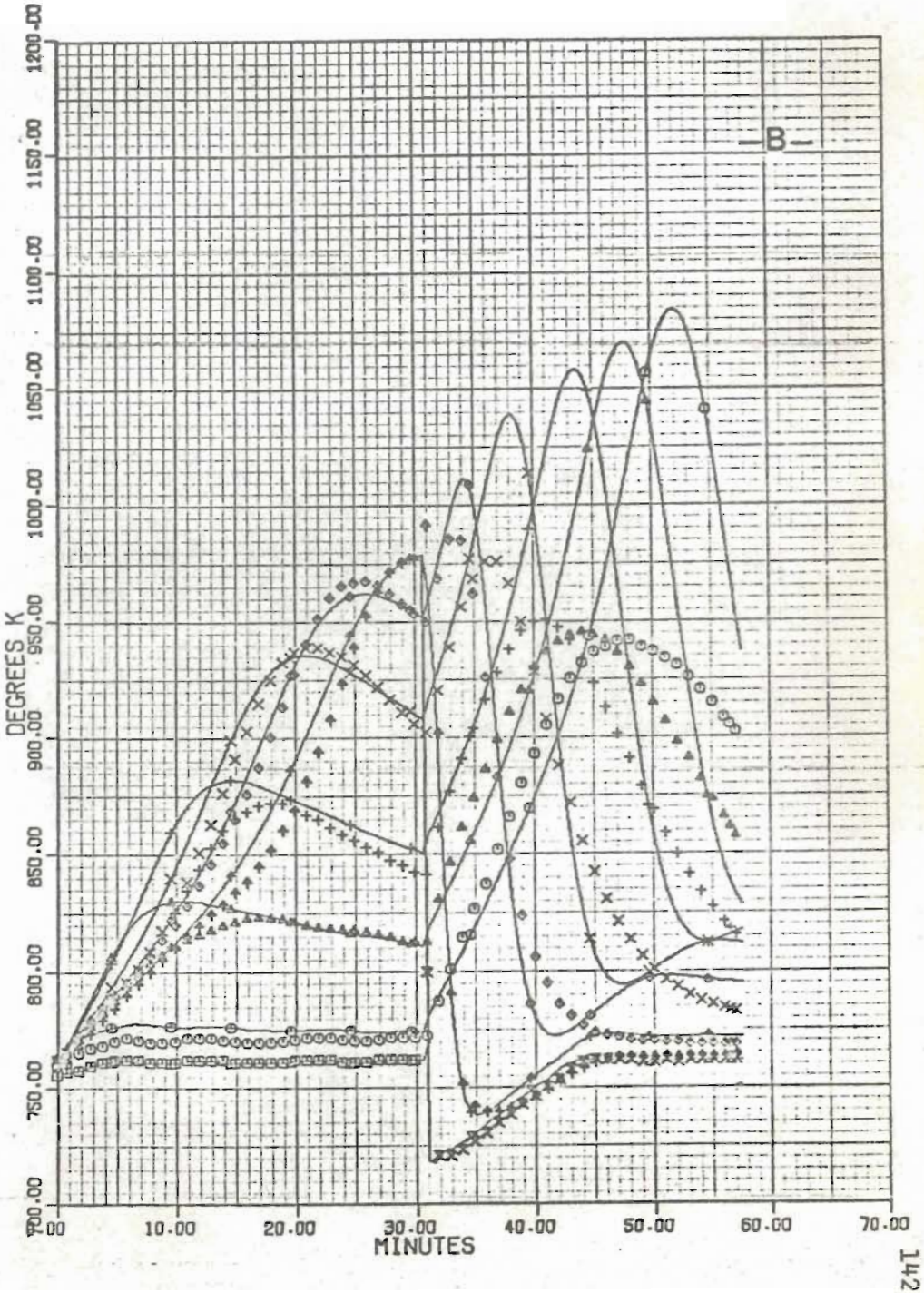

FIGURE 6.28 RUN II

G - 0,949

Co - 0,069

y_o - 0,029

To - 785,

k_o - 9,49

For legend see table 6.2

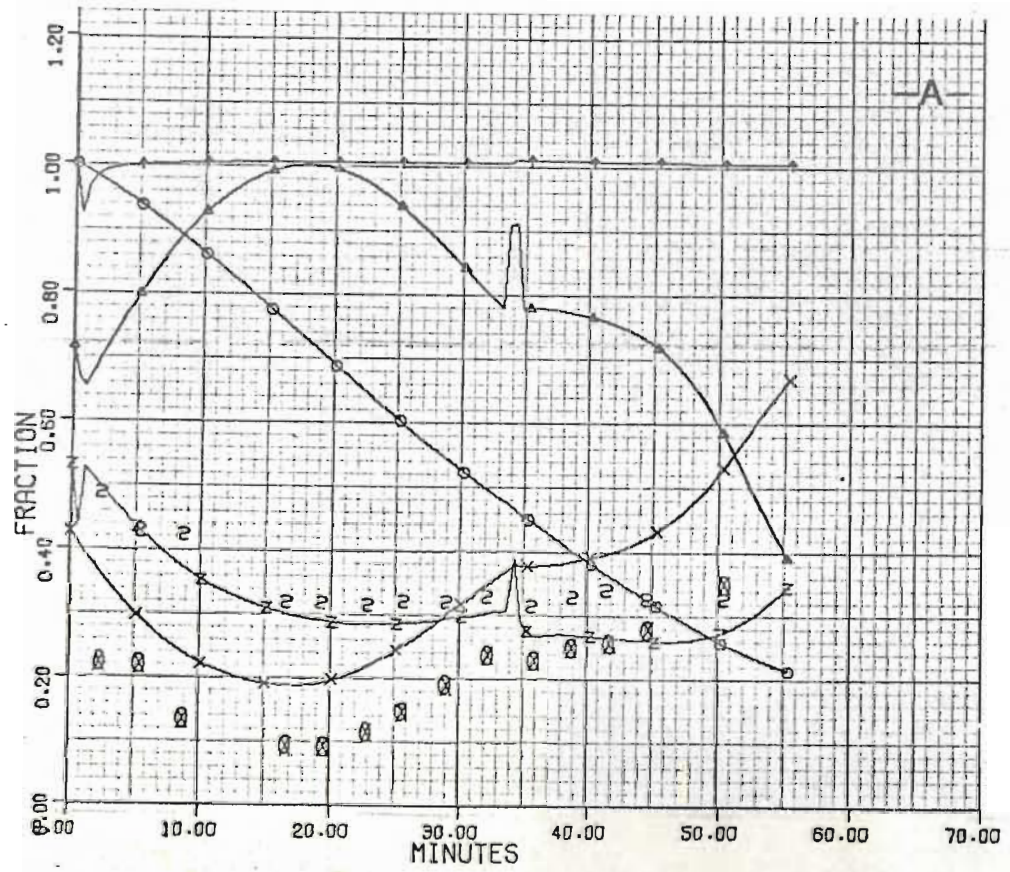

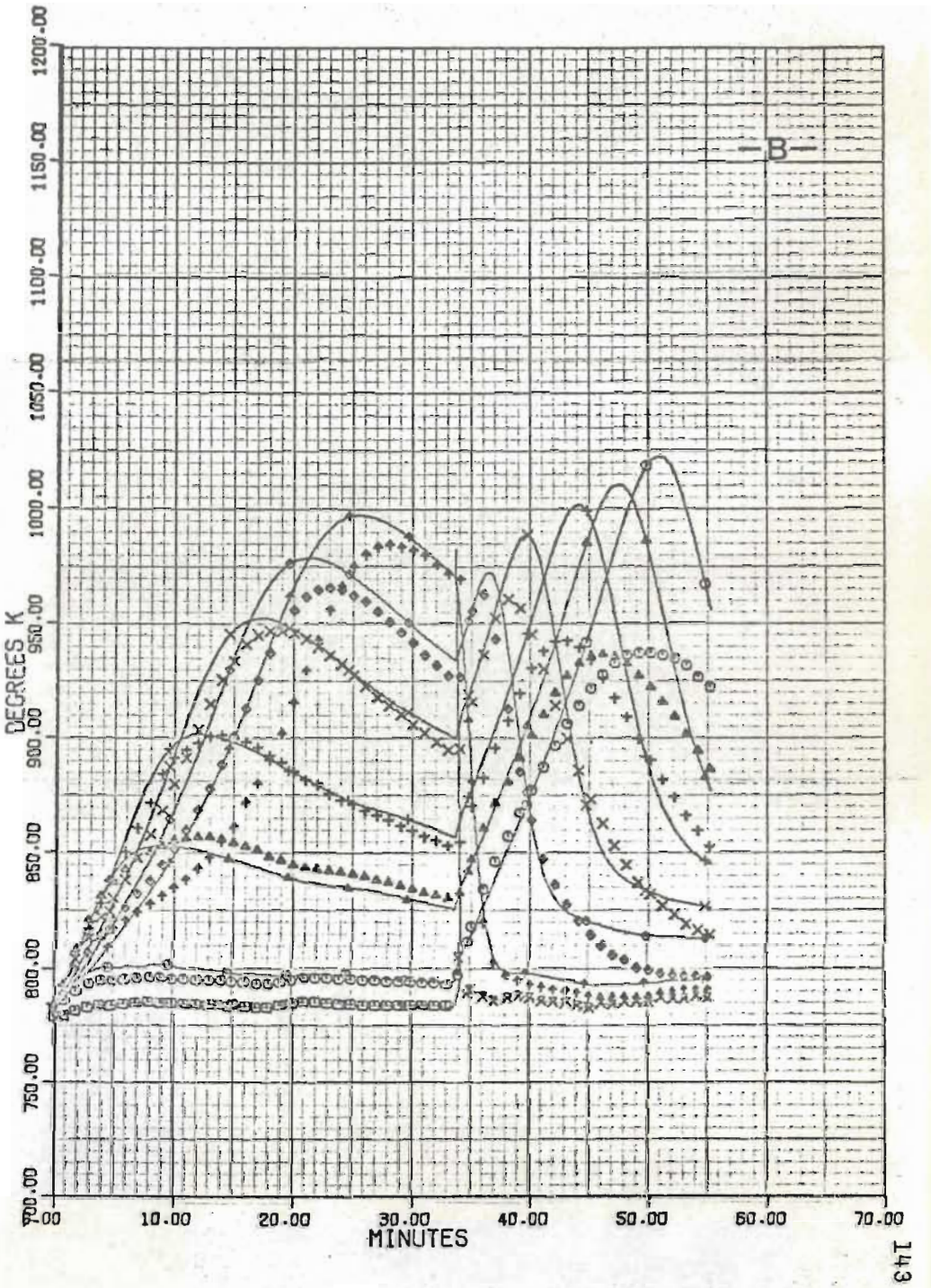

FIGURE 6.29 RUN II(C)

G - 0,841

Co - 0,069

y_o - 0,029

To - 785,0

k_o - 9,29

For legend see table 6.2

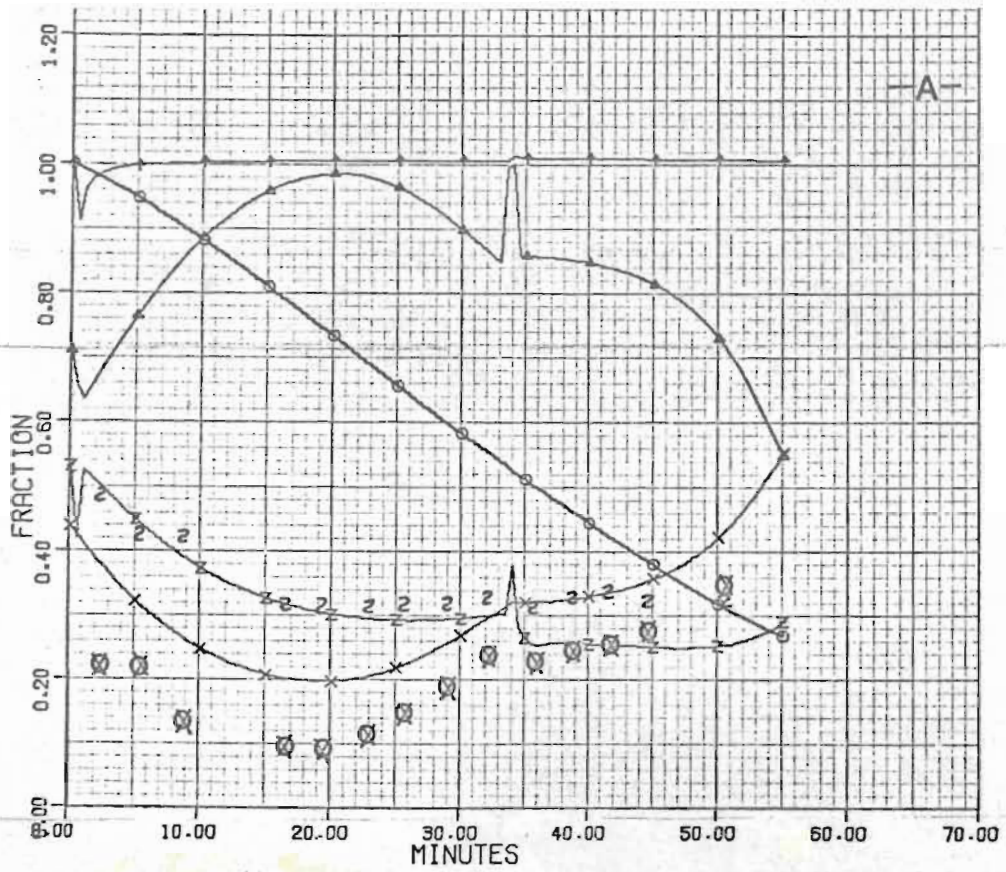

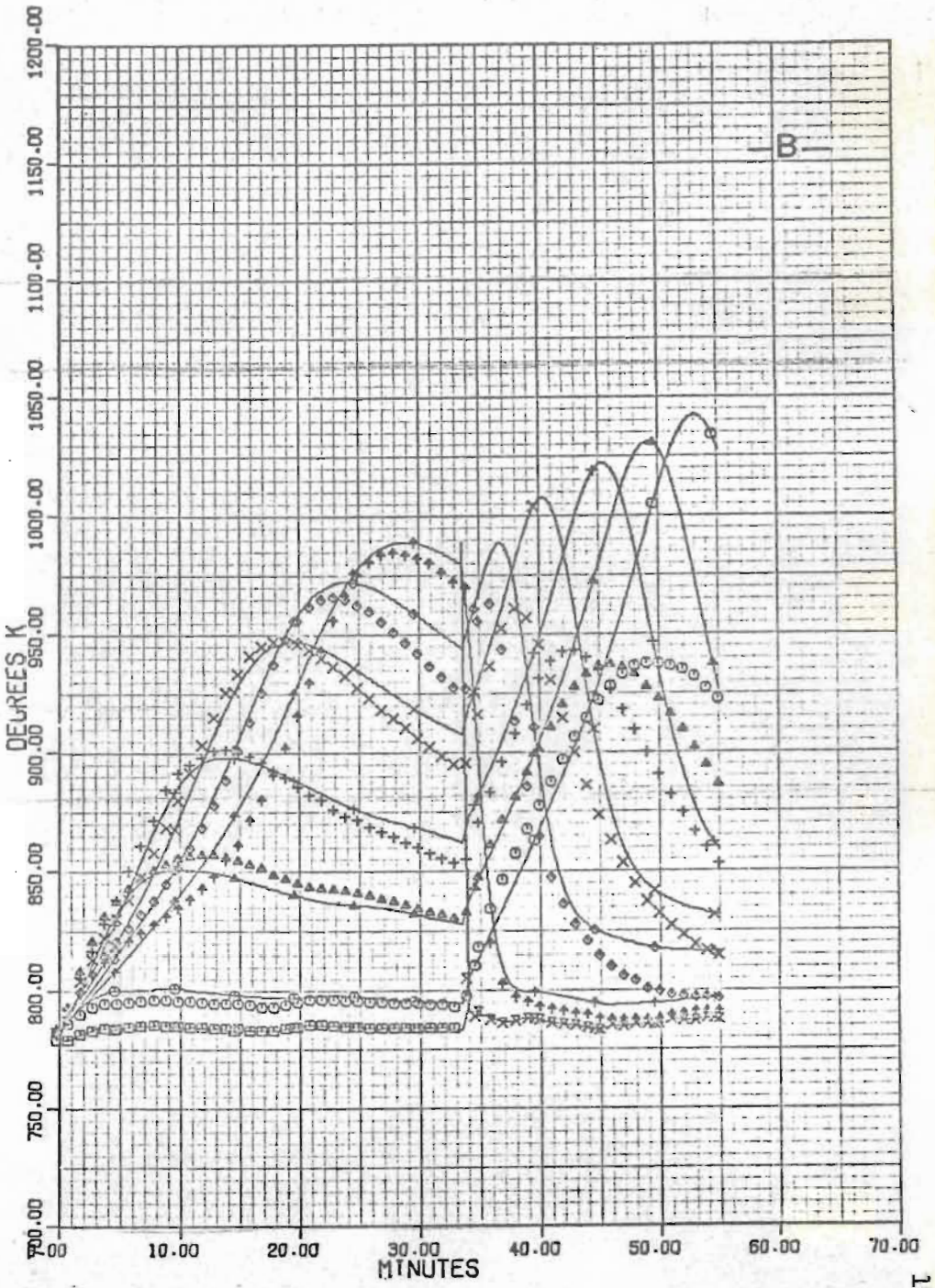

FIGURE 6.30 RUN IH

G - 0,949

Co - 0,048

y_o - 0,030

To - 808,

k_o - 9,74

For legend see table 6.2

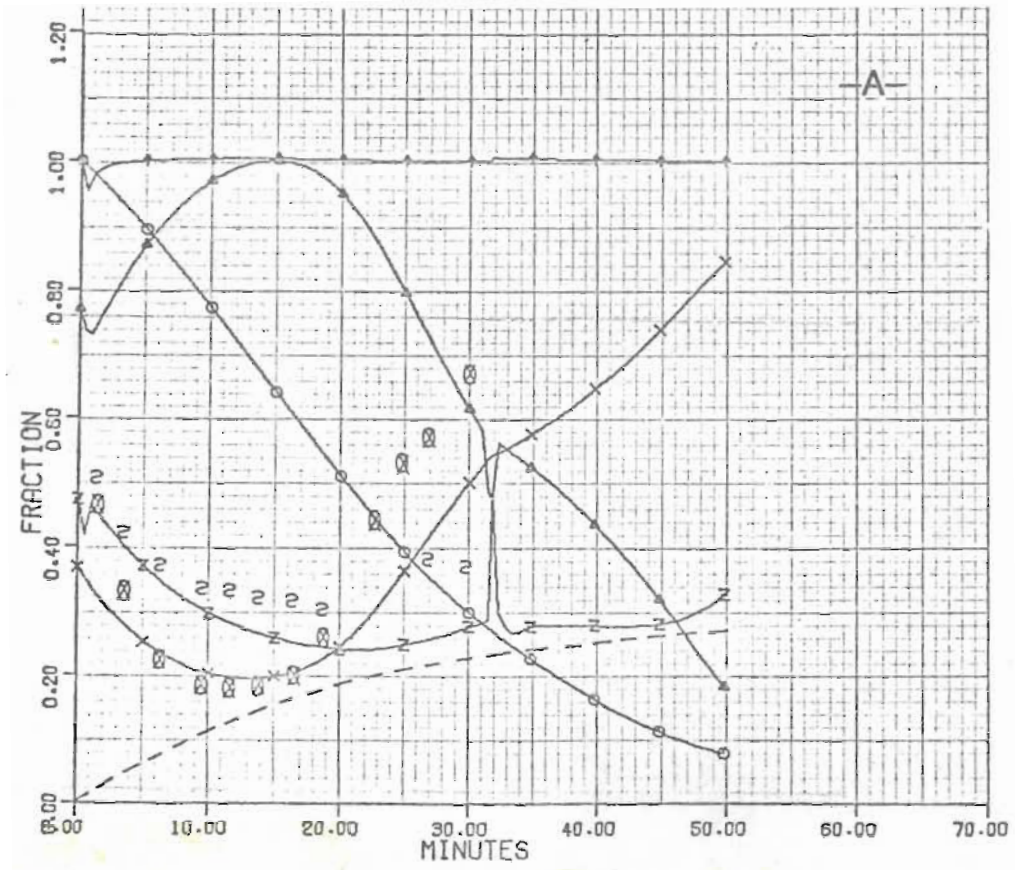

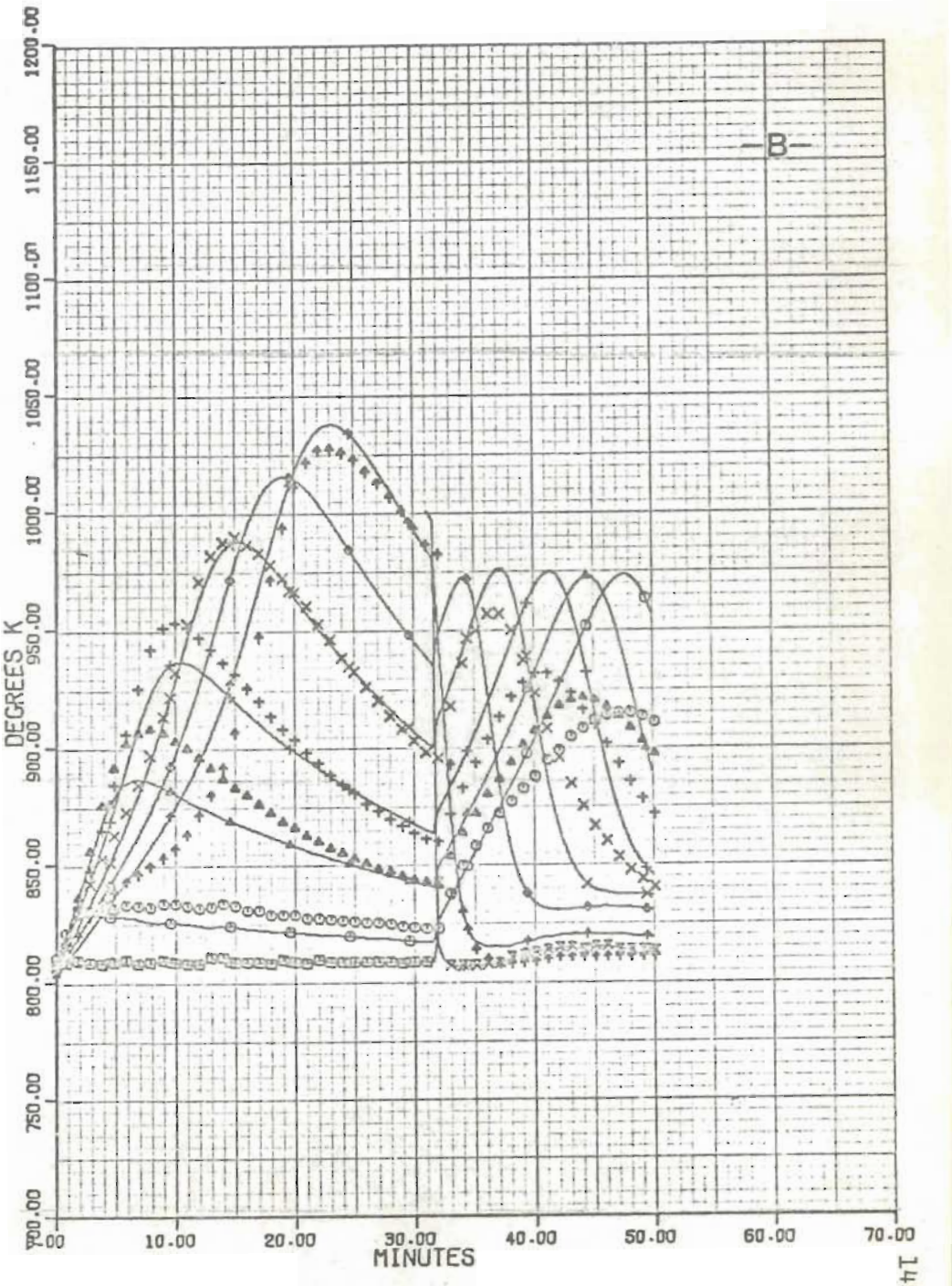

FIGURE 6.31 RUN HL1

G - 1,356
Co - 0,048
y_o - 0,067
To - 755,
k_o - 9,29

For legend see table 6.2

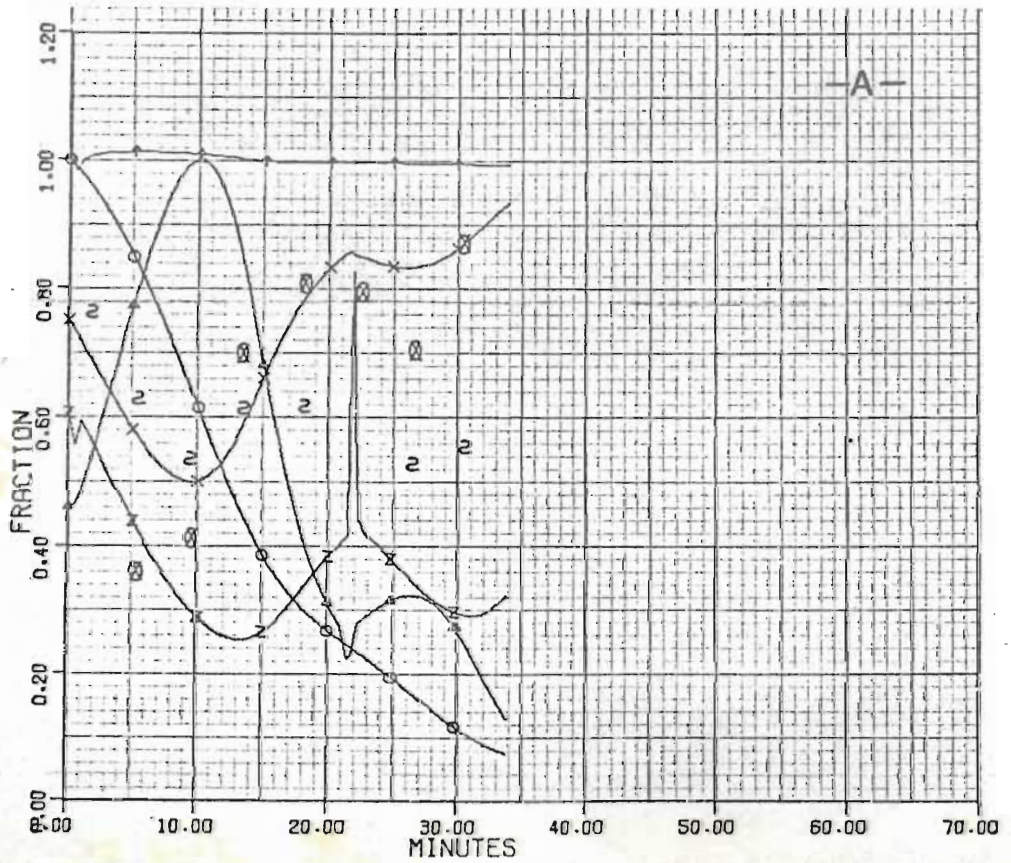

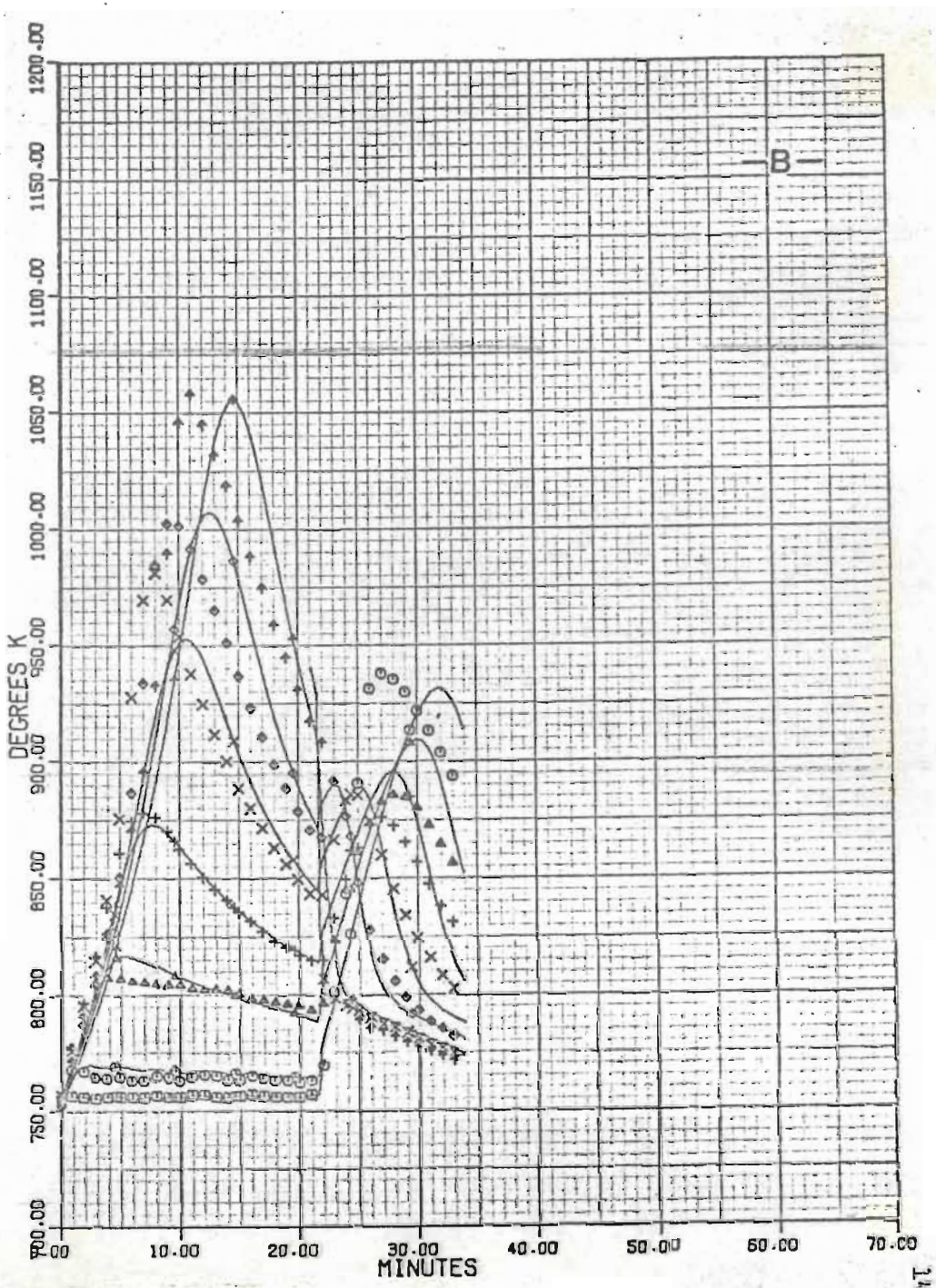

FIGURE 6.32 RUN HL1(C)

G - 1,763

Co - 0,048

y_o - 0,067

To - 755,

k_o - 9,59

For legend see table 6.2

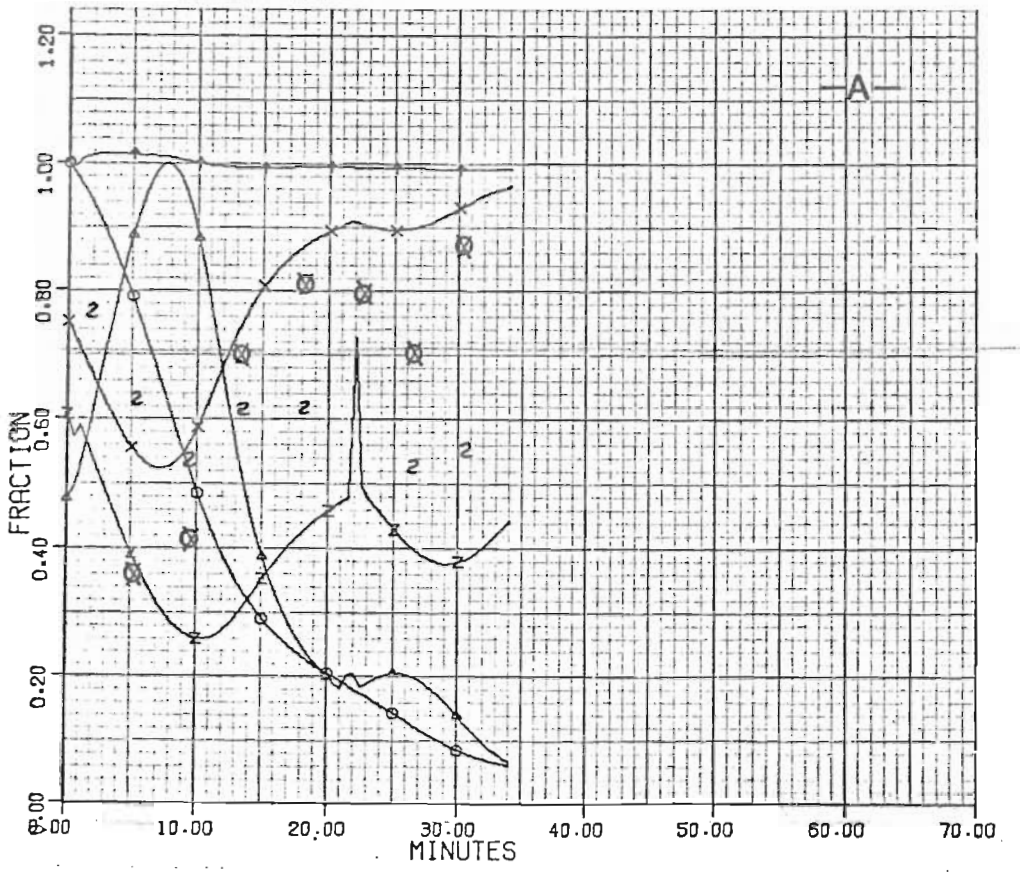

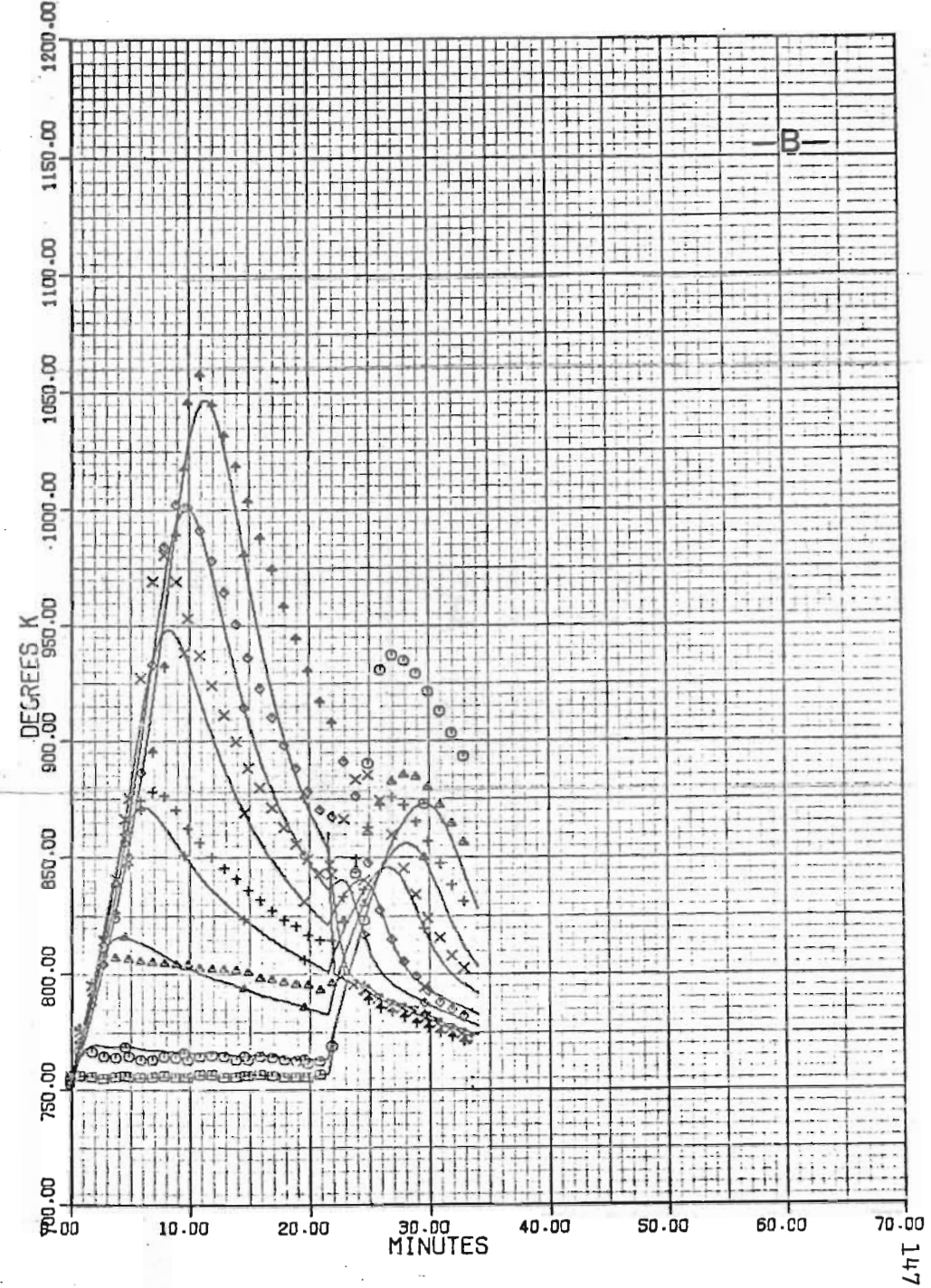

FIGURE 6.33 RUN HL2

G - 1,356

Co - 0,069

y_o - 0,035

To - 752,

k_o - 9,04

For legend see table 6.2

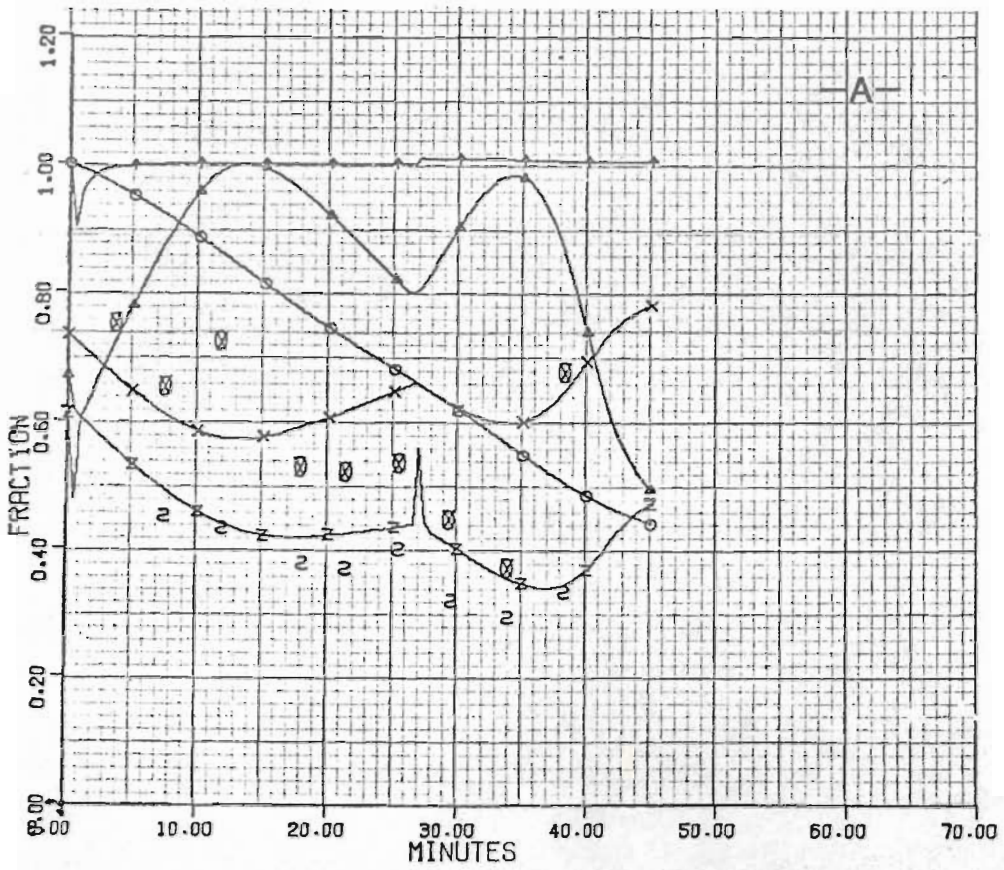

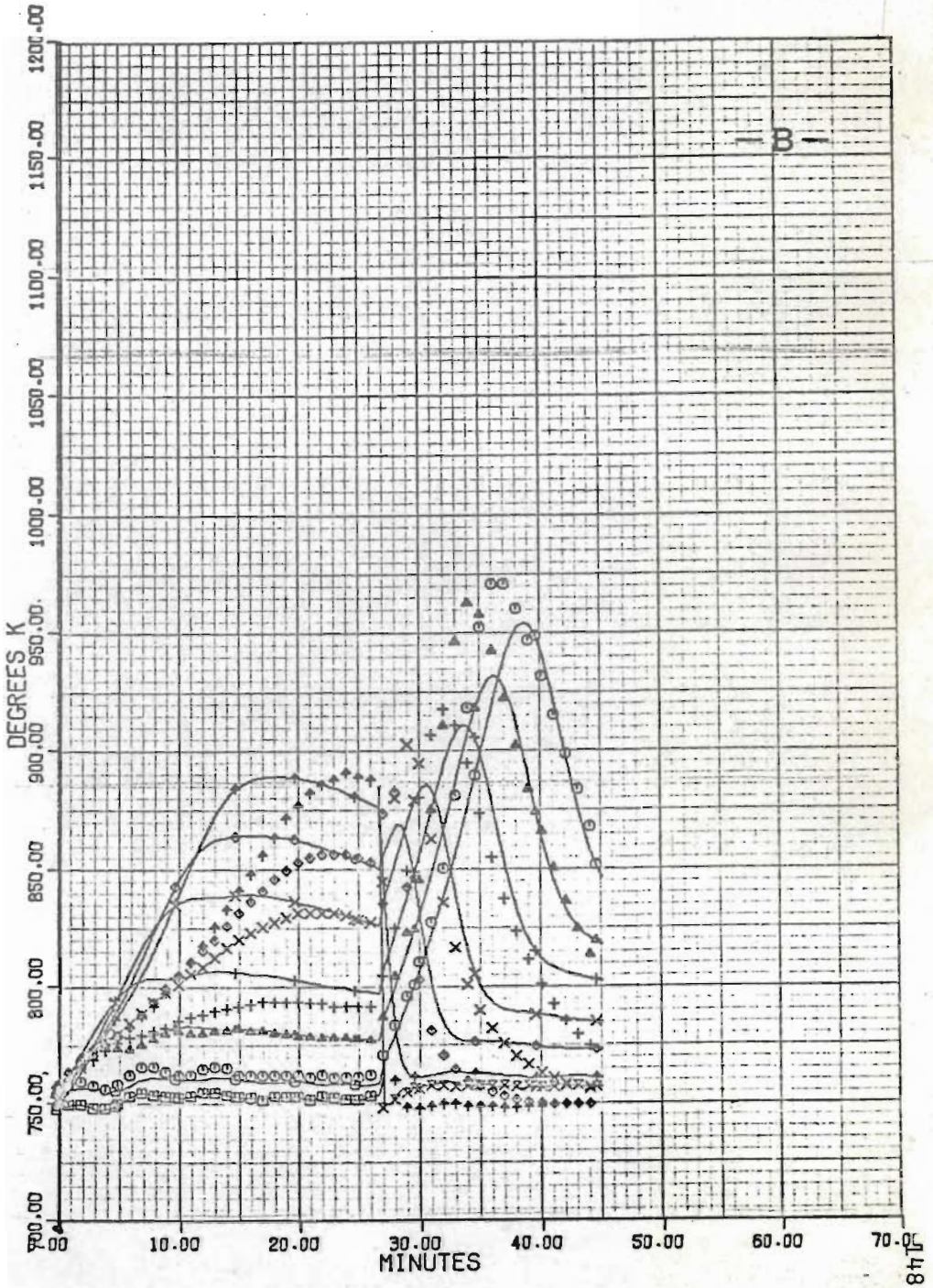

FIGURE 6.34 RUN HL2(C)

G - 1,017

Co - 0,069

y_o - 0,035

To - 752,

k_o - 8,74

For legend see table 6.2

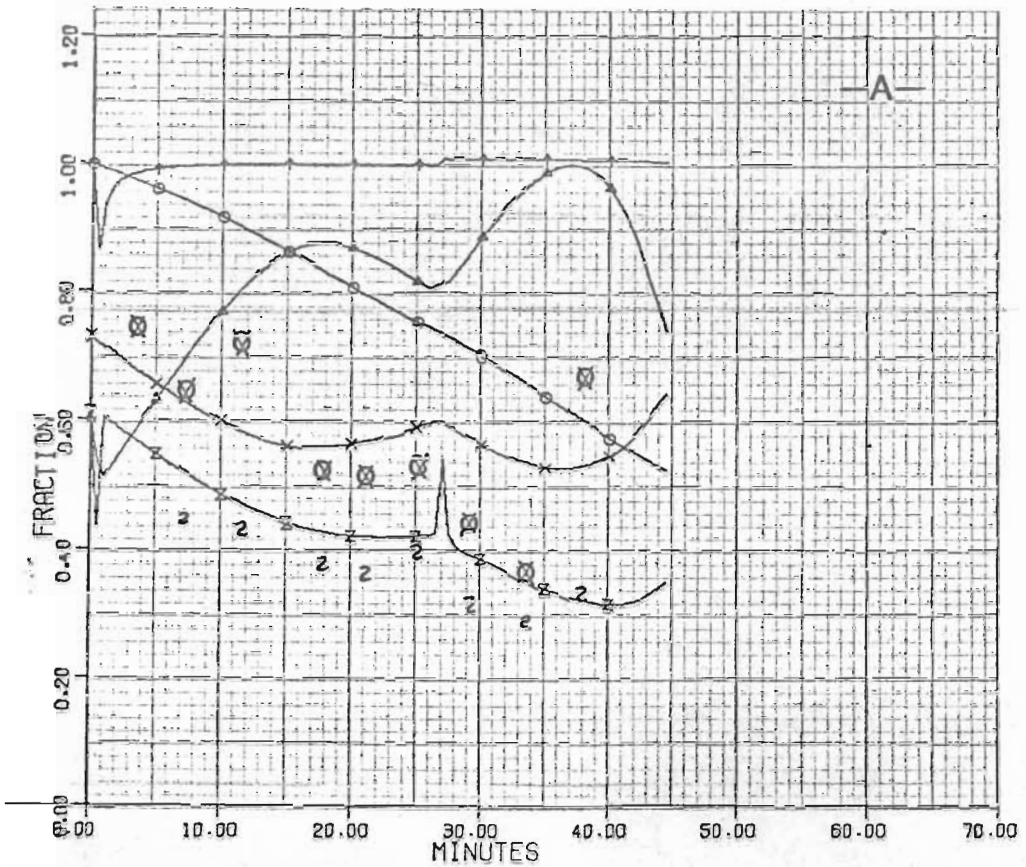

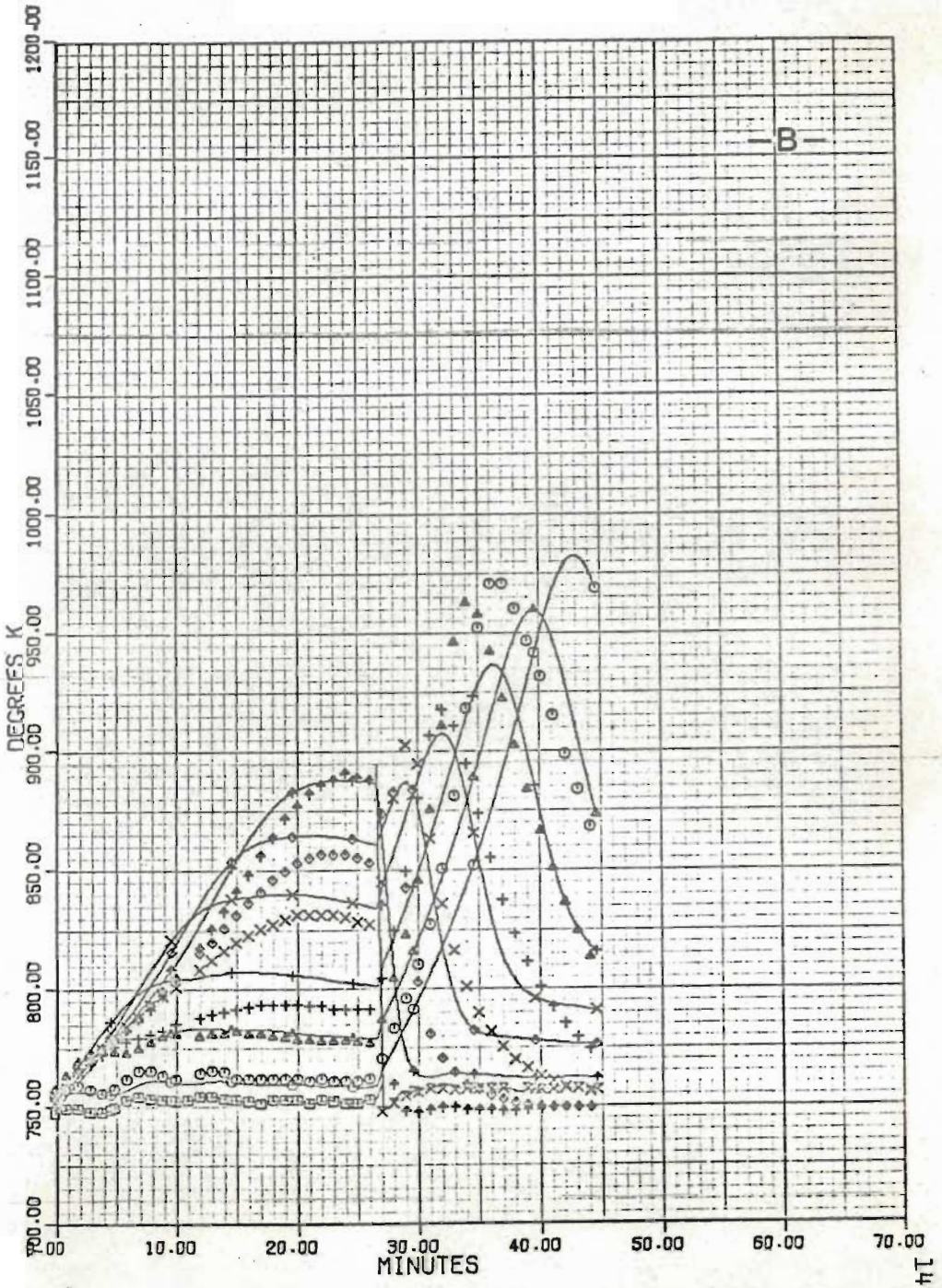

FIGURE 6.35 RUN HI

G - 1,356

Co - 0,048

y_o - 0,030

To - 778,

k_o - 9,24

For legend sec table 6.2

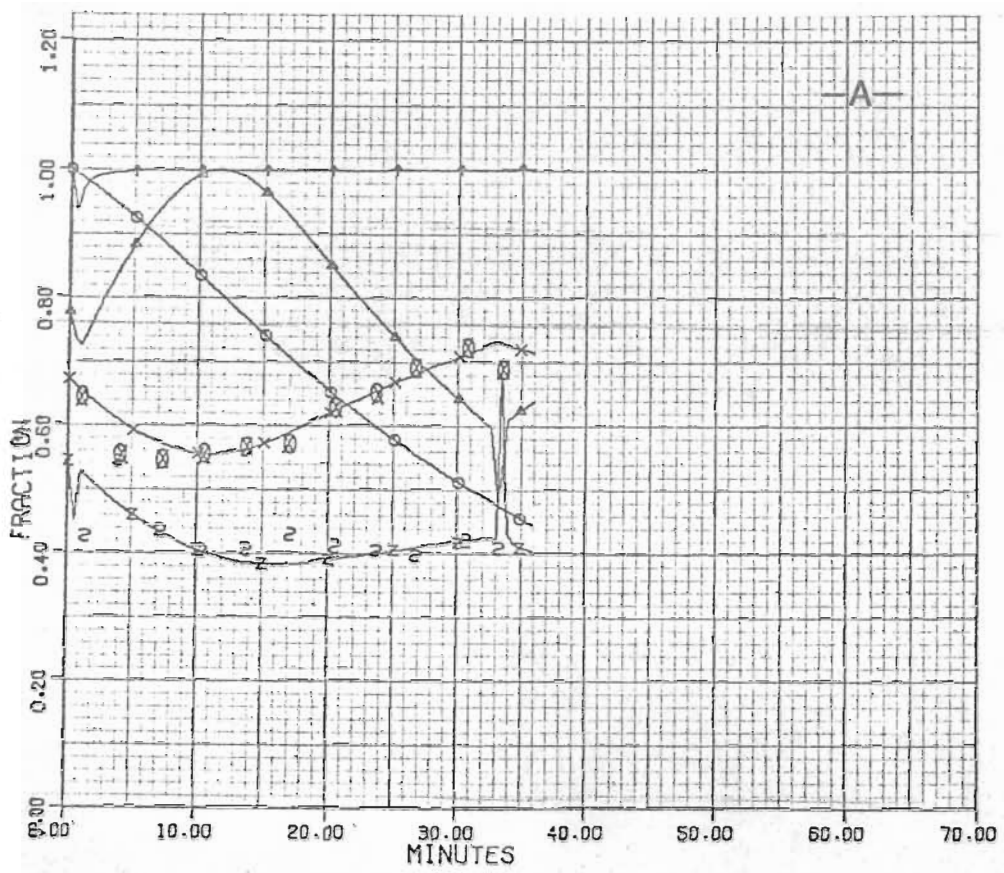

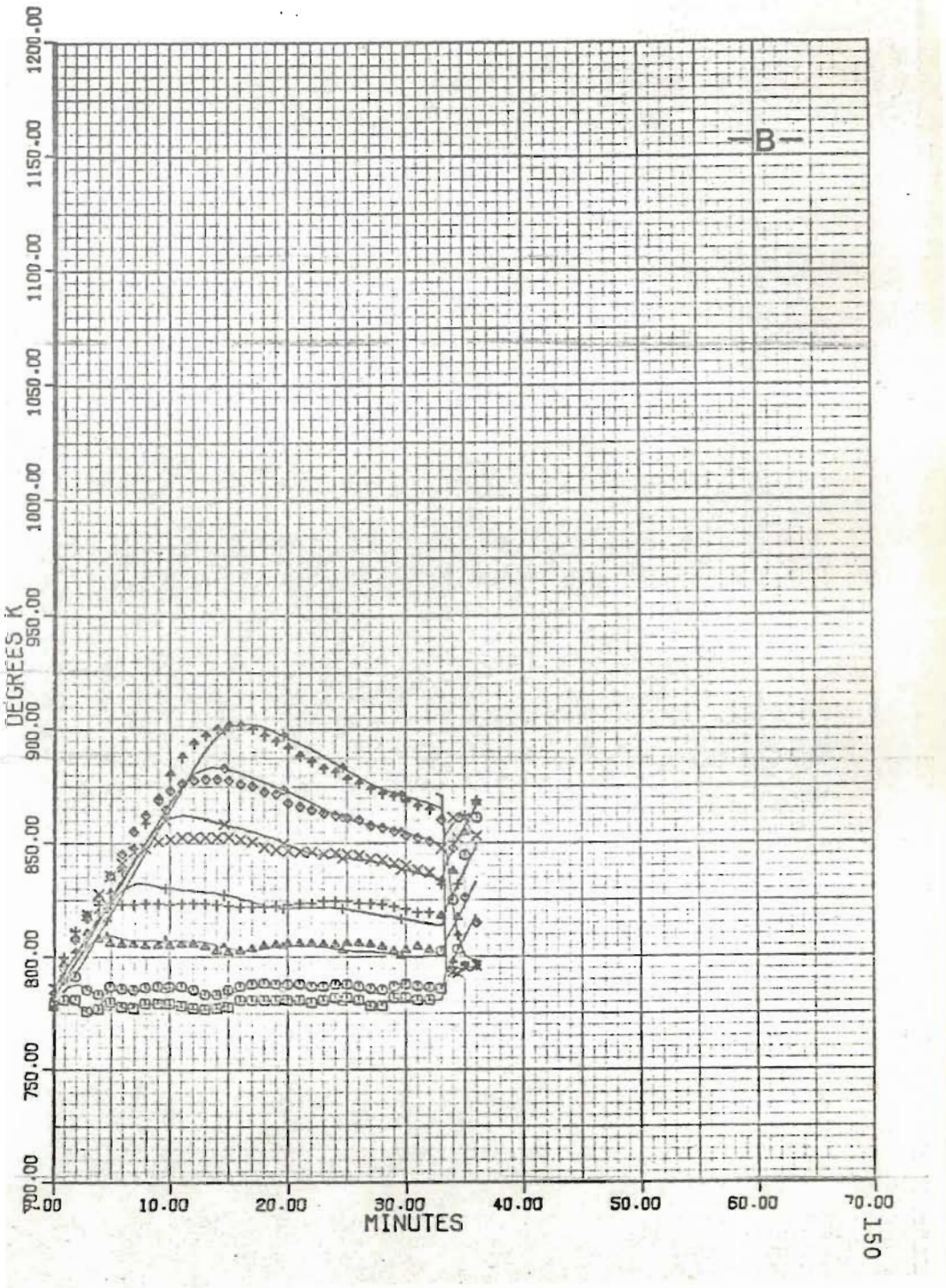

FIGURE 6.36 RUN HH1

G - 1,356

Co - 0,048

y_o - 0,042

To - 810,

k_o - 10,09

For legend see table 6.2

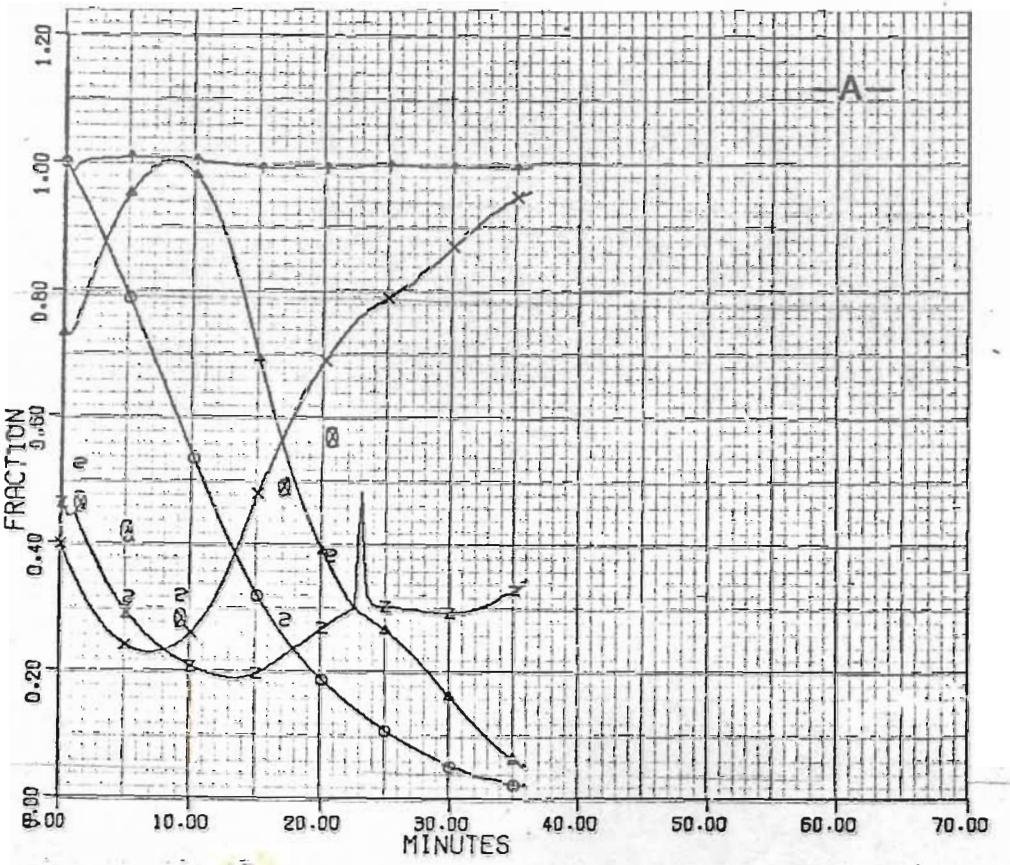

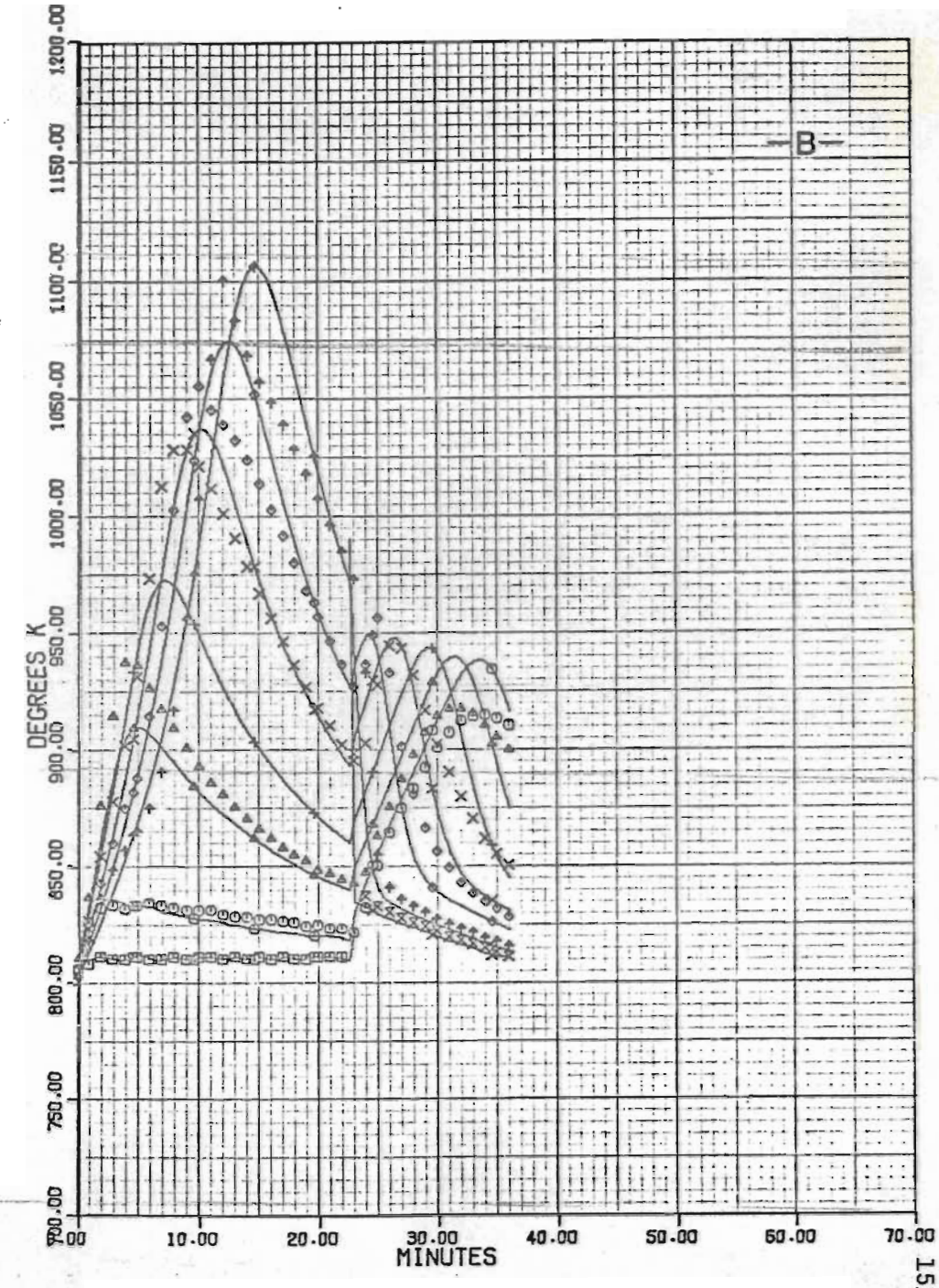

FIGURE 6.37 RUN HH1(C)

G - 1,559

Co - 0,048

y_o - 0,042

To - 810,

k_o - 10,19

For legend see table 6.2

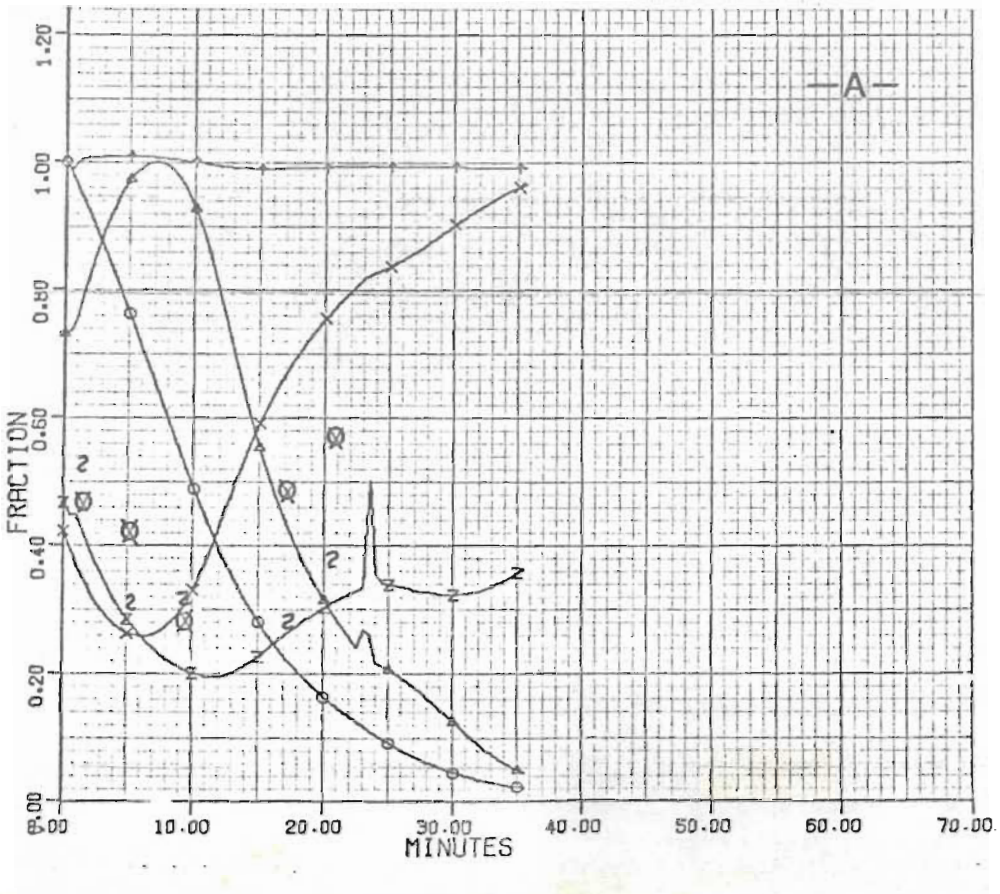

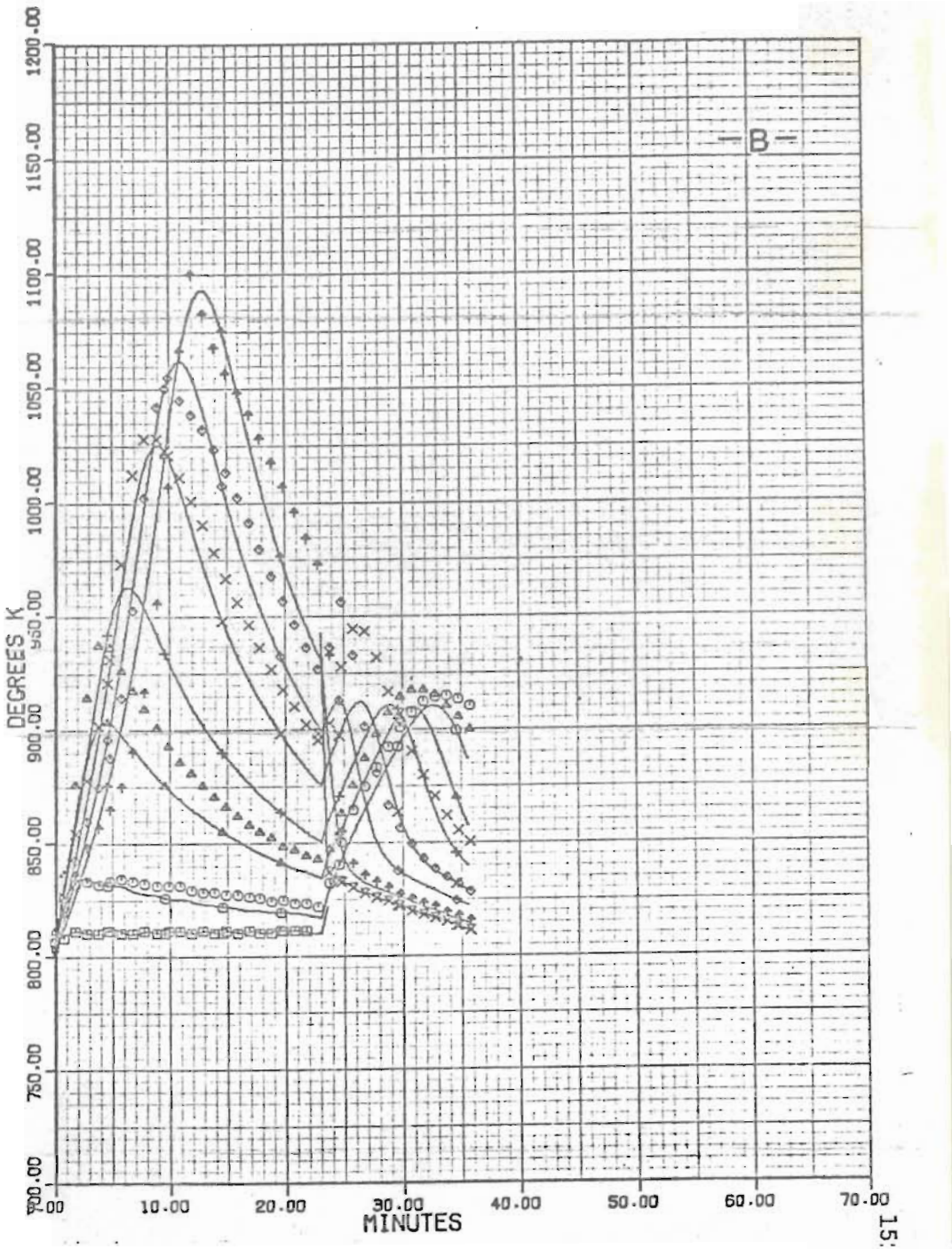

FIGURE 6.38 RUN HH2

G - 1,356

Co - 0,069

y_o - 0,028

To - 808,

k_o - 9,34

For legend see table 6.2

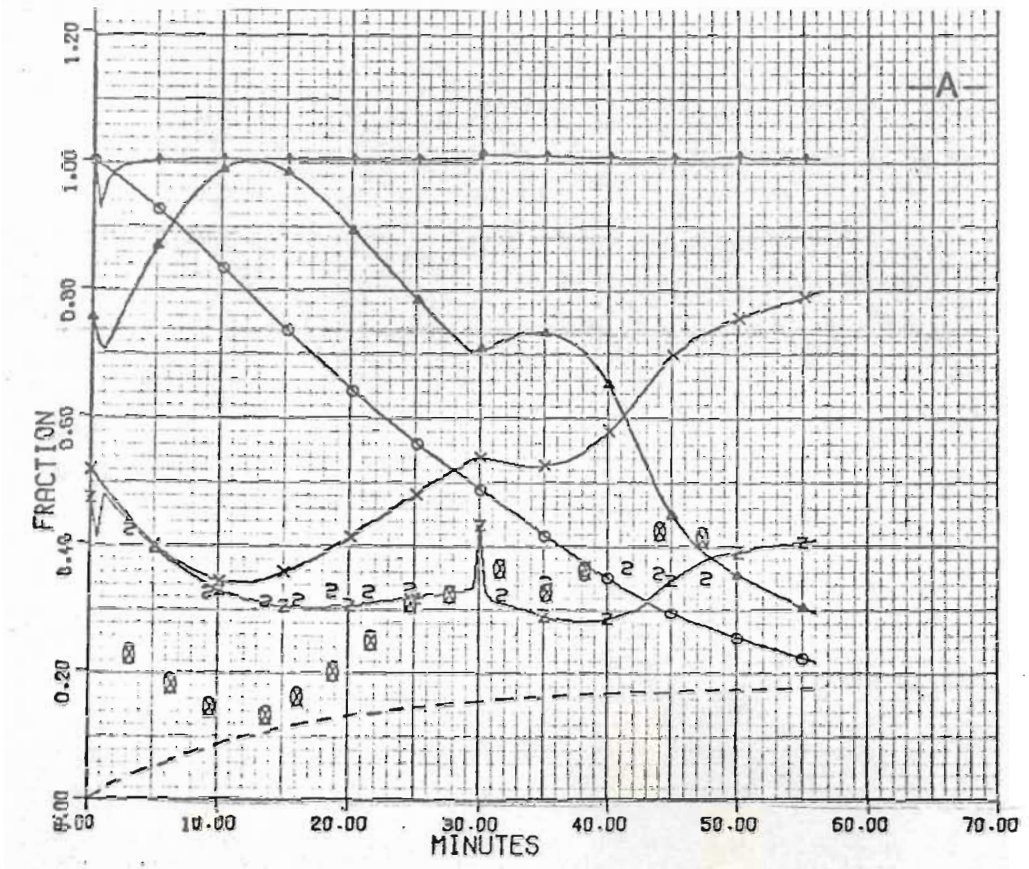

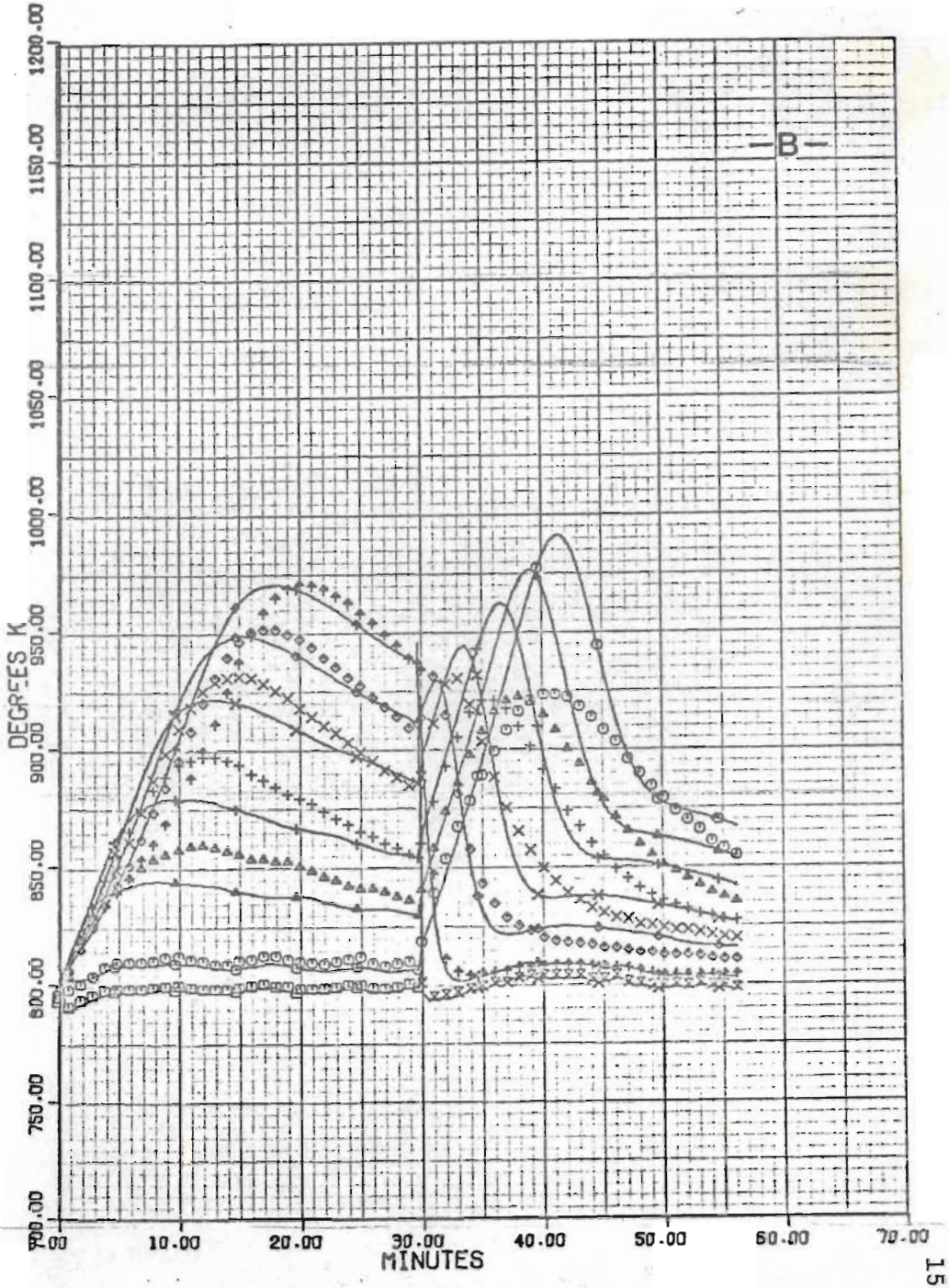

FIGURE 6.39 RUN HH2(C)

G - 1,220

Co - 0,069

y_o - 0,028

To - 808,0

k_o - 9,14

For legend see table 6.2

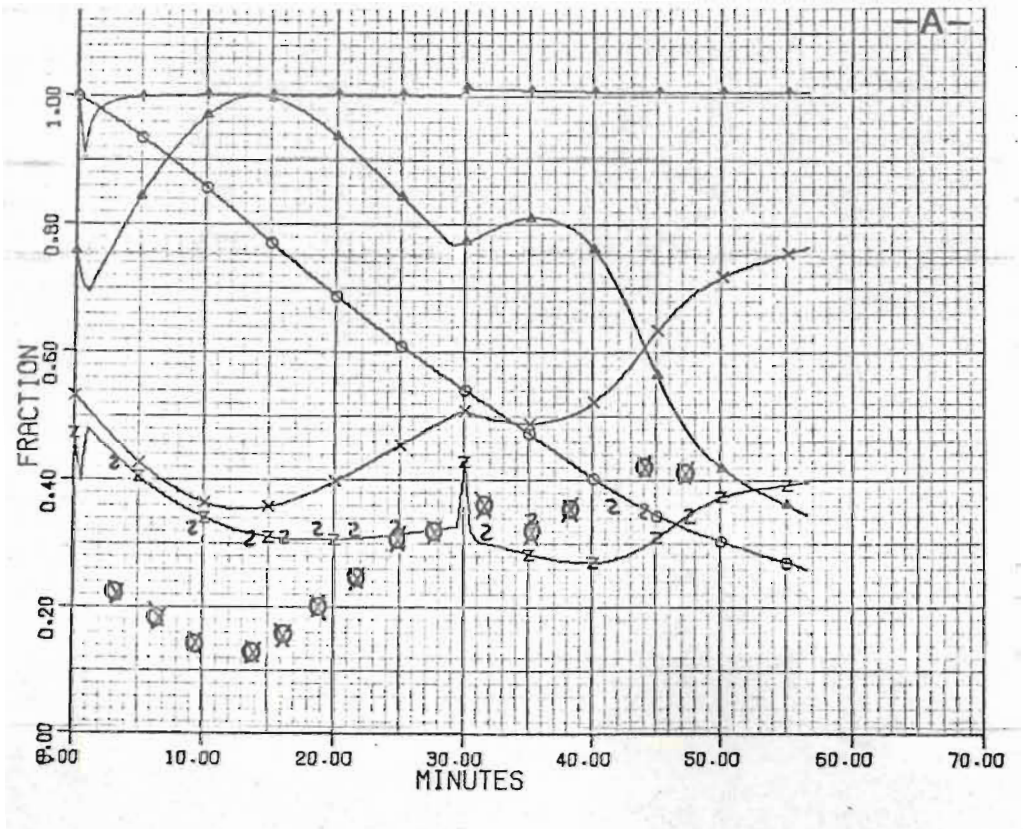

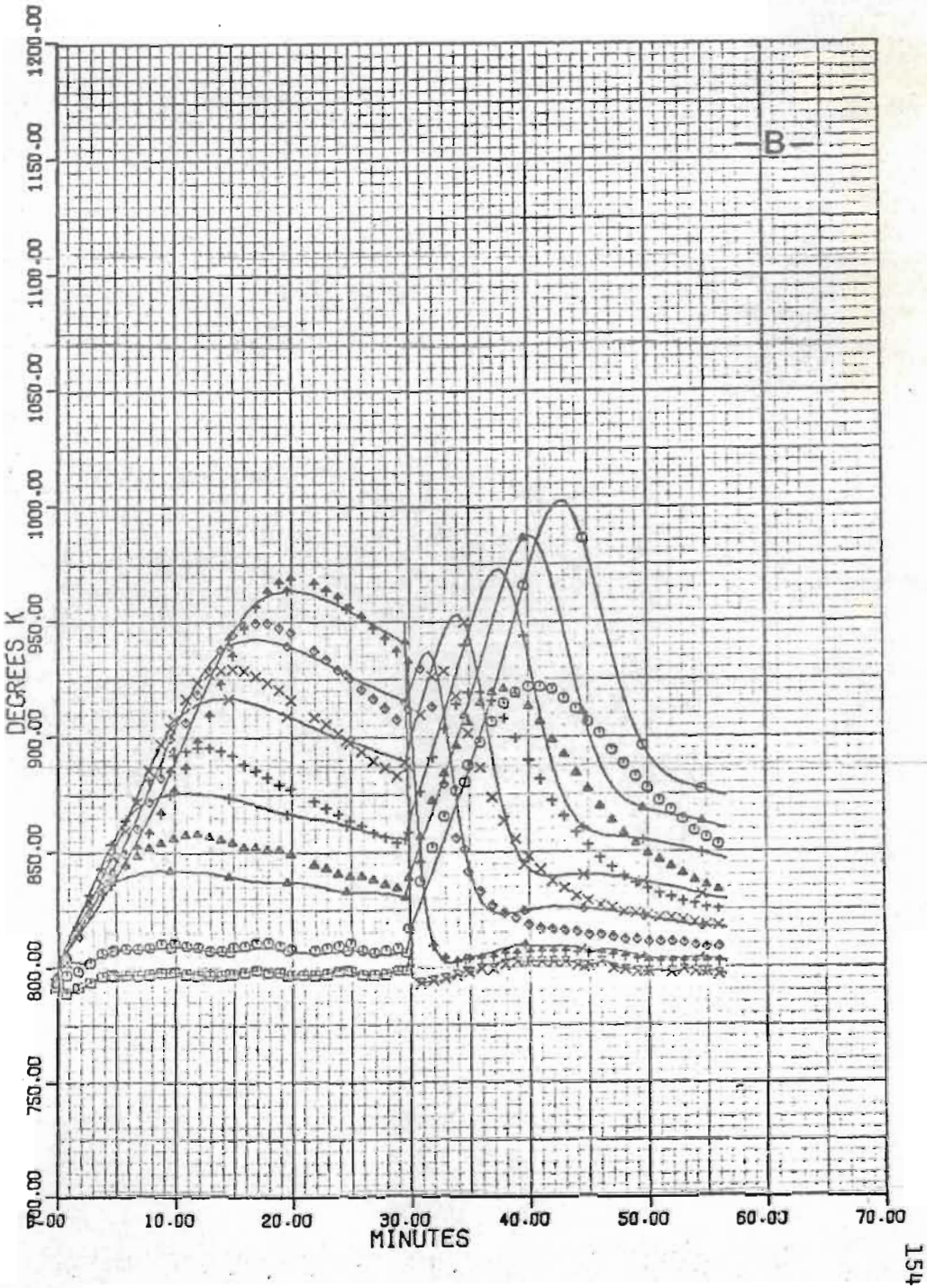

Just after the start of run IL2, figure 6.26, the gas syringe used for gas analysis was damaged and no analysis of the outlet gases was possible for that run. The inlet oxygen concentration however was determined from an inlet gas sample taken during the experiment and analysed after completion of the experiment when a new syringe could be obtained.

6.5.4 Experimental profiles of x', the instantaneous fraction of carbon burned to CO_2 in the outlet.

These profiles are also shown in the "A" parts of figures 6.18 to 6.39 for all the runs but run IL2. They were obtained by interpolating the CO_2 vs time curve to obtain CO_2 values at times for which CO values had been determined. x' is then given by the fraction $CO_2/(CO_2+CO)$ where both CO_2 and CO are outlet gas concentrations.

6.6 Comparison between Experimental and Computed Results.

6.6.1 Preliminary results.

The need for an Arrhenius type of reaction rate expression became apparent soon after this work was started. A regeneration run HUL, with a bed containing 6,9% carbon and a gas flowrate of 1,356 kg/m^2s containing 5% oxygen, was attempted at several nominal base temperatures. Firstly the reactor was taken up to a temperature of 550^oK. When the gas containing 5% oxygen was introduced, no rise in temperature could be discerned at all. The bed was then heated to 663^oK and the gas containing the oxygen was reintroduced. At this level, after 15 minutes the biggest temperature rise in the bed was found to be less than 3^oK. Oxygen flow was again stopped and the bed heated to a uniform 731^oK

before it was introduced again. At this level the temperature profiles shown in figure 6.17 were obtained. Comparing these profiles with those of run HL2, figure 6.33, it appears that although the oxygen concentration for run HUL was 40% greater than that of run HL2, the temperature rise for HUL was only 120°K whereas HL2, which had a nominal base temperature of 752°K, had a temperature rise of 140°K. This difference in performance could not be due only to the small amount of carbon removed at 663°K. In conjunction with the implications of the visual observations made on pellets partly regenerated at different temperatures (figure 3.1) indicating reaction rate control, the need for a temperature dependent reaction rate mechanism became apparent.

6.6.2 Temperature profiles.

6.6.2.1 Regression of experimental temperature profiles.

Of the more important parameters, determining the results obtained by the model, De, the diffusion coefficient for oxygen in the pellet was determined experimentally in chapter 5. It was shown in sections 6.1.3 and 6.1.4 that the effects of Fq, determining the level of the ratio in which CO and CO_2 are produced, and U, the overall wall heat transfer co-efficient, on the temperature profile, were relatively small compared with those of the Arrhenius rate expression parameters k_o and E. It will also be shown in sections 6.6.4 and 6.6.5 that the value for U and Fq = 1,0 used in the standard case are reasonable values. They have also been used for simulating the experimental runs.

Of all the important parameters, the activation energy and the pre-exponential factor of the Arrhenius rate expression were the most critical to be defined. These parameters were to be inferred from the

experimental temperature profiles and a considerable amount of computing was done to regress for these two parameters. Automatic regression proved not feasible due to the difficulties in formulating an objective function. Regression "by eye" however could not only incorporate peak position and peak heights, but also the shape of the curves.

6.6.2.2 The Arrhenius reaction rate parameters k_o and E.

When investigating the effect of k_o and E on the temperature profiles in section 6.1.2, it was shown that the shape of temperature profiles and the relative peak heights at different points in the bed were criteria to be used in evaluating values of k_o and E appropriate to the conditions in the reactor. The effect of the activation energy E, was mainly on the shape of the curves and the relative peak heights, whereas k_o determined the general activity level of the reaction.

Published values for the activation energy range from about 1,0 to $1{,}7\times10^8$ J/kg mole (section A1.4.1). One of the most acceptable values seems to be that by Weisz and Goodwin (1966), who reported $1{,}57\times10^8$ J/kg mole for our type of catalyst. This value however gave peaks that were too steep and too great a spread of peak heights. It was found that using an activation energy of $0{,}78\times10^8$ J/kg mole, i.e. half the value reported by Weisz and Goodwin, gave a steepness to the computed curves which compared well with that found experimentally. Also using this value, on the average the relative heights of profiles obtained at different bed points for the same run compared well with that of the experimental curves. With this value for the activation energy, it was then a matter of choosing the pre-exponential factor which would give the best fit between the experimental and simulated profiles. Regressing

"by eye", k_o values were obtained for best general fit with more weight given to the more important higher temperature profiles. These values are tabulated in table 6.1. The best fits are plotted as continuous lines with the experimental plots in figures 6.18 to 6.39.

For the normal flow parts of the curves, the fits, in general, are fairly good with respect to both shape and peak heights. For some runs however, the correlation with respect to peak positions is not good. For runs LL, LI2 and HL2, figures 6.18, 6.21 and 6.33, the experimental temperature profiles lag the computed profiles quite considerably. The only way that the computed and experimental profiles could be made to correlate, was by adjusting the flow rates used in the simulations. These flow corrected simulations, indicated by adding (C) to the relevant run names, are compared with the appropriate experimental profiles in the figures listed in table 6.1. Only small changes in k_o (listed in table 6.1) were needed to give the best fits for these corrected flow-rates.

The different reaction rates and activation energies reported for the combustion of carbon on Si-Al catalyst, were used to plot the various reaction rates found, against the reciprocal of temperature and compare them with the activation energy and average pre-exponential factor used in this work. The rate data plotted in figure 6.40 is from Hagerbaumer and Lee (1947), Webb and Den Herder (1951), and Pansing (1956), as cited by Olson (1962) and from the authors mentioned in section A1.4. All the data was expressed as rates of combustion (s^{-1}) at a carbon weight fraction of 0,02 and an oxygen mole fraction of 0,02. The average rate used for our simulations is of the same order as that found by other workers. The activation energy used, however, was quite different.

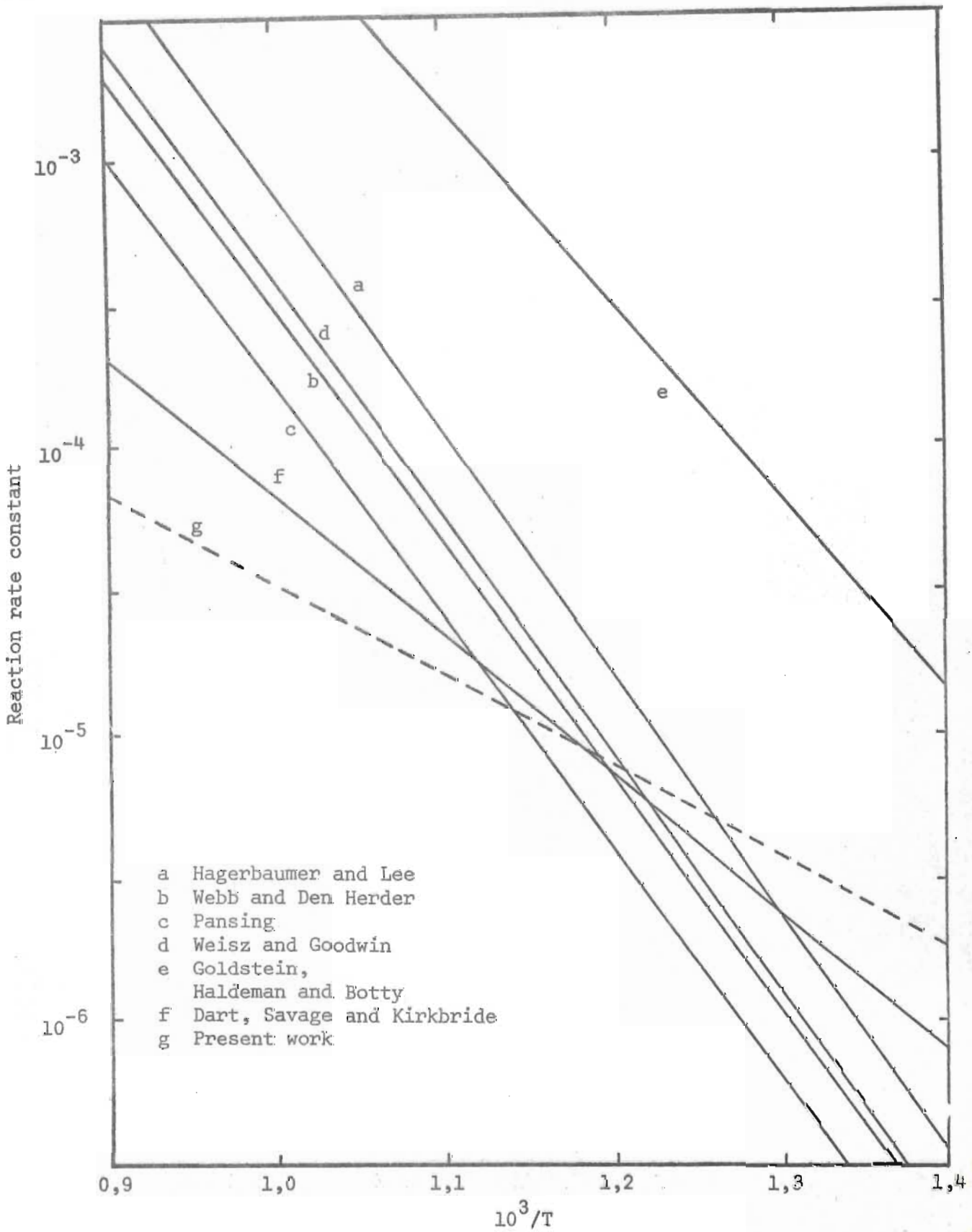

FIGURE 6.40 REACTION RATE CONSTANT vs $10^3/T$

To evaluate the correctness of the choice of the value for the activation energy, the ratios between experimental peak heights at different points in the bed to that obtained at the point 0,864m from the entrance, were compared with ratios obtained by simulation. If the appropriate value of E has been assumed, the two sets of ratios should be identical. The experimental ratios of all runs are plotted against the calculated ratios in figure 6.41 All the computed ratios for uncorrected flowrates and also for most of the corrected flowrates were used. The points obtained are almost evenly distributed and have a mean deviation of 0,066 about the diagonal representing perfect fit for an activation energy of $0{,}785\times10^{8}$ J/kg mole as used in this work.

Comparing the ratios between peak heights at points 0,355 m and 0,864 m from the entrance of the reactor, for different activation energies, the following table can be constructed.

Activation Energy (J/kg mole)	$0{,}393\times10^{8}$	$0{,}785\times10^{8}$	$1{,}57\times10^{8}$
Peak height ratio	0,700	0,569	0,284

Since from figure 6.41 for $E = 0{,}785\times10^{8}$ J/kg mole the peak height ratio is 0,569 ± 0,066, it is quite clear that of the three activation energies shown, the one used is the appropriate one.

On the average, simulated peak ratios are slightly greater than the experimental ones. It should be noticed, however, that at some of the very low corrected flow simulations, stationary state is approached, whereas the experimental plots do not exhibit this tendency to such an extent. Because of this the computed ratios tend to be high. If the

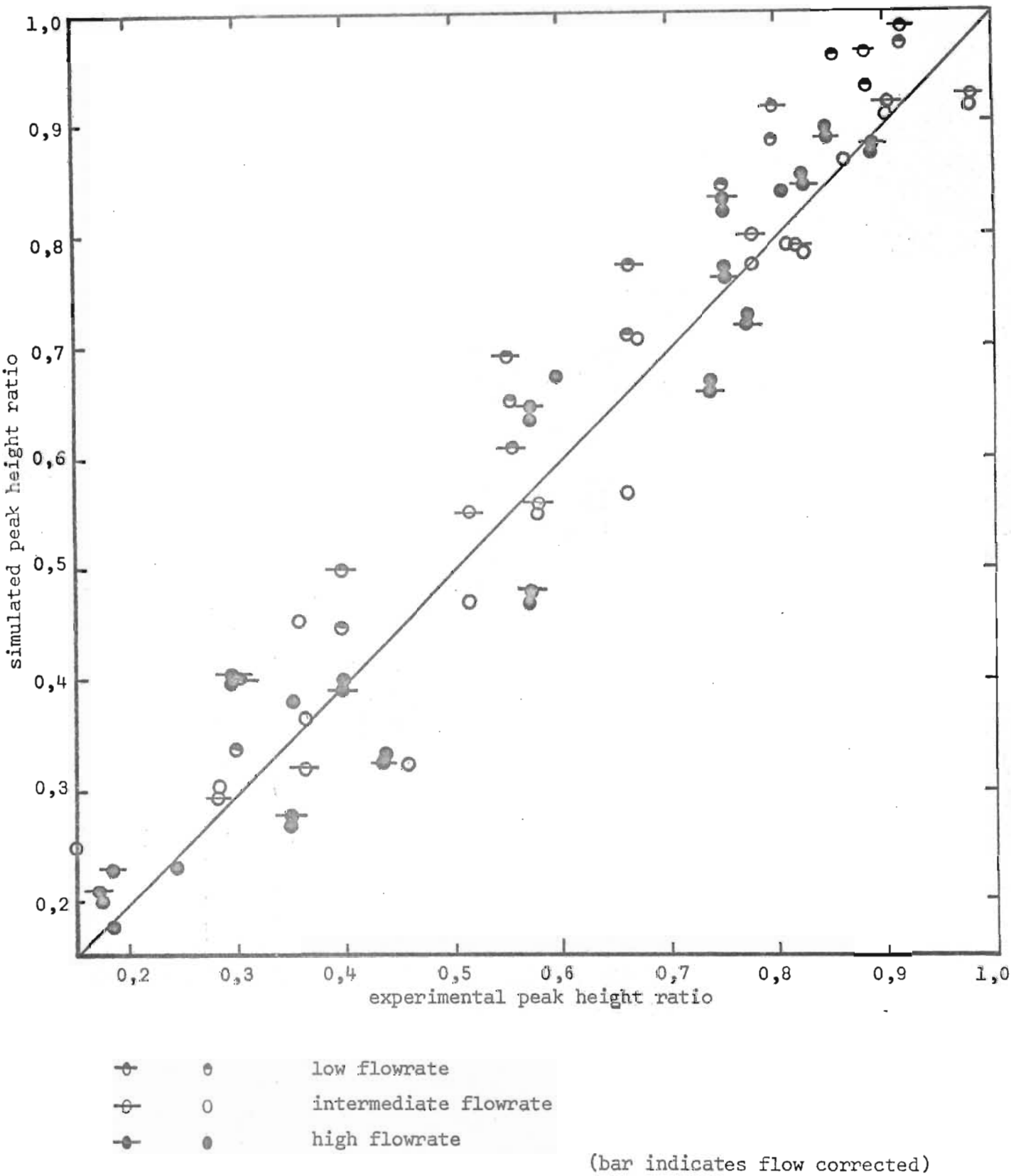

FIGURE 6.41 SIMULATED vs EXPERIMENTAL PEAK HEIGHT RATIOS

difference between the experimental and calculated ratios is real, this would suggest a slight decrease in the activation energy used. The decrease would, however, be smaller than the mean deviation and the time involved in recomputing with a new activation energy does not warrant the slight improvement in average fit which is to be expected. Notwithstanding a general consensus that the activation energy for the combustion of carbon should be $1{,}57\times10^{8}$ J/kg mol, it is clear that the published values of E cannot be used to simulate our experimental data.

It has been shown that for certain runs the fit between experimental and simulated profiles could be improved considerably. The lack of fit without the flow corrections really became apparent only after the experimental program had been finished. The apparatus was then completely stripped and a crack was found in a weld on the gas heater box which was made up from welded sheet metal. It was rather unfortunate that this was discovered at such a late stage in the program. Comparing the original simulated runs with the flow corrected ones, it appears however, that although a much better fit is obtained, only a small adjustment had to be made in the value of k_o, in order to get the best new fit. This may be seen from the k_o values in table 6.1. The change was well within the mean deviation in the average k_o calculated for the three flow regions. The change also brought the means for the different flow regions slightly closer together, although this may not be important as the differences between the three means is much smaller than their mean deviations, through which they overlap considerably.

It was found that for two of the high flowrate runs HL1 and HH1, figures 6.31 and 6.36, the experimental temperature profiles lead the simulated ones. Although the peak positions do not differ greatly, it

cannot be reasonably adjusted by means of flowrates if large increases in flowrate are required to make the peak positions correlate. Since all the peaks for these runs are advanced, it cannot be due to channeling and bypassing of parts of the bed. The reasons for this anomaly are not clear.

6.6.3 Outlet oxygen profiles.

The simulated outlet oxygen profiles are plotted together with the experimental profiles in the A parts of figures 6.18 to 6.39.

The fit between the experimental outlet gas oxygen concentration and the values prediced by the model, varies considerably. For some runs like LI1, LI2, IL1 and HI, figures 6.20, 6.21, 6.25 and 6.35, the fits are quite good. Of these run LI1 was obtained for conditions in which high temperatures were reached. HI also gave a good temperature fit. For LI2 not such a good fit for temperatures is obtained. When this is improved by adjusting the flowrate, the outlet oxygen fit worsens. For some runs the fit is poor, e.g. for HL1, HL2, HHI and HH2, shown in figures 6.31, 6.33, 6.36 and 6.38, although HH2 gave a good temperature fit. Improving the temperature fit by adjusting the flowrate improves the outlet oxygen fit for some runs e.g. II and HL2 but worsens it for others, e.g. LI2 and LH. For run LH, figure 6.23, the computed outlet oxygen values were to some degree consistently lower than those obtained experimentally, but for runs II and HH2, the situation was reversed.

The lowest experimental or simulated values for oxygen concentration anywhere in the reactor bed, were obtained for run LH(C), when the

flowrate was adjusted to 0,475 kg/(m^2s). Outlet oxygen concentrations were low owing to low inlet concentrations combined with high reaction rates due to high inlet temperatures. It was found for this simulated run that the burning zone(arbitrarily defined as the region in which oxygen dopped from 0,95 to 0,10 of the inlet value), extended over at least 0,400 m of the bed. This gives a burning zone length to particle diameter ratio of 63. In all other runs neither experimental nor simulated oxygen concentrations dropped below 0,08 of the inlet value. With a minimum combustion zone length to particle diameter ratio of 63, the variations in oxygen concentration over a single pellet are less than 0,014 of the inlet value. The assumption that conditions along the bed vary continuously (section 3.1) is therefore quite acceptable.

6.6.4 The instantaneous fraction of carbon burned to CO_2, x'

On the whole, the fit between experimental and computed x' profiles, is comparatively good. Some runs like LL, LI2, II and HI, figures 6.18, 6.21, 6.28 and 6.35, gave very good fits. Runs LI1 and HL1, figures 6.20 and 6.31, gave poor fits however. The behaviour of the experimental x' curve for run LI1 is suspect because between 25 and 45 minutes it does not follow a logical trend at all. This is most likely due to malfunction of the gas chromatograph.

Although for run HL2, figure 6.33, the computed values were consistently higher than the experimental values, for most runs without a good fit, the reverse is true. On the whole a good fit for x' values does not seem to be associated with a good fit for outlet oxygen concentrations. Changing flowrates in the simulations only marginally affects the fit of the x' profiles.

For all the simulations shown Fq was taken as 1,0. Reducing Fq for particular runs could improve the fit of the x' curves for those runs. The average fit for all the runs could also be improved to a small extent by reducing the common Fq. In section 6.1.3 it was shown, however, that small changes in Fq hardly affect the temperature profiles. The value of Fq = 1,0 was therefore retained.

6.6.5 The fraction of heat lost through the wall, HW.

Curves representing the computed heat lost through the wall as a fraction of the total heat generated, are shown as broken lines in figures 6.18, 6.30 and 6.38 for runs LL, IH and HH2. These are representative for low, intermediate and high flowrates respectively. The loss through the walls at high flowrates is approximately 17% after 50 minutes. For the intermediate flowrate it is about 27% after 50 minutes and for the high gas flowrate it is about 35%. This trend is as expected since at lower flowrates the gas remains in the reactor for a longer period and will lose more of its heat to the wall of the reactor.

If the value of the overall heat transfer coefficient as estimated in section A2.3.3 were much too high, this would affect the low flowrate runs to a greater extent than the higher flowrate runs and would therefore depress the computed temperature profiles at low flowrates. In order to compensate, one would have to use higher pre-exponential factors in the reaction rate expression to get reasonable computed temperature profiles. Although there seems to be this trend in the average value for k_o for the different flowrates, the mean deviation is so large as to make the trend quite uncertain, especially if run LH, figure 6.23, which needs an exceptionally high k_o value for a good fit, is

excluded from the low flowrate average for k_o (see table 6.1). In that case there is no apparent trend at all. The estimated value of the overall heat transfer coefficient therefore seems to be in order.

6.6.6 Reverse flow temperature profiles.

During the reverse flow period the fits between experimental and computed temperature profiles are not as good as for normal flow conditions. This is to be expected as differences between the experimental and computed profiles built up during the normal flow period, will be carried over into the reverse flow period and be exaggerated. Best fits were obtained for runs IL1, HL1, HL2 and HH1, figures 6.20, 6.31, 6.33 and 6.36.

The runs can be more or less evenly divided between those which show an average predicted temperature higher than the average experimental temperatures and those which predict temperatures on the average lower than those found experimentally. The average reactor activity appears to be the same for the experimental and computed profiles. This indicates that the predicted carbon removed must be similar to that removed experimentally. Lowering simulated flowrates normally raised the reverse flow profiles to some extent, but even then, the predicted carbon removed must have been similar to that removed experimentally. Parameter values used in the model are therefore of the right order.

The overall impression gained from the reverse flow temperature profiles is that flow reversal might be effectively used to speed up the regeneration process, especially at high flowrates or short beds. For run HL2, figure 6.33, for instance, during the normal flow period, the

general activity of the reactor was low and the carbon removal slow. On flow reversal, the reactor was able to operate at higher temperatures; the general level of activity increased considerably and the computed rate of carbon removal also showed a marked increase.

6.7 Comparison with Other Models

It was suggested in section 3.2.2 that in the limit our model should tend to the shrinking core model as used by Olson, Luss and Amundson (1968). This would occur when the reaction rate constant used in our model was made infinitely large. To compare our model with that of Olson, it was therefore applied to the data used by him and for which he computed temperature profiles which were compared with the profiles obtained from the model proposed by Johnson, Froment and Watson (1962). Olson's stoichiometric coefficient α=11,83 gm carbon combusted per gm mol oxygen consumed was equated to our fraction of carbon converted to CO_2 by putting

$$\alpha = 11{,}83 = \frac{12{,}528}{0{,}632+0{,}5x} \qquad \text{(see equation A1.3)}$$

and the equivalent constant value of x was used. The average heat of combustion, for the temperature range involved, was used rather than Olson's temperature dependent expression. The error involved in this assumption was less than 0,1%.

As indicated in section 6.1.5 lowering the flowrate from our 0,542 kg/(m^2s) to 0,0957 kg/(m^2s), the flowrate used by Olson, is roughly equivalent to shortening the bed by a factor of 6. In order to retain an equivalent increment along the bed length, a total bed length a quarter of the one used for our simulations with twice the number of increments

was used. This gave an equivalent increment about 0,7 times that used in our simulations. Making the rate constant infinite, it was found that our model became unstable. It was possible to get a completely stable solution however by increasing the pre-exponential factor by a factor of 10^4 over our standard value. This made diffusion very much the controlling mechanism. The temperature profiles so obtained are shown in figure 6.42 The maximum stationary state temperature rise of 286°K obtained, compares very well with the assymptotic value of 294°K predicted by Olson's model. It should be noted that Olson's initial temperature peak was never observed. For the conditions used in our work there never was any experimental evidence for such an initial temperature peak, nor was this reported by Ishida and Shirai (1969) who did experimental work on diffusion controlled combustion in single spheres. Simulations (see figure 6.14) indicate however, that with a longer bed and smaller flowrates, these initial peaks are likely to occur also for our conditions.

Olson et. al. compare their temperature rises as a function of length along the bed at 7,91 minutes after the start of the reaction with that of Johnson. Superimposing the profiles obtained at 7,91 minutes from our model on theirs in figure 6.43 it appears that the tail end of the profile compares very well but that the temperature peak predicted by our model has moved further into the bed. Also at that stage, our model has not approached the stationary state temperature rise as closely as the models by Johnson and Olson.

Although x_s, the fraction of carbon burned to CO_2 was made constant and equal to 0,854 to fit Olson's data, from the material and energy balances, values of x_M = 0,88 and x_H = 0,70 were obtained. This indicates

that relative to the carbon consumed there was an excess oxygen consumed and not enough heat produced. When the overall rate of combustion is diffusion controlled, the carbon gradients and hence the oxygen gradients in the pellet are very steep. With the limited number of grid points used for the pellet, the oxygen and carbon profiles at the burning zone in the pellet cannot be adequately represented and the model begins to break down. From the comparison with Johnson and Olson's models, it is clear though, that our model can be applied for a wide range of conditions. In order to predict profiles close to those obtained by Johnson and Olson, our model had to assume extremely high reaction rates. The standard reaction rate used when simulating our experimental results, when used on Olson's data gave, after 11 minutes, a temperature rise of only 10°K, which implies the inability of Olson's model to predict the behaviour of our bed. The same would apply to Johnson's model.

Although written to accommodate reaction rate control alone or in conjunction with diffusion control, our model is also capable of predicting with a fair degree of accuracy the type of behaviour to be expected when diffusion is solely controlling.

In our work, reaction rate control played a much more important role than as found by other workers. One reason for this is that the pellets used were very porous and the experimentally determined diffusivities were high. Another possible contributing factor is the history of the coke by the time it was burned off. It was kept for extended periods at high temperatures both during the cracking of the sugar and during preheating in the reactor. Most of the hydrogen containing fractions of the coke were probably driven off and an appreciable fraction of the coke graphitised. This possibility, which was

indicated by Bondi, Miller and Schlaffer (1962), was also suggested by observations made when catalyst whose coke was cracked at temperatures considerably higher than those normally used, was found to be more resistant to oxidation by oxygen.

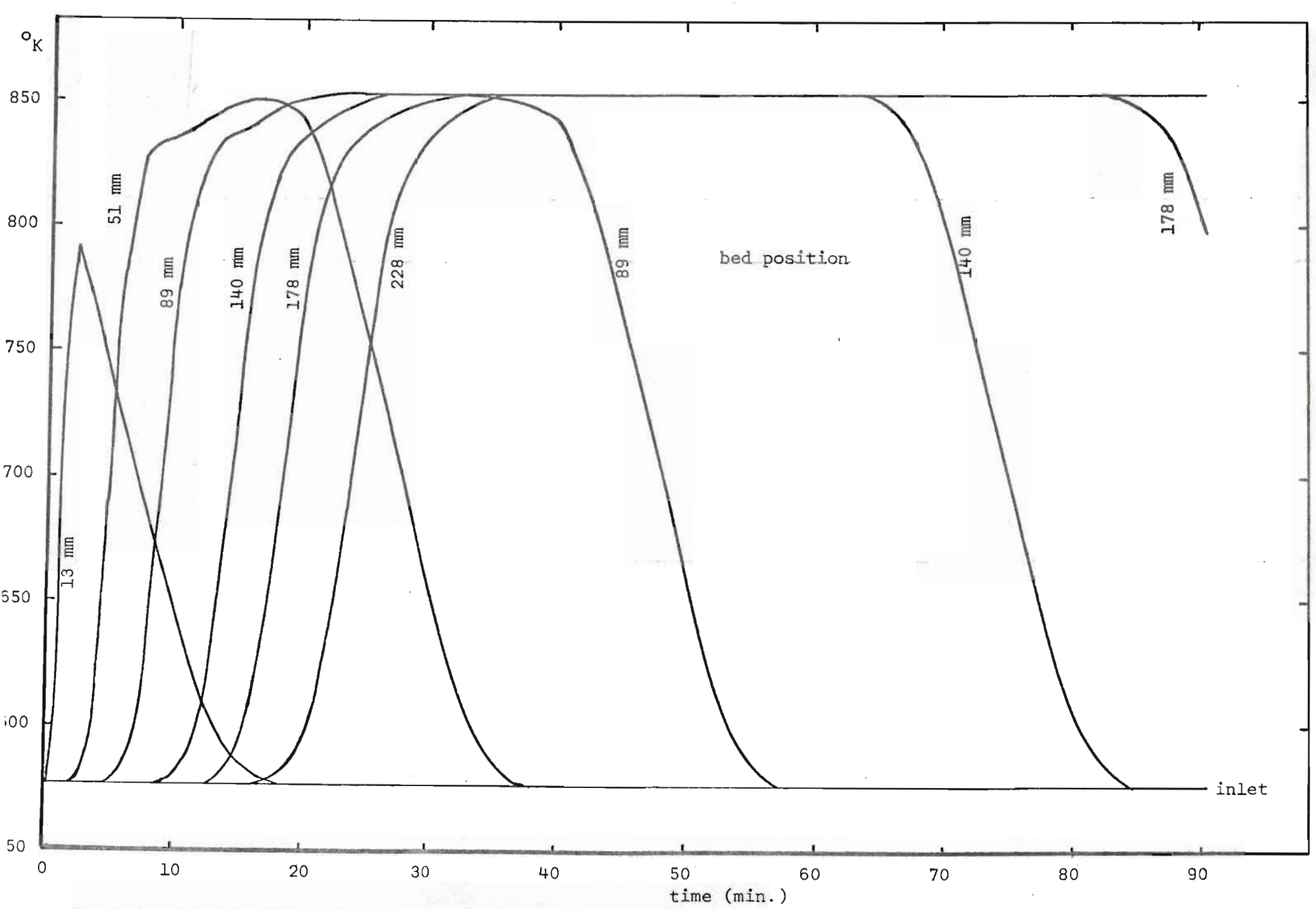

FIGURE 6.42 TEMPERATURE PROFILES FOR OLSON'S DATA

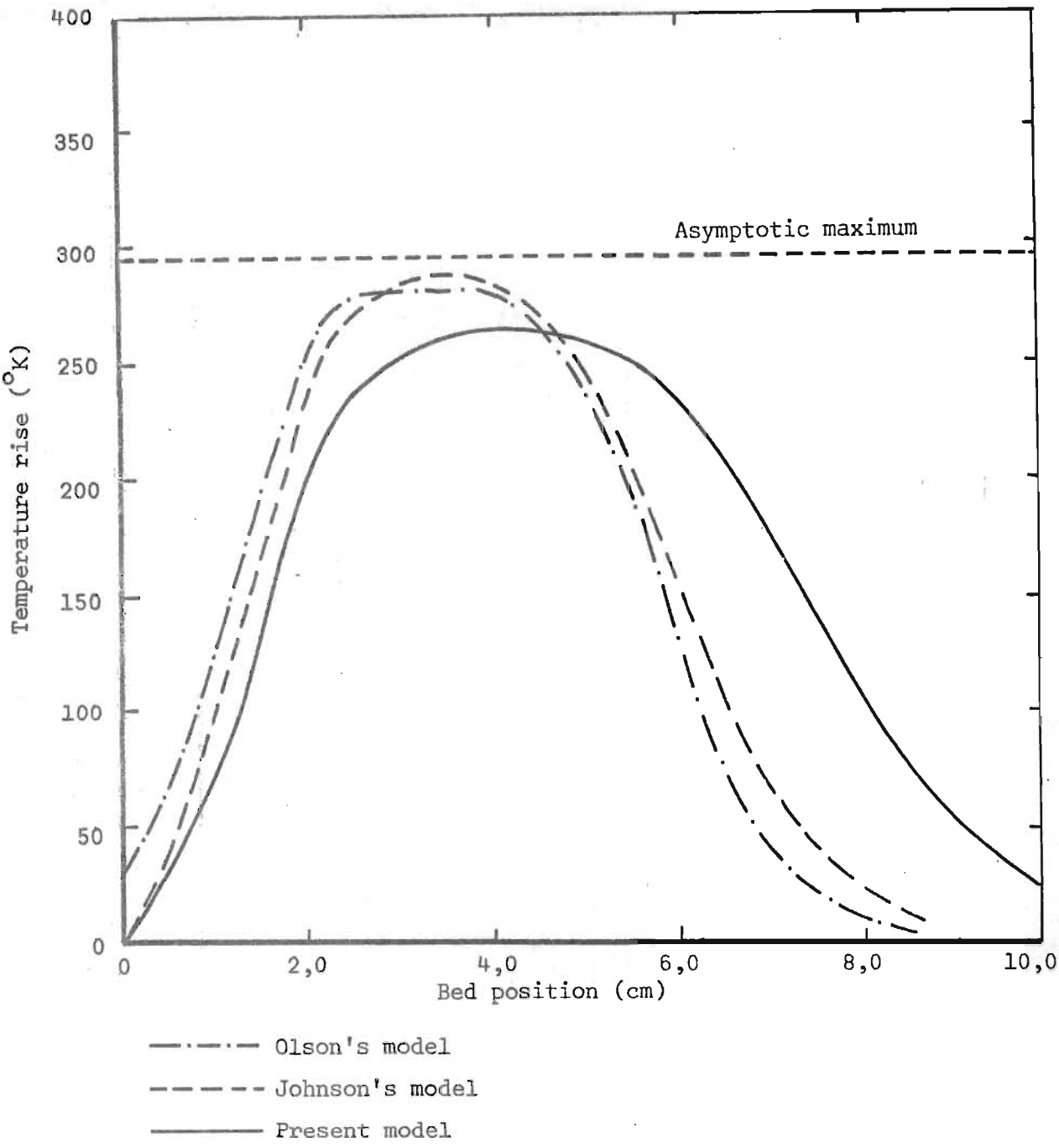

FIGURE 6.43 TEMPERATURE PROFILES AT t=7,91 MINUTES; COMPARISON OF PRESENT MODEL WITH JOHNSON'S AND OLSON'S MODELS

CHAPTER 7

CONCLUSIONS

Models based on diffusion control alone cannot simulate the observed behaviour of a fixed bed of carbonised catalyst pellets during regeneration at low temperatures. In particular, the lack of ignition at temperatures below 660°K cannot be simulated.

A numerical model has been developed for the simulation of the combustion of carbonised pellets in a fixed bed, where the overall rate may be either reaction rate or reaction rate and diffusion rate controlled. Dependence on temperature for most parameters is assumed. Simplifying assumptions made are: that there is no accumulation of oxygen in the bed or pellets, that there is no accumulation of heat in the gas phase, and that there are no radial profiles in the bed.

The model simulates, with fair accuracy, diffusion rate controlled behaviour.

Temperature profiles are predicted for regeneration, which are practically invariant with bed position or gas flowrate, provided L/G, the ratio of position along the length of the bed to gas flowrate, is held constant.

Axial conduction of heat in a fixed bed is unimportant for the conditions considered in this work.

Pre-exponential factors k_o, and a value of the activation energy E, were obtained to fit the experimental data. The value of E found is significantly lower than the best values that are available in the literature for the uncatalysed combustion of carbon.

This could be an indication of some anomaly in the combustion process during regeneration. However, because of the large number of dependent variables that simultaneously influence the simulated profiles, it is quite impossible to draw unequivocal conclusions from the experimental results that were obtained.

For short beds or high gas flowrates, reversal of gas flowrate may reduce the regeneration time up to at least 30%, depending on the degree of regeneration required.

CHAPTER A1

THE REACTION SCHEME.

A1.1 The Extents and Relative Rates of the Reactions in the Gas Phase

Walker and co-workers (1959) have reported on the relative rates of different carbon-gas reactions. It appears that in the range of temperatures of interest, the rate of the carbon-oxygen reaction is about 6 to 8 orders of magnitude greater than that of the carbon-carbon dioxide and carbon-steam reactions. Since the average residence time of the gases in the bed is of the order of seconds, it may be assumed that once the CO/CO_2 ratio has been established at the carbon surface only a gas phase reaction will change this ratio. This change may occur through one of the following reaction schemes :

a) $CO + H_2O \rightleftarrows CO_2 + H_2$ (i)

$H_2 + \frac{1}{2}O_2 \rightarrow H_2O$ (ii)

b) $CO + \frac{1}{2}O_2 \rightleftarrows CO_2$

For the first mechanism reaction (ii) is virtually instantaneous, so that only the rate of reaction (i) needs to be considered. Moe (1962) reports some rate data for the water shift reaction over an iron oxide - chromium oxide catalyst. Using most unfavourable conditions of no H_2 and 5% H_2O in the range 750 to 950 ^oK with Moe's data, a maximum rate of about 10^{-5} kg mol/(m^3s) is obtained for this catalyst. Not using the specific catalyst and at lower reactant concentrations, the rate will be much smaller.

For reaction b)

$$Kp = \frac{P_{CO_2}}{P_{CO}(P_{O_2})^{\frac{1}{2}}}$$

where p is the partial pressure. Hence at equilibrium

$$\frac{[CO_2]}{[CO]} = \frac{p_{CO_2}}{p_{CO}} = Kp\ (p_{O_2})^{\frac{1}{2}}$$

where the square brackets indicate concentrations. Walker and co-workers (1959) report values for Kp from which it appears that Kp decreases with temperature. The lowest equilibrium ratio $[CO_2]/[CO]$ will therefore be obtained at high temperatures and low oxygen concentrations. Experimentally the temperatures would remain below $1000^{o}K$ and oxygen would never drop below say 0,3% by volume, which using Walker's data gives a minimum ratio of about 10^{8}. In the gas phase CO would therefore tend to convert to CO_2 in the presence of O_2. Now for the reaction

$$CO + O \rightarrow CO_2$$

Baulch and co-workers (1968) recommend tentatively a rate of

$1{,}78 \times 10^{13} \exp(-2530/RT)[CO][O]$ kg mole/$(m^3 s)$.

Penner (1968 - page 79) reports

$$\frac{[O]}{[O_2]^{\frac{1}{2}}} = 6{,}06 \times 10^{-8}\ (Pa)^{\frac{1}{2}} \quad \text{at } 1000^{o}K$$

Combining these two expressions and taking concentrations for CO and O_2 as 5% by volume this gives in the temperature range of 750 to $950^{o}K$ a rate smaller than 5×10^{-7} kg mole/$(m^3 s)$.

If one considers that the mean residence time of gases in the gas phase is less than 1 second and 1% CO by volume is about $1{,}2 \times 10^{-4}$ kg mol/m^3 at $750^{o}K$, it may be concluded that the effect of the two reaction schemes mentioned on the CO/CO_2 ratio is negligible. All the heat is therefore generated in the pellets.

A1.2 Relative Rates of CO_2 and CO Produced

Walker et. al. (1959), in their review, report from several sources that on combustion of carbon, q, the ratio of moles of CO produced to moles of CO_2 produced, is given by

$$q = 10^{3,4} e^{-6\ 241/T} \quad \text{for } 730 < T < 1173°K$$

Walker et.al. also reported some authors who found similar temperature dependence but lower ratios. It seems that the presence of water vapour would reduce the ratio. For the present work the reported ratio was used, multiplied by a factor Fq, which is to be adjusted to give best fits with the experimental results. In the units used here the ratio may be written : $q = \exp(\ln Fq + 7,83 - 6\ 241/T)$

For $1,0 < Fq < 0,33$ and $750 < T < 950°K$, q was found to vary between 0,22 and 4,24. For the combustion of coke in catalyst Wunderlich and Ivey (1958) measured q values ranging from 0,3 to 0,8. Webb and Den Herder (1951) obtained values of 0,8 for fresh and 0,4 for aged silica alumina catalyst. Hagerbaumer and Lee (1947) found for synthetic catalyst values ranging from 0,5 to 1,2.

Defining x as the fraction of carbon converted to CO_2 and N as the moles of C consumed per mole of O_2 consumed, then from the above expression and the mass balance equation (A1.3)

$$q = (1-x)/x \qquad \text{or} \qquad x = 1/(1+q) \qquad \text{(A1.1)}$$

$$\text{and} \quad N = 1/(0,632 + 0,5x) = (1+q)/(1,132 + 0,632\ q) \qquad \text{(A1.2)}$$

where for $0,33 < Fq < 1,0$ and $750 < T < 950°K$

$$0,22 < q < 4,24$$

$$0,82 < x < 0,19$$

$$0,99 < N < 1,37$$

A1.3 Heat of Combustion

Several authors like Dart and Oblad (1949), Johnson (1956), Weisz and Goodwin (1963) and Goldstein (1966) report H/C values for coke. These values range from 0,041 to 0,083 kg H/kg C. For this work the figure 0,044 kg H/kg C as reported by Dart and Oblad was used. This is equivalent to 0,264 kg mole H_2 per kg mole C or 0,264 kg mole H_2 per 12,528 kg coke. If a fraction x of the carbon consumed, is converted to CO_2 and the rest to CO, the following molecular balances can be written for the combustion of coke.

$$x\,C + x\,O_2 \rightarrow x\,CO_2$$

$$(1-x)\,C + \left(\frac{1-x}{2}\right)O_2 \rightarrow (1-x)\,CO$$

$$0{,}264\,H_2 + 0{,}132\,O_2 \rightarrow 0{,}264\,H_2O$$

$$1\,C + 0{,}264\,H_2 + (0{,}632 + 0{,}5x)\,O_2 \rightarrow x\,CO_2 + (1-x)\,CO + 0{,}264\,H_2O \quad \text{(A1.3)}$$

The heat of reaction at any temperature T, may be calculated by

$$\Delta H = \Delta H_{298^\circ K} + \int_{298^\circ K}^{T} \nabla c_p \, dT$$

Dart and Oblad (1949) report for their coke a heat of combustion (to carbon dioxide and water) of $3{,}89\times10^7$ J/kg at 298°K which they obtained by plotting the heats of combustion against hydrogen content for several hydrocarbons and reading off the heat of combustion for coke at the relevant H/C ratio. Per kg mole of carbon, i.e. per 12,53 kg of coke this gives a heat of reaction of $-4{,}88\times10^8$ J/kg mole C. From Hougen, Watson and Ragatz (1962) the heat of combustion of CO to CO_2 is $2{,}84\times10^8$ J/kg mole CO or $2{,}84\times10^8$ J/kg mole C and the latent heat for water at 298°K is $4{,}404\times10^7$ J/kg mole. Then if a fraction (1-x) of carbon is converted to

CO and 0,264 mole of water per mole of carbon are in the vapour rather than in the liquid phase,

$$H_{298^oK} = -4,71\times10^8 + 2,84\ 10^8(1-x) \quad J/kg\ mole\ C$$

In order to evaluate $\int \nabla c_p\ dT$, heat capacity data for O_2, H_2, CO_2, CO and H_2O at zero pressure obtained from Hougen, Watson and Ragatz (1962) was used. For coke, heat capacity data was obtained from Olson (1962), who estimated it to be somewhere between that of anthracene and naphthalene on the one hand and graphite on the other. He estimates for the range 290 to 970°K for coke

$$c_c = -85,8 + 4,33\ T - 2,14\times10^{-3}T^2 \quad J/(kg\ K)$$

In section A1.2 it is shown that x the fraction of C converted to CO_2, will not lie outside 0,20 and 0,85. In the range 750 to 950°K for x varying from 0,05 to 0,85, $\int \nabla c_p\ dT$ varied between -5,36 and $-1,67\times10^6$ J/kg mole C. The $\int \nabla c_p\ dT$ term was therefore taken as $-(3,52\pm1,85)\times10^6$ J/kg mole C.

From the above the heat of combustion of coke in the range 750°K to 950°K reduces to

$$\Delta H = -1,97\times10^8 - 2,83\times10^8 x \quad J/kg\ mole\ C \qquad (A1.4)$$

For the least favorable condition of x = 0,20 and 950°K the error due to the uncertainity in $\int \nabla c_p\ dT$ is 0,9%. Normally it would be much less.

Dart, Savage and Kirkbride (1949) found that the hydrogen in the coke burned off much faster than the carbon. A 10% removal of carbon was associated with a 50% removal of hydrogen. Comparing the $3,89\times10^7$ J/kg liberated if the coke combusts to CO_2 at 298°K with the values for carbon and hydrogen given in Perry (1950), about 16% of the heat is due to

hydrogen. This indicates that when combustion has just started in a pellet, the heat of reaction is relatively high, after which it will drop to a value lower than the average value for the coke. During most of the combustion coke both rich and poor in hydrogen will be present in the pellet, and most of the overall heat of combustion will be close to the average value of $3{,}89 \times 10^7$ J/kg. For the whole of the bed this averaging process also applies again. It is therefore assumed that equation (A1.4) is valid for the reactor.

A1.4 The Intrinsic Rate of Reaction

A1.4.1 Activation energy.

The literature reports a fairly wide range for the activation energy associated with the intrinsic reaction rate of the combustion of coke in porous catalyst. Dart, Savage and Kirkbride (1949), Johnson and Mayland (1955), Haldeman and Botty (1959), Hall and Rase (1963), Weisz and Goodwin (1966), Goldstein (1966), Ramaswamy and Stermole (1967), Massoth(1967), and Shettiger (1972) report values from about 1,0 to $1{,}7 \times 10^8$ J/kg mole. They were obtained for several different catalysts like Si-Al catalyst and clay cracking catalyst for packed beds, and Si-Mg catalyst for fluid beds. Of the most complete experimental determinations have been reported by Weisz and Goodwin, who report for a Si-Al catalyst for both catalysed and uncatalysed combustion the same activation energy of $1{,}57 \times 10^8$ J/kg mole. The catalysed rates were up to several orders of magnitude higher than the uncatalysed ones. They also showed that for their catalysts the activation energy appears to be independent of the method of coke preparation.

Haldeman and Botty, Dart, et.al., and Massoth found that hydrogen in the coke burned off faster than carbon. Their results indicate that the first material to react has an average formula near CH_2. Since the original coke has an approximate composition of $CH_{0,5}$, a coke richer in carbon is left as the reaction proceeds. Hall and Rase in DTA studies on regeneration of carbonised catalyst, found evidence indicating that at least two reactions, a fast and a slow reaction, occurred. Since combustion moved smoothly from predominantly hydrogen rich to predominantly carbon rich compounds, it is likely that activation energies and pre-exponential factors associated with these reactions also move smoothly through a range of values. It appears then that the reported activation energies represent the overall kinetic behaviour of an essentially complex reaction system.

Bondi, Miller and Schlaffer (1962), comparing regeneration rates obtained in laboratories with those obtained industrially, indicate that the method of deposition of coke may affect its eventual combustion rate. However, cokes with different histories are likely to differ only quantitatively.

Cremer (1955) indicates that for certain types of catalytic reactions, instead of the frequency factors varying independently of the activation energies in a spectrum of reactions, in effect the frequency factor varies with activation energy and there is a so-called compensating effect. It would seem reasonable to assume that a similar situation could exist for a spectrum of reactions as occur during the combustion of coke.

In the light of the above, it is maybe not so surprising that the

activation energy reported by Weisz and Goodwin corresponds well with the $1{,}54 \times 10^8$ J/kg mole obtained by Gulbransen (1952) for graphite, and with the values of $1{,}49 \times 10^8$ to $1{,}67 \times 10^8$ J/kg mole obtained by Effron and Hoeschler (1964) and Essenhigh, Froberg and Howard (1965), also for graphite. Laz'yan, Panchenkov, Kozlov and Zhorov (1969) found an activation energy of $1{,}51 \times 10^8$ J/kg mole to give best fits with their experimental results for a moving bed. Initially the value reported by Weisz and Goodwin was used for simulation purposes, more appropriate values were determined by the closeness of fit with the experimental results.

A1.4.2 Order of reaction with respect to oxygen.

As reported by Walker, et.al. (1959) in their review, the carbon-oxygen reaction is generally accepted to be first order with respect to oxygen. Notable exceptions were reported for very low oxygen concentrations when Gulbransen and Andrew (1952) obtained zero order for oxygen pressures less than 1,5 cm of mercury and first order for oxygen pressures above 10 cm. Blyholder and Eyring (1957) confirmed the zero order behaviour at very low pressures. For coke deposits on porous catalyst material, a first order reaction with respect to oxygen is generally reported, e.g. by Hagerbaumer and Lee (1947), Johnson and Mayland (1955), and Dart, Savage and Kirkbride (1949). For computing purposes a first order reaction with respect to oxygen was normally assumed.

A1.4.3 Order of reaction with respect to carbon.

When insufficient carbon is present to give complete monomolecular layer

coverage in the porous catalyst (see section 5.6), then the rate of reaction will be proportional to the surface covered with carbon and hence proportional to the carbon concentration in the pellet, provided no multilayers are present which would tend to decrease the order of the reaction. Generally a first order reaction with respect to carbon or coke is reported, e.g. by Weisz and Goodwin (1963 and 1966), Ramaswamy and Stermole (1967), Johnson and Mayland (1955), and Hughes and Shettiger (1971). Dart and co-workers (1944) report a second order reaction for carbon concentrations below and first order for concentrations above 2% by weight. Hall and Rase (1963), and Massoth (1967), indicate that carbon deposits in particles rather than in a monomolecular layer, suggesting an order lower than one. Haldeman and Botty (1959) report small uniform coke particles which gave rise to an even burning rate, approximately first order with respect to carbon. Most of the evidence, therefore, points to a first order reaction with respect to carbon, and this was assumed for computing purposes.

A1.4.4 The intrinsic rate expression.

From the above it follows that the intrinsic rate of reaction may be expressed as

$$\exp\left(k_o - \frac{E}{R'T}\right)\left(\frac{yP}{R'Ts}\right)^m C^n \qquad \text{kg mole C/(m}^3\text{s)}$$

with $m \leq 1$ and $n \leq 1$.

CHAPTER A 2

PHYSICAL PROPERTIES

A2.1 Heat Capacities

A2.1.1 Specific heat of the gas phase.

The expression used to calculate the specific heat of the gas phase

$$c_g = 0{,}9181 \times 10^{3} + 2{,}721 \times 10^{-1} T \quad J/(kg\ K)$$

is the one used by Olsen (1962) for the same regeneration problem. This expression he reports to be within 1,3% of the accepted best values and correlates well with the values used by other workers in the field.

A2.1.2 Heat capacity of the solid phase.

The expression used to calculate the heat capacity of the catalyst

$$c_s = 0{,}8926 \times 10^{3} + 3{,}562 \times 10^{-1} T \quad J/(kg\ K)$$

is the one used by Olsen (1962) and is for high purity α - $Al_2 O_3$

Most of the resistance to heat transfer through the walls of the reactor lies in the insulating material lagging them, (see section A2.3.3). The effect of the walls of the reactor should therefore be included when considering the overall heat capacity of the reactor for the simplified, one dimensional model used here. The effective heat capacity c_e, may be obtained by equating the effective heat capacity of the bed to the sum of the heat capacities of the bed and the walls, as follows :

$$c_e = c_s \left[1 + \frac{1}{D^2} \{ 2D(\Delta D) + (\Delta D)^2 \} \frac{\rho_T\ c_T}{\rho_b\ c_s} \right]$$

From the expression for c_s, c_s is about $1{,}20 \times 10^3$ J/(kg K) for the range 750 - 980°K.

Brown (1958) reports for the same range of temperatures for mullite a density of 2427 kg/m^3 and a specific heat of 963 J/(kg K). Using the values of ρ_b = 697 kg/m^3 (section A3.1) and the tube dimensions

$$c_e = 2{,}095\ c_s$$

Since this approach is not very accurate, probable inaccuracies in the expressions for c_s are of relatively little consequence. It is assumed that the temperature effect on the effective heat capacity is the same as for the catalyst, so that

$$c_e = 1{,}958 \times 10^3 + 0{,}782\ Ts \qquad J/(kg\ K)$$

A2.2 Mass Transfer Coefficient in Fixed Bed

For low rates of mass transfer in a multicomponent system Bird, Stewart and Lightfoot (1960) relate the mass transfer rate to the j_D factor by

$$j_D = \frac{k_g\ Mg}{G}\ (Sc)_f^{2/3}$$

where the Schmidt number, Sc, is evaluated at the temperature of the film at the gas-solid interface. Carberry (1960) derived an expression for the j_D factor in terms of flow conditions in a packed bed

$$j_D = \frac{1{,}15}{\sqrt{\varepsilon}}\ Re^{-\frac{1}{2}} \qquad \text{for } 0{,}1 < Re < 380$$

which is in excellent agreement with the experimental results obtained by Wilke and Hougen (1945). For the present work $90 < Re < 260$, which makes the expression applicable here.

Olson (1962) developed expressions for the Reynold and Schmidt numbers as functions of temperatures and compositions to be expected during regeneration of carbonised catalyst, which he used with the above expressions to obtain

$$k_g = 2{,}161 \times 10^{-5} \left(\frac{G}{\varepsilon Rp} \right)^{\frac{1}{2}} Tg^{1/3} \quad kg\ mol/(m^2 s)$$

This expression was used for all computations in this work.

A2.3 Heat Transfer Coefficients

A2.3.1 Interphase heat transfer coefficient in the fixed bed.

Analogous to the expression for the j_D factor (section A2.2), the j_H factor may be related to the heat transfer coefficient by

$$j_H = \frac{h_v}{G\, c_g} (Pr)^{2/3}$$

Evnochides and Thodos (1961) confirmed earlier experimental findings and reported for fixed beds $j_H/j_D = 1{,}06$. Using expressions for the Reynolds and Schmidt numbers as functions of temperature and compositions to be expected during regeneration, Olson similarly as in section A2.2 for k_g, showed that

$$h_a = 0{,}2638 \left(\frac{GT}{\varepsilon Rp} \right)^{\frac{1}{2}} \quad W/(m^2 K)$$

In conjunction with $h_v = 3\, h_a\, (1-\varepsilon)/Rp$, this expression was used for all the computations in this work.

A2.3.2 Apparent effective conductivity in the fixed bed.

Based on a detailed analysis of heat transfer in a packed bed Yagi and Kunii (1957) and Kunii and Smith (1960) developed an expression for the

stagnant conductivity of heat in a fixed bed. The mechanisms they considered were the conduction of heat through the solid and gaseous phases in the bed and through the stagnant film near the points of contact between particles in the bed. They noted that the contribution due to contact between particles was negligible at ordinary pressures. Including the effects of radiant heat transfer between gas filled voids and also between different parts of the solid phase, the expression for k_e, the stagnant conductivity becomes

$$k_e = k_g + 0{,}95\left(h_{rv}\, 2\, Rp\, \varepsilon + \frac{1 - \varepsilon}{\frac{1}{\frac{k_g}{\phi} + 2\, h_{rs}\, Rp} + \frac{0{,}667}{k_s}} \right) \quad W/(m\ K)$$

where h_{rv}, the void to void radiant heat transfer coefficient, and h_{rs} the solid to solid radiant heat transfer coefficient may be calculated using expressions given by Yagi and Kunii (1957). ϕ is a measure of effective thickness of the fluid film adjacent to the contact surface of two particles. Using the method given by Kunii and Smith (1960) ϕ was found to be practically constant and equal to 0,385. From work done by Keyes (1951), Schaefer and Thodos (1959) and Maxwell (1950), Olson (1962) derived an expression, representative within 0,5% for k_g, the thermal conductivity of the gas in the reactor

$$k_g = 2{,}270 \times 10^{-4}\ Tg^{0{,}829} \quad W/(m\ K)$$

From work done by Sehr (1958), Olson derived, for pellets similar to ours, an expression for the conductivity of the solid phase

$$k_s = 1{,}047 \times 10^{4}\ Ts^{-1{,}8} \quad W/(m\ K)$$

Substituting these expressions and the experimental values for Rp and ε into the above expression, it is found that

$$k_e = 0,0715\ (\pm\ 1,3\%) \qquad W/m\ K$$

for the temperature range from 750 to 950°K.

Kunii and Smith (1961) related k, the apparent effective conductivity of the bed (which includes dynamic effects) to k_e by

$$\frac{k}{k_e} = 0,5\left[1 + \left\{1 + \frac{2}{3(1-\varepsilon)}\frac{(PrRe)^2}{\frac{k_e}{k_g}Nu}\right\}^{\frac{1}{2}}\right]$$

provided $\varepsilon \frac{k_g}{k}$ is much smaller than 1.

They report Nusselt numbers obtained by different workers for packed beds for a wide range of Reynold numbers. For the range of Reynold numbers of interest (section A3.3) these results may be represented by

$$Nu = 0,1337\ Re^{0,913}$$

Olson (1962), for conditions in a regenerator, found the Prandtl number to be practically constant and equal to 0,678. Expressing the Reynold number as a function of flowrate and temperature (section A3.3), it is found that the expression relating k and k_e may be simplified considerably. The first term under the square root sign is very much smaller than the last term and may be ignored. Similarly for our conditions, ignoring the first term in the square brackets, introduced an error of only -4%. Neglecting these two terms therefore and substituting for the various parameters k may be expressed as

$$k = 6,13 \times 10^{-2}\ G^{0,5435}\ T^{0,2631} \qquad W/(m\ K)$$

When evaluating the transfer of heat through the reactor wall (in the next section) it is found that most of the resistance to this transfer is associated with the insulation around the reactor wall. Because of

this the heat capacity of the walls was lumped with that of the bed itself (A2.1.2). For the same reason the walls also contribute to the overall conduction of heat along the axial direction of the bed. Using the same method as in section A2.1.2 and the value for k_w as given in the next section, it was found that the k values obtained above had to be multiplied with factors of 1,82 and 1,63 and 1,52 respectively for flowrates of 0,542 and 0,949 and 1,356 kg/(m^2s).

A2.3.3 Heat transfer coefficient at the reactor wall.

Heat lost from the bed through the reactor walls, has to be transferred from the bed to the wall, conducted through the wall and finally conducted through the insulation to the jacket which is assumed to be at a constant and known temperature Tw. Since the overall driving force (T reactor - Tw) is known, it is most convenient to express the heat losses through the wall by means of an overall heat transfer coefficient (relative to the inside reactor tube diameter) U, which is related to the three transfer mechanisms by

$$\frac{1}{U} = \frac{1}{h_i} + \frac{D}{2}\left(\frac{\ln \frac{Do}{D}}{k_w} + \frac{\ln \frac{D_J}{Do}}{k_I}\right)$$

Brown (1958) reports for mullite k_w = 2,08 W/(m K). Morganite Ceramic Fibre Limited report for the packing density and temperature range used for the insulating material k_I = 0,121 W/(m K). Then substituting the dimensions of the reactor assembly into the above equation

$$\frac{1}{U} = \frac{1}{h_i} + 0{,}1077$$

Using the expression for the wall heat transfer coefficient suggested by Hanratty (1954) for cylinders

$$h_i = 0,95 \frac{k_g}{Dp} \left(\frac{Dp\ G}{\varepsilon \mu} \right)^{0,5}$$

and substituting for k_g and μ (sections A2.3.2 and A3.3), it is found that the reciprocal of h_i ranges from 0,0065 to 0,0039 m^2K/W for our conditions. Using the average of 0,0052 the overall heat transfer coefficient then becomes

$$U = 8,84\ W/(m^2K)$$

U is within about 6% determined by the resistance to flow of heat through the insulation. Equating the heat flow on the inside of the reactor wall to that on the outside of the wall at steady state,

$$0,050\ \pi \left(k \frac{\partial T}{\partial r}\right)_{inside} = 0,059\ \pi \left(k \frac{\partial T}{\partial r}\right)_{outside}$$

If the temperature gradient were the same on both sides of the tube wall, then

$$k_{inside} = 1,18\ k_{outside} = 1,18\ k_I = 0,143\ W/(m^2K)$$

If values for the mass flux in the reactor and the temperature are substituted into the expression for thermal conductivity of the bed as derived in the previous section (A2.3.2), it is found that the lowest value of $k = 0,92\ W/(m^2K)$ is obtained at $G = 0,542\ kg/(m^2s)$ and $T = 755^oK$ whereas $G = 1,356\ kg/(m^2s)$ and $T = 975^oK$ give $k = 1,67\ W/(m^2K)$. Comparing these values with that obtained above it appears that the temperature gradient in the bed will be less than one sixth of that in the insulation material at the lower flowrate of 0,542 $kg/(m^2s)$ and less than one tenth at the higher flowrate of 1,356 $kg/(m^2s)$.

CHAPTER A 3

EXPERIMENTAL CONDITIONS

A3.1 Densities and Void Fractions

The bulk density of the bed, ρ_b, was determined from the weight of pellets needed to fill the known reactor volume. Reactor volume is volume of empty tube minus volume of thermocouple assembly.

The density of the pellets, excluding bed voidage and accessible pore volume, $\hat{\rho}$, was determined by the standard method using a specific gravity bottle. The water displaced by a known weight of pellets is found by the difference in weight of water needed to fill the empty specific gravity bottle and of the water required to fill the bottle containing the pellets. The air in the pores of the pellet was displaced by adding the water under vacuum to the previously evacuated specific gravity bottle containing the pellets. After filling with water the vacuum was released and reapplied four times.

For the density of the pellets including the pores, ρ_p, the pore volume was found from the difference between the weights of the soaked pellets (lightly wiped to remove excess of water from the surface) and the dry pellets. The overall volume of the pellets was obtained by adding the pore volume to the volume displaced by the dry pellets.

The void fraction of the bed, ε, and the porosity of the pellets, ε_p, are related to the densities ρ_B, ρ_p and $\hat{\rho}$ by

$$\varepsilon = 1 - \rho_b/\rho_p \quad \text{and} \quad \varepsilon_p = 1 - \rho_p/\hat{\rho}$$

The following results were obtained for fresh pellets :

$\rho_b = 697 \pm 14 \quad kg/m^3$

$\rho_p = 1067 \pm 9 \quad kg/m^3$

$\hat{\rho} = 2200 \pm 5 \quad kg/m^3$

$\varepsilon = 0,35$

$\varepsilon_p = 0,52$

A3.2 Mean Mass Flowrate and Molecular Weight of Gas Phase

The feed gas consisted mainly of inert nitrogen and a few percent of oxygen. The exit gas consisted mainly of nitrogen, some unconverted oxygen and small amounts of carbon monoxide, carbon dioxide and water vapour. Per kg mole of inlet gas the following expressions may be derived from equation A1.

Weight of inlet gas $= 28\ (1 - y_o) + 32\ y_o$

moles of outlet gas $= 1 + (y_o - y_1)\ \frac{1,264-x}{1,264+x}$

weight of outlet gas $= 28\ (1-y_o) + 32\ y_1 + \frac{2(y_o - y_1)}{1,264 + x}\left\{18x0,264 + 44x + \frac{}{28\ (1-x)}\right\}$

where $x = CO_2/(CO + CO_2)$

y_o = molefraction of oxygen in inlet gas

y_1 = molefraction of oxygen in outlet gas.

The larger change in mass flowrate due to combustion will occur at high conversions of oxygen and high inlet oxygen concentrations. Only at very high flowrates were high concentrations used. Under those conditions, conversions of oxygen were normally relatively lower. For the most severe conditions of a 6% inlet concentration and a conversion of about 85%, the ratio of outlet to inlet mass flowrate ranged from 1,030

to 1,021 for $0,191 < x < 0,822$ (see section A1.2). The ratio of outlet to inlet average molecular weight ranged from 1,0057 to 1,0120 for the same range in x. For an inlet concentration of 4% and a conversion of 88% a mass flowrate ratio of 1,022 to 1,015 and a molecular weight ratio of 1,0039 to 1,0082 were obtained.

The average molecular weight of the gas changes little down the bed and the change in mass flowrate although up to 3% in the worst cases, was still smaller than the accuracy to which the inlet flowrate could be set and controlled. For computing purposes the inlet flowrate and average molecular weight were used throughout the reactor.

A3.3 Reynold Numbers

The Reynold number in the present work is defined as

$$Re = \frac{2\ Rp\ G}{\mu}$$

Olson (1962) developed for the multi-component regenerator gas phase an expression for the viscosity as a function of temperature

$$\mu = 4,186 \times 10^{-7}\ T^{0,66} \quad kg/(ms)$$

Substituting this and the experimental values for Rp into the above equation gives

$$Re = 1,517 \times 10^{4}\ G\ T^{-0,66}$$

This gives

TABLE A3.1

$T^{o}K$	Re			
	G = 0,542	G = 0,949	G = 1,356	$kg/(m^2s)$
756	103	181	259	
811	99	173	248	
867	95	166	237	
922	90	159	227	

CHAPTER A 4

COMPUTER SUBROUTINES

All programs were written in Fortran IV for the CDC 1700 computer with 32K words core storage and $3\frac{1}{2}$ million words disc storage.

A4.1 Subroutine SCP

Purpose: To predict $c_{i+1,j,k}$ profiles.

For a particular value of i+1

1. At j=1, $A3_{i,j,k}$ is calculated for k=1,2,...,K from the current values of all the variables involved.

2. For i=1, t=Δt, $c_{1,j,k} = c_{o,j,k} - A3_{o,j,k}\,\Delta t$ for k=1,2...,K

(equation (4.9a))

for i, t>Δt, $c_{i+1} = c_{i-1} - 2A3_{i,j,k}\,\Delta t$ for k=1,2,....K

(equation (4.9))

3. Steps 1 and 2 are repeated for j=2,3,....J

Note: If $c_{i,j,k} \leq 0$, $A3_{i,j,k}$ is not calculated and $c_{i+1,j,k}$ is put equal to zero.

A4.2 Subroutine SCC

Purpose: To correct the $C_{i+1,j,k}$ profiles.

For a particular value of i+1

1. At j=1 using the current values of variables at i and i+1

$A3_{i,j,k}$ and $A3_{i+1,j,k}$ are calculated for k=1,2,..., K

2. $c_{i+1,j,k} = c_{i,j,k} - 0,5\ (A3_{i+1,j,k} + A3_{i,j,k})\ \Delta t$ for k=1,2,...K

(equation (4.10))

3. Repeat steps 1 and 2 for j=2,3,....,J

Note: If $c_{i+1,j,k} \leq 0$, $A3_{i+1,j,k}$ is not calculated and $C_{i+1,j,k}$ is put equal to zero. ($A3_{i,j,k}$ is stored from previous predictor-corrector cycle).

A4.3 Subroutine SYG

Purpose: To calculate Yg profiles.

For a particular value of i

1. $Yg_{i,1}$ is found by a five point Lagrangian interpolation scheme from known inlet values.

2. $A4_{i,j}$ is calculated from current values of all the variables involved for j=1,2,...,J

3. $Yg_{i,j} = Yg_{i,j-1} \exp\{(A4_{i,j} + A4_{i,j-1})\}\frac{\Delta z}{2}$

for j = 2,3,....,J (equation (4.11))

A4.4 Subroutine SY

Purpose: To calculate $Y_{i,j,k}$ profiles.

For a particular value of i

1. $Al_{i,j,k}$ is calculated from current values of all the variables involved for j=1,2,...J and k=1,2,...,K. $A2_{i,j,k}$ is calculated at K.

2. At j=1 a set of simultaneous equations is obtained from equations (4.6), (4.7) and (4.8) such that

$$\begin{bmatrix} (-2-Al_{i,j,1}) & 2 & & & \\ (1-\frac{\Delta r}{r}) & (-2-Al_{i,j,2}) & (1+\frac{\Delta r}{r}) & & \\ & \cdot & \cdot & \cdot & \\ & (1-\frac{\Delta r}{r}) & (-2-Al_{i,j,k}) & (1+\frac{\Delta r}{r}) & \\ & \cdot & \cdot & \cdot & \\ & & 1 & \{-1-0,5Al_{i,j,K} & \\ & & & -(1+\Delta r)A2_K\} & \end{bmatrix} \begin{bmatrix} Y_{i,j,1} \\ Y_{i,j,2} \\ \cdot \\ Y_{i,j,k} \\ \cdot \\ Y_{i,j,K} \end{bmatrix} =$$

$$\begin{bmatrix} 0 \\ 0 \\ \cdot \\ 0 \\ \cdot \\ -(1+r)A2_{i,j,K} \end{bmatrix}$$

This set of simultaneous equations is solved by the Thomas Algorithm to obtain $Y_{i,j,k}$ for k=1,2,...,K

3. Step 2 is repeated for j=2,3,...,J

A4.5 Subroutine STSP

Purpose: To predict $Ts_{i+1,j}$ profiles.

For a particular i+1, using equations (4.17a), (4.18), (4.19) and (4.20).

1. $A9_{i,j}$, $A10_{i,j}$ and $A11_{i,j}$ are calculated from the current values of

all the variables involved for j=1,2,...J

2. At j=1 $Ts_{i+1,1} = All_{i,1} + (1-AlO_{i,1})\, Ts_{i,1} - 2A9_{i,1}\, Ts_{i,2}$

3. At j=2 $Ts_{i+1,j} = All_{i,j} - A9_{i,j}\,(Ts_{i,j-1} + Ts_{i,j+1}) + (1-AlO_{i,j})\, Ts_{i,j}$

4. Repeat step 3 for j=3,4,...,J-1

5. At j=J $Ts_{i+1,J} = All_{i,J} - 2A9_{i,J}\, Ts_{i,J-1} + (1-AlO_{i,J})\, Ts_{i,J}$

A4.6 Subroutine STSC

Purpose: To correct $Ts_{i+\theta,j}$ profiles.

1. For a particular value for i+1 and θ, using the current values of all the variables involved

$$\left.\begin{aligned} A9_{i+\theta} &= \theta.A9_{i+1} + (1-\theta)A9_i \\ AlO_{i+\theta} &= \theta.AlO_{i+1} + (1-\theta)AlO_i \\ All_{i+\theta} &= \theta.All_{i+1} + (1-\theta)All_i \end{aligned}\right\} \text{ for } j=1,2,....J$$

2. At i+θ a set of equations is obtained from equations (4.18), (4.19) and (4.20) such that

$$\begin{bmatrix} (1+A1O_1\theta) & 2A9_1\theta & & & \\ A9_2\theta & (1+A1O_2\theta) & A9_2\theta & & \\ & \cdot & \cdot & \cdot & \\ & A9_j\theta & (1+A1O_j\theta) & A9_j\theta & \\ & \cdot & \cdot & \cdot & \\ & & 2A9_J\theta & (1+A1O_J\theta) & \end{bmatrix} \begin{bmatrix} \Delta Ts_{i,1} \\ \Delta Ts_{i,2} \\ \cdot \\ \Delta Ts_{i,j} \\ \cdot \\ \Delta Ts_{i,J} \end{bmatrix} =$$

$$\begin{bmatrix} A11_1 - A1O_1\, Ts_{i,1} - 2A9_1\, Ts_{i,2} \\ A11_2 - A9_2\,(Ts_{i,1} + Ts_{i,3}) - A1O_2\, Ts_{i,2} \\ \cdot \\ A11_j - A9_j\,(Ts_{i,j-1} + Ts_{i,j+1}) - A1O_j\, Ts_{i,j} \\ \cdot \\ A11_J - 2A9_J\, Ts_{i,J-1} - A1O_J\, Ts_{i,J} \end{bmatrix}$$

This set of simultaneous equations in $\Delta Ts_{i,j}$ is solved by means of the Thomas Algorithm.

3. $Ts_{i+1,j} = Ts_{i,j} + \Delta Ts_{i,j}$ for $j=1,2,\ldots,J$

A4.7 Subroutine STG

Purpose: To calculate $Tg_{i,j}$ profiles.

For a particular value of i

1. At j'=1, $Tg_{i,1}$ is found by a five point Lagrangian interpolation scheme from known feed gas temperatures.

2. At j' = 1, $A5_{i,j'} = A5_{i,j}$ using the current values for the variables involved.

3. $Tg_{i,j'+1} = Tg_{i,j'} + A5_{i,j'} \Delta z'$ (equation (4.13))

4. By a five point Lagrangian interpolation scheme

   $Ts_{i,j'+1}$ and the group $\frac{L h_{v_{i,j'+1}}}{G c_{g_{i,j'+1}}}$

   are calculated from values stored at j=1,2,...,J.

5. $A5_{i,j'+1}$ is calculated from the current values of

   $Ts_{i,j'+1}$, $\frac{Lh_{v_{i,j'+1}}}{G c_{g_{i,j'+1}}}$ and $Tg_{i,j'+1}$

6. $Tg_{i,j'+1}$ is corrected by

   $$Tg_{i,j'+1} = Tg_{i,j'} + 0,5 (A5_{i,j'} + A5_{i,j'+1}) \Delta z'$$

   (equation (4.14))

7. $A5_{i,j'+1}$ is updated using the corrected $Tg_{i,j'+1}$ value.

8. Steps 6 and 7 are repeated till $Tg_{i,j'+1}$ converges to within a predetermined tolerance.

9. Steps 3 to 8 are repeated for j' = 3,4,....,M

A4.8 Subroutine SHMAC

Purpose: To calculate MO, the oxygen consumed by the reactor, HG,

the heat lost through the outlet gas stream and HW, the heat lost through the reactor wall.

1. At i=1, t=o; MO = 0

HG = 0

HW = 0

A12, A14 and A15, which are constants are recalculated.

2. At i=2,

$$MO = MO + A12\ (Yg_{i,1} - Yg_{i,J}) \qquad \text{(equation (4.21))}$$

$$HG = HG + A14 \left[\{c_g(o) + c_g\ (Tg_{i,J})\}\ Tg_{i,J} - \{c_g(o) + c_g\ (Tg_{i,1})\}\ Tg_{i,1}\right] \qquad \text{(equation (4.25))}$$

$$HW = HW + A15 \left[0{,}4\ (Ts_{i,1} - Tw_1 + Ts_{i,J} - Tw_J) + 1{,}1\ (Ts_{i,2} - Tw_{i,2} + Ts_{i,J-1} - Tw_{i,2} - Tw_{J-1}) + \sum_{j=3}^{J-2} (Ts_{i,j} - Tw_j)\right] \qquad \text{(equation (4.28))}$$

3. Repeat step 2 for i=3,4,.....

A4.9 Subroutine SHMIN

Purpose: To calculate MCP, the instantaneous carbon content of the reactor and HA, the instantaneous heat content of the reactor.

1. At i=1, t=o, A13 and A16, which are constants are calculated.

2. At any value of i>1,

2.1 The carbon in the bed at j, as a function of the original carbon present, say Q_j, is calculated for j=1,2,...,J

$$Q_j = 0{,}4\,(K-1)^2\,c_{i,j,k} + 1{,}1\left(c_{i,j,2} + (K-2)^2\,c_{i,j,K-1}\right) + \sum_{k=3}^{K-2}(k-1)^2\,c_{i,j,k}$$

(equation (4.21a))

$$2.2\quad MCP = 0{,}4\,(Q_1+Q_I) + 1{,}1\,(Q_2+Q_{J-1}) + \sum_{j=3}^{J-2} Q_j$$

(equation (4.22))

$$HAP = 0{,}4\left[\{c_s(o) + c_s\,(Ts_{i,1})\}\,Ts_{i,1} + \{c_s(o) + c_s\,(Ts_{i,J})\}\,Ts_{i,J}\right] + 1{,}1\left[\{c_s(o) + c_s\,(Ts_{i,2})\}\,Ts_{i,2} + \{c_s(o) + c_s\,(Ts_{i,J-1})\}\,Ts_{i,J-1}\right] + \sum_{j=3}^{J-2}\{c_s(o) + c_s\,(Ts_{i,j})\}\,Ts_{i,j}$$

(equation (4.27))

3. At i=1 : MCO = MCP

HAO = HAP

A4.10 Subroutine SBAL

Purpose:

1. To calculate $\overline{x}_M$ and $\overline{x}_H$, the fraction of carbon converted to carbon dioxide from the mass balance and from the heat balance respectively.

2. To calculate x', the instantaneous fraction of carbon converted to CO_2 in the outlet gas.

3. To calculate XR, for an implicit check on mass and energy balances.

At any particular value of i

$$HT = HG + HW + (HAP - HAO) \qquad \text{(equation (4.29))}$$

$$MC_i = MCO - MCP_i \qquad \text{(equation (4.24))}$$

$$\bar{x}_M = 2\,(MO/MC_i - 0{,}632) \qquad \text{(equation (4.30))}$$

$$\bar{x}_H = (HT/MC_i - 1{,}97\times10^{8})/2{,}83\times10^{8} \qquad \text{(equation (4.31))}$$

$$\bar{x}_i = 0{,}5\,(\bar{x}_M + \bar{x}_H)$$

$$XR = \bar{x}_M/\bar{x}_H \qquad \text{(equation (4.32))}$$

$$x' = \frac{\bar{x}_i\, MC_i - \bar{x}_{i-1}\, MC_{i-1}}{MC_i - MC_{i-1}} \qquad \text{(equation (4.33))}$$

A4.11 Subroutine SREV

Purpose: To invert X_j profiles (j=1,2,...,J), with respect to j, that is with respcet to z.

At the time of reversal $i=i_{Rev.}$

1. M = (J-1)/2

2. At j=1

   m = J + 1 - j

   DUMMY = X_j

   $X_j = X_m$

   X_m = DUMMY

3. Repeat step 2 for j=2,3,...,M.

Note: If X is a variable $X_{j,k}$ only the index j is changed.

N O M E N C L E A T U R E

$a_1 - a_8$	-	dimensionless constants as defined in section 3.5	
A1, A2	-	parameters, defined in section 4.2	
A3	-	parameter, defined in section 4.3	
A4	-	parameter, defined in section 4.4	
A5	-	parameter, defined in section 4.5	
A6-A11	-	parameters, defined in section 4.6	
A12-A16	-	parameters, defined in section 4.7	
A	-	cross-sectional area of bed	m^2
c	-	C/Co	
c_e	-	effective specific heat of solid phase	J/(kg K)
c_c	-	specific heat of carbon deposited in pellet	J/(kg K)
c_s	-	specific heat of catalyst	J/(kg K)
c_T	-	specific heat of reactor tube	J/(kg K)
c_g	-	specific heat of gas phase	J/(kg K)
∇c_p	-	change in heat capacity of entire reaction system at constant pressure	J/(kg mole K)
c_w	-	carbon concentration	kg C/kg catalyst
c_{wo}	-	initial carbon concentration	kg C/kg catalyst
C	-	carbon concentration	kg mole C/m^3
Co	-	initial carbon concentration	kg mole C/m^3
C'	-	total gas concentration	kg mole/m^3
D	-	inside diameter of reactor tube	m
$\Delta D/2$	-	thickness of reactor tube	
De	-	effective diffusivity of oxygen in pellet	m^2/s
D_J	-	inside diameter of jacket	m
Do	-	outside diameter of reactor tube	m

Dp	-	diameter of catalyst pellet	m
Dz	-	axial mixing coefficient	m^2/s
E	-	activation energy	J/kg mole
Fq	-	proportionality constant determining level of CO/CO_2 produced	
G	-	gas flowrate	$kg/(m^2s)$
h_a	-	film heat transfer coefficient	$W/(m^2K)$
h_i	-	wall heat transfer coefficient	$W/(m^2K)$
h_{rs}	-	heat transfer coefficient for radiation between pellets	$W/(m^2K)$
h_{rv}	-	heat transfer coefficient for radiation between voids in the bed	$W/(m^2K)$
h_v	-	film heat transfer coefficient	$W/(m^3K)$
H	-	Nusselt number, h_a Rp/ks	
$-\Delta H$	-	heat of combustion of coke	J/kg mole C
HA	-	heat accumulated in bed	J
HAO	-	initial heat content of bed	J
HAP	-	heat content of bed	J
HG	-	total heat lost through gas stream	J
HW	-	total heat lost through the reactor wall	J
HT	-	total heat generated	J
k	-	apparent thermal conductivity of the solid phase	W/(m K)
k_o	-	natural logarithm of Arrhenius frequency factor	
k_e	-	solid phase contribution to stagnant conduction in bed	W/(m K)
k_g	-	film mass transfer coefficient for oxygen	kg mole/(m^2s)

k_g	-	thermal conductivity of gas phase (section A2.3.2 only)	W/(m K)
k_I	-	thermal conductivity of insulating material	W/(m K)
k_w	-	thermal conductivity of tube reactor	W/(m K)
k_s	-	thermal conductivity of catalyst pellet	W/(m K)
L	-	length of reactor	m
	-	length of cylindrical catalyst pellet (Chapter 5 only)	m
m	-	order of reaction with respect to oxygen	
M	-	Sherwood number, k_g Rp/(De C') (section 3.2.4 only)	
	-	number of subdivisions of Δz	
Mc	-	molecular weight of carbon	kg/kg mole
Mg	-	molecular weight of gas phase	kg/kg mole
MCO	-	total initial carbon content of bed	kg mole
MCP	-	total carbon content of bed at time t	kg mole
MC	-	total carbon consumed at time t	kg mole
MO	-	total oxygen consumed at time t	kg mole
n	-	order of reaction with respect to carbon	
$n_i\lambda_i$	-	latent heat due to n moles of species i	J/kg mol
N	-	moles of carbon burned per mole oxygen consumed	
N_{av}	-	Avogadro's number	
P	-	total pressure	atm.
Pr	-	Prandtl number, $C_g\mu/k_g$	
q	-	CO/CO_2 ratio produced on combustion of coke	

Q	-	dummy variable defined in text	
r	-	R/Rp, dimensionless radial position in pellet	
Δr	-	dimensionless radial increment in pellet	
$\hat{r}$	-	pore radius	Å
R	-	radial position in pellet	m
Re	-	Reynolds number (G Dp/μ)	
Rp	-	radius of pellet	m
R'	-	gas constant	
R*	-	rate of reaction as defined by equation 3.1	kg mole C/(m^3s)
R*o	-	initial rate of reaction at inlet conditions	kg mole C/(m^3s)
S	-	total active surface of catalyst	m^2/kg
t	-	time	s
Δt	-	time increment	s
T	-	temperature	°K
Tg	-	gas phase temperature	°K
Ts	-	solid phase temperature	°K
ΔT	-	$Ts_i - Ts_{i-1}$	°K
Tw	-	temperature of jacket (pipe) around reactor	°K
U	-	overall wall heat transfer coefficient	W/(m^2K)
x	-	fraction of carbon converted to CO_2 - $CO_2/(CO + CO_2)$	
x'	-	$CO_2/(CO + CO_2)$ in outlet gas	
$\bar{x}_M$	-	overall fraction of carbon converted to CO_2 calculated from mass balance	
$\bar{x}_H$	-	overall fraction of carbon converted to CO_2 calculated from heat balance	
XR	-	$\bar{x}_M / \bar{x}_H$, a material and heat balance check parameter	
y	-	mole fraction of oxygen	
$y_o(t)$	-	mole fraction of oxygen in inlet gas	

y_o	-	initial mole fraction of oxygen in inlet gas	
y_g	-	mole fraction of oxygen in bulk gas phase	
y_p	-	mole fraction of oxygen in pellet	
y_{Rp}	-	mole fraction of oxygen at surface of pellet	
Y	-	y_p/y_g	
Yg	-	y_g/y_o	
z	-	Z/L, dimensionless length	
Δz	-	increment in z	
$\Delta z'$	-	1/(J-1) M	
Z	-	distance into bed	m
β	-	dimensionless group defined in section 3.2.4	
γ	-	dimensionless group defined in section 3.2.4	
ε	-	void fraction in the bed	
ε_p	-	porosity of pellet	
θ	-	interpolation factor, $0 \leq \theta \leq 1$	
ϕ	-	dimensionless group defined in section 3.2.4	
ρ_b	-	bulk density of bed	kg/m^3
ρ_g	-	density of gas phase	kg/m^3
ρ_p	-	density of pellet	kg/m^3
ρ_T	-	density of reactor tube material	kg/m^3
$\hat{\rho}$	-	density of catalyst material	kg/m^3
μ	-	viscosity of gas	kg/(m s)

indexes

i	-	denotes time, $1 \leq I \leq \infty$
j	-	denotes axial position in bed $1 \leq j \leq J$
k	-	denotes radial pellet position, $1 \leq k \leq K$

I - denotes total simulation time

J - denotes total length of reactor

K - denotes outside radius of pellet

B I B L I O G R A P H Y

Aris, R., Chem. Eng. Sci., 6, 262 (1957).

Ausman, J.M., and Watson, C.C., Chem. Eng. Sci., 17, 323 (1962).

Balder, J.R., and Petersen, E.E., J. Cat., 11, 195 (1968).

Baulch, D.L., Drysdale, D.D., and Horne, D.G., "High Temperature Reaction Rate Data. 2." Dept. Phys. Chem., Univ. of Leeds, 1968.

Bird, R.B., Stewart, W.E., and Lightfoot, E.N., "Transport Phenomena", Wiley Inc., New York, 185 (1960).

Bischof, K.B., Chem. Eng. Sci., 18, 711 (1963).

Bischof, K.B., Chem. Eng. Sci., 20, 783 (1965).

Blyholder, G., and Eyring, H., J. Phys. Chem., 61, 682 (1957).

Bondi, A., Miller, R.S., and Schlaeffer, W.G., Ind. Eng. Chem., Process Des. Develop., 1, 196 (1962).

Bowen, J.H., and Cheng, C.K., Chem. Eng. Sci., 24, 1829 (1969).

Bowman, W.H., Sc. D. Thesis, Mass. Inst. Tech., 1955. (Cited by Olson (op. cit.)).

Brown, R.W., Chem. Eng. (New York), 65, Apr., 135 (1958).

Carberry, J.J., A.I.Ch.E. J., 6, 460 (1960).

Carberry, J.J., Ind. Eng. Chem., 58, No.10, 40 (1966).

Carberry, J.J., and Wendel, M.M., A.I.Ch.E. J., 9, 129 (1963).

Cremer, E., Adv. Cat., 7, 75 (1955).

Dart, J.C., and Oblad, A.G., Chem. Eng. Prog., 45, 110 (1949).

Dart, J.C., Savage, R.T., and Kirkbride, C.G., Chem. Eng. Prog., 45, 102 (1949).

Effron, E., and Hoelscher, H.E., A.I.Ch.E. J., 10, 388 (1964).

Essenhigh, R.H., Froberg, R., and Howard, J.B., Ind. Eng. Chem., 57, No. 9, 32 (1965).

Evnochides, S., and Thodos, G., A.I.Ch.E. J., 7, 78 (1961).

Finkelstein, N.P., National Institute for Metallurgy, Johannesburg, South Africa, Private Communication, 1969.

Froment, G.F., Ind. Eng. Chem., 59, No. 2, 18 (1967).

Goldstein, M.S., Ind. Eng. Chem., Process Des. Develop., 5, 189 (1966).

Gonzales, L.O., and Spencer, E.H., Chem. Eng. Sci., 18, 753 (1963).

Gulbransen, E.A., Ind. Eng. Chem., 44, 1045 (1952).

Gulbransen, E.A., and Andrew, K.F., Ind. Eng. Chem., 44, 1034 (1952).

Gunn, R.D., Dissertation, Univ. of California, 1976.
(Cited by Balder and Petersen (op. cit.)).

Hagerbaumer, W.A., and Lee, R., Pet. Ref., 26, No. 6, 123 (1947).

Haldeman, R.G., and Botty, M.C., J. Phys. Chem., 63, 489 (1959).

Hall, J.W., and Rase, H.F., Ind. Eng. Chem., Process Des. Develop., 2, 25 (1963).

Hanratty, T.J., Chem. Eng. Sci., 3, 209 (1954).

Hill, G.R., Chemtech, May, 292 (1972).

Hirschfelder, J.D., Curtiss, C.F., and Bird, R.B., "Molecular Theory of Gasses and Liquids", Wiley Inc., New York, 10, 15 (1964).

Hougen, O.A., Watson, K.M., and Ragatz, R.A., "Chemical Process Principles. Part I. 2nd. Ed., Wiley Inc., New York, 298 (1962)

Hughes, R., and Shettigar, U.R., J. Appl. Chem. Biotechnol., 21, 35 (1971).

Ishida, M., and Shirai, T., J. Chem. Eng. Jap., 2, 180 (1969).

Ishida, M., and Wen, C.Y., A.I.Ch.E. J., 14, 311 (1968).

Johnson, B.M., Ph.D. Thesis, Univ. of Wisconsin, 1956.

Johnson, B.M., Froment, G.F., and Watson, C.C., Chem. Eng Sci., 17, 835 (1962).

Johnson, M.F.L., and Mayland, H.C., Ind. Eng. Chem., 47, 127 (1955).

Keyes, F.G., Trans. A.S.M.E., 73, 589 (1951).

Kunii, D., and Smith, J.M., A.I.Ch.E. J., 6, 71 (1960).

Kunii, D., and Smith, J.M., A.I.Ch.E. J., 7, 29 (1961).

Lapidus, L., "Digital Computation for Chemical Engineers", Chapter 2, McGraw-Hill Book Co., New York, 1962.

Laz'yan, V.I., Panchenkov, G.M., Kozlov, M.V., and Zhorov, Y.M., UDC 66.042.886:542.921, Translated from Khim. i Tekhnol. Topl. i Masel., 6, June, 37 (1969).

Lee, J.C.M., and Luss, D., Ind. Eng. Chem., Fundam., 8, 596 (1969).

Luss, D., Can. J. Chem. Eng., 46, 154 (1968).

Luss, D., and Amundson, N.R., A.I.Ch.E. J., 15, 194 (1969).

Massoth, F.E., Ind. Eng. Chem., Process Des. Develop., 6, 200 (1967).

Maxwell, J.B., "Data Book on Hydrocarbons", Van Nostrand Co., New York, 88, 216 (1950).

Moe, J.M., Chem. Eng. Prog., 58, No. 3, 33 (1962).

Morganite Ceramic Fibres Limited, Triton Kaowool - M40(M)/11.68/3M, Neston, Wirral, Cheshire.

Olson, K.E., Ph.D. Thesis, Univ. of Minnesota, 1962.

Olson, K.E., Luss, D., and Amundson, N.R., Ind. Eng. Chem., Process Des. Develop., 7, 96 (1968).

Ozawa, Y., Ind. Eng. Chem., Process Des. Develop., 8, 378 (1969).

Pansing, W.F., A.I.Ch.E. J., 2, 71 (1956).

Penner, S.S., "Thermodynamics for Scientists and Engineers", Addison - Wesley Publ. Co., Reading, Massachusets, 79 (1968).

Perry, J.H., "Chemical Engineers Handbook", 3rd Ed., McGraw-Hill Book Co., New York, 1959.

Prater, C.D., Chem. Eng. Sci., 8, 284 (1958).

Ralston, A., and Wilf, H.S., "Mathematical Methods for Digital Computers", Wiley Inc., New York, 121 (1960).

Ramaswamy, V., and Stermole, F.J., J. Chem. Eng. Data, 12, 552 (1967).

Satterfield, C.N., "Mass Transfer in Heterogeneous Catalysis", M.I.T. Press, 1970.

Schaefer, C.A., and Thodos, G., A.I.Ch.E. J., 5, 367 (1959).

Schulman, B.L., Ind. Eng. Chem., 55, No. 12, 44 (1963).

Schwartz, C.E., and Smith, J.M., Ind. Eng. Chem., 45, 1209 (1953).

Sehr, R.A., Chem. Eng. Sci., 9, 145 (1958).

Shettigar, U.R., and Hughes, R., Chem. Eng. J.(Loughborough), 3, 93 (1972).

Shettigar, U.R., and Hughes, R., Chem. Eng. J.(Loughborough), 4, 208 (1972).

Shettigar, U.R., and Hughes, R., J. Appl. Chem. Biotechnol., 22, 787 (1972).

Strijbos, R.C.W., Chem. Eng. Sci., 27, 800 (1973).

Van Deemter, J.J., Ind. Eng. Chem., 45, 1227 (1953).

Van Deemter, J.J., Ind. Eng. Chem., 46, 2300 (1954).

Walker, P.L., Rusinko, F., and Austin, L.G., Adv. Cat., 11, 133 (1959).

Weast, R.C., (Ed.), "Handbook of Chemistry and Physics", 49th Ed., Chemical Rubber Publ. Co., Cleveland, B188 (1968-1969).

Webb, G.M., and Den Herder, M.J., A.I.Ch.E., Kansas City, Mo., May 13-16, 1951.
(Cited by Olson (op. cit.)).

Wei, J., Chem. Eng. Sci., 21, 1171 (1966).

Weisz, P.B., and Goodwin, R.B., J. Catal., 2, 397 (1963).

Weisz, P.B., and Goodwin, R.D., J. Catal., 6, 227 (1966).

Wilke, C.R., and Hougen, O.A., Trans. A.I.Ch.E., 41, 445 (1945).

Wunderlich, O.A., and Ivey, F.E., Petr. Ref., 37, No. 2, 135 (1958).

Yagi, S., and Kunii, D., J. Chem. Soc. Jap., 56, 131 (1953).

Yagi, S., and Kunii, D., A.I.Ch.E. J., 3, 373 (1957).